

Formulation of catalysts based on the upcycling of the cathode of spent Mn-Zn batteries for the
combustion of methane

Edwing Alexander Velasco Rozo

Tesis presentada como requisito para optar al título de: Doctor en Ingeniería Química

Director

Víctor Gabriel Baldovino Medrano

Ph.D. en Ingeniería Química

Codirector

Edgar Mauricio Morales Valencia

Ph.D. en Ingeniería Química

Asesora

Luz Marina Ballesteros Rueda

Ph.D. en Ingeniería Química

Universidad Industrial De Santander

Facultad de Ingenierías Físicoquímicas

Escuela de Ingeniería Química

Doctorado en Ingeniería Química

Bucaramanga

2022

Dedicatoria

Lessly Vanessa Serrano Gómez

Te dedico cada letra, cada frase o planteamiento, cada hallazgo o mérito alcanzado en esta tesis. Desde el inicio hasta la concepción de este manuscrito, tu aporte en mi vida personal y académica fueron incalculables: fuiste el motor que me impulso todo este tiempo, y aunque en la cúspide, en el clímax de mi desarrollo científico te ausentaste de mi vida, no pasó un momento sin que usara el gran amor que te tengo para avanzar hasta el día de hoy. Tus aportes a mis ideas y tu discusión de la etiología y motivación de mis formulaciones, indudablemente influyeron en mi capacidad para aterrizar el contenido de este trabajo. Cada café con galletas, cada palabra de aliento, cada juego de voleibol, cada caminata, cada jornada de trabajo, cada sonrisa, cada desvelo y consejo, fueron el catalizador más activo para el desarrollo de mi tesis. Tu presencia y respaldo, considerando que eres la persona más interesante, hermosa e inteligente que conozco, me llenaron de confianza en mis capacidades, y de convicción en que podía terminar con éxito esto que ahora te dedico.

Más que el profundo agradecimiento por todo aquello que sacrificaste para que lograra terminar con éxito mi tesis, resalto que, si este manuscrito es un aporte a la ciencia, ese aporte lo realizo

en honor a ti.

Aless

Agradecimientos

A Dios, mi dueño y escultor, quién guio mis ideas hasta convertirlas en este manuscrito.

A los profesores Sonia Giraldo y Aristóbulo Centeno, quienes me abrieron la puerta al mundo de la ciencia y la catálisis.

A mi director, el profesor Víctor Baldovino, quién me dio la oportunidad de ingresar al programa doctoral, y me formó como investigador tanto en lo académico como en lo personal.

A mi codirector y amigo, Mauricio Morales, por sus sabios consejos, su apoyo y su confianza en mí.

A MINCIENCIAS y la ANH por la beca doctoral otorgada en el marco de la convocatoria 721.

A la familia UNIPAZ, y en particular a la Escuela de Ingeniería de Producción, por la oportunidad laboral flexible y oportuna.

A mi madre, Luz Marina Rozo Camacho, por su voz de aliento, su ternura y sonrisa que siempre me mantuvieron firme ante las adversidades.

A mis amigos y familiares, en especial a Iván Mora, Javier Rozo y Luz Mery Rozo por haber sido un soporte en lo personal, académico y económico durante el desarrollo de mi tesis.

Al TEAM: Angélica Aguas, Máveris Castro y Miller Guzmán, por su compañía, sus chistes, sus consejos y por haber sido un polo a tierra para mí.

A Lessly Serrano e Isaac Matías Pérez, por haber sido la parte bonita del doctorado, por tantas alegrías y sueños cumplidos; por ser mi inspiración.

Content

	Page.
Introduction.....	13
1. A review of the catalyst synthesis from manganese-based waste.....	25
1.1 Availability and effects of natural and anthropogenic manganese	28
1.2 Waste processing to manganese recovery.....	34
1.2.1 Solid waste processing.....	35
1.2.1.1 Pyrometallurgical processing.....	35
1.2.1.2 Hydrometallurgical processing.	39
1.2.1.3 Bio-metallurgical processing.	49
1.2.2 Wastewater treatment to recovery manganese.....	52
1.3 Catalyst synthesis from Mn-based waste	57
1.4 Concluding remarks	68
1.5 Acknowledgment	69
2. Single step synthesis of MnO _x nanorods from spent batteries used for the combustion of methane	69
2.1 Materials and Methods.....	71
2.1.1 Materials	71
2.1.2 Methods.....	72
2.1.2.1 Cathode recovery from spent batteries.	72
2.1.2.2 Single step synthesis of nanorods.	73

2.1.2.3 Characterization tests	74
2.1.2.4 Catalytic evaluation.	77
2.1.2.5 Experimental specific reaction rate calculation.	79
2.1.2.6 Theoretic activity calculation of a mixture of crystalline phases.	79
2.1.2.7 Activity factor calculation of the individual crystalline phases in MnO _x -based materials.	80
2.2 Results and discussion	82
2.2.1 MnO _x -based nanorods.....	82
2.2.2 Chemistry of the synthesis.....	85
2.2.3 Catalytic performance	89
2.3 Conclusion	92
3. Influence of alumina and kaolinite on the mechanical strength and methane combustion activity of spent battery cathode-based pellets	94
3.1 Experimental.....	98
3.1.1 Pellets catalyst synthesis	98
3.1.2 Materials characterization.....	100
3.1.3 Catalytic tests	103
3.2 Results.....	105
3.2.1 Characterization of the raw material.....	105
3.2.2 Extrusion of the cathode powder	106
3.2.3 Mechanical performance of the pellets	110
3.2.4 Study of the catalytic activity	112
3.2.5 Relation between mechanical resistance, activity and stability of the pellets	116

3.3 Conclusion 118

4. General conclusions 119

References Bibliographical 121

Appendices 160

List of Figures

	Page.
Figure 1. Potential energy diagram for a catalyzed reaction	17
Figure 2. Possible mechanism for the catalytic oxidation of methane	18
Figure 3. Flowchart of stages to obtain value added products from Mn residue.....	34
Figure 4. Method to calculate the activity factors of the crystalline phases presented in MnO _x - based materials synthesized in this work	81
Figure 5. Physical and chemical properties of raw cathode and MnO ₂ -based nanorods (n-rods).	84
Figure 6. Physical and chemical properties of NaOH-washed cathode (NaOH-cathode) and MnO ₂ -based nanorods (n-rods).....	85
Figure 7. Scheme representing the physicochemical transformations at the cathode of spent alkaline batteries during the single step synthesis of nanorods.	89
Figure 8. Comparison between catalytic activity, and the oxygen reducibility and mobility.	92
Figure 9. Mechanical test to determine Fracture strength (A) and radial bed rigidity (B).	103
Figure 10. Morphologic and semiquantitative analysis of the pellets.	109
Figure 11. Specific surface area (A) and the percentage of surface blocking (B) on the pellets as a function of % wt. of additives and the alumina fraction.....	110
Figure 12. Mechanical analysis of the pellets.....	112

Figure 13. Specific reaction rate (R_{CH_4}) (A), theoretic thermal conductivity (k_{pellet}) (B), reaction rate monitoring through the reactions (C) of the pellets as a function of additives content and the alumina mass fraction. The dashed horizontal lines represent the value of raw pellets. 114

Figure 14. Comparison of the normalized reaction rate and fracture strength of the pellets (A), and the analysis of stability for a specific pellet formulation (B)..... 117

List f Table

	Page.
Table 1. General description of the types, functions and materials applied as additives in the manufacture of technical catalysts	22
Table 2. List of Mn-bearing minerals.	29
Table 3. Pyrometallurgical recovery of manganese-based residues.	38
Table 4. Hydrometallurgical recovery of Mn from residues.	43
Table 5. Byo-hydrometallurgical recovery of Mn from residues.	50
Table 6. Catalyst preparation and evaluation from Mn-based waste.....	58
Table 7. Extrudable pastes composition.	99

List of Appendixes

	Page.
Appendix A. Method for the highly accurate quantification of gas streams by on-line chromatography	160
Appendix B. A Method for the Accurate Quantification of Gas Streams by Online Mass Spectrometry	225
Appendix C. Supplementary information chapter 2	289

Resumen

Título: Formulación de catalizadores basados en el reciclaje del cátodo de baterías gastadas de Mn-Zn para la combustión de metano*.

Autor: Edwing Alexander Velasco Rozo**

Palabras Clave: Fuentes secundarias, lixiviación ácida, nanobarras de MnOx, pellets de MnOx, oxidación catalítica.

Descripción:

Como se demostró, las fuentes secundarias de manganeso como el cátodo de las baterías gastadas, podrían usarse para producir catalizadores basados en óxidos de manganeso activos en procesos de combustión catalítica de metano. En este sentido, convertimos el polvo de cátodo recuperado de las baterías alcalinas gastadas de Zn-Mn en nanobarras de MnOx reducibles y oxidantes en un solo paso basado en los procesos simultáneos de disolución del cátodo y cristalización de MnO_x. Entre las nanobarras sintetizadas, las basadas en ε-MnO₂ fueron catalíticamente tan eficientes en la combustión de metano como el polvo de γ-MnO₂ de referencia. Encontramos que esto último se debió a un equilibrio adecuado entre la reducibilidad, la concentración de oxígeno en la superficie y en la red, y el estado de oxidación promedio del manganeso. Por otro lado, reproducimos una formulación de catalizador a partir del cátodo recuperado, adaptable a un proceso industrial. Se sintetizaron pellets de tipo cilíndrico activos para la reducción de metano usando un proceso de síntesis circular y verde, mediante la extrusión de una pasta compuesta de agua y polvos de cátodo recuperado, caolinita y alúmina. La composición influyó tanto en las propiedades mecánicas como catalíticas de los pellets: la caolinita mejora la resistencia mecánica, pero afecta negativamente la actividad catalítica porque bloquea el acceso de los reactivos al interior del pellet; la alúmina, por el contrario, disminuye la resistencia mecánica y aumenta la actividad debido a que rompe la continuidad de la matriz de caolinita, aumentando la porosidad del pellet. En particular, por la contribución adicional de la alúmina a la conductividad térmica de los pellets, las formulaciones basadas en 20 % en peso del cátodo recuperado y 50 % en peso de alúmina fue la más activa, y térmica y mecánicamente estable.

* Tesis doctoral

** Facultad de Ingenierías Físicoquímicas. Escuela de Ingeniería Química. Doctorado en Ingeniería Química. Director: Prof. Víctor Baldovino Medrano. Codirector: Ph.D. Edgar Mauricio Morales Valencia.

Abstract

Title: Formulation of catalysts based on the upcycling of the cathode of spent Mn-Zn batteries for the combustion of methane*.

Author: Edwing Alexander Velasco Rozo**

Keywords: Secondary sources, acid leaching, MnO_x nanorods, MnO_x pellets, catalytic oxidation.

Description:

As demonstrated, secondary sources of manganese, such as the cathode of spent batteries, could be used to produce catalysts based on active manganese oxides in catalytic methane combustion processes. In this sense, we converted the cathode powder recovered from the spent Zn-Mn alkaline batteries into reducible and oxidant nanorod-like materials in a single step based on the simultaneous processes of dissolution of the cathode and MnO_x crystallization. Among the synthesized nanorods, those based on ε-MnO₂ were as catalytically efficient in the combustion of methane as a benchmark γ-MnO₂ powder. We found that the latter was due to an adequate balance between reducibility, surface and lattice oxygen concentration, and the average oxidation state of manganese. On the other hand, we reproduce a catalyst formulation based on the recovered cathode, adaptable to a catalytic industrial process. Cylindrical-like pellet catalysts active for methane abatement were synthesized based on a circular and green synthesis process. They were formed by extruding a paste composed of water and the powders of recovered cathode, kaolinite, and alumina. The composition influenced both mechanical and catalytic properties of the pellets: kaolinite improves the mechanical resistance, but it negatively affects the catalytic activity because it blocks the access of the reactants to the interior of the pellet; the alumina, on the other hand, decreases the mechanical resistance and increases the activity of the pellets due to disrupt the continuity of the kaolinite matrix, increasing the porosity of the pellet. In particular, by the additional contribution of the alumina to the pellet thermal conductivity, the formulations based on 20 % wt. of recovered cathode and 50 % wt. of alumina was the most active and thermally and mechanically stable.

* Ph.D. thesis

** Facultad de Ingenierías Físicoquímicas. Escuela de Ingeniería Química. Doctorado en Ingeniería Química. Director: Prof. Víctor Baldovino Medrano. Codirector: Ph.D. Edgar Mauricio Morales Valencia.

Introduction

Methane is considered one of the main responsible for inducing global warming; its potential as a greenhouse gas is approximately 21 times greater than that of carbon dioxide (Elvidge et al., 2018). Due to this, the progressive reduction of its emissions has been a priority in environmental matters worldwide for more than a decade. Among the sectors that generate the highest emissions into the atmosphere is the oil industry, which scores points in the indiscriminate release of methane, ethane, propane and butane with more than 175 billion cubic meters emitted in 2017 alone (Ismail & Umukoro, 2016; Soltanieh, Zohrabian, Gholipour, & Kalnay, 2016). Despite that currently most of the refineries and oil facilities around the world have flaring systems for the elimination of gaseous wastes, it has been shown that this methodology is inefficient, not only because the products of combustion and hydrocarbons that are not burned release soot, but also partially oxidized hydrocarbons, CO and NO_x are emitted (Soltanieh et al., 2016). Additionally, the flare is generated outdoors, and there is an important amount of energy released from the reaction which must be equivalent to the energy to activate the reagents plus heat losses, causing high temperatures to be reached around 1100 and 1400 °C, which represents a risk for operators and the ecosystem in general (Fawole, Cai, & Mackenzie, 2016).

Thermal incinerators are equipment that allow combustion processes to be carried out at temperatures between 650 and 1000 °C, lower than those of torch burning (Baynham, Randall, & Hancy, 2017). The key element of these systems is that the reaction is carried out in isolation, which allows heat losses to be considerably reduced. Due to the fact that the potential barrier of the reactants must be overcome for their activation, these systems are forced to preheat the reagents

to their autoignition temperature (approx. 650 °C for methane), which generates enormous energy consumption. This, added to the fact that, depending on the composition of the feed gas, there may be low conversions and the formation of CO, making thermal incineration a mere palliative to the need to efficiently eliminate methane.

Catalytic combustion is one of the most effective technologies for methane removal, which was born as an alternative to the aforementioned processes (J. Chen, Arandiyan, Gao, & Li, 2015). Although it is carried out in a similar way to thermal incineration, the use of catalysts allows the combustion reactions to follow a path of lower activation energy, which means that they can occur at temperatures below 500 °C, achieving conversions and selectivities to CO₂ close to 100% (Gancarczyk et al., 2018). An adequate choice of catalyst is essential for the performance of the process. It is known that not only the catalyst must have activity, selectivity and stability at low temperatures, but also it must have other characteristics such as: ideal geometry to adjust to reactors of up to tens of cubic meters, minimizing the limitations of mass and heat transfer; high mechanical strength to withstand pressure gradients inside the reactor; and a long shelf life (Sie & Krishna, 1998; Tomašić & Jović, 2006).

The main problem around the development of industrial catalysts is the cost of the active phase. At the beginning of the 90s it was established that the catalysts with the greatest potential for this process were based on monoliths of noble metals such as Pt, Pd and Rh (López, Gígola, Borio, & Bucalá, 2001), however, their high cost and rapid deactivation by coke prevented them from being used at an industrial level. Such drawbacks opened the door to the study of cheaper active phases based on transition metals. Manganese oxide, thanks to its unique redox properties, has exhibited excellent catalytic performance in the oxidation of CO, ethanol, propane, CH₄, and formaldehyde (Lamaita, Peluso, Sambeth, & Thomas, 2005); its catalytic properties are related to

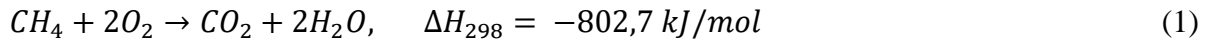
the variability of the oxidation state of the metal and the oxygen storage capacity in the crystal lattice (Xiuyun Wang et al., 2018).

An even more attractive feature of this material, even than its activity, is the possibility of obtaining it from toxic wastes such as spent batteries (Abid Charef, Affoune, Caballero, Cruz-Yusta, & Morales, 2017a). It has been reported that between 40 and 60% of the cathode mass of Zn-MnO₂ batteries corresponds to manganese oxides (Farzana et al., 2020). However, its easy access and its potential activity are not enough to glimpse the possibility of using it as a solution to the problems associated with methane emissions. For its implementation at an industrial level, it must become a technical catalyst, which means, to go from being a powder with particle sizes of the order of microns, to becoming a material of the order of millimeters or centimeters (Kreutzer, Kapteijn, & Moulijn, 2006).

Methane combustion

Methane is a tetrahedral molecule with four equivalent C–H bonds. Its electronic structure is described by four bonding molecular orbitals resulting from overlapping valence orbitals at C and H. Like other hydrocarbons, methane is a very weak acid (pK_a ~ 56). The main chemical reactions of methane are combustion, synthesis gas steam reforming, and halogenation. As for combustion, to start it requires energy to force di-oxygen into a spin-paired state, or singlet oxygen, which is extremely reactive (Y. Wang, Liu, Cao, Wang, & Che, 2011). The process continues with the extraction of the hydrogen atom from the fuel to oxygen to give a hydroperoxide radical (HOO•), which reacts forming a hydroperoxide, which breaks down to obtain hydroxyl radicals (Dunlop & Tully, 1993). Oxidizing species involved in the process include singlet oxygen, hydroxyl radical, monatomic oxygen, and the hydroperoxyl radical (Sotudeh-Gharebagh & Chaouki, 2008). Such intermediates are short-lived and cannot be isolated, however, non-radical

intermediates are stable and are produced on incomplete combustion. An example is the formation of carbon monoxide, which is of special importance due to its toxicity, however, it is economically useful for the production of synthesis gas. Equations 1 and 2 show the complete and incomplete combustion reactions of methane, respectively.



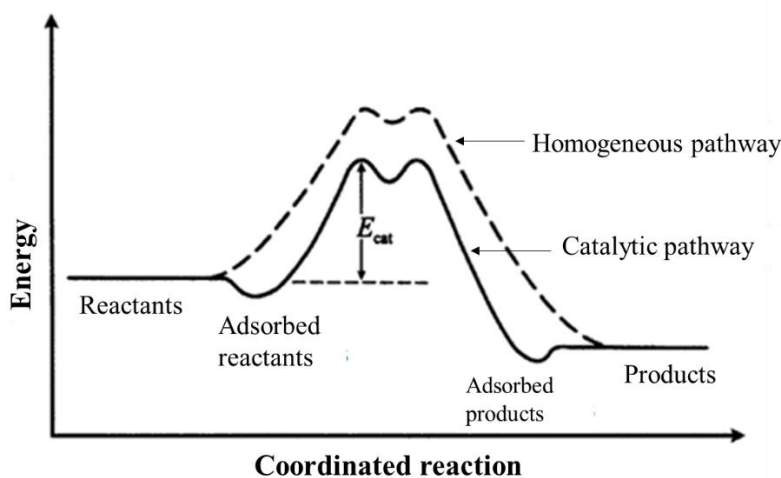
Since the energy to activate the reactants is supplied as heat and the reaction produces heat, as long as methane and oxygen are supplied, the reaction is self-perpetuating. Combustion in the gas phase can only occur with given flammability limits, reaching temperatures close to 1400 °C. At these temperatures, when there is an excess of oxygen, the oxidation of nitrogen is thermodynamically favored (in cases in which combustion occurs in the presence of air) giving rise to the formation of NO_x, recognized for its high toxicity (Elvidge et al., 2018).

Catalytic combustion of methane

Catalytic combustion involves the use of a solid catalyst (L. He, Fan, Bellettre, Yue, & Luo, 2020). The role of the catalyst is to provide an alternative reaction pathway between the reactants and products that require a lower activation energy, as shown in Fig. 1. In the catalytic process, the reactants (methane and oxygen) initially have a certain amount of energy, however, when adsorbed on the surface of the catalyst, they move slightly to a state of lower energy because the adsorption is usually exothermic, which causes it to lose energy. Subsequently, the reactants must overcome the activation energy and form an adsorbed complex. The adsorbed intermediates can then react to form the adsorbed products, which are then desorbed into the gas phase as products (H. Xu et al., 2017). Fig. 1 shows that the homogeneous pathway (in the gas phase) has a higher energy barrier than the catalytic pathway.

Figure 1.

Potential energy diagram for a catalyzed reaction

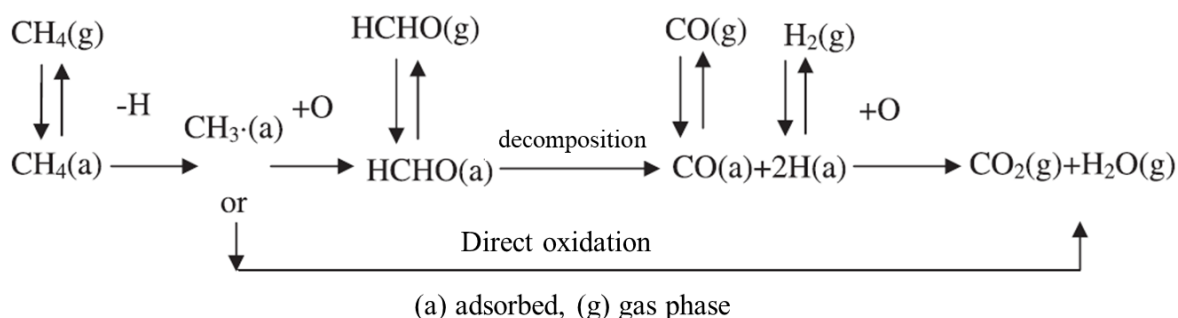


Note: Adapted from Hayes, (1997)

A possible mechanism for the catalytic oxidation of methane is presented in Fig. 2. It is observed that the CH_4 , after its adsorption and activation (dehydrogenation), gives way to the formation of the adsorbed complexes CH_3^* and O , which react to produce a new adsorbed intermediate species HCHO , which decomposes to produce adsorbed CO ; the latter reacts with H on the surface and produces CO_2 which is desorbed and passes into the gas phase. An alternate route of direct oxidation prevents the formation of HCHO and CO (J. Chen et al., 2015).

Figure 2.

Possible mechanism for the catalytic oxidation of methane



Note: Adapted from Chen et al. (J. Chen et al., 2015)

Catalysts for combustion based on noble metals

The development of catalysts based on noble metals such as Pd, Pt, Ru and Au, among others, has been widely documented in the literature (Okal, Zawadzki, & Baranowska, 2016; Todorova, Stefanov, Naydenov, & Kolev, 2014). Among them, the most attractive catalysts for methane combustion are based on Pd (L. He, Fan, Luo, Bellettre, & Yue, 2020). Although there are still some differences in the literature about which is its most active state, metallic Pd, PdO or a mixed PdO/PdO_x phase, a majority lean towards PdO as the most active phase for oxidation. It is known that this phase decomposes into metallic Pd in the range 650-850 °C, depending on the partial pressure of O₂ and the composition of the reactive gas mixture. Among the negative aspects, in addition to the cost and its high rate of poisoning, especially with chlorinated and sulfur compounds, it has been reported that the transformation of PdO into Pd negatively affects the catalytic reaction by reducing the conversion (Qi et al., 2016). However, these catalysts are easily regenerated after reoxidation of Pd to PdO. The development of Pd catalysts supported on γ -Al₂O₃ have also shown high activity and have managed to correct the stability drawbacks of bulk catalysts

(L. He, Fan, Luo, et al., 2020). Pt-based catalysts, despite having lower catalytic activity, are more resistant to poisoning compared to Pd-based materials.

Catalysts for combustion based on non-noble metals

Non-noble metal oxides have an important application in catalytic oxidation, and this is mainly because metals, particularly transition elements, have multiple valence states and can easily form a redox cycle between the high and low states oxidation, and at the same time, the oxygen network can be released and restored (C. He et al., 2019). Compared with noble metal-based catalysts, these oxides have abundant raw materials which are much cheaper (Sihaib et al., 2017).

Active manganese oxides for methane combustion. The Mn-O system is composed of different crystalline phases such as Pyrolusite (MnO_2), β -Bixbyite ($\beta\text{-Mn}_2\text{O}_3$), α -Hausmanite ($\alpha\text{-Mn}_3\text{O}_4$), β -Hausmanite ($\beta\text{-Mn}_3\text{O}_4$), Manganosite (Mn_{1-x}O), Mn_5O_8 , α -Mn (Mn), β -Mn (Mn), γ -Mn (Mn), and δ -Mn (Mn), which can be obtained by modifying the variables of the thermal treatment of their precursor salts (Post, 1999; Reidies, 2000). It is possible to synthesize several phases at the same temperature, which allows obtaining multivalent manganese oxides. Most of these manganese oxide phases consist of tunnel structures built from MnO_6 octahedrons (Reidies, 2000; C. Zhou et al., 2018).

Other characteristics of the Mn-O system are the variability of the oxidation state of Mn (going from Mn^{2+} to Mn^{3+} or from Mn^{3+} to Mn^{4+} , depending on the phase), and the oxygen storage capacity in the crystal lattice due to the "oxygen mobility", represented by the following equation:



Where the symbol \square represents an oxygen vacancy.

Mn oxides have been shown to be active in the oxidation of volatile organic compounds such as propylene, ethylene and toluene, among others, and methane. Its activity has been

attributed mainly to its unique redox properties as a consequence of the easy oxidation state transition, and the availability of oxygen from the oxide crystal lattice. It is also considered that the oxygen network of MnO_x catalysts is responsible for activating C–H bonds in hydrocarbons, especially when the reaction temperature is higher than 400 °C. One of the main disadvantages of this material is that, at temperatures above 700 °C, its activity drops dramatically due to sintering (J. Chen et al., 2015).

Recovery of Mn oxides from spent batteries

The high consumption of primary Zn-Mn batteries is due to their reliability, safety, and low cost, among other reasons. They are used in many daily applications, to the point that more than 300,000 tons of zinc batteries are sold each year; an average of six units per person (Melchor-Martínez et al., 2021). Despite the wide variety of Zn-Mn batteries on the market, more than 80% of all batteries sold are alkaline. Different chemical species are needed for its manufacture, which include Zn and MnO₂ as active electrochemical materials, KOH as electrolyte, polymers as separators, carbon as additive conductor, and stainless steel for the case. The widespread use of these products has led to a rapid increase in the accumulation of spent batteries, the disposal of which requires methods that are consistent with sustainable development. In this sense, strong regulations have been generated against conventional methods such as waste disposal or incineration. The latter has generated controversy because it causes the predictable release of heavy metals and toxic organic compounds into the atmosphere.

Recycling and further reuse of spent battery materials is perhaps the most successful option for mitigating environmental problems arising from poor disposal (P. Liu, 2018). The main metals in zinc-carbon and alkaline batteries are manganese and zinc (Abid Charef et al., 2017a). These valuable metals can be recovered for reuse either as raw materials in battery production, or for

other purposes. Several methods to recover metal from batteries are described in the literature, but industrial routes generally employ pyrometallurgical or hydrometallurgical processes. Although pyrometallurgical processes are more commonly used, hydrometallurgical processes are gaining relevance due to their lower environmental footprint, lower cost, and ability to treat even low-zinc materials on a small scale. It has been shown that the battery cathode contains Mn, Zn, C, K, Cl, Fe, which can be physically treated until a mixture of Mn, Zn and C is obtained. It is known that Zn can be removed from this mixture by basic treatments and that the phase of the resulting Mn can be modulated by chemical treatments either by dilution or precipitation and thermal treatment (Dwivedi, Randhawa, Saroj, & Jana, 2017).

Shaping of catalysts

An essential task in manufacturing catalysts at an industrial level is a unit operation known as "forming" (Kreutzer et al., 2006). In this, different powders composed of active phases (laboratory-scale catalysts) are structured using a specific method in macroscopic bodies, giving rise to something known as the technical catalyst (Mohammadzadeh & Zamaniyan, 2002). Most of the industrial shaping methods, be it spray drying, granulation or extrusion, among others, rely on powder agglomeration (Sie & Krishna, 1998). Powders can be agglomerated dry (granulation), or in the presence of a liquid (usually water) to allow processing as pastes (extrusion and wet granulation) or as slurries (spray drying) (Mitchell, Michels, & Pérez-Ramírez, 2013). The quality of the resulting technical body depends on the uniform densification of the components, which is strongly influenced by the attributes of the particles (i.e. size and morphology, surface chemistry and bulk density), the rheological behavior of the feed and the action of additive phases (Christensen, 2007). Three elements are common to all structuring processes: (i) the powdered raw materials must be mixed initially until they form a homogeneous medium, (ii) the premixes must

be agglomerated into bodies with the required shape, and (iii) the shaped bodies they must be hardened to meet the mechanical demands. Table 1 presents a summary of the recommended additives according to the forming operation.

Table 1.

General description of the types, functions and materials applied as additives in the manufacture of technical catalysts

Additive	Function	Applicable Materials	Examples
Binder	Increases mechanical resistance	Inorganic oxides with refractory properties	Alumina, aluminum phosphate, silica, silica-alumina, natural clays, titania and zirconia
Filler species	Dilute the active phase to optimize the content of the coating staff	Low cost inorganic oxides	Natural clays and alumina
Lubricant	Reduces friction during mixing and forming operations	Oil or other viscous liquid	Ethylene glycol, glycerin, graphite, mineral oil, propylene glycol, and aluminum stearate
Modifier	Improves technical catalyst performance	Promoters, co-catalysts, metal or coke traps, passivators	Precursors of metals or metal oxides, clays, zeolites
Peptizing	Disperses particles to improve feed homogeneity before or during shaping	Organic or inorganic acids or some bases	Acetic, citric, formic, hydrochloric, nitric or sulfuric and phosphoric acids
Plasticizer	Lowers the viscosity of feed mixes for easier processing	Polar and non-polar material	Hydroxyethylcellulose, polyethylene glycol, starch, sugars and water
Porogen	Increases intraparticle porosity in the technical body	Any material of defined shape that can be removed by thermal decomposition	Coal, sawdust, flours of different sizes

Note: Adapted from Mitchell et al. (Mitchell et al., 2013).

Scope of the thesis

As far as is known, secondary sources of manganese such as the cathode of spent batteries, in an ideal scenario, could be used for the production of catalysts based on active manganese oxides in catalytic methane combustion processes. Eventually, the implementation of a strategy of this nature would have a sustainable and circular approach since a waste is recovered, but it is also part of the solution of an environmental problem that scales globally. However, to make this alternative technically feasible, several questions associated with the first level in the development of a catalytic process at an industrial level must first be answered, and that has to do with the design of the catalyst: i) What is the method and most promising conditions for obtaining an active phase in catalytic methane combustion processes, starting from a manganese-based residue? ii) What is the effect of the chemical modification of the active phase obtained from manganese residues, in terms of improving catalytic performance, determining the factors that influence the modification of its activity as a basis for the design of active phases from waste?, iii) Understanding that industrial catalysts must meet certain requirements of geometry and mechanical resistance, What is the influence of the conformation of the active phase on the mechanical properties, and how do they influence the catalytic performance?

To answer the first question, in chapter 1 an in-depth analysis of the manganese recovery processes from waste is carried out, clarifying which of them have advantages for obtaining active phases. Likewise, a compendium of the conditions reported in the literature is made, for the preparation of catalysts from residues, discriminating the type of residues, the type of manganese recovery treatment and obtaining the active phase, the conditions and performance in the catalytic evaluation. With this analysis of the literature, it is possible to clarify which is the most promising residue, as well as the method and adequate conditions for obtaining an active phase for

combustion processes. Consecutively, based on this information, to answer the second question, a method for refining a residue based on manganese was formulated and explained in chapter 2, which allows increasing the catalytic performance thanks to the modification of the morphology and chemical structure of the species present in the waste leading to the enhancement of its oxidizing capacity. Thanks to a systematic analysis of the physicochemical and catalytic properties of the synthesized active phases, this chapter also establishes the main causes of the improvement in catalytic activity. Finally, answering the third question, in chapter 3 a method of shaping one of the active phases studied in chapter 2 is proposed, and the effects of the formulation of the pellets (shaped materials) on the mechanical and catalytic properties are analyzed. From the analysis of these properties, it is shown under which conditions the improvement of the mechanical properties influences the catalytic activity.

At an experimental level, this work addressed an additional challenge associated with catalytic processes in the gas phase, and it has to do with the certainty in the quantification of methane combustion reactions used to tested the catalytic activity of the materials synthesized. Therefore, two high-precision quantification methods were developed, one for a catalytic system coupled online to gas chromatography and the other for a system coupled to mass spectrometry. Thanks to the development of these methods, presented in annexes 1 and 2, it was possible to establish conversions of the reactants (CH_4 and O_2) with a margin of error of less than 1%, verified with closures in the carbon balances, which allowed to generate more relevant information about the catalytic activity of the formulated materials.

1. A review of the catalyst synthesis from manganese-based waste

Manganese is found in everyday human life as part of various products, whether for ferrous applications such as ferroalloys or steel, or non-ferrous applications such as batteries, fertilizers, animal feed, and brick dye (Malcolm, Wood, & Kingdom, 2004; Reidies, 2000). Throughout history, its enormous availability has made it one of the metals with substantial exploitation and interest at an industrial level (Kloprogge, Ponce, & Loomis, 2020). Currently, there are two challenges associated with the chain of exploitation and use of this metal: i) the search for alternative sources of Mn because of the depletion of high-grade Mn ore reserves (Toro, Jeldres, Órdenes, Robles, & Navarra, 2020), and ii) the development of waste management programs since both the extraction and the final disposal of Mn-based products have caused the spread of this metal in soil, air and water in a range of concentrations that are as high to be harmful to humans, flora and fauna, but so low that recovery processes are technically and economically unfeasible (Das, Ghosh, Mohanty, & Sukla, 2014a; Shu et al., 2020; Shu, Liu, Liu, Chen, & Tao, 2016a). Given these circumstances, it is necessary to implement immediate measures to mitigate the effects on the environment and human beings of the cycle of use of Mn-based materials. Consistent with the principles of environmentally sustainable management, recycling is currently the most attractive alternative to mitigate these negative aspects (Hagelstein, 2009). The Mn recycling products are prioritized within high waste generation fields (metallurgical and batteries). In the metallurgical area, the reuse of scrap as a substrate for alloys has been documented (Hagelstein, 2009), while the Mn extracted from electronic waste is not mainly reused to obtain electronic products, but rather has various applications (İşıldar, Rene, van Hullebusch, & Lens, 2018).

Despite this obvious bias towards this type of waste, other types, such as pyrometallurgical sludge, sludge from water treatment, wastewater from mining processing, or during electrolytic processes, are also part of the research focused on Mn recycling (B. S. Kim, Lee, Jeong, Lee, & Kim, 2010; Kularatne, Kasturiarachchi, Manatunge, & Wijeyekoon, 2009; Mocellin et al., 2017; Peng, Pan, Liu, Yang, & Wang, 2018).

In general, recycling has three stages: i) collection/processing, ii) manufacturing and iii) marketing of new products made from recycled materials (US EPA, 2021). Specifically, the first stage in the manganese-based waste recycling has two purposes: to increase the purity of Mn in the waste by dissolution or evaporation of other pollutants and the separation of the manganese from the waste (generally by its dissolution) and subsequent recovery in a high purity metal, oxide or salt. Both of these can be achieved by a varied set of metallurgical methods. Within the recent scientific publications, there is a considerable number of reviews that address various aspects of said waste treatments. Dwivedi et al. (Dwivedi et al., 2017) summarized the different hydrometallurgical and pyrometallurgical routes reported for Mn recovery. Zhan et al. (W. Zhang & Cheng, 2007a, 2007b, 2007c) studied multiple Mn extraction and recovery metallurgical methods. Although these authors studied the technique without evaluating the influence of the Mn source, the reported information is applicable to waste treatment. Ghosh et al. (Ghosh, Mohanty, Akcil, Sukla, & Das, 2016) reviewed the recycling processes by bioleaching methods. Bal et al. (Mohanty, Ghosh, Bal, & Das, 2018) reviewed the literature associated with manganese recovery by metallurgical methods. Mohanty et al. (Mohanty et al., 2018) also conducted a study of biotechnological processes for Mn recovery. Canda et al. (Canda, Heput, & Ardelean, 2016) analyzed the different ways to recover heavy metals from industrial waste, including Mn in their list. The control of the conditions of each process and the type of waste play an essential role in

the quantity and purity of recovered species (Dwivedi et al., 2017). Naturally, the choice of the former must be combined with the desired physicochemical properties of the metal or its species.

The second stage of manganese-based waste recycling concerns value-added product manufacturing (Zimmerman, Anastas, Erythropel, & Leitner, 2020). In this sense, the applications development scientifically at the lab scale is classified into five groups: cement and related materials, ceramics for construction, bricks, road materials, and adsorbent materials (Du, Zhou, & Duan, 2014; Kumar, García-Triñanes, Teixeira-Pinto, & Bao, 2013; M. Li, Hu, et al., 2021; Wu, Li, Zhong, & Wang, 2016). In the first four groups, Mn is implemented as a filler, with thermal and chemical stability and mechanical strength being the properties of interest for the synthesized compounds. Regarding the adsorbents, the surface area and the type of surface species of Mn are included as final properties of the material. He et al. (S. He, Jiang, Hong, & Liu, 2021) performed a systematic review of the different works published on obtaining products in these five categories for a particular type of waste. An emerging group of value-added products from manganese-based residues are the manganese oxides-based catalysts. Manganese oxidant properties play an important role on catalytic applications, such as: chemical looping gasification, reduction of nitric oxide, esterification of acetic acid, oxygen evolution reaction, azo dyes degradation, and volatile organic compounds abatement (Cano, Mackey, & McGlacken, 2018; Lyu et al., 2020a). The fact that extracting these oxides from residues has attracted the attention of scientists around the world. In this case, the control of properties of manganese oxides recycled such as thermal, mechanical, and chemical resistance, surface and morphological properties, and surface composition in terms of concentration and nature of Mn species is desirable (Pulleri et al., 2021; Wei, Ni, Li, & Zhao, 2017). However, unlike the other groups of value-added products, there are no reviews in the literature on obtaining catalysts from manganese-based residues. Understanding that the opening

of a discussion about the technical feasibility of the production of catalysts from manganese residues is essential to stimulate the development of sustainable processes that have an impact on the reduction of pollution associated with the uncontrolled releasing of manganese o the environment, the objective of this work is to carry out a systematic review of the literature, clarifying the vast amount of waste that can potentially be reused, the processes for this purpose, and what are the routes proposed for obtaining catalysts, highlighting their effect on the physicochemical and mechanical properties and their catalytic activity. Likewise, it seeks to propose various routes that lead to a set of special characteristics in the materials. Not every route that allows the maximum extraction of Mn guarantees that the catalyst is active. There are deeper aspects that have a greater influence on activity than simply the quantity and purity of the metal used. This review focuses on establishing currently what are the processes and residues used to prepare catalysts, leaving comparisons that allow visualizing the most important aspects to control in the synthesis of a catalyst depending on the type of waste. In addition to showing the current panorama for the use of waste that is not currently used.

1.1 Availability and effects of natural and anthropogenic manganese

Manganese is a silver-gray transition metal like iron. It is hard, brittle, and difficult to fuse. It has 25 electrons arranged in an $[\text{Ar}] 3d^5 4s^2$ electron configuration. All the 7 electrons of the sublevels 4s and 3d can participate in chemical reactions, indeed, in manganese-based compounds, it can have oxidation states of up to 7+ (R.D.W. Kemmitt and R.D. Peacock, 1973). The complete range of oxidation states of manganese goes from -3 to +7, however, in the environment only compounds with Mn^{2+} , Mn^{3+} , and Mn^{4+} naturally originated (Kloprogge et al., 2020). In terms of

the stability of Mn ions in an aqueous solution, Mn^{2+} is the only species that can form a free ion. Mn^{3+} is only stable if it is forming complexes; it tends to deprotonate in states 2+ and 4+. The manganese species Mn^{4+} and Mn^{5+} are not stable in neutral solutions. The Mn^{7+} is only stable forming the permanganate ion (MnO_4^-) (Das, Sukla, Pradhan, & Nayak, 2011). The reactivity of manganese is similar to iron; it oxidizes superficially in air and forms rust in moist air. It also burns in air or oxygen at elevated temperatures to give manganese (2+ and 3+) oxide (Mn_3O_4 or $MnOMn_2O_3$). Although the elemental form of Mn does not exist naturally in the environment, this metal makes up at least 100 minerals (Malcolm et al., 2004; Maynard, 2010). Of these, the most common forms are oxides, carbonates, silicates, and sulfates (Post, 1999). Table 1 shows some of the most important manganese minerals, related to their empirical formula, approximated Mn composition, and its occurrence.

Table 2.

List of Mn-bearing minerals.

Mineral	Empirical Formula	Mn composition	Occurrence
Alabandite a,b	$Mn^{2+}S$	Mn= 57.09- 63.15 %	May be in large quantities in epithermal polymetallic sulfide vein and especially in low-temperature manganese deposits.
Bementite a,b	$(Mn^{2+})_5Si_4O_{10}(OH)_6$	MnO_2 = 39.22- 54.64 %	Layered parallel to the walls of secondary veins of calcite in a metamorphosed stratiform zinc orebody
Braunite a,c	$Mn^{+2}(Mn^{+3})_6SiO_{12}$	Mn= 66.6 %	Occurs by metamorphism of manganese silicates and manganese oxides
Cryptomelan e a,b	$K_{1-1.5}(Mn^{+4}, Mn^{+3})_8O_{16}$	MnO_2 = 83-87 % MnO= 2-2.5 %	Widespread in oxidized manganese deposits as open-space fillings or replacing primary manganese-

Mineral	Empirical Formula	Mn composition	Occurrence
			bearing minerals; commonly replaced by other secondary manganese minerals
Franklinite a,b	$(\text{Fe}^{+2}, \text{Zn}, \text{Mn}^{+2}) (\text{Fe}^{+3}, \text{Mn}^{+3})_2\text{O}_4$	MnO=6.6-9.96 %	In beds and veins formed by high-temperature metamorphism of Fe, Zn, Mn-rich marine carbonate sediments. As a minor mineral in some manganese and iron deposits.
Hausmannite e a,b	$\text{Mn}^{2+}(\text{Mn}^{3+})_2 \text{O}_4$	MnO=91.38-93.01 %	A primary mineral in hydrothermal veins. Also produced by metamorphism of manganiferous rocks
Kutnohorite a,b	$\text{Ca} (\text{Mn}^{2+}, \text{Mg}, \text{Fe}^{2+}) (\text{CO}_3)_2$	MnO= 23.76-32.99 %	Typically, in deposits associated with manganiferous sediments.
Manganite a,b	$\text{Mn}^{3+}\text{O}(\text{OH})$	MnO= 79.55-80.66 %	Formed in low-temperature hydrothermal or hot-spring manganese deposits; replacing other manganese minerals in sedimentary deposits; a component in some clay deposits and laterites.
Romanechite a,b	$(\text{Ba}, \text{H}_2\text{O})_2(\text{Mn}^{4+}, \text{Mn}^{3+})_5\text{O}_{10}$	MnO ₂ = 66.62-66.87 % MnO= 7.09-8.23 %	A product of weathering of manganese-bearing oxides, carbonates, silicates; in sedimentary deposits; as replacement deposits in limestones and dolostones; a principal component of "psilomelane" and "desert varnish" (manganese oxide-rich coatings formed on rocks in arid regions); in some plume agates
Pyrolusite a,b	Mn^{4+}O_2	MnO ₂ =98.72 %	Formed under highly oxidizing conditions in manganese-bearing hydrothermal deposits and rocks; in bogs and lakes, under shallow marine conditions; commonly an alteration product of manganite.
Rhodochrosite a,b	$\text{Mn}^{2+}\text{CO}_3$	MnO= 60.87-61.71 %	A primary mineral in low- to moderate-temperature

Mineral	Empirical Formula	Mn composition	Occurrence
			hydrothermal veins; in metamorphic deposits; common in carbonatites; authigenic and secondary in sediments; uncommon in granite pegmatites.
Rhodonite a,b	(Mn ²⁺ ; Fe ²⁺ ; Mg; Ca)SiO ₃	MnO= 50.54 %	In manganese-bearing deposits formed by hydrothermal, contact and regional metamorphic, and sedimentary processes.

Note: ^aWebMineral database (<http://webmineral.com/>), ^bHandbook of Mineralogy (Anthony, Bideaux, Bladh, & Nichols, 2006), ^cDwivedi et al. (Dwivedi et al., 2017)

The abundance of manganese is one of the pluses of this metal since it constitutes 0.1% of the earth's crust representing the twelfth more abundant element. It is distributed principally in South Africa and Ukraine with 74 % and 10 %, respectively, and a minor proportion in Australia, India, China, Gabon, and Brazil (Survey, 2020). The pyrolusite and Rhodochrosite sedimentary deposits are the major sources of Mn for commercial use (Reidies, 2000). In 2020 the mineral production of Mn was 18,500,000 tons. An alternative source of Mn is the sea nodules or ferromanganese concretions which contain approximately 30–36 % Mn and are mostly found in the Pacific Ocean, along with the Atlantic Ocean (Dwivedi et al., 2017; Ghosh et al., 2016). Industrially, manganese has several metallurgical applications such as the manufacture of steel and ferro-alloys, specifically, in the desulfurization and reinforcement of steel and cast iron, to improve their strength, toughness, hardness, and workability. Likewise, non-metallurgical applications include the production of batteries, fertilizers, animal feed, ceramics, glass, and pigments, among other chemical applications (Reidies, 2000). Globally, the annual consumption of manganese is above 1,500,000 metric tons, and it has an increasing trend; about 90% of manganese is used in

metallurgical applications while the remaining 10% is used in non-metallurgical applications (U.S. Geological Survey, 2021). The production of metallic manganese, used for metallurgical applications, begins with the reduction of MnO_2 to MnO through thermal treatment at 700–900 °C, followed by acid leaching (frequently made with H_2SO_4) until obtaining the Mn^{2+} ion, which is recovered by diaphragm electrolysis in presence of SO_2 or SeO_2 as an antioxidant (Lu, Dreisinger, & Glück, 2014). Before the electrolytic process, impurities (such as Fe, Pb, Ni, and Co) can be precipitated by the addition of MnO or H_2S . In cases where the starting mineral is a carbonate, the reduction step is not required. On the other hand, the production of manganese dioxide, used in non-metallurgical applications, can be carried out by two routes: one mediated by electrodeposition to obtain electrolytic manganese dioxide (EMD) and other strictly chemical to obtain chemical manganese dioxide (CMD) (Fu, He, Wang, Liang, & Guo, 2010). The EMD, mostly $\epsilon\text{-MnO}_2$, is obtained by a route analogous to the production of metallic manganese, including the stages of reduction, leaching, purification, and electrodeposition by anodic oxidation of MnSO_4 solution with inert electrodes. The CMD, mainly $\gamma\text{-MnO}_2$, is obtained through the stages of reduction, leaching until obtaining the Mn^{2+} ion, removal of metallic impurities by neutralizing the leaching agent, precipitation of Mn in the form of salt (preferably carbonates), and finally, calcination of manganese salt in an air atmosphere (W. Zhang & Cheng, 2007a).

One of the main drawbacks of the extraction processes and the manufacturing of manganese-based products is the unsustainable generation of waste (Blight, 2011). Due to the excessive use at an industrial level and the natural discharge of manganese to the environment by the weathering of rocks and sediments rich in manganese, Mn has been classified as an emerging pollutant (Das, Ghosh, Mohanty, & Sukla, 2014b). Among the main solid and liquid waste generated throughout the manganese use cycle, the most important are solid waste and wastewater

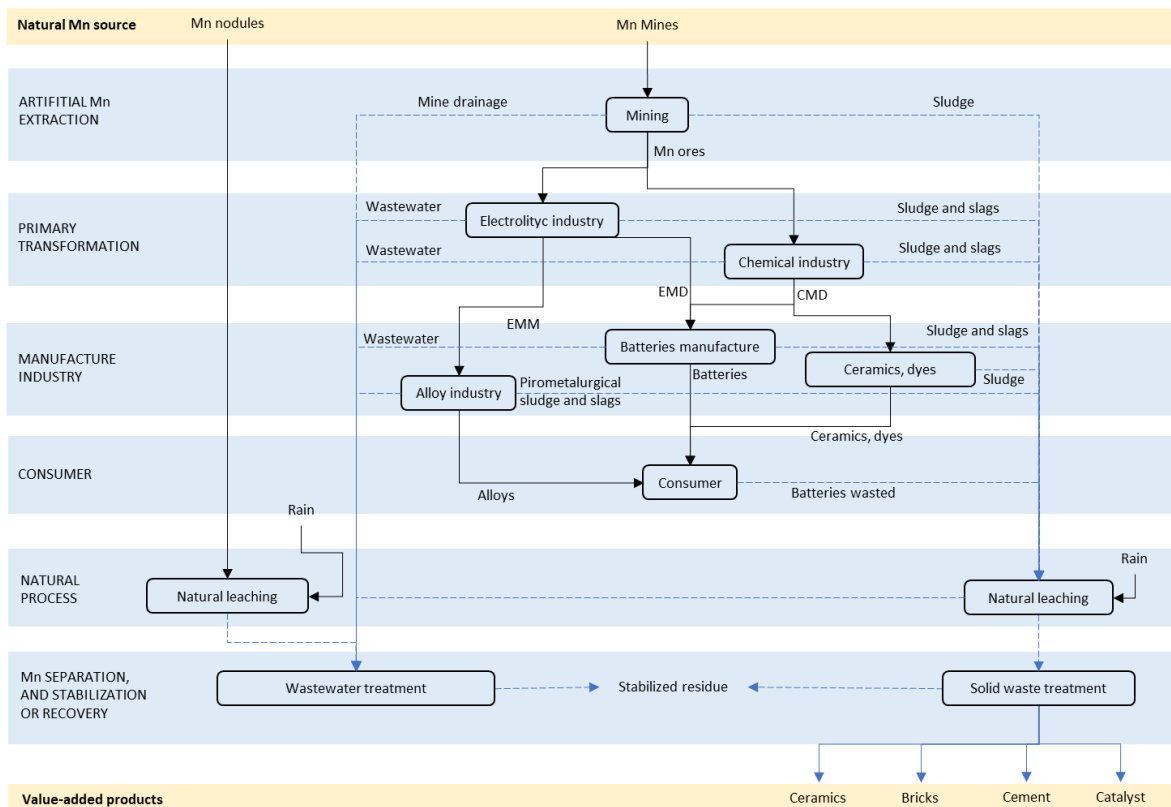
from the metallurgical industry, which are between 10-12 tons of electrolytic manganese waste (EMR) (Duan, Fan, Changbo, Chunlei, & Hongbing, 2010) and 4.5 tons of wastewater per ton of EMM, respectively; the drains from the mining activity, which present a variable composition that usually includes the primary phases of the non-leached minerals, leaving a manganese concentration in the range of 9 to 352 mg/L (Larsen & Mann, 2005); and waste from the battery industry (Bernardes, Espinosa, & Tenório, 2004). In this last segment, spent batteries are included as waste since they present a high turnover due to their relatively short useful life (3 months). In particular, EMD use in alkaline batteries exceeded 230,000 tons per year, while more than 160,000 tons of spent batteries are released into the environment each year. Air pollutants include industrial emissions (such as the production of ferroalloys and iron and steel smelters, power plants and coke ovens), and the combustion of fossil fuels. Global emissions of Mn are estimated to exceed 70,000 tons per year by far (S. He, Jiang, et al., 2021).

Among the main effects of the exaggerated release of manganese wastes by land, water, and air, are the impact to the ecosystem and the health effects. The inadequate management of metallic effluents results in the mobilization of heavy metals to the surrounding environment, contaminating the soil, surface and underground water bodies and the air (Herndon & Brantley, 2011). Under aquatic conditions, Mn is absorbed and spread to different particles in the form of sediment. Extreme Mn exposure in aquatic systems affects animals' invertebrate immune system and neuromuscular transmission. In the soil, high amounts of Mn are dangerous for the vegetation due to the alteration of the chemical properties. Among the effects for human health, it causes abnormalities in psychiatric condition, movement disorders and decreases cognitive capacity such as Parkinson's disorder, it is also associated with the appearance of ataxia, weak tendons and ligaments, loss of appetite and other neurological disorders. After entering the Mn through the

digestive or respiratory tract, it is absorbed by the bloodstream until it reaches the cells of the human body (Takeda, 2003).

Figure 3.

Flowchart of stages to obtain value added products from Mn residue.



1.2 Waste processing to manganese recovery

As previously commented, the processing of manganese-based residues to form and/or concentrate the manganese oxides must be the first stage in circular catalyst production. Two types of residues potentially can work as a source of manganese oxides, the solids residues and the wastewater characterized in Fig. 1. Following, a detailed review of these residues and the

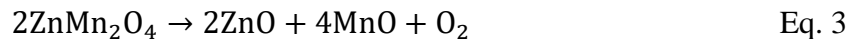
treatments reported to recover manganese oxides or manganese species that can easily be transformed into manganese oxides, will be present.

1.2.1 Solid waste processing

Solid waste is the most important source of manganese, and the concentrations of this metal can achieve 45 % wt., e.g., Zn-C spent batteries (Sayilgan et al., 2009). It is known that the slags or sludges from alloys and MnO₂ manufacturing industry, and the recycled cathode from spent batteries, are the most residues processed for manganese recovery reported in the literature. There are two principal purposes in the treatment of these residues: i) the increase in the manganese concentration in the residue by the removal of the other compounds present, and ii) the separation of manganese from the residue as metal, salt, and oxide. To achieve these purposes, a variety of processes have been reported, which can be classified into thermal, leaching, and bioleaching treatments.

1.2.1.1 Pyrometallurgical processing. Pyrometallurgical methods are the most widely used in industry due to their simple operating conditions. They are based on the volatilization and condensation of different species of interest present in the residue by heating in an oven under an inert atmosphere. The use of that method for the spent battery cathode recycling is reported in the literature, which is focused on the selective removal of Zn species to increase the content of Mn (Belardi, Lavecchia, Medici, & Piga, 2012). The volatilization of metallic Zn occurs at temperatures close to 907 °C. Around 950 °C, the ZnO present in the residue is reduced through carbothermic reactions (Eq. 1 and Eq. 2) obtaining metallic Zn, which is separated by evaporation

(Ebin, Petranikova, Steenari, & Ekberg, 2019). In this case, the hetaerolite phase (ZnMn_2O_4) decomposes carbothermally between 1000 and 1200 °C (Eq. 3 to 5) to obtain MnO, Mn_3O_4 , and ZnO. At this temperature, ZnO decomposes into Zn vapor, which allows its separation. Under the conditions mentioned, carbothermic reactions are viable thanks to the presence of C in the spent battery waste. A recovery between 75 and 85% of the Zn contained in the cathode of spent batteries with a purity of 99% under an N_2 atmosphere at 1000 °C can be achieved, using residence times of 10 and 30 min, respectively (Ippolito, Belardi, Medici, & Piga, 2016). Like the thermal processing of the spent battery cathode, the electrolytic manganese residue (S. He, Wilson, Lundström, & Liu, 2021), manganese dust (B. S. Kim et al., 2010), and iron-bearing manganese residues (Peng et al., 2018), has been thermally processed to separate impurities as Zn, or promote the formation of a specific manganese crystalline phase as Mn_3O_4 or MnO. In these cases, the volatilization of Zn or ZnO was conducted by carbothermal reactions in an inert atmosphere, and the manganese phase transformation was carried out by roasting in airflow. A detailed review of thermal treatment methods and their conditions for different types of manganese-based waste is presented in Table 2.



A way to achieve a higher concentration of Mn is the high volatilization of the contaminants as the Zn present in the residue. For this, the occurrence of carbothermal reactions is essential (Eqs. 1 and 2), which use carbon as a reducing agent. Such carbon can be supplied by

the same waste, as in the case of the Zn-Mn spent batter cathode, or can be added from external carbon sources such as "car-fluff" (containing plastics, fibers, glass, foam, rubber, wood, sand, dirt and other materials that remain after the grinding and separation of metals). It has been shown that a stoichiometric excess of carbon with respect to the contaminant promotes a greater yield of volatilization. To avoid the concurrent reaction of carbon with oxygen from the air, the reaction must be carried out in an inert atmosphere. Thermal desorption tests carried out in different atmospheres; air, CO₂, and N₂, and in the presence or absence of carbon for Zn evaporation showed that the highest recoveries, at any temperature, were achieved using N₂. Moreover, it was achieved 57, 97, and 99% of zinc volatilized at 850, 1000, and 1200°C, respectively (Kononov, Ostrovski, & Ganguly, 2008).

As presented above, the pyrometallurgical process is expensive because it requires high power consumption. However, it is a fast process and requires simple operating conditions. There exist some negative points from the catalyst development point of view. Firstly, after the pyrometallurgical processes, the residual solid, enriched in Mn content, presents a variety of species and crystalline structures of Mn_xO_y thanks to the diversity of oxidation states of Mn, which means that pyrometallurgical transformation is not selective to a particular manganese oxide. Secondly, carrying out the pyrometallurgical process above 900°C causes the material to sinter and, consequently, have a reduced surface area (~ 9.6 m²·g⁻¹). And thirdly, depending on the initial composition of the waste, other metals such as Fe can also be concentrated in the residual solid.

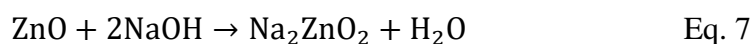
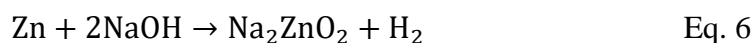
Table 3.
Pyrometallurgical recovery of manganese-based residues.

Mn-based waste	Target species	Treatment methods	Treatment conditions	Separation or recovery efficiencies (%)	Recycling products	Ref.
EMR (dried and grounded)	Mn water-soluble and bulk	Successive roasting, and neutral leaching	Two stages: i) roasting, Air flow, 60 min, 600 °C; ii) natural leaching, distilled water S/L 1:4	67.12 % Mn	MnCO ₃	(S. He, Wilson, et al., 2021)
Manganese Dust (washed and dried)	Mn, Zn bulk	Carbothermal reduction	11.7 mL/s N ₂ , 1223 K, 9 Wt.% of C	100 % Zn	MnO and Mn ₃ O ₄	(B. S. Kim et al., 2010)
Iron-bearing manganese residues (MnFe ₂ O ₄)	Mn, Fe bulk	Successive roasting, reductive roasting and magnetic separation	Three stages: i) roasting, 750 °C, air flow, 30 min; ii) reductive roasting, CO flow, 750 °C, 30 min; iii) magnetic separation, weak magnetic intensity of 1000 G, strong magnetic separation of 12,000 G.	72.29% of Fe (grade 62.21%), 90.75% of Mn (grade 35.21%)	Fe ₃ O ₄ , Mn ₃ O ₄ , MnO	(Peng et al., 2018)
Spent Zn–C and alkaline batteries mixture (separated cathode)	Zn, Mn, Hg bulk	Successive thermal treatments	Two stages: i) Hg removal, air flow, 400 °C, 10 min; ii) Zn separation, N ₂ flow, 1200 °C, 30 min	100 % Hg, 99% Zn (grade 97%), 86% Mn (grade 87%)	MnO and Mn ₃ O ₄	(Belardi et al., 2012)
Spent Zn-C cells (separated cathode)	Zn, Mn bulk	Thermal treatment	1.8 L/min N ₂ , 1200 °C, 30 min	99% Zn (grade 96%), 90-100% Mn (grade 90%)	Zn, Mn ₃ O ₄ in air and MnO	(Belardi, Medici, & Piga, 2014)
Spent alkaline batteries	Zn, Mn bulk	Pyrolysis	1 L/min N ₂ , 950 °C, 1 h	97% Zn	Zn, MnO	(Ebin, Petranikova, Steenari, &

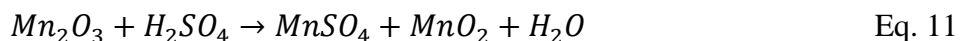
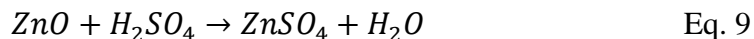
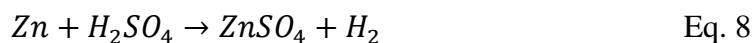
Mn-based waste	Target species	Treatment methods	Treatment conditions	Separation or recovery efficiencies (%)	Recycling products	Ref.
						Ekberg, 2016)
Spent alkaline batteries	Zn, Mn bulk	Carbothermic reduction	1 L/min N ₂ , 11 Wt. % C, 950°C	99% Zn	Zn, MnO	(Ebin et al., 2019)
Spent Zn-C battery (dried SEPARATE D cathode)	Zn, Mn bulk	Thermal treatment	1 L/min Ar, 900 °C	10 Wt. % ZnO, 48 Wt % MnO	ZnO, MnO	(Farzana, Rajarao, Hassan, Behera, & Sahajwalla, 2018)
Spent Zn-C and alkaline batteries mixture (separated cathode)	Zn, Mn bulk	Carbothermic reduction	900% stoichiometric excess of car-fluff (68% C), 1000 °C, N ₂	99% Zn (grade 97%), Mn in residue (57% grade)	Zn, MnO	(Ippolito et al., 2016)

1.2.1.2 Hydrometallurgical processing. The hydrometallurgical process consists of stages that seek the selective leaching of a metal, or a set of metals present in the waste. The purposes of the leaching can be dissolving compounds different from manganese to concentrate this metal in the residue, or to selectively dilute the manganese (W. Zhang & Cheng, 2007a). In the last case, the process must include additional stages to recover the diluted manganese by its transformation into an insoluble solid as metal, hydroxide, salt, or oxide. The leaching stage, which is perhaps the most important due to its influence on the metal recovery performance, can be neutral, acidic or acid-reducing, alkaline, or due to metal complexing. Each of these depends on the nature of the leaching agents as well as the process variables such as pH and temperature. Neutral leaching corresponds to the use of deionized water for the extraction of electrolytes and other soluble components from the waste. Species such as Cl⁻, K⁺, Na⁺, SO₄⁻, etc. are generally

removed (H. Chen, Liu, Shu, & Li, 2015). The alkaline leaching uses a strong base as a leaching agent, e.g., NaOH. This treatment was used to remove the Zn from the residue of Zn-Mn spent batteries cathode (Eqs. 6 and 7) (M. Buzatu, Săceanu, Ghica, Iacob, & Buzatu, 2013). Due to the alkaline and neutral leaching are inefficient for manganese dissolution, these treatments are frequently used to wash the residue removing impurities and increasing the concentration of Mn in the waste.



Acid leaching is the hydrometallurgical treatment most used for the dilution of Mn present in the residues. The efficiency of this process is mainly influenced by experimental conditions such as the type of acid and its concentration, the mass ratio between the solid residue and the leaching solution, the temperature, and residence time of treatment (S. He, Jiang, et al., 2021; W. Zhang & Cheng, 2007a). In general, acid such as HCl, H₃NO₄ and mainly H₂SO₄ are used due to their low cost and dissolution yields. Organic acids such as citric, malic, formic and oxalic offer a less corrosive and more environmentally friendly alternative (de Oliveira Demarco, Stefanello Cadore, da Silveira de Oliveira, Hiromitsu Tanabe, & Assumpção Bertuol, 2019), however, most studies focus especially on H₂SO₄ as a leaching agent for the extraction of manganese from residues. Among the residues more used for manganese recovery purposes they can be mentioned the electrolytic manganese residue, slags from the electrolytic manganese residue, pyrometallurgy sludge, groundwater treatment sludge, spent catalyst sludge, and probably the most reported, the spent batteries (specially Zn-Mn batteries). For manganese recovery from spent Zn-Mn batteries, the reactions expected during the acid leaching with H₂SO₄ are presented by Eqs. 8-12, which include the reactions with Zn also present in the waste.



As observed in Eqs. 8-13, the MnO_2 cannot be dissolved by sulfuric acid. To achieve close to 100% MnO_x solubilization with both H_2SO_4 and organic acids, it is necessary to use acid leaching assisted by a reducing agent. Carbon, H_2O_2 , ascorbic acid, glucose, etc. are the most used for this purpose (Yunqing Li & Xi, 2005; A. Sobianowska-Turek, Szczepaniak, Maciejewski, & Gawlik-Kobylińska, 2016). However, the process is required to be carried out under certain conditions for maximum yield, e.g., for batteries cathode processing, the concentrations of H_2SO_4 and organic acids (mentioned before) in which there is greater leaching of Mn are between 1.5 and 2 M. Moreover, the increase in temperature during the leaching process with H_2SO_4 improves the yield of the process (T. Buzatu, Popescu, Birloaga, & Săceanu, 2013). That improvement in efficiency occurs in the same way in solutions of citric, formic, and malic acid, the latter presenting the best leaching efficiency. However, these organic acids require a higher temperature (90 ~ 100°C) to obtain the highest possible efficiency compared to H_2SO_4 (> 25°C) (de Oliveira Demarco et al., 2019). For the leaching using both inorganic and organic acid, it was found that the optimal solid waste/acid liquid solution (S/L) ratio to carry out leaching processes is close to 1 g/20 ml. This relationship allows a higher concentration of the acid, and a greater contact of it with the material to be leached, which facilitates the transfer of ions in the solution. An increase in the value of this parameter generally causes a decrease in the dilution efficiency due to the saturation of the leaching solution, but an increase to 1 g/50 ml did not modify the metal leaching

yield (de Oliveira Demarco et al., 2019). Variables such as the particle size or the concentration of the reducing agent were little studied. On the other hand, as mentioned above, after the leaching of manganese they are carried out treatments for the recovery of manganese in the solid state. Among the most relevant and used, it is reported precipitation (H. Chen et al., 2015; Mocellin et al., 2017), electrodeposition (Biswal et al., 2015; RÁCZ & Ilea, 2013), evaporative crystallization (Andak, Özduğan, Türdü, & Bulutcu, 2019), and solvent extraction (Lannoo, Vilas-Boas, Sadeghi, Jesus, & Soares, 2019; Leite, Carvalho, de Lemos, Mageste, & Rodrigues, 2019) of ionic manganese. Among these, precipitation is the technique most used due to its low cost, and high yields. Some points of the chemistry of this process are presented in the wastewater processing section (next to this section).

In general, focusing on catalyst synthesis by manganese-based waste processing, the hydrometallurgical processes have some benefits over pyrometallurgical processes, such as low cost, possible recovery of the leaching agent, and less air pollution. However, one of the most important challenges in these processes is leaching selectivity; because the waste has a variety of contaminants, leaching dilutes much of them, making the chemical recovery of a particular metal more complex. With the aim of grouping the different leaching and recovery methods that made it possible to obtain manganese oxides from waste, Table 3 presents detailed review of leaching treatments and their conditions for different types of manganese-based waste.

Table 4.

Hydrometallurgical recovery of Mn from residues.

Mn-based waste	Target species	Treatment methods	Treatment conditions	Separation or recovery efficiencies (%)	Recycling products	Ref.
EMR	Mn, NH ₄ ⁺ -N water-soluble	Neutral leaching	L/S 2:1	99,96 % Mn, 99.15% NH ₄ ⁺ -N	Leachate of Mn and NH ₄ ⁺ -N	(H. Chen et al., 2015)
	Leachate of Mn and NH ₄ ⁺ -N	NH ₄ ⁺ -N Stripping and Mn precipitation	8 Wt.% CaO, 60 °C, air 800 ml/min, 60 min.	99,99 % Mn, 99.73% NH ₄ ⁺ -N	Mn ₂ O ₃ , (NH ₄) ₃ H(SO ₄)	
EMR	Mn water-soluble	Neutral leaching	L/S 5:1, 72 h, room temperature, constant agitation	-	Leachate of Mn	(Du, Zhou, Li, Guo, & Wang, 2015)
	Leachate of Mn	Precipitation	Na ₂ CO ₃ (Mn ²⁺ /CO ₃ ²⁻ molar ratio of 1:1), 30 °C, 190 rpm	98% Mn	MnCO ₃	
Slag (EMR)	Mn water-soluble and bulk	Reductant acid leaching assisted by ultrasound	Leaching medium of H ₂ SO ₄ -HCL (4:0.3 v/v), S/L 4:1, 60 °C, ultrasound bath for 35 min, 8 mg citric acid/g slag.	88.6 % Mn	Leachate of Mn	(H. Li, Zhang, Tang, Li, & Zhang, 2008)
Pyrometallurgy sludge	Mn and Zn water-soluble and bulk	Simultaneous acid and reductant acid leaching	Two stages leaching: i) 0.25 M H ₂ SO ₄ , solid/liquid ratio of 1:10, 30 min, 700 rpm. ii) 0.05-0.25 M H ₂ SO ₄ and MnO ₂ /Na ₂ S ₂ O ₅ ratio fixed at 0.5, 120 min and 150 rpm	80.8-100 % Zn, 77.6-95.9 % Mn (depending on sludge nature)	Leachate of Mn and Zn	(Mocellin et al., 2017)
	Leachate of Mn and Zn	Successive precipitation of Zn and Mn	Zn precipitation: Na ₂ S (S/Zn molar ratio of 10) , pH 5.6, 8 h. Mn Precipitation: Na ₂ CO ₃ (CO ₃ /Mn molar ratio of 1.2), pH=8.5	99.9 % Mn, coprecipitation of Ca (90.4%)	ZnS, MnCO ₃	
	Mn, NH ₄ ⁺ -N water-soluble and bulk	Electric field enhanced reductant acid leaching	35 mA/cm ² , 120 min, 40 °C, pH 2.97, S/L 1:5, 3.33 Wt.% H ₂ O ₂ , 9.15 Wt.% H ₂ SO ₄	88.07% Mn, 91.50% NH ₄ ⁺ -N	leachate of Mn and NH ₄ ⁺ -N	
EMR	Mn, NH ₄ ⁺ -N water-soluble and bulk	Electric field enhanced reductant acid leaching	35 mA/cm ² , 120 min, 40 °C, pH 2.97, S/L 1:5, 3.33 Wt.% H ₂ O ₂ , 9.15 Wt.% H ₂ SO ₄	88.07% Mn, 91.50% NH ₄ ⁺ -N	leachate of Mn and NH ₄ ⁺ -N	(Tian et al., 2019)

Mn-based waste	Target species	Treatment methods	Treatment conditions	Separation or recovery efficiencies (%)	Recycling products	Ref.
EMR	Leachate of Mn and NH_4^+ -N	Successive precipitation of Mn and struvite	Mn precipitation: Na_2CO_3 (CO_3/Mn molar ratio of 1:3), pH 9.23. N- NH_4^+ precipitation: $\text{NaH}_2\text{PO}_4 \cdot 2\text{H}_2\text{O}$ and MgCl_2 (N:P:Mg molar ratio of 1:1.3:1.1), pH 9.53 and stirred for 30 min.	98.6% of MnCO_3 and 98.0% of struvite	MnCO_3 and struvite	(N. Wang et al., 2016)
	Mn water-soluble	Neutral leaching	S/L 1:5, 72 h	Mn final concentration of 2872 mg/L	leachate of Mn	
	Leachate of Mn	Precipitation with ammonia assisted with CO_2	Two stages: i) NH_3/Mn molar ratio of 3:1, bubbling 2 L/min CO_2 for 2 min; ii) agitation at 190 rpm, 25 °C, 12 min	94.2% Mn	MnCO_3 and Mn_3O_4	
Pyrometallurgical sludge	Mn and Zn water-soluble and bulk	Successive acid and reductant acid leaching	Two stage leaching: i) 0.25 M H_2SO_4 , solid/liquid ratio of 1:10, 20 °C, 150 rpm, three 20-min steps of leaching. ii) 0.25 M H_2SO_4 and $\text{Na}_2\text{S}_2\text{O}_5/\text{Mn}$ ratio of 1, 120 min, 150 rpm, two leaching steps.	75 % Zn (first leaching), 100 % Mn (second leaching)	Independents leachates of Zn and Mn	(Mocellin, Mercier, Morel, Blais, & Simonnot, 2015)
Groundwater treatment sludge	Mn and Fe water-soluble and bulk	Reductant acid leaching	0.3 M H_2SO_4 , 0.8 M H_2O_2 , S/L 1:27.5, 150 rpm, 25 °C	100 % Mn, 80 % Fe	leachate of Mn and Fe	(Ong, de Luna, Pingul-Ong, & Kan, 2018)
	Leachate of Mn and Fe	Simultaneous precipitation of Fe and Mn	0.4 M KOH added by dropping until pH 6	Fe 100 %, Mn 20 %	$\text{Mn}(\text{OH})_2$, $\text{Fe}(\text{OH})_2$	
Groundwater treatment sludge	Fe, Al, Mn Bulk	Acid leaching	5 M HCl, 70 °C, 90 rpm, 30 min	93% Mn, 90.2% Fe, and 100% Al	leachate of Mn, Fe and Al	(C. Liu et al., 2021)
	leachate of Mn, Fe and Al	Consecutive hydrothermal recovery of	Fe/Al Precipitation: 1.9 g of NaNO_3 and 0.7 g of glucose/10.4	97.1 % Fe, 94.8 % Al, 98 % Mn	Hematite y bohemite, Hausmannite	

Mn-based waste	Target species	Treatment methods	Treatment conditions	Separation or recovery efficiencies (%)	Recycling products	Ref.
Groundwater treatment sludge		Fe/Al and precipitation Mn	g sludge hydrothermal treated at 270 °C for 20 h. Mn precipitation: 6 M NaOH, pH 8.3.			(Ong et al., 2021a)
	Mn Bulk	Reductant acid leaching	0.3 M H ₂ SO ₄ , 0.8 M H ₂ O ₂ , 150 rpm, 5 min, 25 °C	100 % Mn	leachate of Mn	
	Leachate of Mn	Precipitation	0.02 M KMnO ₄ , 300 rpm, 90 °C.	-	MnO ₂	
Spent catalyst sludge	Mn, Co Bulk	Acid leaching	10 % v/v H ₂ SO ₄ , 30 min, S/L 1:5, 75 °C.	100 % Mn, 100 % Co	leachate of Mn and Co	(Biswal et al., 2015)
	Leachate of Mn and Co	Co precipitation and electrodeposition of EMD	Co precipitation: NaS, 30 °C. EMD electrodeposition: current density of 200 A m ⁻² , at 90 °C, anode of Pb and cathode of stainless steel	88 % Co, 96% EMD	CoS, EMD	
Spent alkaline batteries	Mn, Zn bulk	Acid leaching	2M H ₂ SO ₄ , 3 h, S/L 1:10, 80 °C, 200 rpm	100 % Zn, 82 % Mn	Leachate of Mn and Zn	(Abid Charef, Affoune, Caballero, Cruz-Yusta, & Morales, 2017b)
	Leachate of Mn and Zn	Electrowinning	Current density of 0.02 A cm ⁻² , at 25 °C, 1.5 h, anode of lead and cathode of aluminum	73 % MnO ₂ , 71 % Zn	Zn, MnO ₂	
Spent alkaline batteries	Bulk Mn and Zn	Alkaline leaching	6.5 M NaOH, 3 h, S/L 1:10, 80 °C, 200 rpm	52 % Zn	Leachate of Zn	(Andak et al., 2019)
	Leachate of Zn	Electrowinning	Current density of 0.125 A cm ⁻² , at 60 °C, 3 h, anode of stainless steel and cathode of platinum	65% Zn, 35% Mn	Zn, ZnO	
Spent zinc-carbon and alkaline battery mixtures	K, Zn, Mn bulk	Successive neutral and acid leaching	Two stages leaching: i) K leaching, Distilled water, liquid/solid ratio of 10, 25 °C; ii) Zn and Mn leaching, H ₂ SO ₄ , pH 2, L/S 10:1, 60 °C.	99.2 % K, 99.2 % Zn, 37.6 % Mn	Leachate of K and leachate of Zn and Mn	

Mn-based waste	Target species	Treatment methods	Treatment conditions	Separation or recovery efficiencies (%)	Recycling products	Ref.
Spent zinc-carbon battery	Leachate of Zn and Mn	Evaporative crystallization	Two stages: i) Zn Evaporative crystallization, 40 °C. ii) Mn cooling crystallization, 15 °C.	-	MnSO ₄ ·H ₂ O and ZnSO ₄ ·7 H ₂ O	(T. Buzatu et al., 2013)
Spent alkaline battery	K, Zn bulk	Neutral and alkaline leaching	Two stages leaching: i) Neutral leaching, water 60 °C, S/L 1:5; ii) alkaline leaching, 6 M NaOH, for 2 h, S/L 10:1, 80 °C.	98.4 % K+, 82% of zinc		
Spent zinc-carbon and alkaline battery mixtures	K, Zn, Mn bulk	Neutral and acid leaching	Two stages leaching: i) Neutral leaching, water 60 °C, S/L 1:5; ii) acid leaching, 2 M H ₂ SO ₄ , 1 h, 80 °C, 200 rpm, S/L 1:10	98.4 % K+, 96% Cl-, 96% Zn, 43% Mn		
Leachate of Zn and Mn from spent batteries treated with H ₂ SO ₄	Leachate of Zn and Mn	Electrolysis	Anode: titanium, 2 pieces, current density – 1.2 A/dm ² ; cathode: aluminum, 1 piece, cathode current density – 2.4 A/dm ² ; cell voltage 3.5 V, current intensity 3.6 A, 30 mm anode–cathode distance, electrolyte recirculation speed 20 l/h. 96 °C, 24 h, pH final 4.	85.87 % Zn, 93.71 % MnO ₂	Zn, MnO	(M. Buzatu et al., 2013)
Spent lithium-ion batteries	Co, Li, Mn bulk	Reductant acid leaching	6 % (v/v) H ₂ O ₂ , 2M Malic acid, S/L of 1:20, 95 °C, 60 min	90.57 % Co, 93.22 % Li, 99.53 % Mn	leachate of Co, Li, Mn	(de Oliveira Demarco et al., 2019)
	Co, Li, Mn bulk	Reductant acid leaching	1 % (v/v) H ₂ O ₂ , 2M Citric acid, S/L of 1:20, 65 °C, 60 min	43.39 % Co, 63.25 % Li, 19.09 % Mn	leachate of Co, Li, Mn	
	Co, Li, Mn bulk	Reductant acid leaching	1 % (v/v) H ₂ O ₂ , 2M Formic acid, S/L of 1:20, 65 °C, 60 min	20.67 % Co, 82.18% Li, 18.82 % Mn	leachate of Co, Li, Mn	
Spent zinc-carbon and alkaline battery mixtures	K, Zn, Mn bulk	Neutral and acid leaching	Two stages leaching: i) neutral leaching, water, 60 °C, 10% w/v pulp density; ii)	96.4 % K, 99% Zn, 20% Mn	Residual solid from leaching	(Ferella, De Michelis,

Mn-based waste	Target species	Treatment methods	Treatment conditions	Separation or recovery efficiencies (%)	Recycling products	Ref.
			acid leaching: 3 h, 80 °C, 10% w/v pulp density, 1.5 M H ₂ SO ₄			& Vegliò, 2008)
	Residual solid from leaching	Roasting	900 °C (10 °C/min), 30 min, in oven.	100% Mn	Mn ₂ O ₃ , Mn ₃ O ₄	
Spent zinc-carbon and alkaline battery mixtures	Zn, Mn bulk	Reductive acid leaching	40 °C, 20% pulp density, 1.8 M H ₂ SO ₄ , citric acid 40 g/L	100% Zn, 97% Mn	Leachate of Zn and Mn	(Ferella, De Michelis, Beolchini, Innocenzi, & Vegliò, 2010)
Spent alkaline batteries	Zn, Mn bulk	Reductive acid leaching assisted by microwave	S/L 1:10, 1.5 M H ₂ SO ₄ and 20 g/L glucose, domestic microwave oven (800W, 2.45 GHz), 2 cycles of 30 s	84 and 95 % for Mn and Zn	Leachate of Zn and Mn	(Lannoo et al., 2019)
	Lechate of Zn and Mn	Successive solvent extraction and ion exchange	60% (v/v) of Cyanex 302 in kerosene mixed with lechated v/v ratio of 1, for 15 min.	98.9 % Zn	Zn-Cyanex 302 complex	
Alkaline batteries	Zn, Mn bulk	Reductive acid leaching	2 h at 60 °C, 5% v/v H ₂ SO ₄ , 4% v/v H ₂ O ₂ , S/L 1:30	-	Leachate of Zn and Mn	(Leite et al., 2019)
	Lechate of Zn and Mn	Extraction by aqueous two-phase systems	2 g Copolymer solution (L64 and extracting agent dithizone 10.0 mmol/kg) + 2 g lechate and salt (Na ₂ SO ₄) solution, pH 3, 12 h, 25 °C.	(93 ± 5) % Zn, (9.1 ± 0.1)% Mn	Zn-dithizone complex	
Spent Zn–Mn batteries cathode	Bulk	Reductive acid leaching	2 mol/L HCl; 3 % Wt. % H ₂ O ₂ , 50 °C, 50 min	80 % of total residue	Leachate of Zn and Mn	(Yunqing Li & Xi, 2005)
Spent alkaline batteries	Zn, Mn bulk	Microwave assisted acid leaching	Microwave (800 W, 2.45 GHz, 1 cycle, 30 s), 1 M H ₂ SO ₄ , S/L ratio 1:10.	94% of the Zn, 20 % Mn	Leachate of Zn and Mn	(Maryam Sadeghi, Vanpeteghem,

Mn-based waste	Target species	Treatment methods	Treatment conditions	Separation or recovery efficiencies (%)	Recycling products	Ref.
		Ultrasound assisted acid leaching	Ultrasound (200W, 20 kHz \pm 500 Hz, 2 min, 0.1p, 20% amplitude), 1 M H ₂ SO ₄ , S/L ratio 1:10.	92% of the Zn, 20 % Mn	Leachate of Zn and Mn	Neto, & Soares, 2017)
		Microwave assisted alkaline leaching	Microwave (800 W, 2.45 GHz, 1 cycle, 3 min), 4 M NaOH, S/L ratio 1:10.	80 % Zn, 0.01 % Mn	leachate of Zn and Mn	
		Ultrasound assisted alkaline leaching	Ultrasound (14 min, 0.1p, 20% amplitude), 4 M NaOH, S/L ratio 1:10.	80 % Zn, 0.01 % Mn	leachate of Zn and Mn	
Spent Zn–MnO ₂ batteries	Zn, Mn bulk	Neutral complexion media	5 M NH ₄ Cl, S/L ratio 1:20, 100 °C, 4 h	72 % Zn, 1 % Mn	leachate of Zn and Mn. Mn-based solid	(Nogueira & Margarido, 2015)
Spent zinc-carbon and alkaline battery mixtures	Zn, Mn bulk	Successive acid fusion and neutral leaching	Two stages: i) acid fusion, 500 °C, 4 h, KHSO ₄ /sample mass ratio = 1.3; ii) neutral leaching, distilled water (30 mL g ⁻¹), 90-100 °C, 30 min, 200 rpm	98 Wt.% of zinc and 92 Wt.% of manganese	Leachate of Mn and Zn	(Quintanilha, Afonso, Vianna, Gante, & Mantovano, 2014)
		Selective precipitation	Two stages: i) Zn recover, 0.1 M H ₂ C ₂ O ₄ , 200 rpm, 50 °C, pH 1 adjusted with 3 M H ₂ SO ₄ ; ii) Mn Recover: 6 M KOH, pH 11, 25 °C, 200 rpm	98 Wt.% Zn, 99.5 Wt.% Mn	ZnC ₂ O ₄ ·2H ₂ O, MnO(OH) ₂	
Spent Zn-MnO ₂ batteries	Zn, Mn bulk	Acid leaching	1M H ₂ SO ₄ , 1 h	95 Wt.% Zn, 14-16 Wt.% Mn	Acid leachate of Zn and Mn. Mn-based solid	(RÁCZ & Ilea, 2013)
		Acid lechate of Zn and Mn	Electrochemical	Cathode: aluminum, energy ⁻¹ .1 V, pH 2.6; anode: Pb-Ag, energy 1.73 V, pH 0.5, 20	91 Wt. % Zn, 85 Wt. % Mn	

Mn-based waste	Target species	Treatment methods	Treatment conditions	Separation or recovery efficiencies (%)	Recycling products	Ref.
Spent Nickel-metal hydride (Ni-MH) battery	Ce, La, Co, Fe bulk	Acid leaching	°C, 1 h, 5A dm ⁻² , 4.4 V cell voltage. 3 M H ₂ SO ₄ , S/L 1:10, 75 min, 500 rpm	Ce - 97.7%, La - 88.7%, Co - 79.4%, Fe - 68.5%, Mn - 91.9%, Ni - 66.2%, Zn - 100%.	Acid leachate of Ce, La, Co, Fe, Mn, Ni, Zn	(Agnieszk a Sobianow ska-Turek, 2018)
Spent zinc-carbon and alkaline battery mixtures	Mn, Zn bulk	Successive neutral, reductive acid and neutral leaching	Three stages of leaching: i) water, S/L 1:6, 200 rpm, ambient temperature, 120 min; ii) S/L 1:15.96, 45-57 °C, 63 % H ₂ SO ₄ , 60 min, 200 rpm, 88 g oxalic acid/133 ml acid solution, iii) same of step i	100% Mn, 86% Zn, 59% Cd, 43% Cu, 42% Co, 33% Ni, 22.5% Fe 9% Cr. Only stage one, 100% Na, 85% K.	Acid leachate of Mn and Zn	(A. Sobianow ska-Turek et al., 2016)
	Acid leachate of Mn and Zn	Precipitation	50 °C, 300 rpm, 1.0 M NH ₄ OH, 3.0 M NH ₄ HCO ₃ , pH 7-7.5	Mn, Fe, Co, Cd, Cr 100%, Co 98%, 95.5% Zn, Cu, Ni 85%	-	

1.2.1.3 Bio-metallurgical processing. Another form of leaching is bioleaching; in this case, the leaching agents are obtained by the metabolization of microorganisms such as *Acidithiobacillus ferrooxidans* or *thiooxidans*, *Alicyclobacillus* and *Sulfobacillus*, among others (Duan, Zhou, Chen, Jiang, & Xin, 2011; Ghosh et al., 2016). There are two types of bioleaching: by non-contact with microorganism, which implied the formation of acid by metabolization ex situ to the waste leaching, or by contact which correspond to the processes where the acid is formatted at a time that the waste is leached. For the non-contact test, the chemistry and conditions effect of the leaching process can be analyzed according to presented above for hydrometallurgical processing, and the yield to the acid formation depends directly on the conditioning and

maintenance of the microorganism. For the contact test, it is necessary to establish the effect of waste leaching products on the performance of the microorganism. However, it has been reported that contact experiments promote a higher yield of manganese recovered (Xin, Jiang, Aslam, et al., 2012). Table 4 summarizes the principal metallurgical process to leach the manganese from the waste, and the experiments for its recovery in a solid form. Regarding pyrometallurgical and hydrometallurgical methods, bioleaching offers a sustainable way to carry out the separation of metals of interest, however, the process yields of recovery manganese keep still lower and unattractive. Nevertheless, as will be seen, this method has been successfully tested for the preparation of the manganese-based catalyst.

Table 5.

Byo-hydrometallurgical recovery of Mn from residues.

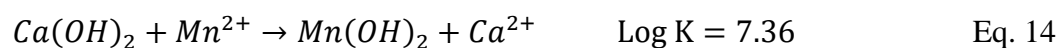
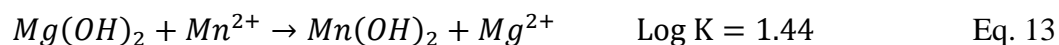
Mn-based waste	Target species	Treatment methods	Treatment conditions	Separation/recovery efficiencies (%)	Recycling products	Ref.
EMR	Mn water-soluble and bulk	Bioleaching-non-contact mechanism	SOB Medium (Acidithiobacillus, sulfur/Pyrite), 5 d, 1% slag pulp, final pH: 1.2-1.3	99.7% Mn	Leachate containing Mn	(Duan et al., 2011)
Mining waste residues	Mn	Bioleaching	Acinetobacter sp., 20 d, 2% pulp density, 30 °C, 200 rpm. Initial pH: 6.5	76% Mn	Leachate containing Mn	(Ghosh & Das, 2017)
EMR (Crushed)	Mn, Mg, Fe, NH ₃ -N, SO ₄ water-soluble and bulk	Bioleaching	Bioleaching medium (Bacteria isolated from EMRs., waste molasses as carbon/nutrient source), S/L 1:2.5, 8 d, 30 °C and 160 rpm	78-88% SO ₄ ⁻² , 85-98% Mn, 75-85% Mg, 88-95% Fe, 95-99% NH ₃ -N	Leachate containing ions	(Lan et al., 2019)
		Precipitation	NaOH, pH: 8.5-9.0, 30 min	99.73 % NH ₃ -N,		

Mn-based waste	Target species	Treatment methods	Treatment conditions	Separation/recovery efficiencies (%)	Recycling products	Ref.
EMR	Mn water-soluble and bulk	Successive bioleaching	Two leaching stages: i) SOB medium (Acidithiobacillus, 4.0 g/l sulfur), S/L 1:10, 9 d. ii) PLB Medium (Acidithiobacillus, 4.0 g/l pyrite), S/L 1:10, 9 d	79.22% SO ₄ ²⁻ 93% Mn	(NH ₄) ₂ ·6H ₂ O and (NH ₄) ₂ ·Fe(SO ₄) ₂ ·6H ₂ O Leachate containing Mn	(Xin, Chen, Duan, & Zhou, 2011)
Spent alkaline and Zn-C batteries mixture	Zn, Mn bulk	Bioleaching non-contact mechanism	Bioleaching medium (Acidithiobacillus thiooxidans, CO ₂ from the air as carbon source and Sulphur)	90 % Zn, 20% Mn	Lechate containing Mn and Zn	(Falco, Quina, Gando-Ferreira, Thomas, & Curutchet, 2014)
		Solvent extraction	0.3 M Cyanex 272 diluted in kerosene, pH 4, A/O = 1, 25 °C	95% Zn, 80 % Mn	Cianex 272-Mn ⁺²	
Spent alkaline button-cell batteries (Cathode and anode)	Zn, Mn bulk	Bioleaching	Bioleaching medium (Acidithiobacillus ferrooxidans), 10 g/L, 21 days, initial pH: 2 (adjusted with 98% sulfuric acid), 30 °C.	99 % Zn, 53% Mn	leachate containing Mn and Zn	(Sadeghabad, Bahaloo-Horeh, & Mousavi, 2019)
Spent Zn–Mn batteries	Zn, Mn bulk	Separated Non contact bioleaching and contact bioleaching	Bioleaching medium (Alicyclobacillus sp. 5% v/v and Sulfobacillus sp. 5% v/v, 2.0 g/l elemental sulfur + 2.0 g/l pyrite, 8–10 days), 1 % pulp density, 13 days	Non contact: 96% Zn, 36 % Mn; Contact: 96% Zn, 97% for Mn	leachate containing Mn and Zn	(Xin, Jiang, Aslam, et al., 2012)
Spent Zn–Mn batteries	Zn, Mn bulk	Bioleaching	Bioleaching medium (Alicyclobacillus sp. 5% v/v and Sulfobacillus sp. 5% v/v, 2.0 g/l elemental sulfur + 2.0 g/l pyrite, 8–10 days), 4 % pulp density, 13 days	100% Zn, 94 % Mn	Leachate containing Mn and Zn	(Xin, Jiang, Li, et al., 2012)

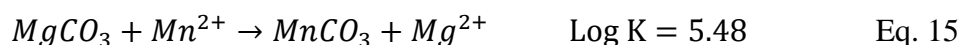
1.2.2 Wastewater treatment to recovery manganese

Wastewater is considered as water contaminated by any combination of domestic, industrial, commercial, agricultural activities, surface runoff, or rainwater, which can be collected by sewage systems or that can generate an anthropogenic effect on the environment. In the case of wastewater contaminated with manganese, the main distinguishing features are the waters contaminated with residues from mines or mining activities (Le Bourre, Neculita, Coudert, & Rosa, 2020; Yongchao Li, Huang, Xu, Ma, & Guo, 2020) and the wastewater from metallurgical activities for the production of metallic manganese or manganese dioxide (Koivula et al., 2009; Shu, Liu, Liu, Chen, & Tao, 2016b). Regarding the acid drainage of the mines, especially those abandoned or without waste management, the waste is generated by the effect of rain or surface runoff which, when in contact with the tailings or mineral deposits, promotes the oxidation of the sulfur phases and dissolves salts as $\text{MnSO}_4 \cdot \text{H}_2\text{O}$, $(\text{NH}_4)_2\text{Mn}(\text{SO}_4)_2 \cdot 6\text{H}_2\text{O}$, and $(\text{NH}_4)_2\text{SO}_4$, $\text{Mg}(\text{NH}_4)_2(\text{SO}_4)_2 \cdot 6\text{H}_2\text{O}$ among others, releasing gradually acidic fluids rich in sulfates and metals to the environment around the slag dump (Neculita & Rosa, 2019). These mine effluents can have manganese concentrations greater than 352 mg/L. On the other hand, several types of wastewaters are distinguished in the industrial production of metallic manganese and manganese dioxide. Some are generated by the release of manganese leachates generated in the production of electrolytic manganese metal, or by the leaching of manganese sulfates present in the electrolytic manganese residues. In both cases, due to the leaching processes occurring in an acid medium, these wastes generally have low pH along with a significant number of species such as Cr (VI), $\text{NH}_3\text{-N}$, Mg, Na, Ca, Fe and Al, among others (Shu et al., 2019). Although these metals are found in a lower proportion than Mn, they are of consideration in manganese recovery processes.

There are various processes for the removal of manganese from wastewater. Patil et al. (Patil, Chavan, & Oubagaranadin, 2016) published a detailed review of technologies for manganese removal from wastewaters. In general, those processes seek to chemically isolate manganese ions to later separate them by physical or chemical processes. Chemical precipitation is the most efficient and widely used method for this purpose. This technique is based on the conversion of the soluble manganese ion into an insoluble precipitate. Precipitation reactions generally occur at basic pH. There are different chemical mechanisms of precipitation that depend on the nature of the precipitant and the pH of the medium. Hydroxides, e.g., manganese or calcium have been widely used to precipitate manganese (Eqs. 13 and 14) (W. Zhang & Cheng, 2007b). Since only pH greater than 8.5 yields greater than 99% are achieved in the removal of manganese and high selectivity towards $Mn(OH)_2$, one of the disadvantages of this method is the need for high amounts of base and in higher operating cost effect as well as the generation of other types of alkaline waste.

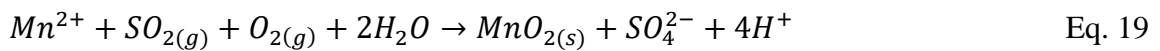
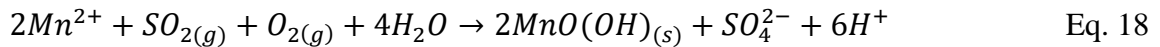
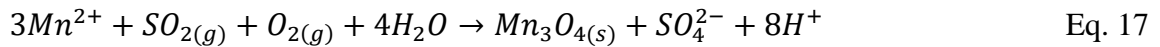


Similar to the process with hydroxides, precipitation with carbonates (Eqs. 15 and 16) can be carried out at a pH greater than 8.5 with yields greater than 99%. This technique has proven to be efficient in concentrated solutions. However, for low concentration solutions, excessive coprecipitation may occur. The equilibrium constants of the equations presented show that the selectivity's towards manganese depend strongly on the cation of the precipitating agent. The combination of carbonates has proven to be a good alternative to avoid coprecipitation, working at a pH lower than 8.5.



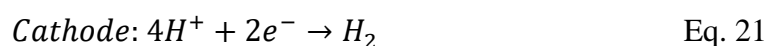
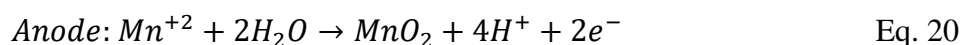


Oxidative precipitation, unlike the previously mentioned processes, occurs in an acid medium and provides the highest selectivity for the recovery of manganese as MnO₂/Mn₂O₃, over other species such as Zn²⁺, Ni²⁺, Co²⁺, Mg²⁺, and Ca²⁺. This type of precipitation is carried out by bubbling SO₂ and O₂ in the Mn solution to promote oxide reduction reactions that allow the formation of the Mn³⁺ and Mn⁴⁺ oxides (Eqs. 17 to 19) (W. Zhang & Cheng, 2007a). In this process, pH control plays a crucial role because it influences the solubility of SO₂.



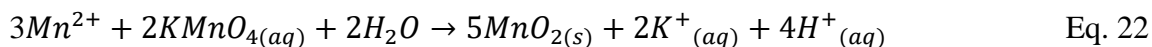
Sulfide precipitation, contrary to oxidative precipitation, does not involve oxidation-reduction reactions, but rather a simple substitution of cations, similar to processes with hydroxides and carbonates, but at a pH close to neutral. In this process, it is customary to bubble sulfides such as hydrogen sulfide (H₂S), sodium sulfide (Na₂S), or ammonium sulfide ((NH₄)₂S) into the manganese solution. Like the SO₂ process, gas solubility is essential for removal efficiency. At this point, the control of pH and temperature have a significant influence on the removal of Mn²⁺. This process offers a particular difference in relation to the other precipitation techniques and is associated with the high solubility of MnS in relation to the sulfides of Cu²⁺, Zn²⁺, Co²⁺, Ni²⁺ and Fe²⁺; in this case, after the initial precipitation of other pollutants, co-precipitation would not represent a problem, as if it occurs in precipitation with hydroxides or carbonates. Analogous to the precipitation, other way to recover the manganese oxides from solution is the electrowinning. This process is conventionally used to produce electrolytic manganese dioxide and electrolytic manganese, according to Eqs. 20 and 21, starting with the anodic oxidation of ionic manganese

(like $MnSO_4$ or $MnCO_3$ solution) with inert electrodes. As Zhang et al. reported (W. Zhang & Cheng, 2007a), there are several limitations to use efficiently this process, as impurities, the concentration and nature of initial electrolyte, the additives in the solution and the anode types. According to that, this process has been rarely used to recover manganese from wastewater and in fact, it was not mentioned by Li et al. (Yongchao Li, Xu, Ma, & Hursthouse, 2019) and Deepti et al. (Patil et al., 2016) in their reviews about wastewater treatments for manganese recovery.



On the other hand, coagulation/flocculation is a widely used method for the removal of heavy metals from drainage waters, but with the intention of reducing the ion load of a solution but not the recovery of any particular metal (Yongchao Li et al., 2019). In this process, coagulating agents are added to the wastewater to promote the stabilization of manganese ions and their aggregation, so that they can be easily separated from the solution (Patil et al., 2016). Among the most used coagulants for wastewater treatment are those based on iron and aluminum. The factors that have the greatest influence on coagulation performance are the coagulant dose, pH, temperature, and the oxidation state of heavy metals. Among the limitations of this process are the high operational costs due to the high volume of chemical reagents, as well as the enormous amounts of sludge generated. Conventionally, precipitation or coagulation/flocculation processes are accompanied by filtration operations (Rashid, Shafiq, Akhter, Iqbal, & Hussain, 2021). Due to the insoluble nature of the precipitated species, they can be trapped in sieves or membranes with pore sizes smaller than the particle sizes of the precipitate and separated from the liquid. There is an alternative technique, and it is oxidation/filtration, which involves loading the sieves with oxidizing agents such as potassium permanganate in a way that allows generating of them a layer

of manganese oxide (Eq. 22) which is retained in the sieve. Other filtration operations include the use of semi-permeable membranes; microfiltration, ultrafiltration, nanofiltration, reverse osmosis, and electrodialysis are the different membrane filtration techniques. In the case of membrane filtration, the recovery of filtered manganese is a rather expensive operation since it involves back-flow operations and the use of diluents.



Contrary to filtration, processes such as ion exchange or adsorption seek the trapping of the diluted ionic species, and are not precipitated or added (Rashid et al., 2021). In the first process, the ions dissolved in a liquid are exchanged with ions in a solid matrix. Generally, the ions of the solid medium correspond to surface functional groups intentionally anchored by functionalization processes. The exchange mechanism is generated between ions of similar charge, although it is expected that the dilute ions of the solution are exchanged for ions of the solid medium with a lower oxidation state, while the concentrated ions are balanced with the other ions of similar charge. Mn ions can be removed with ion exchange zeolites. This process is the most efficient for removing very dilute fractions of heavy metals, as well as being the most environmentally friendly. One of its major disadvantages is the need for regeneration after treating large amounts of water contaminated with heavy metals. For its part, the adsorption process refers to the accumulation of one substance on the surface of another, which remains adhered by the formation of chemical complexes with the surface of the adsorbent or by electrostatic attraction. Due to the wide variety of adsorbents available on the market, there is an enormous diversity of mechanisms and species that can intervene in adsorption. Activated carbon, adsorbent polymers, natural adsorbents such as minerals, plants, biomass-based biomaterials, and microorganisms are distinguished. Both ion

exchange and adsorption have the drawback of the difficulty of recovering the removed Mn (Chai et al., 2021).

1.3 Catalyst synthesis from Mn-based waste

Manganese oxides are known for their oxidizing properties, which are associated with the reducibility of manganese. Due to the lability of its bond with oxygen, Mn is capable of acting both as a reducing agent and as an oxidizing agent, acting in both cases as an active component of the redox system. Furthermore, due to the multivalent nature of manganese, its oxides generally exhibit high oxygen storage capacity and a high oxygen mobility in the crystal lattice (Reidies, 2000; C. Zhou et al., 2018). As an excellent oxidizer, manganese oxides have been successfully tested in a wide variety of catalytic applications. The synthesis of these oxides for catalytic purposes has traditionally been carried out through the use of commercial precursors extracted from primary sources of manganese. Conventional routes to produce these oxides have been reported to be precipitation of manganate salts, solution combustion, hydrothermal synthesis, or sol-gel routes (Bach, Henry, Baffier, & Livage, 1990; Lyu et al., 2020b; Piumetti, Fino, & Russo, 2015; W. Zhang & Cheng, 2007a). In the last decade, with the increase in both environmental problems and the reported effects on human health due to the spread of manganese, whether due to natural or anthropogenic causes, the circular production of manganese-based products from waste has charged great interest. On the particular topic of catalyst production, at least on a laboratory scale, there is a considerable published literature. Table 5 summarizes the publications on the production of catalysts from manganese-based residues, discriminating the type of waste, the methods and conditions of catalyst synthesis, the relevant properties of the catalyst, the

catalytic test conditions and the catalytic performance. It was found that the main applications of these catalysts were chemical looping gasification, nitric acid reduction, acetic acid esterification, oxygen evolution reaction, azo dyes degradation and volatile organic compounds removal, these being last two the most reported. Additionally, the most used residues in the synthesis of the catalyst were electrolytic manganese residues with a manganese content between 16-31.9 % wt. or MnO of 41 % wt., and spent batteries either lithium-ion, Zn-C or alkaline with a content of Mn > 34 % wt.. The processing of the residues to obtain the catalyst was mainly based on hydrometallurgical or bio-metallurgical methods. The first basically consisted in three stages: i) leaching stage using nitric, sulfuric and citric acids, or ammonia, ii) precipitation with oxalic acid or NaOH, and iii) thermal treatment for drying (up to 200 °C during 2 h in oven) and/or roasting (up to 750 °C during 4 h in muffle furnaces). The second is similar to the first, but included a previous stage for the production of acid by the metabolism of the microorganism. Finally, the most common characteristics in the obtained catalyst from residues are the crystalline phases MnO₂, Mn₂O₃ and Mn₃O₄, surface areas between 4 and 45 m²/g, molar ratio Mn³⁺/Mn²⁺ XPS between 0.99 and 1.5, and a surface Mn average oxidation state between 2.4 and 3.5.

Table 6.

Catalyst preparation and evaluation from Mn-based waste

Mn-based waste	Catalyst synthesis	Relevant properties	Catalytic test conditions	Catalyst activity	Ref.
<i>Chemical looping gasification</i>					
Waste manganese and (18.1 % Fe, 34.3 % Si, 6.5 % Al, 0.7 % Ca)	Two stages: i) wet ball milling method, waste manganese sand to Ca(OH) ₂ mass ratio 1:1, deionized water, 2 h; ii) calcination, air, 1100 °C, 4 h	CaMn _{0.7} Fe _{0.3} O _{2.845} , Bulk density (g/ml): 1.82, Crushed strength (N): 3.70, Surface area (BET, m ² .g ⁻¹): 1.98	Catalyst mass: 10.59 g, coal mass 3 g, Reaction temperature 950 °C, Gasification agent 50% H ₂ O, 1.04 g/min, Inert gas N ₂ , 1 L/min, Oxidation gas Air, 1 L/min	Gas yield (Nm ³ /kg): 1.2 H ₂ , 0.5 CO ₂ , 0.3 CO, 0.04 CH ₄	(Ren, An, Hu, Ma, & Guo, 2021)

Mn-based waste	Catalyst synthesis	Relevant properties	Catalytic test conditions	Catalyst activity	Ref.
<i>Reduction of nitric oxide</i>					
Manganese slag (31.89 % Mn, 12.21 % Fe, 5.85 % Al, 1.07 % Ca and 24.92 % Si) and chromium wastewater (2779 ppm Cr, 237 ppm Zn, 54 ppm Fe, 23 ppm Ni and 13 ppm Cu)	Three stages: i) Mn activation, 1M ammonia S/L 1:25, 2 h; ii) impregnation with Cr wastewater, S/L 0.2/45 (molar ratio of Mn:Cr was 3:1). iii) dried, 105 °C	Mn(Cr) ₂ O ₃ , Mn ₃ O ₄ . Manganese distribution: Mn ⁴⁺ 25.2%, Mn ³⁺ 36.5%, Mn ⁺² 38.3%. weak and medium acid sites: 0.99 mmol/g, strong acid sites: 0.08 mmol/g	Fixed-bed reactor (4 mm inner diameter), NO (961.54 ppm: balance Ar), 0.3 ml/min of NH ₃ (10%, balance Ar) and 1.0 ml/min of O ₂ (99.9999, when necessary), GHSV 14 400 1/h (= 30.0 mL/min*60 min/ (0.20 g/1.59 g/mL))	NO removal: 97.2 ± 1.6%, 150 °C	(G. Wang et al., 2018)
Manganese slag (41.83% of MnO, 43.38% of SiO ₂ and 9.65% of Al ₂ O ₃)	Four stages: i) microwave digestion, slag: HNO ₃ (1 M) 1:30, 65 °C; ii) silica-gel precipitation, pH 3.2 (adjusted with 6 M ammonia); iii) Mn precipitation, pH 9 (adjusted with 6 M ammonia); iv) Calcination, 400 °C for 3 h	MnO ₂ , Mn ⁺² 20.63%, Mn ⁺³ 39.89%, Mn ⁺⁴ 39.62%	Fixed-bed reactor (4 mm inner diameter), 30.0 ml/min of NO (1000 ppm, balance Ar), 0.3 ml/min of NH ₃ (10%, balance Ar) and 1.0 ml/min of O ₂ (99.9999), GHSV 15,000 h ⁻¹ .	NO removal: 78.31% at 100 °C	(G. Wang, Zhang, Zhou, & Qian, 2019)
<i>Esterification of acetic acid with n-butanol</i>					
Manganese nodule leached residue (Mn 28.8 %, Fe 2.55%, Al ₂ O ₃ 19.8 %, SiO ₂ 0.35%, SO ₄ % 2– 5.58)	i) water-washed: S:L 1:10, 4h; ii) calcination, 400 °C, 3 h, in muffle furnace	Surface area (m ² /g): 175, Bronsted acid sites (mol/g): 89.5, Surface oxygen (mmol/g): 10.92, Surface hydroxyl groups (mmol/g): 0.322	Acetic acid: n-butanol = 1:16, 4h, 98 °C, 0.025 g catalyst.	76.6% conversion having 100% selectivity towards n-butyl acetate	(Dash & Parida, 2007)
<i>Oxygen evolution reaction</i>					
Spent Zn-C battery (Zn 18.53±0.14%, Mn 42.84±7.8%, Fe 2.03±1.61%,	Three stages: i) manually separation of cathode black mass; ii) Thermal treatment of black mass, Ar atmosphere, 900°C, 1 h, iii) second	Mn ₃ O ₄ nanoparticles (10– 60 nm)	MnO ₂ and Mn ₃ O ₄ based electrodes (Stainless steel painted with a sonicated mix of 5 mg of MnO ₂ or Mn ₃ O ₄ into a 0.4 ml solution of 5% Nafion diluted with ethanol in a ratio of 1:3),	Onset potential of 1.51 V vs RHE, 360 mV overpotentia 1 (to reach 10 mA cm ⁻²	(Farzana et al., 2020)

Mn-based waste	Catalyst synthesis	Relevant properties	Catalytic test conditions	Catalyst activity	Ref.
Cl 11.74±4.45%)	thermal treatment of black mass, air atmosphere, 800°C, 1h		0.1 M KOH medium, graphite Rod (auxiliar electrode)	in alkaline medium)	
<i>Azo dyes degradation</i>					
EMR	Two stages: i) ultrasound treatment: 100 g EMR, 0.2 g EDTA-2Na, and 200mL NaOH (2M), 30-min, 80 °C, 100 W (15 KHz) ultrasound; ii) hydrothermal treatment, 5 h, 130 °C.	Honeycomb structure (100-200 nm), 265.3 m ² /g, Mn ₂ O ₃	H ₂ O ₂ 0.04 x 10 ³ M; catalyst 3 mg; pH 3.0; 35 °C, 100 ml (100 mg/L) of azo dyes (X-3B, Methyl Orange, Methylene blue and Acid Orange 7), indoor weak light	99.99% removal of azo dyes	(Lan et al., 2020)
Electrolytic manganese slag (O 38.92%, Si 8.98%, Ca 11.82%, Mg 5.62%, Fe 8.82%, Mn 16.41%, Ti 0.21%, S 5.87%, Na 0.21%, K 0.45%)	Two stages: i) 40 g slag, 1.0 L of 4.0 g/L Na ₂ CO ₃ , 25°C, 170 rpm, 20 min; ii) 1 M of HNO ₃ , 30 min	O 41.22%, Si 12.53%, Ca 0.06%, Mg 1.11%, Fe 16.94%, Mn 26.38%, Ti 0.11%, S 0.24%, Na 0.16%, K 0.38%.	0.8 g/L Catalyst, 0.4 g/L peroxymonosulfate, 100 mg/L Thiol collectors, 298 K.	Remotion efficiency: 100% diethyl dithiocarbamate and 97.3% butyl xanthate in 10 min, 93.2% ester-200 and 85.6% butyl amine in 30 min	(M. Li, Zhong, et al., 2021)
Electrolytic manganese slag (CaSO ₄ (H ₂ O) ₂ , SiO ₂ , α-Fe ₂ O ₃ , Mn ₃ O ₄)	Two stages: i) 4.0 g slag, 20 mL of 4.0 g/L Na ₂ CO ₃ , 170 rpm, 25 °C, 20 min; ii) 7.0 mL of HNO ₃ (65%), 73 mL of ultrapure water	84.1 m ² /g, atomic composition: 0.170 Mg, 4.93 Fe, 8.19 Mn, 68.25 O, 18.16 C; MnO ₃ , Mn ₃ O ₄ , CaCO ₃ , SiO ₂ , α-Fe ₂ O ₃	0.8g/L Catalyst, 0.4 g/L peroxymonosulfate, 20 mg/L levofloxacin, 298 K, natural pH	levofloxacin remotion: 82.6 %	(M. Li et al., 2020)
Electrolytic manganese anode slag	i) leaching stage: 5 g waste, 30 mL H ₂ SO ₄ 1M, 25 °C, 40 min, stirred in magnetic stirrer; ii) dried: 50 °C, 12h	α-MnO ₂ , 97.59 m ² /g.	1 mM peroxymonosulfate, 0.3 g/L catalyst, 40 ppm tetrachlorophenol, 50 min	degradation of tetrachlorophenol: 85%	(X. Zhou et al., 2021)

Mn-based waste	Catalyst synthesis	Relevant properties	Catalytic test conditions	Catalyst activity	Ref.
Mn residue from production process of qualified manganese sulfate (28.67 % Fe, 15.66 % Si, 10.44 % S, 2.88 % Mn, 2.22 % Al, 1.04 % K, 1.01 % Ba, 0.62 % C)	Four stages: i) pre-roasted of Mn residue, 600 °C (10 °C/min, 1 h, air atmosphere; ii) milling a mix of pre-roasted and starch (20 Wt. %), 1 h, 400 rpm, 50 °C; iii) freeze dried, 24 h; iv) reduction roasting, 700 °C (10 °C/min), 1h.	SiO ₂ , Fe ₃ O ₄ , Mn ₃ O ₄ , FeO, 2SiO ₂ FeO; Surface area (BET) (m ² /g): 41.3,	1.0 g/L catalyst, 4 mL/L H ₂ O ₂ , 50 mg/L Safranin-T, shaking incubator (120 rpm), 20 min, 50 °C, pH 3	Safranin-T remotion: 99.1%	(Cai et al., 2020)
spent Zn–MnO ₂ batteries (MnO ₂ , Mn ₃ O ₄)	Three stages: i) leaching stage, 8.0413 g of cathode powder with 250.0 mL of 0.5 mol L ⁻¹ HNO ₃ and 6.0 mL of 30 % (v/v) H ₂ O ₂ , 4 h at 80 °C; ii) co-precipitation, 23 g ferric chloride added to leaching solution and precipitated with ammonium hydroxide; iii) thermal treatment: 450 °C, 2 h, muffle furnace.	MnFe ₂ O ₄ (615.5 ± 12.0 mg Fe/g 45.2 ± 1.0 mg Mn/g), surface area 25.2 m ² /g,	50.0 mL of dye solution (methylene blue (5.4 mg/L) in H ₂ SO ₄ (pH 3.0)), 20 mg of ferrite, and 3.0 mL of 0.5 mol L ⁻¹ H ₂ O ₂), ultraviolet light irradiation (365 nm at 20 W), 120 min	degradation of methylene blue: 98 %	(Morais et al., 2020)
Spent ternary lithium-ion batteries (LiNi _x Co _y Mn _z O ₂ and LiMn ₂ O ₄ .)	i) cathode separation; ii) dried, 300 °C for 20 min; iii) leaching, ammonia, ammonium sulphate, sodium sulphite and deionized water, pulp density of 10g/L, 500 rpm at 353K for 6 h; iv) filtered, filtrate washed and dried	DRX phases: Mn ₃ O ₄ , NiMn ₂ O ₄ ; BET surface area: 2.64 m ² /g	100 ml Methylene Blue solution (100 mg/L), 10 ml H ₂ O ₂ (30%), 25±1 mg catalyst, 300 rpm, initial pH 145 of 6.0, 250 min	Methylene Blue degradation: 10 %	(Shen et al., 2019)

Mn-based waste	Catalyst synthesis	Relevant properties	Catalytic test conditions	Catalyst activity	Ref.
	(55 °C for 24 h); v) thermal treatment (600-900 °C, 5 °C/min) for 1h. i) cathode separation; ii) dried, 300 °C for 20 min; iii) leaching, ammonia, ammonium sulphate, sodium sulphite and deionized water, pulp density of 10g/L, 500 rpm at 353K for 6 h; iv) filtered, filtrate washed and dried (55 °C for 24 h); v) thermal treatment (600-900 °C, 5 °C/min) for 1h; vi) ball milling, 15 min, 18 Hz,	DRX phases: Mn ₃ O ₄ , NiMn ₂ O ₄ ; BET surface area: 6.34 m ² /g		Methylene Blue degradation: 40 %	
Spent Li-MnO ₂ button-cell batteries	i) Cathode separation; ii) washed, 400 g/L; iii) dried, 60 °C overnight.	BET surface area: 22.3265 m ² /g, Average Mn oxidation state 3.10,	100 mL of 10 mg/L Rhodamine B (RhB) solution, 180 rpm at 25 °C, catalyst 0.1 g/L and oxone (0.15 g/L), 0.02 g/L phosphate buffer solution, 30 min	Rhodamine B degradation: 98.2%	(Xu Wang et al., 2018)
VOCs remotion					
Spent alkaline and zinc-carbon batteries (47% Mn, 25% Zn)	Three stages: i) bioleaching media, Acidithiobacillus thiooxidans, initial pH 2.5, powdered sulfur (2 Wt.%) as energy source, 30 C; ii) non-contact bioleaching, S/L 1:14, 3 h, 0.3 M H ₂ SO ₄ , iii) thermal treatment of solid residue: air, 500 °C, 2 h.	Mn ₃ O ₄ , Mn ₂ O ₃ and C, 7 m ² /g, Mn average oxidation state 2.4,	Continuous flow tubular glass reactor, atmospheric pressure, 100 cm ³ /min VOC (1% Vol in air), 1 g catalyst, 350 °C,	Ethanol conversion: 98%; n-heptane: 60 %	(Gallegos, Falco, Peluso, Sambeth, & Thomas, 2013)

Mn-based waste	Catalyst synthesis	Relevant properties	Catalytic test conditions	Catalyst activity	Ref.
	<p>Four stages: i) bioleaching media, Acidithiobacllus thiooxidans, initial pH 2.5, powdered sulfur (2 Wt.%) as energy source, 30 °C; ii) non-contact bioleaching, S/L 1:14, 3 h, 0.3 M H₂SO₄; iii) electrolysis of leachate, stainless steel electrodes, current of 3 A dm², pH 5 to 1.5; iv) thermal treatment: air, 500 °C, 2 h.</p>	<p>Mn₂O₃, MnO₂, 44 m²/g, Mn average oxidation state 3.5</p>		<p>Ethanol conversion: 98%; n-heptane: 80 %</p>	
	<p>Four stages: i) bioleaching media, Acidithiobacllus thiooxidans, initial pH 2.5, powdered sulfur (2 Wt.%) as energy source, 30 °C; ii) non-contact bioleaching, S/L 1:14, 3 h, 0.3 M H₂SO₄; iii) selective precipitation, 100 mL of KMnO₄ (0.1 M) dropwise, 100 mL leachate, stirred, 30 °C, 1 h; iv) thermal treatment: air, 500 °C, 2 h.</p>	<p>Mn₂O₃, MnO₂; 49 m²/g, Mn average oxidation state 3.4</p>		<p>Ethanol conversion: 100 %; n-heptane: 90 %</p>	
Spent alkaline and Zn/C batteries (34 Wt.% Mn and 22 Wt.% Zn)	<p>Four stages: i) bioleaching media, Acidithiobacllus thiooxidans, initial pH 2.5, powdered sulfur (2 Wt.%) as energy source, 30 °C; ii) non-contact bioleaching, S/L</p>	<p>MnO₂, Mn₂O₃; 37 m²/g, Mn/Zn AA 2.5</p>	<p>Flow U-shape glass reactor, atmospheric pressure, 100 mg of catalyst, 100 cm³ min⁻¹ (2 vol% of VOC in air), gas hourly space velocity of 36000 h⁻¹, 300 °C</p>	<p>Ethanol conversion: 100 %</p>	(Gallegos et al., 2017)

Mn-based waste	Catalyst synthesis	Relevant properties	Catalytic test conditions	Catalyst activity	Ref.
	1:14, 3 h, 0.8 M H ₂ SO ₄ ; iii) selective precipitation, 100 mL of KMnO ₄ (0.1 M) dropwise, 100 mL leachate, stirred, 30 min; iv) thermal treatment: air, 500 °C, 2 h.				
	Four stages: i) bioleaching media, Acidithiobacillus thiooxidans, initial pH 2.5, powdered sulfur (2 Wt.%) as energy source, 30 °C; ii) non-contact bioleaching, S/L 1:14, 3 h, 0.8 M H ₂ SO ₄ ; iii) selective precipitation, 100 mL of NaOH dropwise, 100 mL leachate, final pH 8, stirred, 30 min; iv) thermal treatment: air, 500 °C, 2 h.	ZnMnO ₃ , ZnO, Mn ₂ O ₃ ; 33 m ² /g, Mn/Zn AA 0.4		Ethanol conversion: 90 %	
	i) leaching stage, S/L 20 g/L, citric acid 1.5 M, glucose 0.3 g/g, 80 °C; ii) dried, 105 °C overnight; iii) thermal treatment of dried powders, 350 °C (5 °C/min), 3 h.	LiNi _{0.18} Mn _{1.82} O ₄ ,		Toluene conversion a 300 °C: 67 %	
Spent Ternary Lithium-ions Batteries	i) leaching stage, S/L 20 g/L, citric acid 1.5 M, glucose 0.3 g/g, 80 °C; ii) precipitation, 50 mL acid leachate, 4 g acid oxalic, iii) dried, 105 °C overnight; iv) thermal treatment of	MnO _x -M-350, CuNi _{0.5} Mn _{1.5} O ₄ , 26.80 m ² /g; Mn ³⁺ /Mn ²⁺ XPS molar ratio 0.99; Mn ⁴⁺ /Mn ³⁺ XPS molar ratio 0.7	On-stream reaction experiments, toluene concentration of 1000 ppm (900-1100 ppm) and GHSV of 60,000 mL·h ⁻¹ ·g ⁻¹ ; 300°C	Toluene conversion a 300 °C: 95 %	(M. Guo, Li, Liu, Zhang, Guo, et al., 2019)

Mn-based waste	Catalyst synthesis	Relevant properties	Catalytic test conditions	Catalyst activity	Ref.
	dried powders, 600 °C (5 °C/min), 3 h; v) acid leaching of calcined powders, nitric acid, 50 °C; vi) dried, 105 °C overnight; vii) thermal treatment, 350 °C, 180 min.				
Spent ternary lithium-ions batteries (Mn, nickel, cobalt, aluminum, and copper and their contents are 65.59%, 20.54%, 8.05%, 3.62% and 1.73%, respectively)	i) leaching stage, S/L 20 g/L, citric acid 1.5 M, glucose 0.3 g/g, 80 °C; ii) precipitation, acid leaching solution 50 mL, four times stoichiometric molar of oxalic acid, 40 °C, 120 min; iii) dried, oven at 105 °C overnight; iv) thermal treatment, 600 °C for 180 min in a muffle furnace	LaMnO ₃ , 27.22 m ² /g, Mn ³⁺ /Mn ²⁺ XPS molar ratio 1.12; Mn ⁴⁺ /Mn ³⁺ XPS molar ratio 1.15	50 mg of as-prepared catalyst, 1000 ppm (900-1100 ppm) toluene vapor (21 vol.% O ₂ and 79 vol.% N ₂ as balance gas) with the total flow rate of 50 mL·min ⁻¹ , corresponding to WHSV of 60,000 mL·g ⁻¹ ·h ⁻¹ , 300 °C.	Toluene conversion: 95 %	(M. Guo, Li, Liu, Zhang, Hu, et al., 2019)
Spent lithium-ion batteries	i) leaching stage, 20 g·L ⁻¹ of solid-liquid ratio, 1.5 mol·L ⁻¹ of citric acid, 0.3g·g ⁻¹ of glucose and 80 °C; ii) precipitation, 3 g oxalic acid was added into 80 ml of acid leaching solution; iii) dilution of precipitate, 30 ml dilute of HNO ₃ ; iv) dilution of metal nitrate, Gd(NO ₃) ₃ ·6H ₂ O and citric acid (C ₆ H ₈ O ₇ ·H ₂ O) stoichiometric ratio of 1:1:1.5, v) dried, 80 °C; vi) thermal	GdMnO ₃ , GdMn ₂ O ₅ , Gd ₂ O ₃ ; 20.458 m ² ·g ⁻¹ ; Mn ³⁺ /Mn ²⁺ XPS molar ratio 1.43; Mn ⁴⁺ /Mn ³⁺ XPS molar ratio 0.77	50 mg of catalyst, 50 ml·min ⁻¹ (1000 ppm VOCs mixture), GHSV of 60 000 ml·g ⁻¹ ·h ⁻¹ , 300 °C	Toluene conversion: 96 %; 2-ethoxy-ethanol conversion: 96 %	(M. Guo et al., 2021)

Mn-based waste	Catalyst synthesis	Relevant properties	Catalytic test conditions	Catalyst activity	Ref.
	treatment, 200 °C (2 h), 750 °C (3 h) i) leaching stage, 20 g·L ⁻¹ of solid-liquid ratio, 1.5 mol·L ⁻¹ of citric acid, 0.3g·g ⁻¹ of glucose and 80 °C; ii) precipitation, g oxalic acid was added into 80 ml of acid leaching solution; iii) metal solution preparation, precipitated, 30 ml dilute of HNO ₃ ; iv) 1.5 times stoichiometry of citric acid; v) dried, 80 °C; vi) thermal treatment, 200 °C (2 h), 750 °C (3 h)	Cu _{1.5} Mn _{1.5} O ₄ ; 185.892 m ² ·g ⁻¹ ; Mn ³⁺ /Mn ²⁺ XPS molar ratio 1.67; Mn ⁴⁺ /Mn ³⁺ XPS molar ratio 0.65		Toluene conversion: 96 %; 2-ethoxy-ethanol conversion: 92 %	
Spent lithium-ions manganate batteries	i) leaching stage, 20 g·L ⁻¹ of solid-liquid ratio, 1.5 mol·L ⁻¹ of citric acid, 0.3g·g ⁻¹ of glucose and 80 °C; ii) 80 mL acid leaching solution, 6g oxalic acid; iii) metal solution preparation, precipitated, 30 ml dilute of HNO ₃ ; iv) doping stage, 10 % Ce/total amount of active metal ions	Mn ₅ O ₈ , Mn ₂ O ₃ , 34.894 m ² /g; Mn ⁴⁺ /Mn ³⁺ XPS molar ratio 0.87	50 mg of catalyst, 50 ml·min ⁻¹ (1000 ppm VOCs mixture), GHSV of 60 000 ml·g ⁻¹ ·h ⁻¹ , 300 °C	1-methoxy-2-propyl acetate conversion (220 °C): 100 %	(M. Guo et al., 2020)
Spent alkaline batteries	i) H ₂ SO ₄ (0.5% v/v), solid/liquid ratio: 1/60 (gr/ml), 70 C for 4 h; ii) filtrated and dried 110 °C for 12 h; iii) thermal treatment, 600°C, 12 h	DRX phases: Mn ₂ O ₃ , BET surface area: 51.6 m ² /g,	Thermal combustion: 300 °C, BTC contaminated Air 200 ml/min, Catalyst 2 g.	98, 96 and 44% for benzene, toluene and xylene,	(Hoseini, Rahemi, Allahyari, & Tasbihi, 2019)

Mn-based waste	Catalyst synthesis	Relevant properties	Catalytic test conditions	Catalyst activity	Ref.
Spent alkaline batteries	i) H ₂ SO ₄ (0.5% v/v), solid/liquid ratio: 1/60 (gr/ml), 70 °C for 4 h; ii) filtrated and dried 110 °C for 12 h; iii) thermal treatment, 600°C, 12 h; iv) wet impregnation, 1.5 h, 10 % MnO ₂ /Al ₂ O ₃ ; v) thermal treatment, 600 °C for 3 h.	DRX phases: Mn ₂ O ₃ , Al ₂ O ₃ ; BET surface area: 116.8 m ² /g; EDX atomic composition: 8.07 % C, 48.46 % O, 39.23 % Al, 3.63 % Mn, 0.62 % Zn.	Plasma combustion, BTC contaminated Air 200 ml/min, Catalyst 2 g, Voltage 10 kV, High voltage electrode was a steel rod, ground electrode was an aluminum sheet	97.82, 99.59, 74 % for benzene, toluene and xylene,	
	i) cathode separation; ii) H ₂ SO ₄ (0.5% v/v), solid/liquid ratio: 1/60 (gr/ml), 70 °C for 4 h; iii) filtrated and dried 110 °C for 12 h; iv) thermal treatment, 600°C, 12 h		Plasma combustion, BTC contaminated Air 200 ml/min, Catalyst 2 g, Voltage 10 kV, High voltage electrode was a steel rod, ground electrode was an aluminum sheet	98.55, 98.07 and 57.99% for benzene, toluene and xylene,	(Hoseini, Rahemi, Allahyari, Tasbihi, & Gharehabani, 2020)
waste alkaline batteries	i) cathode separation, ii) washing stage, S/L 2/50 g/ml, 150 rpm for 5 h at around 25 °C.; iii) filtration and dried, overnight at 80 °C in an oven; iv) thermal treatment, 400 °C, 4 h, furnace.	DRX phases: Mn ₃ O ₄ , ZnMn ₂ O ₄ , C ₂ K ₂ , ZnO, BET surface area: 17.66 m ² /g; EDX atomic composition: 9.15 % C, 17.9 % O, 1.2 % Na, 0.20 % K, 1.29 % Al, 0.66 % Si, 0.83 % Cl, 41.37 % Mn, 5.84 % Fe, 21.56 % Zn	60 mg catalyst, VOC 1,000 ppm, GHSV of 40,000 h ⁻¹ , 450 °C	100 % benzene, 100 % o-xylene	(Park, Kim, et al., 2021a)
Spent alkaline battery	i) cathode separation; ii) 0.1 N H ₂ SO ₄ , S/L 3g/200 mL; iii) filtration, washed (pH 7) and dried (80 °C, 24 h); iv) thermal treatment, 400 °C, 4h, furnace.	DRX phases: ZnMnO ₂ , Mn ₃ O ₄ , C, C ₂ K ₂ ; BET surface area: 45.16 m ² /g; ICP/OES Wt. % composition: 35.37 % Mn, 13.58 % Zn, 4.68 % Fe, 0.26 % K.	60 mg, VOC 1000 ppm, gas hourly space velocity of 40,000 h ⁻¹ , 340 °C	Toluene 100 %	(Park, Song, et al., 2021)
	i) cathode separation; washed	DRX phases: ZnMnO ₂ , Mn ₃ O ₄ ,		Toluene 8 %	

Mn-based waste	Catalyst synthesis	Relevant properties	Catalytic test conditions	Catalyst activity	Ref.
Zn-C and Zn-Mn battery	(pH 7) and dried (80 °C, 24 h); iv) thermal treatment, 400 °C, 4h, furnace.	C, C ₂ K ₂ , ZnO; BET surface area: 17.66 m ² /g; ICP/OES Wt. % composition: 27.74 % Mn, 23.37 % Zn, 3.14 % Fe, 0.22 % K, 0.07 % Pb.			
	i) Cathode separation; ii) leaching, H ₂ SO ₄ , 180 rpm, 68 °C; iii) Precipitation, NaOH, 3 h, 60 °C, pH 10.	BET surface area: 4.98m ² ·g ⁻¹ ; XPS atomic composition: 21.7 % C, 59.5 % O, 5.8 % Mn, 7.3 Fe, 5.7 Zn	3 cm ³ (d= 0.6–1.2 mm) of catalyst, liquid flow of 3 cm ³ h ⁻¹ , 460 °C	1-butanol conversion: 100 %	(Winiarska et al., 2019)

1.4 Concluding remarks

In general, a knowledge gap is detected in carrying out an in-depth analysis of the nature and behavior of catalysts, although a series of processes are mentioned that improve the morphological and physicochemical characteristics of these catalysts against the oxidation of different hydrocarbons, there is no evidence of further study that is linked to the kinetics and reaction mechanisms involved during combustion processes. Similarly, no information is found on an experimental development that evidences the possible existence of mass transfer limitations in the synthesized catalysts. Another aspect to take into account is that, in general, the different research groups focused their attention on aromatic hydrocarbons, leaving aside the alkanes that cause high environmental pollution, such as methane. Added to this, no development of pilot tests of MnO_x catalysts recovered from spent battery cathodes for possible use at an industrial level was found.

1.5 Acknowledgment

Funding: This work was supported by Agencia Nacional de Hidrocarburos -ANH- and Minciencias, Colombia, within the frame of the projects 1102-721-50962: “Desarrollo de alternativas catalíticas para la reducción y valorización de emisiones de gases de efecto invernadero típicas de pozos y refinerías petroleras por combustión catalítica de VOCs y transformación de CO₂ y CH₄ en gas de síntesis”.

2. Single step synthesis of MnO_x nanorods from spent batteries used for the combustion of methane

Manganese oxides have become one of the most investigated materials for the catalytic combustion of hydrocarbons owing to their lower cost, higher thermal stability, and larger availability than noble metals. The multivalent nature of Mn allows it to produce MnO₆ octahedra that arrange in diverse polymorphs such as α , β , δ , γ , and ϵ -MnO₂ as well as α and γ -Mn₂O₃, and Mn₃O₄ (Reidies, 2000; C. Zhou et al., 2018). Previous studies have demonstrated that MnO_x nanostructures are more reactive towards hydrocarbons combustion as compared to larger-scale undefined morphologies (Akbari, Alavi, Rezaei, & Larimi, 2021; K. Zhang et al., 2019a). Most of the explanations for such an improvement are based on considerations that take into account the total specific surface area of the material, the presence of surface defects such as oxygen vacancies in the crystal lattice, the type and morphology of crystal structure, the degree of oxidation of

manganese and the number of surface active sites (Gangwar & Rath, 2021; K. Li et al., 2019; Liang, Teng, Bulgan, Zong, & Zhu, 2008; L. Sun et al., 2021). Conventional routes for producing these oxides are the precipitation of manganate salts, solution combustion, hydrothermal synthesis, or sol-gel routes which demand the use of structure directing agents (Bach et al., 1990; Lyu et al., 2020b; Piumetti et al., 2015; W. Zhang & Cheng, 2007a). On the other hand, taking advantage of the fact that alkaline Zn-Mn batteries have a relatively higher loading of Mn per gram of battery than other batteries, several investigators have proposed recycling manganese from spent Zn-Mn batteries to upgrade this problematic waste into MnO_x-based catalysts within the frame of circular economy principles (Işıldar et al., 2018; Z. Sun et al., 2017) and partly as a response to the constant growing demand for manganese, whose reserves are starting to decrease (Işıldar et al., 2018; Z. Sun et al., 2017).

Focusing on the purity of MnO_x, two hydrometallurgical ways of upcycling the cathode of spent Zn-Mn batteries have been successfully proved: first, the selective dissolution of the metals or cations of the cathode powders, leaving a solid based solely on MnO_x (Park, Kim, et al., 2021b), and second, the total dissolution of the cathode powder followed by the selective precipitation or electrodeposition of Mn compounds (Abid Charef et al., 2017b; Park, Song, et al., 2021). Among those hydrometallurgical processes, although the second option involves the use concentrated acid solutions, reductant agents, more than two chemical steps and various unit operations (W. Zhang & Cheng, 2007b), the first one is rarely used to synthesize catalyst because the resulting solids have a hetero-composition and irregular morphology, which is related to a low oxidant capacity. However, one argument to re-evaluate the efficiency of such selective dissolution to prepare the catalyst is the possibility that the contamination of the cathode powder such as graphite may play a role in the formation MnO_x-based crystalline nanostructures. In this sense, some researchers

have found that graphite promotes the formation of crystalline nanostructures based on MnO_x at acidic pH (X. Liu, Shi, Jiang, Zhang, & Huang, 2018; Ruizhi Yang, Wang, Dai, & Chen, 2005).

We thus took advantage of the fact that the cathodes of spent alkaline Zn-Mn batteries contain between 3 to 5 % wt. of graphite and performed a single step acid treatment to produce MnO_x-based nanorods. Motivated by the interesting morphology and physicochemical properties of these MnO_x-based nanorods synthesized, and knowing that methane is a greenhouse gas whose potential is ~20 times higher than that of CO₂ (L. He, Fan, Bellettre, et al., 2020), the produced materials were tested in the catalytic combustion of methane in a continuous fixed bed reactor under kinetic regime. Among the produced materials, MnO₂-based nanorods were as efficient as a pure g-MnO₂-based benchmark catalyst for the combustion reaction. The analysis of the characteristics of the materials and of the catalytic performance allowed proposing how each one of the crystalline phases of the produced manganese oxides contributes to the methane reaction rate.

2.1 Materials and Methods

2.1.1 Materials

All the reagents used were analytical grade. The spent household AA type Zn-Mn alkaline batteries of 3 commercial brands (Energizer, Duracell and Varta) were taken from a recycling point in the UIS campus, Bucaramanga, Colombia. Water type 1 was collected from an OmniaPure equipment (Stakpure). Sodium hydroxide pellets (NaOH, ≥ 97 %), concentrated sulfuric acid (H₂SO₄, ≥ 98 %) and granules about 1-2.5 mm of Silicon dioxide (SiO₂, ≥ 97 %) were purchased

from Merck. Commercial γ -MnO₂ ($\rho_{\text{App}}=1800 \text{ g/m}^3$, particle size $<100 \text{ }\mu\text{m}$) used as benchmark catalyst was provided by Erachem, Comilog (Faradiser M, LOT 622). CH₄, O₂, and N₂ (Grade 5.0) was provided by Linde Colombia. The Whatman® qualitative filter paper, Grade 1, was provided by Merck. The potassium bromide (KBr, $\geq 98 \%$) was provided by Merck.

2.1.2 Methods

2.1.2.1 Cathode recovery from spent batteries. The cathode used for the nanorods synthesis was recovered from the spent batteries. The batteries were manually dismantled, removing the pvc label, the conjunct of negative terminal/collector/ protective layer, the steel case, and finally, separating the cathode black mass from the ion separator and the anode (Fig S12). Mass balance details of the batteries dismantling are shown in Table S5. By analysis of the mass balance, a correlation between the cathode and anode specific weight and the batteries residual voltage was established as is presented in Fig. S1 and discussed in Supplementary text. The cathode black mass was then macerated to reduce its particle size until the range 45-180 μm . The resultant powder was rinsed five times to remove soluble ionic impurities (based on K, Cl, Na, Fe, among others), each one, by suspension of the solids into type 1 water maintaining a solid:liquid (S:L) ratio of 1 g:100 ml, during 30 min, under constant agitation of 800 rpm and temperature of 25 °C. After each rinsed, the wet solids were separated by filtration. After the last filtration, or when the conductivity of the water used was not up to 0.005 μS , the wet solids were dried in an oven at 120 °C in overnight. The resultant raw cathode powder was optionally washed with a 6M NaOH solution assuring a solid:liquid (S:L) ratio of 1 g:100 ml, a temperature of 80 °C and a residence time of 3 h. The NaOH-washed of the cathode was also by suspension and posterior filtration. The

chemical effect of the NaOH washing over the cathode has been documented in the literature (Abid Charef et al., 2017b). After that, the solids were again rinsed five times with type 1 water, and dried, as commented above. So, two types of cathode powder were obtained: raw and NaOH-washed.

2.1.2.2 Single step synthesis of nanorods. The cathode powder, raw or NaOH-washed, was suspended in a 2 M H_2SO_4 solution under constant temperature and agitation of 80 °C and 300 rpm, respectively, for 3 h, maintaining a S:L ratio of 1 g:10 ml. During this acid treatment, the pH, conductivity and ζ -potential of the leach liquor were sensed using a pH-Meter (Hanna Instruments). After the acid treatment, the suspension was decanted and filtered. The filtered leach liquor was analyzed by UV-Vis spectrometry and atomic absorption spectrometry, as it is described in the characterization section. On the other hand, the filtered solids were rinsed five times until removing all soluble ions (as described previously), and dried until eliminating all moisture. Finally, the dried powder was calcined under continuous airflow of 100 ml min^{-1} following the next temperature program: 6 h isotherm at 120 °C (5 °C· min^{-1}), 6 h isotherm at 500 °C (5 °C· min^{-1}), and natural cooling. Two types of nanorods were obtained, MnO_2 -based from the raw cathode, and Mn_2O_3 -based from the NaOH-washed cathode. The general flowsheet of the cathode powder processing until the nanorods obtention is presented in Fig. S13.

2.1.2.3 Characterization tests

UV-Vis spectroscopy analysis

The nature of the species presents in the leachates were analyzed by UV-Vis spectroscopy using a Genesys 10s UV-VIS (Thermo Scientific) in the range of wavelength between 200-800 nm. For the analysis the liquid samples were placed on 10 mm path length cuvettes.

Atomic absorption spectroscopy (AAS) analysis

The amount of Zn and Mn in leachates and solids from leaching processes were determined by AAS using an AGILENT SPECTRAA 240 S by flame mode (air-acetylene-nitrous oxide). Prior to the analysis, the solids were dissolved by mixing with 40 % Wt. hydrofluoric acid solution in S:L ratio of 1 g:10 mL, under constant agitation of 300 rpm and temperature of 70 °C.

N₂-Physisorption analysis

The surface area porosity of the samples was assessed by adsorption-desorption isotherms of molecular nitrogen at -196°C. For these measurements, samples of ca. 0.1500 g of each material were weighed inside 9 mm diameter cells made of borosilicate glass (Micromeritics). After weighing, the cells were placed in an outgassing unit (Vac Prep 061, Micromeritics) and heated for 2 h at 200°C in order to remove adsorbed gases. The duration of the outgassing procedure was defined after finding that the vacuum in the cells reached ca. 0.05 mbar. The recorded weight of the outgassed samples was used as input data for recording the adsorption-desorption isotherms. The adsorption-desorption isotherms for each sample were measured in a 3FLEX™ (Micromeritics) instrument. Data were recorded in the relative pressure range (P/P_0) between 0.0025 and ~0.9900 using an equilibration time of 10 s. The total pore volume and the pore size distributions were calculated with the Barret-Joyner-Halenda (BJH) method produced distribution

can only be considered for comparison purposes since the software is restricted to pores with cylindrical geometry. In addition, the total specific surface area -SSABET- of the solids was estimated by the Brunauer-Emmett-Teller, BET, method.

Scanning Electronic Microscopy (SEM) and Energy-Dispersive Spectroscopy (EDS) analysis

The morphology was observed by SEM using a QUANTA FEG 650 microscope dotted with an Everhart Thornley detector (ETD) and a Back scattered electron detector (BSED) type SSD, operating at a high vacuum with an acceleration voltage of 25 KV. The analyzed samples were placed on top of carbon adhesive tape and coated with gold for alleviating differential charging effects during the tests. During the microscopy runs, a semiquantitative analysis to obtain the chemical composition was made by SEM-EDS using an EDAX APOLO X detector with a resolution of 126.1 eV (Mn $K\alpha$) and the EDX Genesis software.

Infrared Spectroscopy (FTIR) analysis

The chemical groups were analyzed by FTIR using a Nicolet iS50 Fourier Transform Infrared spectrometer (ThermoScientific) using tablets of 1 % Wt. of the material in KBr. The tables were prepared by tableting in a hydraulic press using a compression force of 5 tons for 2 min.

X-ray diffraction (XRD) analysis

The crystalline structure was recorded by XRD using a D8 advance X-ray diffractometer (Bruker) that works at 40 kV y 40 mA with Cu $K\alpha$ 1 radiation, taking the XRD patterns between $2\theta = 2.0$ and 70° , with a step time of 0.6 s which corresponds to a 2θ step of 0.02035° . The diffractometer was equipped with a 2.5° Soller slit, 0.6 mm divergence slot, 0.02 mm nickel filter, and a LynxEye detector. The analysis of the recorded diffractograms was done with the MATCH[®]

software. A Rietveld refinement allowed a better estimation of the unit cell and crystal system (Table S1). It was performed using a wavelength of 1.541874 Å and a Cu-K α radiation source, using a FullProf refinement intentionally focused on analyzing only the MnO $_x$ crystalline phases. Parameters as the Chi-square (χ^2) and the final weighted average Bragg R-factor were considered during the Rietveld refinement.

Temperature-Programmed Reduction (H $_2$ -TPR) analysis

The H $_2$ -TPR assays were carried out using an automated reaction system (CATLAB, Hiden Analytical) coupled online to a Mass Spectrometer QGA (Hidden Analytical), which is thoroughly described by Velasco-Rozo *et al.* (Velasco-Rozo, Ballesteros-Rueda, & Baldovino-Medrano, 2021). The MS was equipped with both an internal dual electron multiplier detector, SEM, and a Faraday detector, and with a precision quartz inlet heated capillary (QIC) sampling interface. For the H $_2$ -TPR analysis, the CATLAB quartz microreactor was loaded with 50 mg of sample and heated from 20 to 700 °C (2 °C min $^{-1}$) under a 50 mL·min $^{-1}$ continuous flow of 4 % V/V H $_2$ in Ar. The samples analyzed were pretreated at 500 °C in a continuous flow of 4 % V/V O $_2$ in Ar during 2 h. The consumption of hydrogen and the production of water were followed on-line with the MS. The sensitivity factors provided by the Hiden QMS library were used for quantification. The instrument was calibrated with H $_2$ pulses of 10 μ L for quantification purposes.

Temperature-Programmed Desorption (O $_2$ -TPR) analysis

The O $_2$ -TPD assays were carried out in the same CATLAB microreactor described before, using 50 mg of sample and heating from 20 to 700 °C (2 °C min $^{-1}$) under a continuous flow of Ar. The samples analyzed were pretreated at 500 °C in a continuous flow of 4 % V/V O $_2$ in Ar during 2 h. The consumption of oxygen was followed on-line with the MS. The sensitivity factors

provided by the Hiden QMS library were used for quantification. The instrument was calibrated with O₂ pulses of 10 μL for quantification purposes.

X-ray photoelectron spectroscopy (XPS) analysis

Surface elemental composition and chemical speciation of the materials were assessed by XPS. The spectra were recorded in the XPS/ISS/UPS-A.Centeno surface characterization platform (SPECS). The platform is equipped with a PHOIBOS 150 2D-DLD analyzer and a monochromatic Al K α X-ray source (FOCUS 500). The X-ray source was operated at 100 W and 12 kV. For the analyses, the samples were deposited on a carbon conductive tape which was mounted on a metallic sample holder. For the spectra record, the pass energy of the analyzer was set at 100 eV and the energy step equal to 1.000 eV, for recording general surveys and 15 eV, energy step equal to 0.050 eV, for recording high-resolution spectra of specific core lines. The over-charge due to the photoelectron emission process was compensated with an electron flood gun (FG 15/40-PS FG500) operated either between 1-10 eV or between 58-70 μA. The stability of the samples during the analyses was verified by taking spectra from the C 1s core level at the beginning and at the end of each run. Quantification of species was made in the CasaXPS software (Casa Software Ltd.) using U 3 Tougaard (Walton, Alexander, Fairley, Roach, & Shard, 2016) type baseline and LA(y₁,y₂) line shapes.

2.1.2.4 Catalytic evaluation. The catalytic tests based on the methane combustion were carried out in a continuous fixed-bed quartz tubular reactor (i.d. 1.04 cm) fed by a set of independent mass flow controllers (Alicat Scientific) with an accuracy of ± 0.1 % of full scale, repeatability of ± 0.08 % of full Scale, a turndown of 1:200 and a temperature sensitivity of 0.02% of full Scale / °C. The reactor temperature was controlled by a programmable logic controller

(PLC, Rockwell Automation) connected to a concentric tubular furnace and a thermocouple placed inside the catalytic bed. The outlet of the reactor was connected online to a Gas Chromatograph (GC-2014 instrument, Shimadzu Corporation) to make the online analysis of the reaction products. The GC was provided with a set of packed columns and with a TCD-Methanizer-FID array for detection and quantification. The scheme of the reactor system is presented in Fig. S15. The gaseous stream from the reactor outlet was analyzed every ~20 min. In each catalytic test, the reactor was loaded with a bed composed of a 1:10 weight ratio mixture of catalyst (40-180 μm) and SiO_2 (40-60 μm) particles. The use of quartz as a diluent avoids artifacts due to temperature gradients. Further homogenization of the temperature of the reactor as well as reaching plug-flow in the system was achieved by placing a glass wool plug on top of the catalytic bed. The catalytic bed was dried in situ at 120 $^\circ\text{C}$ (5 $^\circ\text{C min}^{-1}$) for 90 min with a flow of 90 ml min^{-1} N_2 at a space velocity of 108000 $\text{ml g}^{-1} \text{h}^{-1}$. Then, the reactor feed was changed by a mixture of CH_4 (7.7 % V/V.), O_2 (18.4 % V/V), and N_2 as gas balance, keeping the same flow conditions mentioned above. The temperature of the reactor was raised to 500 $^\circ\text{C}$ (5 $^\circ\text{C min}^{-1}$), which was the selected reaction temperature, after the complete stabilization of the flow fed to reactor. The reactions had a duration of 6 h. The reactor effluents were intentionally analyzed by chromatography before and after the reaction to quantify the feed of the reaction. The reaction conversion was determined by comparing the feed analysis with the reaction products analysis. In a typical test, reaction products started to appear from 300 $^\circ\text{C}$. The details of the reaction system including GC conditions and calibration, and the quantification method can be extended by Sandoval-Bohorquez et al. (Sandoval-Bohorquez, Rozo, & Baldovino-Medrano, 2020).

2.1.2.5 Experimental specific reaction rate calculation. To analyze the catalytic activity, some parameters were calculated. The feed and product analyzed by GC allowed to calculate the reactant conversion using Eq. S1:

$$X_{reac}(\%) = \frac{F_{reac}^0 - F_{reac}}{F_{reac}^0} * 100\% \quad \text{Eq. S1}$$

Where F_{reac}^0 and F_{reac} are the molar flow (mol h⁻¹) of reactant at inlet and outlet of the reactor, respectively. Additionally, from conversion assuming that the reactor operates in a differential form (i.e. conversions below 15 %), the specific reaction rate (r_{CH_4} , mol g⁻¹ h⁻¹) was determined by Eq. S2.

$$R_{reac} = \frac{F_{reac}^0 X_{reac}}{W} \quad \text{Eq. S2}$$

Where W is the weight of the catalyst (g).

2.1.2.6 Theoretic activity calculation of a mixture of crystalline phases. The activity of a catalyst composed by a mixture of crystalline phases is not commonly calculated as the sum of the individual contributions of each phase to the total activity. As in the present work, the materials catalytically tested were composed by several crystalline phases, and it is known that each known phase has a particular activity, we proposed an alternative method to determine the individual contribution of each phase to the total activity. For that, the total activity must be expressed as the sum of the activity of each phase as in Eq. S3.

$$R_j = \sum_i^n (R_{ij}) \quad \text{Eq. S3}$$

Where R_j is the experimental activity of material j , R_{ij} is the activity of the phase i in the material j , and n is the total number of the phases in the material j . Then, the activity of each phase

must be expressed in terms of the mass or molecular fraction of each phase in the material (f_{ij}) and a metric called *activity factor* (\aleph_i) that represent the normalized specific activity of each phase, as is described in Eq. S4.

$$R_{ij} = f_{ij} \times \aleph_i \quad \text{Eq. S4}$$

In a system with several materials and phases, the Eq. S4 can be written as Matrix S1.

$$\begin{pmatrix} f_{11} & f_{21} & \cdots & f_{i1} \\ f_{12} & f_{22} & \cdots & f_{i2} \\ \vdots & \vdots & \vdots & \vdots \\ f_{1j} & f_{2j} & \cdots & f_{ij} \end{pmatrix} \times \begin{pmatrix} \aleph_1 \\ \aleph_2 \\ \vdots \\ \aleph_i \end{pmatrix} = \begin{pmatrix} R_1 \\ R_2 \\ \vdots \\ R_j \end{pmatrix} \quad \text{Matrix S1}$$

Note that for the system of equations to be solvable, i must be less than or equal to j . By solving the Matrix S1, it is possible to know the *activity factor* for all the phases. With these values, not only is known the individual contribution of each phase, but could be possible to predict the activity of others materials composed by the same crystalline phases.

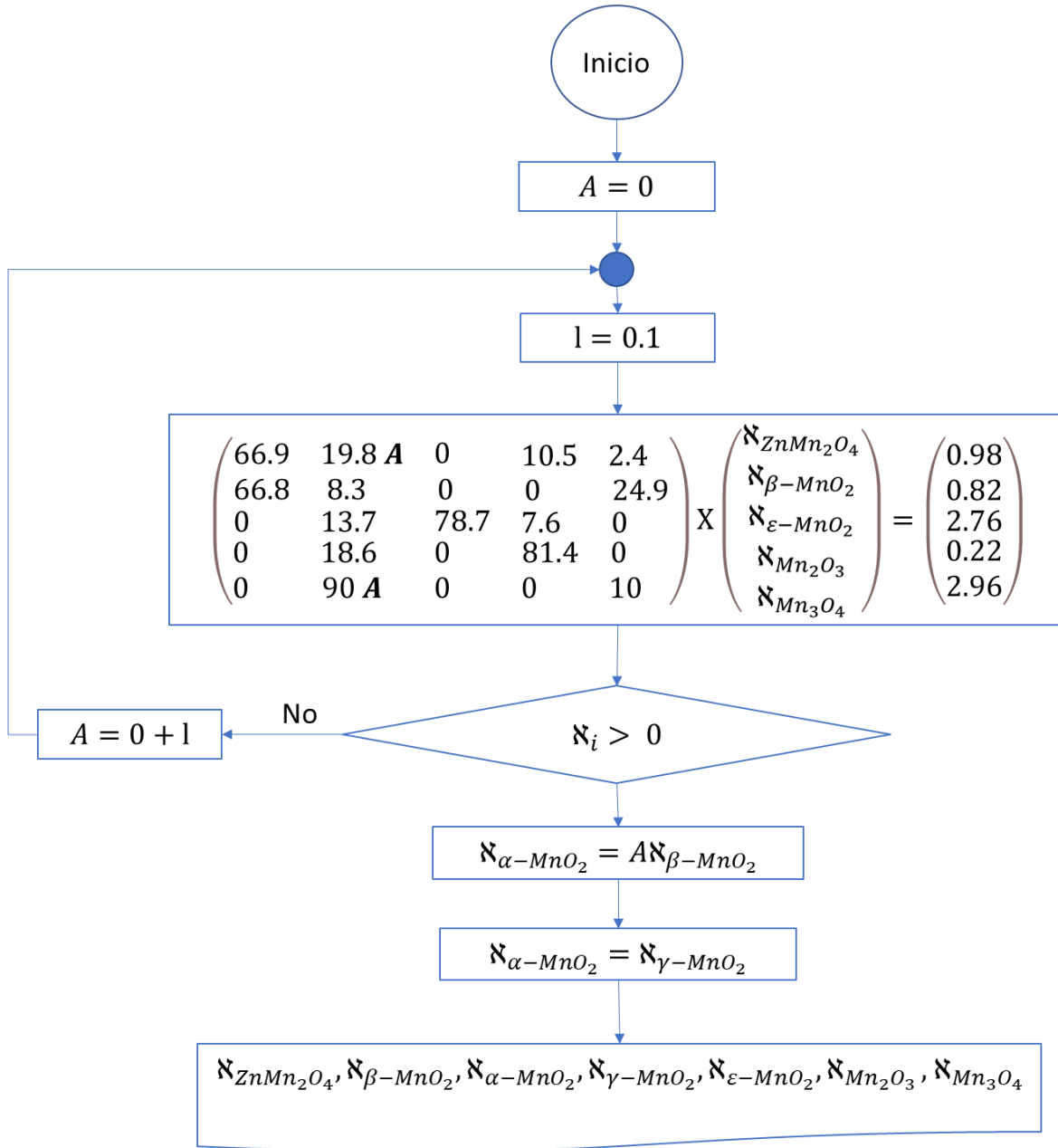
2.1.2.7 Activity factor calculation of the individual crystalline phases in MnOx-based materials. As commented above, the activity of the MnOx materials synthesized in this work was determined in terms of the specific reaction rate. Moreover, the molecular fraction of each phase was determined by XRD Rietveld analysis (Table S1). Given that the number of the crystalline phases was less than the number of materials, the next suppositions were made:

- i) $\aleph_{\alpha-MnO_2} \approx \aleph_{\gamma-MnO_2}$
- ii) $\aleph_{\alpha-MnO_2} \approx A \aleph_{\beta-MnO_2}$, where A is a proportionality coefficient
- iii) $\aleph_i > 0$, which means that no crystalline phase has inhibitory effects on the global specific reaction rate.

By using these suppositions and replacing the values of f_{ij} and R_j in the matrix S1, the next algorithm was run to determine the *activity factors*:

Figure 4.

Method to calculate the activity factors of the crystalline phases presented in MnOx-based materials synthesized in this work



2.2 Results and discussion

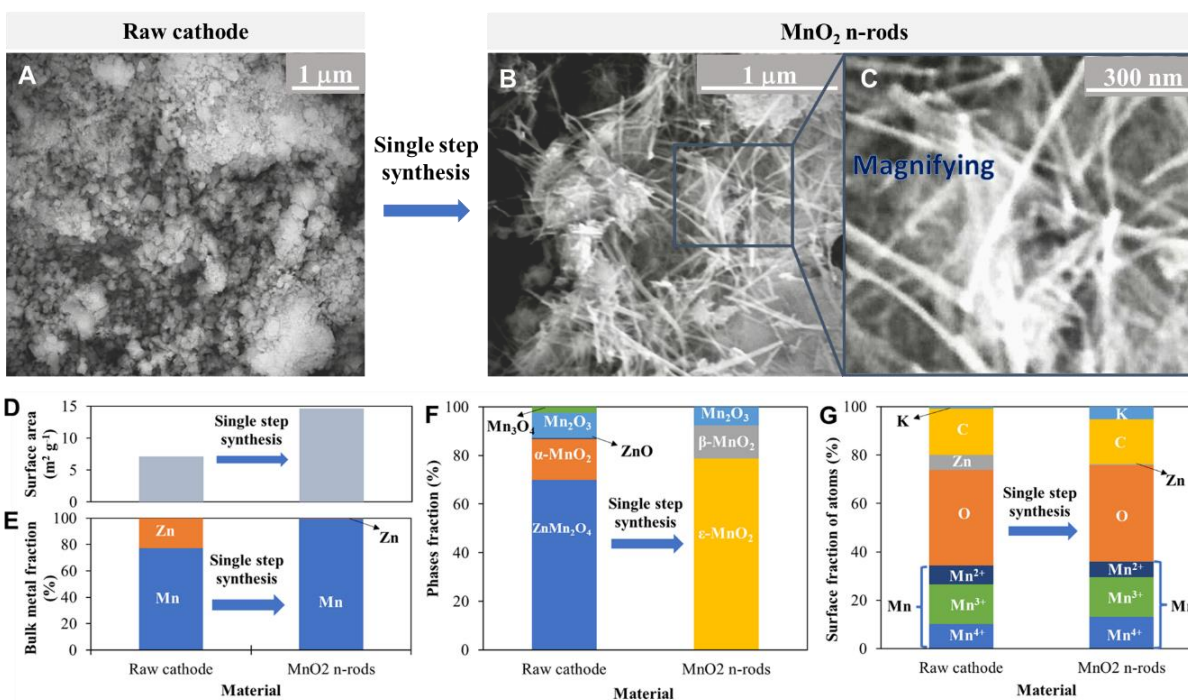
2.2.1 MnO_x -based nanorods

MnO_x -based nanorods were synthesized from the cathode powder, either raw or NaOH-washed, which was recovered from spent alkaline Zn-Mn batteries. A first type of nanorods based on MnO_2 were obtained by means of the raw cathode (Fig. 1, A to C). Specifically, these nanorods were characterized by having dimensions of 32 ± 9 nm in diameter, 693 ± 295 nm in length, and by an irregular organization pattern (Fig. 1, B and C, Fig. S1A). The composition of the observed nanorods was mainly based on a rare crystallographic phase, ϵ - MnO_2 (78.7 %), and on β - MnO_2 (13.7 %) and Mn_2O_3 (7.6 %), according to X-ray diffraction (Fig. S2) and Rietveld refinement (Table S1) analysis. The above composition was coherent with the Fourier-transformed infrared spectroscopy (Fig. S3) spectra of the materials showing bands for the Mn-O, Mn-O-Mn, Mn-OH, and Mn-O-OH bonds. The latter agreed with previous reports concerning nanostructures of MnO_x produced by other synthetic routes (Akbari et al., 2021; Ruizhi Yang et al., 2005). The bulk of the nanorods was mainly composed by Mn (53 % wt.), as measured by atomic absorption spectroscopy, (Table S2), and their surface was composed by Mn, O, C, K, and Zn with concentrations of 35.9, 40, 0.3, 18.7 and 5.1 % at., respectively, as shown by X-ray photoelectron spectroscopy results (Fig S4, Table S3). Surface manganese was found to be a mixture of Mn^{4+} (37 %), Mn^{3+} (46 %), and Mn^{2+} (17 %) species. Comparing these characteristics with those of the raw cathode, it was observed that the latter had irregular morphology (Fig. 1A, Fig. S1B), half the surface area (Fig. 1D, Fig S5, Table S4) and a larger oxides poly-composition including Zn species (Fig. 1, E to G).

A second type of nanorods were also obtained from the cathode powder (Fig. 2, A to C, Fig. S1, C and D), however, in this case, the cathode used was previously washed with a NaOH solution. Comparatively, this NaOH-washed cathode had a similar morphology (Fig 2A, fig. S1D) and textural properties (Fig 2D, Fig. S5, table S4) to the raw one, but a more reduced bulk chemical state (Fig. 2F, Table S3): higher quantity of oxides with a lower manganese oxidation state (Mn_3O_4), and a lower amount of MnO_2 , besides its lower content of ZnO and graphite. As the first type of nanorods, those from NaOH-washed cathode powder had a special morphology and a particular composition. They had 44 ± 9 nm of diameter and 389 ± 110 nm of length and were organized around a core; i.e., a sea urchin type morphology (Fig 2, A to C, Fig. S1C). Their composition was based on Mn_2O_3 (81.4 %) and $\beta\text{-MnO}_2$ (13.7 %) (Fig. S2, table S1), which was coherent with the Fourier-transformed infrared spectroscopy (Fig. S3) and atomic absorption spectroscopy (Table S2) analysis. Comparing these nanorods with those based on MnO_2 , they showed similar textural properties (Fig S5, Table S4) and bulk manganese content (Figs. 1E, 2E) but a lower Mn average oxidation state at both the bulk and at the surface (Fig. 1F, 1G, 2F and 2G). All of those characteristics found for the synthesized materials prove that the raw material was upcycled from a toxic residue to a well-defined high purity nanomaterial hence potentially contributing to fulfilling circular economy purposes (Işıldar et al., 2018; Z. Sun et al., 2017). In what follows, we discuss the chemistry that made possible the upcycling of the spent cathode powder into the produced manganese oxide nanorods.

Figure 5.

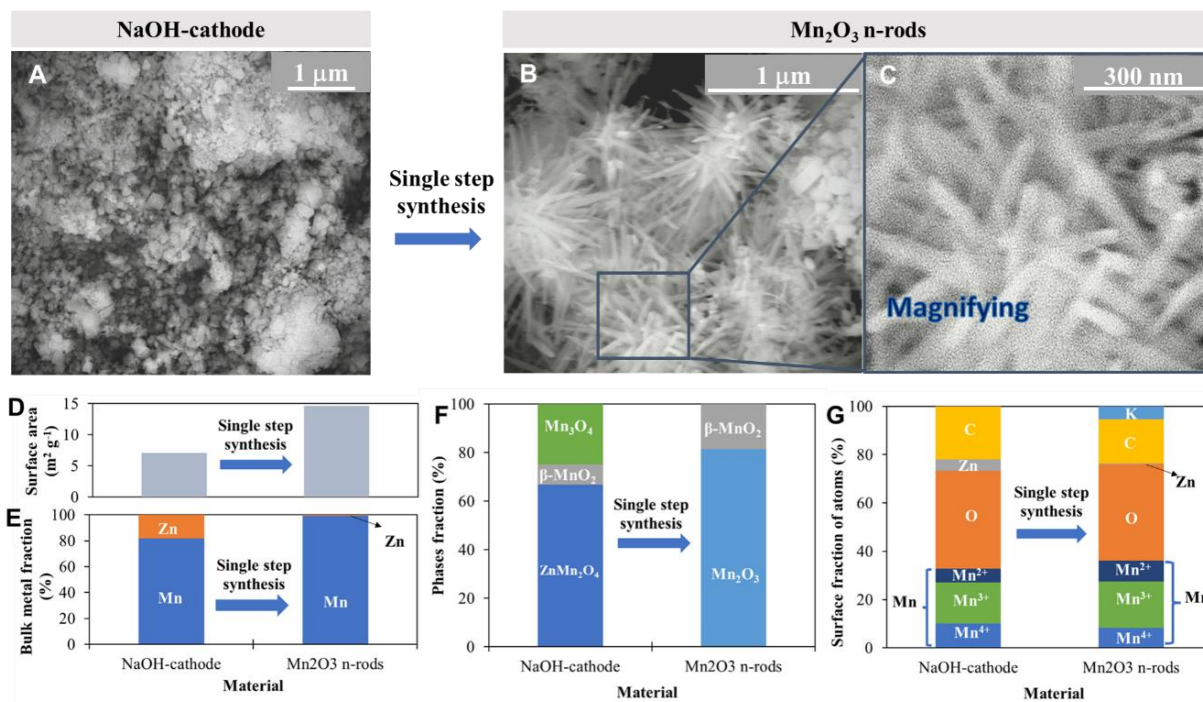
Physical and chemical properties of raw cathode and MnO₂-based nanorods (n-rods).



Note: SEM images of the raw cathode (A) and MnO₂ n-rods (B and C). Comparison between the composition of the raw cathode and the MnO₂ n-rods in terms of surface area (D), Mn bulk fraction (E), the crystalline phases fraction (F), and surface atomic composition (G).

Figure 6.

Physical and chemical properties of NaOH-washed cathode (NaOH-cathode) and MnO₂-based nanorods (n-rods).

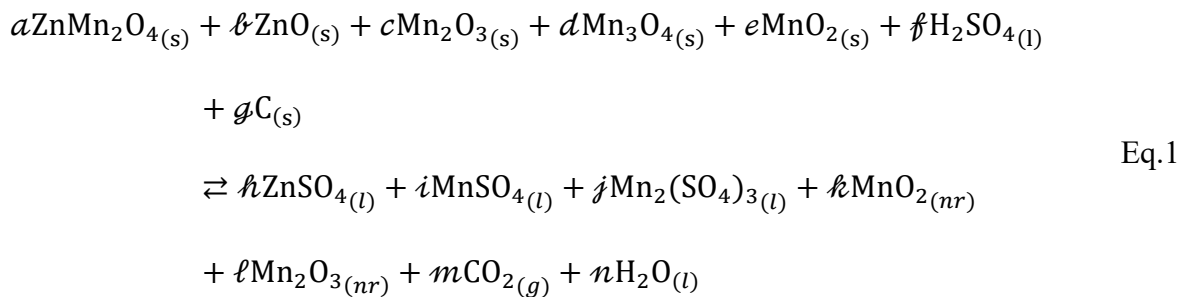


Note: SEM images of the NaOH-cathode (A) and Mn₃O₄ n-rods (B and C). Comparison between the composition of the raw cathode and the Mn₃O₄ n-rods in terms of surface area (D), Mn bulk fraction (E), the crystalline phases fraction (F), and surface atomic composition (G).

2.2.2 Chemistry of the synthesis

All the transformations that occurred in the cathode powder (either raw or after NaOH washing) in morphology and composition to become the nanorods occurred in a single step, only by exposing it to an aggressive acid medium (pH close to 0) (Fig. 3). Comparing the composition of the raw cathode with that of the MnO₂-based nanorods (Fig. 1D, Table S1), it was observed that

the acid treatment had an oxidizing chemical effect in addition to the removal of Zn species. However, that oxidation can be limited when the cathode powder has a lower bulk manganese average oxidation state, as occurred in the acid treatment of the NaOH-washed cathode that produced Mn₂O₃-based nanorods (Fig. 2D). The same oxidizing chemical effect was also observed after analysis of the leach liquors resulting from the acid treatments. It was determined that among the species dissolved by the chemical attack of the acid on MnO_x (Zn²⁺, Mn²⁺ and Mn³⁺ cations making up the sulphates), the most oxidized specie (Mn³⁺) predominated in the leach liquor from the raw cathode, as observed by UV-Vis spectrometry (Fig. S6A). Such a finding was qualitatively supported by the reddish color of the leached solution that was more intense in this treatment than in that of the NaOH-washed cathode (Fig. S6B) (Hanf, Henschel, Diehl, Winter, & Nowak, 2020; Jee, Pestovsky, & Bakac, 2010; Lee, Lee, You, Choi, & Kim, 2015). According to the evidence presented above on the transformation of cathode powder oxides and the products detected during the acid treatment, the chemical reaction that globally describes the process is represented by Eq. 1; note that the nanorods (nr) were intentionally distinguished from the solid (s), liquid (l) and gaseous (g) products.

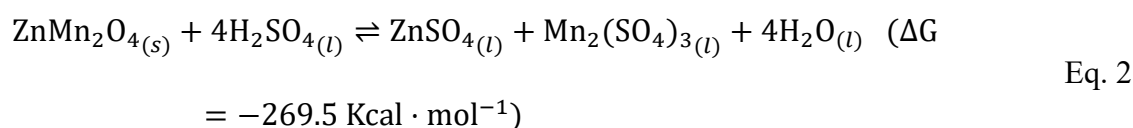


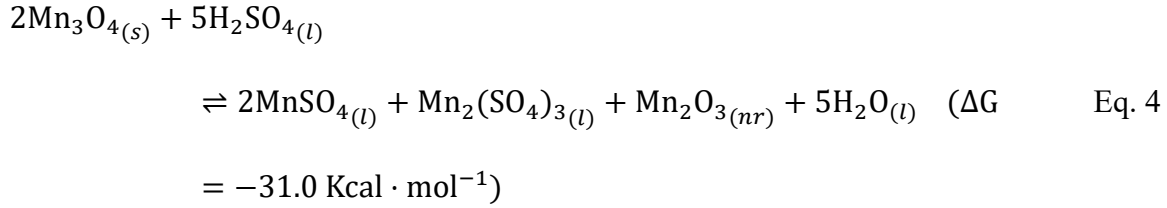
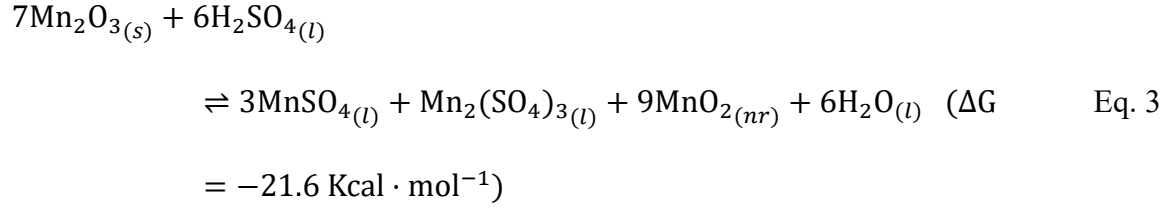
Since the pH close to 0 and the ζ -potential of 0.4 mV detected during the acid treatment, according to Mn-Zn-H₂O Pourbaix's diagram (Bischoff et al., 2020; B. R. Chen et al., 2018; Rubel et al., n.d.), favors the dissolution of MnO_x from the cathode powder (Fig. S7), and the nanorods are structurally different to the structures in the cathode (Fig. 1, A to C, Fig. 2, A to C), we proposed

that during the single-step synthesis (Eq. 1), two simultaneous chemical processes occurred: namely, the dissolution of MnO_x via the formation of ZnSO₄, MnSO₄, and Mn₂(SO₄)₃, as represented by eqs. 2 to 4, which is influenced by the composition of the cathode powder, and the crystallization of manganese into MnO_x-based nanorods. For the crystallization process, the most plausible explanation is that Mn₂(SO₄)₃ must disproportionate into MnSO₄ and MnO₂ or Mn₂O₃ depending if the cathode powder was used raw or NaOH-washed (eqs. 5 and 6), respectively (expanded analysis on Supplementary text). Additionally, the consumption of graphite (Table. S2) and the fact that a bubbling was observed during the acid treatment, it was determined that graphite acted as a co-reactant being oxidized to CO₂ during the crystallization. Furthermore, the literature shows that graphite promotes the formation of nanostructures (X. Liu et al., 2018; Ruizhi Yang et al., 2005; Zeng et al., 2016).

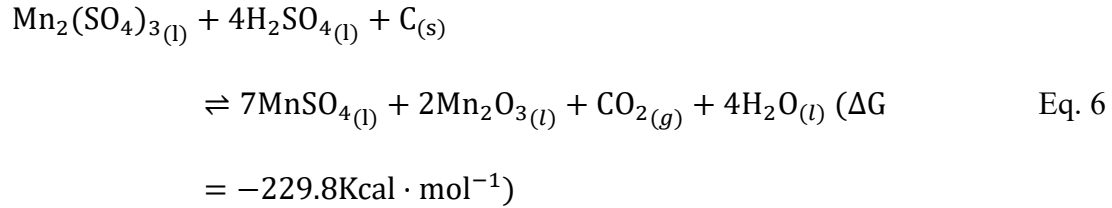
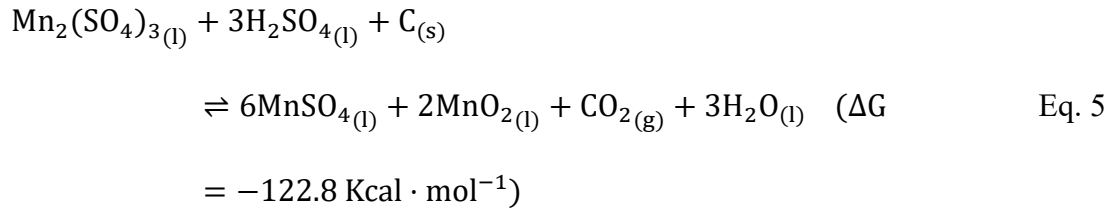
At the conditions of the single step synthesis, one may consider that the dissolution and crystallization processes are at equilibrium between themselves. An indirect proof of such an equilibrium was the stabilization of the pH, the ζ-potential, and of the conductivity of the leach liquor during the acid treatment process (Fig. S8). Moreover, the amount of dissolved Mn in the leach liquor after the acid treatment (equivalent to ~19.9 g·L⁻¹ for raw cathode and ~15.1 g·L⁻¹ for NaOH-washed) was found in the same order of the solubility of Mn²⁺ and Mn⁺³ in concentrated H₂SO₄ at 85 °C (~8.5 and 1 g·L⁻¹, respectively) (Vaudano, Pierre; Plattner, Eric; Comminellis, 1995) indicating that the synthesis was carried out near the saturation limit of the H₂O-H₂SO₄ system by ionic species.

Dissolution reactions





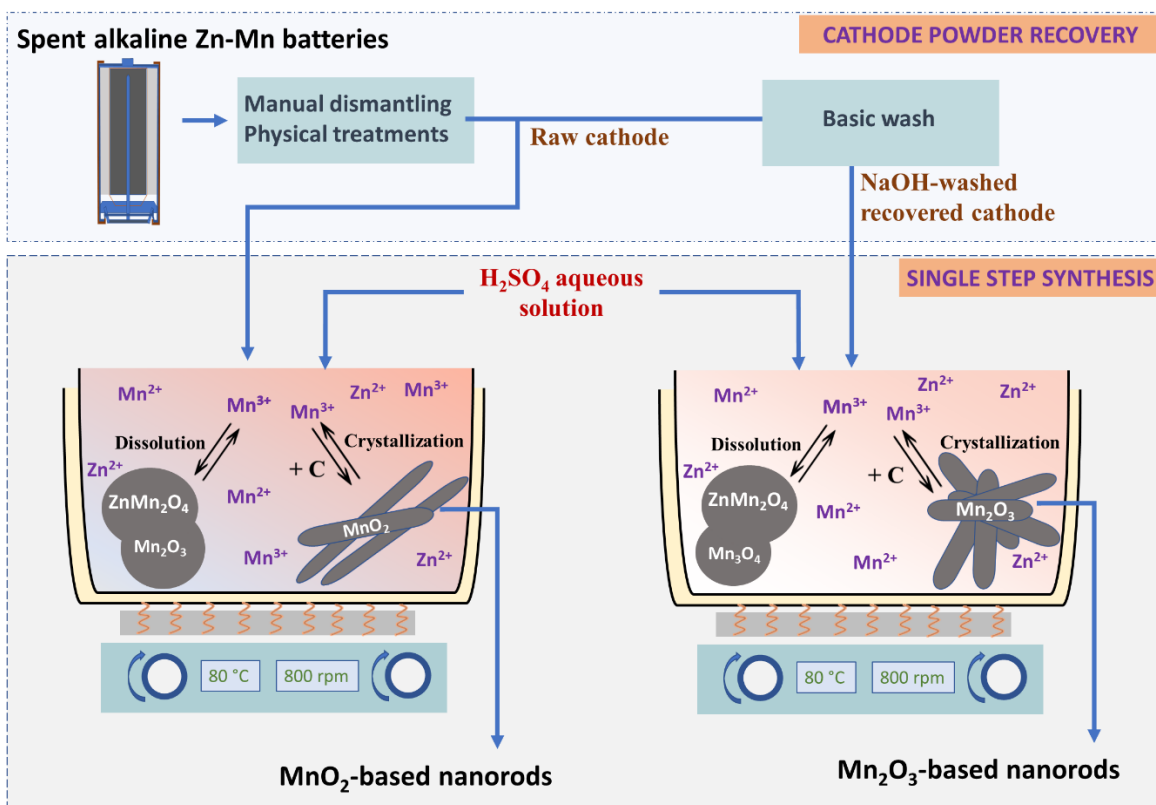
Crystallization reactions



In addition to our proposal, the transformation of ZnMn_2O_4 , Mn_2O_3 and Mn_3O_4 into MnOx has already been explained under acidic conditions (Bischoff et al., 2020; B. R. Chen et al., 2018; Rubel et al., n.d.). However, since that analysis do not apply to the formation of nanostructures with the participation of graphite, nor do that include the formation of dissolved Mn^{3+} species, these routes reported in the literature can be seen as side processes to the main ones exposed.

Figure 7.

Scheme representing the physicochemical transformations at the cathode of spent alkaline batteries during the single step synthesis of nanorods.



2.2.3 Catalytic performance

Since methane is a greenhouse gas and manganese oxides have been used for its catalytic removal, the materials developed in this work, whether recovered waste such as cathode powder or its value-added products such as nanorods, were tested in the catalytic methane combustion. Among these materials, the MnO_2 -based nanorods showed the highest specific rate of combustion of methane (R_{CH_4}): MnO_2 -based nanorods \gg raw cathode $>$ NaOH-washed cathode \gg Mn_2O_3 -based nanorods (Fig. 4 A). Moreover, in Fig 4A, the activity of the tested materials was compared

with a γ -MnO₂ benchmark (see physical properties in Fig. S1E and supplementary methods) which has shown a catalytic activity for hydrocarbon oxidation highest than other MnO₂ and Mn₂O₃ crystalline phases (Baldovino-Medrano, Kartheuser, & Gaigneaux, 2019a; Lahousse et al., 1998; Lamaita et al., 2005). It was found that the activity of MnO₂-based nanorods was very close to that shown by the γ -MnO₂ benchmark. According to the trends found in Fig. 4A, the differences in catalytic performance were neither directly correlated to the specific surface area nor to the bulk Mn content of the materials, nor to the concentration of Mn and O at the surface. Instead, the reaction rate can be estimated as the sum of the individual contributions of each crystalline phase composing the materials tested ($R_{CH_4,i}$) (Figs. 1D, 2D, 4B). These contributions were quantified defining a metric called *activity factor* (\aleph_i), see Eq. 7.

$$R_{CH_4} = \sum_i^n (R_{CH_4,i}) = \sum_i^n (\aleph_i * \% XRD\ phase_i) \quad \text{Eq. 7}$$

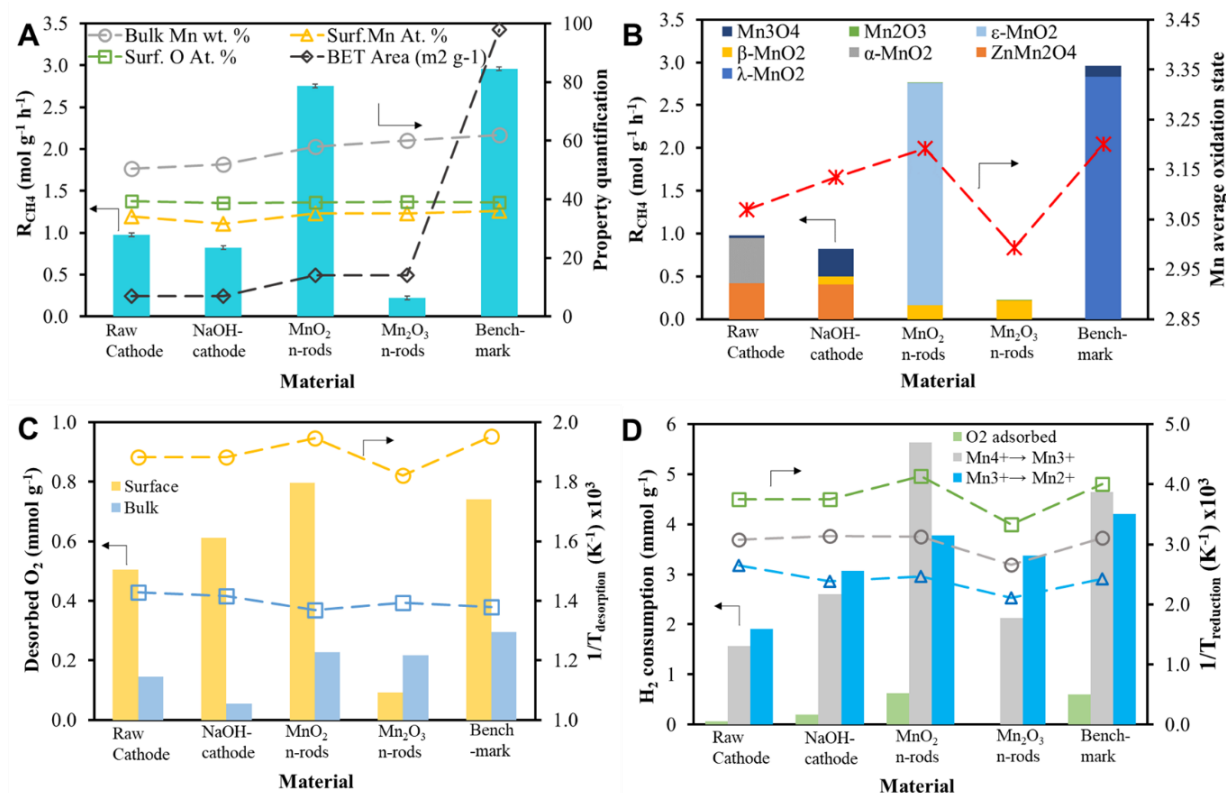
Where % XRD $phase_i$ corresponds to the percentage of each crystalline phase composing the materials tested determined by XRD Rietveld refinement. Accordingly, the following trend of \aleph_i was established: 0.033, ϵ -MnO₂ > 0.031, γ -MnO₂ \approx 0.031, α -MnO₂, \gg 0.013, Mn₃O₄ > 0.012, β -MnO₂ \gg 0.006, ZnMn₂O₄ \gg 4.08x10⁻⁵, Mn₂O₃ (quantification details are found in the supplementary methods). The statistical fitting (Fig. S9) of the metric indicated that possible synergistic effects between the different crystalline phases were negligible. The higher *activity factor* found for ϵ -MnO₂, even than for γ -MnO₂, can be related to its nanorods-like morphology, since MnO₂-based nanostructures are generally associated with a higher density of surface defects favoring oxygen mobility, which is a faculty of oxidant catalysts (Shi et al., 2012).

According to the literature, the active sites for oxidation over manganese oxides may consist of a Mn-O (or Mn-vacancy) pair site configuration (Xiuyun Wang et al., 2018). Such pair

sites can vary in terms of surface density and the strength and amount of oxygen bound to Mn, depending on the crystalline phase of the manganese oxide (C. He et al., 2019). Hence, a straightforward correlation between the average oxidation state of manganese and the apparent catalytic reaction rate was found (Fig. 4B). Further analysis on the contribution of the different oxygen species to the catalytic performance was assessed by temperature programmed oxygen desorption and hydrogen reduction profiles (Fig. S10, Fig. S11). The distinction of both surface and bulk lattice oxygen was made (Fig. S10, Fig. S11, Table S3). The analysis of the desorption and reduction profiles allowed establishing a direct correlation between the concentration of the adsorbed and surface lattice oxygen and the reaction rate (Fig. 4, C and D). In addition, the results plotted in Fig. 4, C and D showed a correlation between the reaction rate and the reducibility, expressed as the inverse of the desorption or reduction temperature. Depending on the reaction mechanisms (Xiuyun Wang et al., 2018), the control of the combustion reaction rate has been attributed to both surface lattice oxygen considered as nucleophilic (Gallegos et al., 2017; Piumetti et al., 2015), and adsorbed oxygen considered as electrophilic (Gallegos et al., 2017).

Figure 8.

Comparison between catalytic activity, and the oxygen reducibility and mobility.



Note: Catalytic conversion and common evaluated properties (A). Specific reaction rate (R_{CH_4}) as a function of Mn crystalline phase, and the average oxidation state of surface Mn from catalyst (B). Amount and temperature of desorbed surface and bulk oxygen (C). Amount and temperature of reducible oxygen (D). For all the graphs, the bars are quantized with the y-axis on the left, and the dashed lines with the y-axis on the right.

2.3 Conclusion

Treating powders recovered from the cathode of spent alkaline batteries with a strong acidic solution of H_2SO_4 proved to be an easy alternative to upcycle this waste into MnO_x

nanorods. The treatment thus becomes a single-step synthesis method in which the dissolution of MnO_x from the solid and its crystallization in the form of nanorods occur simultaneously. The equilibrium between dissolution and crystallization process depends on the solubility of manganese at pH close to zero. By this route, two types of nanorods were synthesized; namely, thin and elongated nanorods mainly composed of $\epsilon\text{-MnO}_2$, and sea urchin-like nanorods mostly constituted by Mn_2O_3 . The production of the second type of nanorods was made by pretreating the solid raw material with a NaOH solution. According to the results, residual graphite from the cathode powders plays a key role in the chemistry of the process. Concerning the use of the produced materials as catalysts for the combustion of methane, the nanorods based on MnO_2 showed the same catalytic performance than a $\gamma\text{-MnO}_2$ benchmark; the latter being recognized as one of the most active phases of manganese oxide in oxidation. The catalytic trends were well correlated with the relative concentration of each manganese oxide crystalline phase present in the tested materials as well as with the average surface oxidation state of manganese, the reducibility of the oxides, and to the availability of surface lattice oxygen. Introspectively, this work highlights the fact of seeing a waste in an integral way, not as a set of contaminants, but as a mixture of possible active phases or structuring agents. This approach would be beneficial when designing e-waste recycling, which is based on several hydrometallurgical and electrochemical steps. A change in this traditional methodology represents an advance not only in terms of circular economy, but also in the sustainability of the process.

3. Influence of alumina and kaolinite on the mechanical strength and methane combustion activity of spent battery cathode-based pellets

Catalytic combustion is one of the most effective technologies for the removal of methane, which is seen as an alternative to replace the traditional process of flaring (or tea type) used in refineries and oil facilities around the world, which has been strongly questioned in environmental matters due to its low combustion yields (which favors the release of greenhouse gases) accompanied by the formation of toxic compounds such as NO_x and CO (Anejionu, Whyatt, Blackburn, & Price, 2015; Elvidge et al., 2018; Fawole et al., 2016). Because the use of the catalyst allows the combustion reactions to follow a path of lower activation energy, catalytic combustion can occur at temperatures below 500 °C, reaching a conversion of the hydrocarbon and a selectivity towards CO₂ close to 100 % (Arai & Machida, 1991; L. He, Fan, Bellettre, et al., 2020). Since the catalyst is the heart of the catalytic process, its proper design is essential to obtain a viable technology at an industrial level (Mitchell et al., 2013; Sie & Krishna, 1998). There are different stages in the design of a catalyst. The first one has to do with the choice and synthesis of the active phase, which in the first instance controls the speed and stability of the chemical process. At the beginning of the 90s, it was determined that the active phases with the greatest potential for oxidation processes were based on noble metals such as Pt, Pd and Rh, thanks to their ability to activate methane (Abbasi, Wu, Wanke, & Hayes, 2012; L. He, Fan, Luo, et al., 2020), however, their high cost and easy deactivation due to coke formation, quickly motivated the search for cheaper and more stable active phases based on transition metals (C. He et al., 2019). Among the most promising, manganese oxides (MnO_x) have stood out due to their low cost, higher thermal

stability and higher availability than noble metals (H. Xu et al., 2017; K. Zhang et al., 2019b). The multivalent nature of Mn allows it to produce MnO_6 octahedrons that are organized in various polymorphs such as α , β , δ , γ and ϵ - MnO_2 , as well as α and γ - Mn_2O_3 and Mn_3O_4 , which have been associated with the formation of oxygen vacancies in the crystal lattice that favor the storage and mobility of oxygen during oxidation reactions (L. He, Fan, Bellettre, et al., 2020; K. Li et al., 2019; Shi et al., 2012; Xiuyun Wang et al., 2018). Conventional routes to produce these oxides are precipitation of manganate salts, solution combustion, hydrothermal synthesis, and sol-gel routes that require structuring agents (Bach et al., 1990; Lamaita et al., 2005; Lin et al., 2016; Piumetti et al., 2015). Other routes, covered by the circular economy approach, are based on the chemical extraction of Mn oxides from waste such as pyrometallurgical sludge, process sediments to obtain electrolytic and chemical manganese oxides, and spent batteries (Yongchao Li et al., 2020; P. Liu, 2018; Ong et al., 2021b). This last type of waste is considered the largest secondary source of Mn, since the battery cathode (e.g. Zn-Mn) can contain between 40-60 % wt. of Mn (Gallegos et al., 2013; Park, Song, et al., 2021). Among the most questioned aspects of the chemical treatment of residues for the recovery of Mn oxides, are the multiple hydrometallurgical and electrolytic steps to isolate the Mn species with significant purities (<95%), the generation of acid residues and the high amounts of energy used. However, despite these chemical challenges, secondary sources represent the most responsible alternative for future Mn extraction.

The second stage of the synthesis process of an industrial catalyst is the scaling of the active phase to a rigid body (Sie & Krishna, 1998). This increase in the size of the catalyst particles, from the order of microns (generally powders of mass or supported active phases) to the order of millimeters, allows the catalysts to meet a series of geometric and mechanical requirements such as the minimization of the limitations of mass and heat transfer within the reactor; the high

mechanical resistance to withstand pressure gradients and interparticle compression and shear stresses within the catalytic bed; and a long service life (Klusacek & Schneider, 1981; Thüne & Niemantsverdriet, 2009). At the end of the 90's, the most promising industrial catalysts for combustion consisted of monolithic honeycomb arrangements (Tomašić & Jović, 2006), however, as mentioned, their high cost and instability made technological developments unfeasible. Although there is little evidence on the scaling of transition metal oxides such as MnO_x, tableting has been used to obtain rigid bodies from MnO₂ powders, with promising activity and mechanical strength results (Baldovino-Medrano, Kartheuser, & Gaigneaux, 2019b). One of the drawbacks of this type of scaling is that, due to the large pressure gradients used for the formation of the tablets, the internal fraction of the catalyst remains inaccessible, so only the sites on the external surface are activated. Extrusion is another scaling alternative in which pellets with cylindrical and tubular shapes, among others, can be obtained (Akhtar, Andersson, Ogunwumi, Hedin, & Bergström, 2014; Blackburn & Wilson, 2008). Due to the fact that a lower compressive stress is used in this operation, the materials generally present a higher internal diffusion coefficient, however, they also have a low mechanical resistance. In the case of the extrusion of manganese oxides, due to the lower cohesion of their particles, the pellets formed can be conditioned to a low mechanical resistance, that is, they do not remain intact when handled. According to Mitchell et al. (Mitchell et al., 2013), among a wide variety of possible additives, binders and plasticizers can improve the mechanical properties of the shaped material since they increase the cohesion of the particles, as well as lubricants and peptizers can help flow during extrusion, and homogenize the extruded paste. These additives can remain in the pellet or be removed by heat treatment or washing after shaping. Whatever the strategy, the search for mechanical resistance does not have to sacrifice the

catalytic performance of the pellets. However, to the best of our knowledge, it is still unknown how additives affect those properties in manganese oxides pellets.

A final problem, inherent to the different levels in the catalyst preparation, either in the manganese oxides synthesis or in their forming, at laboratory or industrial scale, is the generation of large volumes of residues. It is known that during metal impregnations operations or by electrolytical and chemical obtention of manganese oxides, among others, residues as acid sludges and wastewaters are generated (Gunarathne et al., 2020; F. Xu et al., 2014; W. Zhang & Cheng, 2007a). Despite that way of contamination is strongly associated to the current industrial model of massive production, the green chemistry apports a series of principles (Zimmerman et al., 2020) that with time can change the actual paradigm of manganese catalyst preparation, in fact, some scientific advances are in sight (Stegarescu et al., 2020). Considering the problems in the development of manganese-based catalysts for industrial applications (phase active synthesis, scaling up and environmental implications on the chemical processes associated), we proposed a circular and residue-free synthesis of active pellets in methane combustion, by extruding the cathode of spent household batteries (extracted without chemical processes), using kaolinite as plasticizer, alumina as a binder and water as lubricant. The central topic of discussion is the analysis of the relationship between the mechanical resistance and the catalytic activity of the pellets and how the additives content can modify this relationship.

3.1 Experimental

3.1.1 Pellets catalyst synthesis

Pellets catalyst were prepared by the extrusion of the cathode powder recovered from spent Zn-Mn alkaline batteries. The batteries, AA-type, were recycled in a collection point in the UIS campus and manually dismantled until recovering the cathodes, which were dry mixed, macerated and sieved to obtain a powder of particle size of 80-160 μm (details of mass balance of dismantling operation can be consulted in [REF]). After that, the cathode powder was five times rinsed with type-1 water keeping a solid:liquid (S:L) ratio of 1 g:10 ml and a residence time of 30 min by each rinsed, in order to remove water soluble ionic species as Na^+ , K^+ , Cl^- , SO_4^- . In the last rinsed, the conductivity of the resultant water was below 0.005 $\mu\text{S}/\text{cm}$. Posteriorly, the wet cathode was separated and dried overnight in oven at 120 $^\circ\text{C}$. The resulting powder was again adjusted for particle size at 80-160 μm . For the extrusion of that cathode powder as catalyst active phase, it was used kaolinite as a plasticizer, alumina as a binder and water as lubricant. The kaolinite powder (Laboratorios León). was washed with 0.1 M H_2SO_4 solution keeping a S:L ratio of 1 g:5 ml and a residence time of 30 min, in order to leach metallic and soluble ionic contaminants. After that, the wet kaolinite was separated from acid solution, rinsed to remove acid residues and dried following the same procedures described above. The alumina in pellets (99 % $\gamma\text{-Al}_2\text{O}_3$, Sasol) and the resultant washed dry kaolinite were mixed macerated and sieved to obtain a powder of particle size of 80-160 μm .

All of the powders, cathode, kaolinite and alumina were dried and mechanically mixed in different mass proportions until homogeneity. The resultant powder mixtures were wetted

dropwise with type-1 water and vigorous macerated until an extrudable paste of homogeneous consistency was obtained. The mass of additives and water used for each composition was reported in Table 1. The pastes were extruded by manual compression using a 10 ml syringe forming cylinders of 2 mm diameter and a length between 2 to 10 cm, depending on paste composition (Fig. S1). During extrusion, the syringe was placed near a flat glass and slid horizontally in a straight line, allowing the extruded to continuously fall onto the glass plate. In all the extrusions, the pressure was between 0.45 and 0.5 MPa, and the mass of water used (Table 1) was just the need to reach said pressure range. After that, the extruded were dried at 120 °C in overnight, and posteriorly cut manually to form pellets of 6-8 mm length. Finally, the pellets were calcined at 500 °C (5 °C·min⁻¹) for 6 h in a muffle furnace.

Table 7.

Extrudable pastes composition.

Additives (% wt.)	Alumina fraction (g·g ⁻¹ additives)	Weigth (g)			
		Cathode	Alumina	Kaolinite	Water
20	0	8.02	0.00	1.99	1.93
	0.25	8.02	0.50	1.50	2.92
	0.5	8.00	1.00	1.00	3.91
	0.75	8.00	1.50	0.50	4.90
	1	8.01	2.00	0.00	5.87
40	0	6.00	0.00	4.00	3.30
	0.25	6.02	1.02	3.01	4.66
	0.5	6.00	2.00	2.00	5.40
	0.75	6.00	3.03	1.02	6.27
	1	6.00	4.00	0.00	7.94
60	0	4.01	0.00	6.00	3.40
	0.25	4.01	1.50	4.52	5.56
	0.5	4.00	3.01	3.01	7.77
	0.75	4.01	4.50	1.50	9.80
	1	4.01	6.01	0.00	11.00
80	0	2.01	0.00	7.99	4.02
	0.25	2.00	2.00	6.00	6.50
	0.5	2.00	4.01	4.01	8.92
	0.75	2.00	6.02	2.06	10.73
	1	2.00	8.00	0.00	13.10

3.1.2 Materials characterization

The chemical groups were analyzed by infrared spectroscopy in a Nicolet iS50 Fourier Transform Infrared (FT-IR) spectrometer (ThermoScientific) using tablets of 1 % wt. sample in KBr (Merck, Analytic grade). The crystalline structure was recorded by X-ray diffraction (XRD) using a D8 advance X-ray diffractometer (Bruker) that works at 40 kV y 40 mA with Cu K α 1 radiation, taking the XRD patterns between 2 θ angles of 3.5-70 with a 0.02 step size. The diffractometer was equipped with a 2.5° Soller slit, 0.6 mm divergence slot, 0.02 mm nickel filter, and a LynxEye detector. The reduction profiles were evaluated by hydrogen Temperature-Programmed Reduction (H₂-TPR) and Oxygen Temperature-Programmed Desorption (O₂-TPD) analysis, using an automated reaction system (CATLAB, Hiden Analytical) coupled online to a Mass Spectrometer QGA (Hidden Analytical), which is thoroughly described in (Velasco-Rozo et al., 2021). For the H₂-TPR analysis, the CATLAB microreactor was loaded with 50 mg of sample and heated from 20 to 700 °C (2 °C·min⁻¹) under a continuous flow of 4 % V/V H₂ in Ar. For the O₂-TPD analysis, the CATLAB microreactor was loaded with 50 mg of sample and heated from 20 to 700 °C (2 °C·min⁻¹) under a continuous flow of Ar. In both reduction analysis, the samples were pretreated at 500 °C in a continuous flow of 4 % V/V O₂ in Ar during 2 h. Surface elemental composition and chemical speciation of the Recovered Cathodes materials were assessed by X-ray photoelectron spectroscopy (XPS). The spectra were recorded in the XPS/ISS/UPS-A.Centeno surface characterization platform (SPECS). The platform is equipped with a PHOIBOS 150 2D-DLD analyzer and a monochromatic Al K α X-ray source (FOCUS 500), operated at 100 W and 12 kV. Quantification of species was made in the CasaXPS software (Casa Software Ltd.) using

U 3 Tougaard (Walton et al., 2016) type baseline and LA(y_1, y_2) line shapes. Full details of the characterization of the samples are presented in Supplementary Methods.

The bulk density (ρ_p) was determined at 25 °C and atmospheric pressure by the pycnometer method (Blake, 2015), which consists in comparing the weight of a pycnometer (~24.7 ml) empty (W_a), filled with water (W_w), filled with the pellets up to 30 % of the pycnometer volume (W_p), and filled with a mixture of 30 % V/V pellets and 70 % V/V water (W_{pw}), by using the Eq. 1. The textural properties of the degassed samples at 300 °C (5 °C·min⁻¹) during 6 h at 0.05 mbar, were determined by N₂-physisorption of 0.15 g of sample at -196 °C in a relative pressure range of 0.0025 – 0.995 with an equilibrium interval of 10 s, using a 3FLEX TM (Micromeritics) instrument. The total pore volume and the pore size distributions were calculated with the Barret-Joyner-Halenda (BJH) method (Barrett et al., 1951), using the MicroActive® software provided with the instrument. However, the produced distribution can only be considered for comparison purposes since the software is restricted to pores with cylindrical geometry. In addition, the total specific surface area of the solids was estimated by the Brunauer-Emmett-Teller, BET, method. The morphology was observed by Scanning Electron Microscopy (SEM) using a QUANTA FEG 650 microscope dotted with an Everhart Thornley detector (ETD) and a Back scattered electron detector (BSED) type SSD, operating at a high vacuum with an acceleration voltage of 25 kV. During the microscopy runs, a semiquantitative analysis to obtain the chemical composition was made by Energy-Dispersive Spectroscopy (EDS) using an EDAX APOLO X detector with a resolution of 126.1 eV (Mn K α) and the EDX Genesis software. The transversal section of some pellets was also characterized by EDS elemental mapping.

$$\rho_p = \frac{\rho_w(W_p - W_a)}{(W_p - W_a) - (W_{pw} - W_w)} \quad \text{Eq. 1}$$

Where ρ_w is the density of the water.

Preliminary mechanical tests were applied to qualitative characterize the crushing and impact properties of the pellets. They consisted in the verification of the pellet's integrity after dropping them from 1 meter height and after the pellet compression with the fingers, wearing nitrile gloves (Castellanos-Beltran, Assima, & Lavoie, 2018). Additionally, quantitative mechanical tests were performed. Attrition tests were carried out by shaking in an orbital shaker (Heidolph, model 036130520) at 500 rpm and 25 °C, 2 g of pellets randomly packed inside a test tube of 1.05 cm internal diameter. The resultant fines were sieved in order to determine their particle size distribution. Fracture strength of the individual pellets was determined by a three-point cutting test using a TA-TX Plus texture analyzer (Fig. 2A). Each pellet was placed horizontally on a two-point support and then transversally bent until broken by contact with a flat plate which was aligned transversely with the middle of the pellet. The plate was connected to a 5 kg_f load cell and went down vertically with a speed of 1 mm·s⁻¹, applying a force of 0.5 kg_f and a break sensitivity of 1x10⁻⁴ kg_f. The quantification of fracture strength (σ_f) was made according to Eq. 3, reported in literature for pellets analysis (Yongdan Li, Wu, & Lin, 2004; Staub, Meille, Le Corre, Chevalier, & Rouleau, 2015).

$$\sigma_f = \frac{8FL}{\pi D^3} \quad \text{Eq. 3}$$

Where F is the maximum force recorded prior to fracture, L is the two-point support span, and D is the pellet diameter. Reported fracture strength was the average of the results from 7 replicates. The radial bed rigidity was determined as the maximum deformation of the pellets bed achieved by the bed compression, using the TA-TX Plus texture analyzer (Fig. 2B). In this test, A set of 10 pellets was stacked on a flat plate inside a 1.05 cm internal diameter test tube and radial compressed with a parallel flat plate connected to a load cell moving downward at a speed of 2

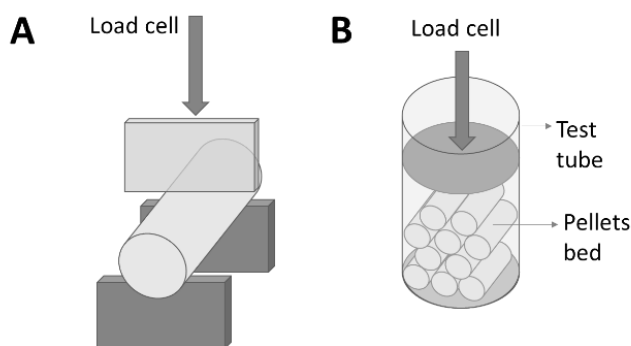
mm·s⁻¹ applying a constant vertical force of 4.5 kg_f as it is shown in Fig. 2B. The radial bed rigidity (R_b) was calculated according to Eq. 4 (Ying, Lu, & Abdou, 1998).

$$R_b = \frac{F^*}{\varepsilon} \quad \text{Eq. 4}$$

Where F^* is the compression force and ε is the maximum bed strain.

Figure 9.

Mechanical test to determine Fracture strength (A) and radial bed rigidity (B).



3.1.3 Catalytic tests

The pellets were tested in the methane combustion reaction using an automated reaction system, composed by a continuous fixed-bed quartz reactor (i.d. 1.04 cm) fed by a set of independent mass flow controllers (Alicat Scientific) with an accuracy of ± 0.1 % of full scale, repeatability of ± 0.08 % of full scale, a turndown of 1:200 and a temperature sensitivity of 0.02% of full Scale / °C. The reactor temperature was controlled by a programmable logic controller (PLC, Rockwell Automation) connected to a concentric tubular furnace and a thermocouple placed inside the catalytic bed. The outlet of the reactor was connected online to a Gas Chromatograph (GC-2014 instrument, Shimadzu Corporation) to make the online analysis of the reaction products.

The instrument was provided with a set of packed columns and with a TCD-Methanizer-FID array for detection and quantification. The schematic of the reactor system is presented in Fig. S2. Samples from the gaseous stream from the reactor outlet, were analyzed every ~20 min. In each test, the catalytic bed was composed of a 1:2 weight ratio mixture of catalyst (40-180 μm) and quartz (SiO_2) particles (40-60 μm). The use of quartz as a diluent avoids artifacts due to temperature gradients. Further homogenization of the temperature of the reactor as well as reaching plug-flow in the system was achieved by placing a glass wool plug on top of the catalytic bed. The catalyst was dried in situ at 120 $^\circ\text{C}$ (5 $^\circ\text{C}\cdot\text{min}^{-1}$) for 90 min with a flow of 90 $\text{ml}\cdot\text{min}^{-1}$ N_2 at a space velocity of 108000 $\text{ml}\cdot\text{g}^{-1}\cdot\text{h}^{-1}$. Then, the reactor feed was changed by a mixture of CH_4 (7.7 % V/V), O_2 (18.4 % V/V), and N_2 as gas balance, keeping the same flow conditions mentioned above. The temperature of the reactor was raised to 500 $^\circ\text{C}$ (5 $^\circ\text{C}\cdot\text{min}^{-1}$), the reaction temperature, either after 30 min or until complete stabilization of the flow fed to reactor. The tests had a duration of 6 h. The chromatographic analysis of reactor effluents was made before and after the reaction (feed analysis) and during the reaction (products analysis). In a typical test, reaction products started to appear from 300 $^\circ\text{C}$. The reaction system including GC conditions and the quantification method are provided by Sandoval-Bohorquez et al. (Sandoval-Bohorquez et al., 2020).

To analyze the catalytic activity of the pellets, some parameters were calculated. From feed and product GC analysis the reactant conversion was calculated using Eq. 5:

$$X_{\text{reac}}(\%) = \frac{F_{\text{reac}}^0 - F_{\text{reac}}}{F_{\text{reac}}^0} * 100\% \quad \text{Eq. 5}$$

Where F_{reac}^0 and F_{reac} are the molar flow ($\text{mol}\cdot\text{h}^{-1}$) of reactant at inlet and outlet of the reactor, respectively. Additionally, from conversion assuming that the reactor operates in a

differential form (cause conversions below 15 %), the specific reaction rate (r_{CH_4} , mol g⁻¹ h⁻¹) and the apparent turnover frequency (TOF*, h⁻¹) was determined by next equations (Eqs. 6-8):

$$R_{reac} = \frac{F_{reac}^0 X_{reac}}{W} \quad \text{Eq. 6}$$

$$TOF^* = \frac{R_{reac}}{[Mn]} \quad \text{Eq. 7}$$

$$[Mn] = \frac{Mn}{O}_{XPS} O_{TPR} \quad \text{Eq. 8}$$

Where W is the weight of the catalyst (g), [Mn] is the Mn pseudo-content near to the surface of the catalyst determined by product of the ratio of Mn to O calculated by XPS analysis (Mn/O_{XPS} , mol Mn·mol⁻¹ O) and the specific oxygen amount calculated by H₂-TPR analysis (O_{TPR} , mol O·g⁻¹ catalyst).

3.2 Results

3.2.1 Characterization of the raw material

The cathode powder used as active phase of the pellets-like catalyst, was manually recovered from spent alkaline Zn-Mn batteries by an easy and green method, with no chemical steps. This powder was characterized by an irregular morphology formed by the aggregation of particles of about 122 ± 42 nm. About textural properties, the cathode presented and specific surface area of $7.9 \text{ m}^2 \cdot \text{g}^{-1}$ with a mean width pore of 20 nm. Its composition was based principally on 50.4 % wt. of manganese and 14.9 % of zinc (from AAS analysis), distributed in the crystalline phases ZnMn₂O₄, Mn₃O₄ and MnO₂, according to XRD analysis. Those species were coherent with the chemical groups Mn-O, Mn-OH and Zn-O detected by FTIR analysis. At the surface, the

cathode powder presented an average Mn oxidation state around 3.07+ (by XPS analysis) with a reducible oxygen amount of 4.36 mmol·g⁻¹ determined by hydrogen temperature programmed reduction and 0.65 mmol·g⁻¹ from oxygen temperature programmed desorption test. These values of oxygen were contrasted with the thermogravimetric reduction analysis. On the other hand, additives used for the extruded formation (kaolinite and alumina) were also analyzed. Kaolinite powder, used as plasticizer and binder, was morphologically characterized by sheets of a length of 400 ± 80 nm irregularly organized. Its mesoporous surface area was about 20 m²·g⁻¹ with a pore width of 20 nm. The chemical groups detected in kaolinite by FTIR were Si-O, Al-O and Al-OH. The alumina, 99 % wt. γ -Al₂O₃, with irregular morphology, was also used as binder in the pellets forming. It was characterized by a mesoporous surface area of 250 m²·g⁻¹ and a pore width of 20 nm, and by the chemical groups Al-O and Al-OH (determined by FTIR analysis). Results of AAS, FTIR, XPS and SEM analysis for the cathode powder were presented in the previous chapter.

3.2.2 Extrusion of the cathode powder

The cathode, kaolinite and alumina powders were dry mixed in different mass proportions and slowly wetted to form extrudable pastes, which after extrusion, drying and calcination, became a set of cylindrical pellets of ~2 mm diameter. For this process no chemical agents were used and it was free of residues. The rigid bodies obtained presented a physical property that strongly depended on their composition. In terms of morphology, the surface of the pellets presented a variable topography that going from a totally cracked heterogeneous matrix (Fig. 2, A and B), to a homogeneous matrix with less cracked area (Fig. 2, C and D). The formation of cracks seems more evident in the pellets with lower concentration of kaolinite respect to the cathode powder or

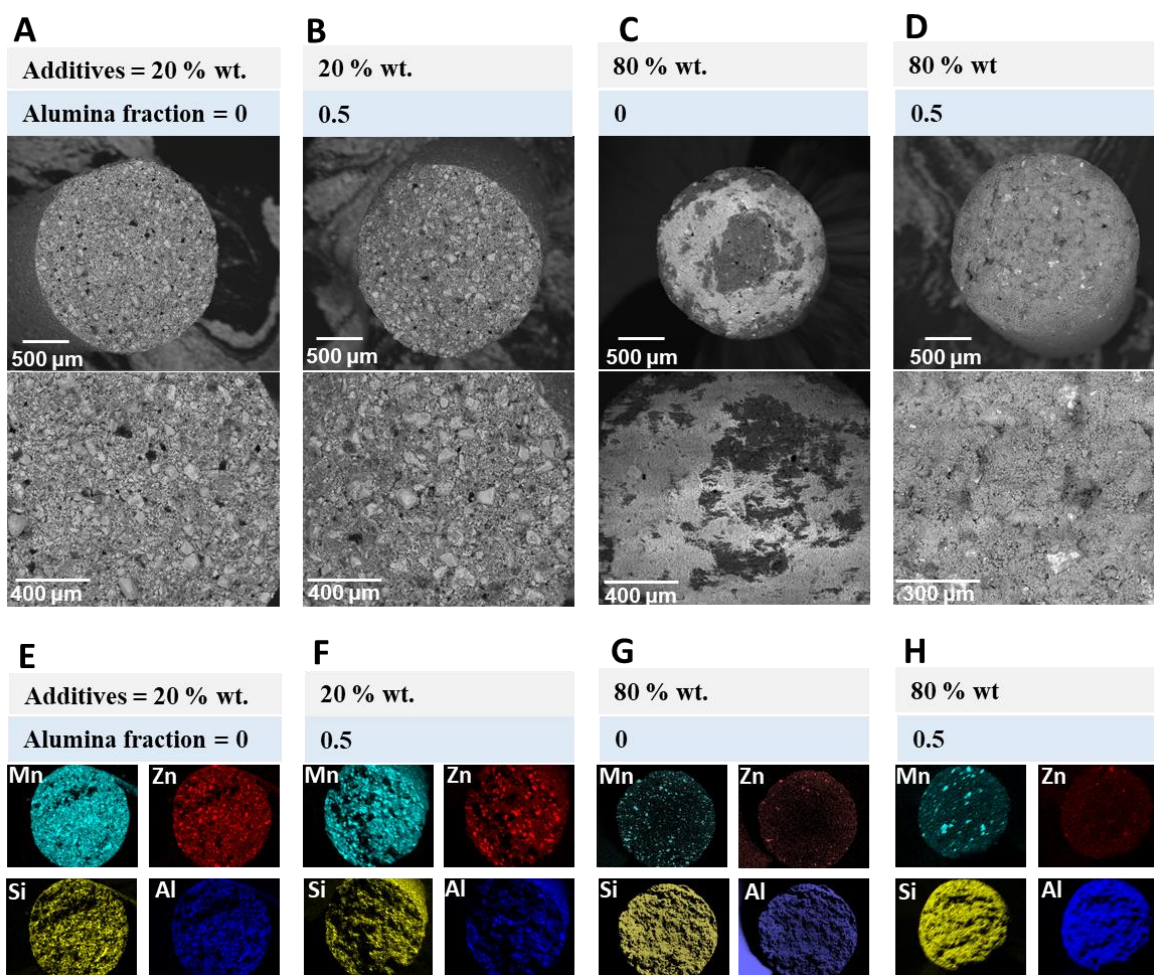
the alumina. Internally on the pellet, it was observed by Mn and Zn SEM-EDS analysis that the cathode powder is aggregated with lower content of additives (Fig. 2, E and F), but is disaggregated with the increase of additives (Fig. 2, E and F). The alumina content seems not to affect considerably this aggregation. The specific surface area increased linearly with the increment of alumina concentration (Fig. 3A). However, the pore distribution shows that the pores width was not modified with the concentration of additives indicating that the extrusion operation did not affect the size of the pores (Fig. S2). The specific area of the pellets S_A was compared with a theoretical area S_A^{cal} calculated with the area of the powders before the pellets extrusion (Eqs. 9 and 10), using a metric called blocked surface area (B_{surf}), as it is shown in Fig. 3B.

$$B_{surf} (\%) = \frac{S_A - S_A^{cal}}{S_A} * 100 \quad \text{Eq. 9}$$

$$S_A^{cal} = \sum_i^n S_{A_i} * \omega_i \quad \text{Eq. 10}$$

Where S_{A_i} and ω_i are the specific surface area and the mass fraction of the powder i in the pellet. Notice that for the N_2 -physisorption test, B_{surf} represent the restriction to the inlet of N_2 to the pellet. Two outside behaviors for the blocking (Fig. 3B) were observed: the kaolinite was the most blocked while alumina was the lowest. This indicates that the kaolinite formed a rigid body where the external surface area is only accessible and the area of the particles inside the pellet is inaccessible. This result is coherent with the fact that kaolinite particles have a high cohesion which led to gain cross-linking properties. In contrast, alumina powder with lower cohesion forms a cracked pellet body where its internal mass is accessible. Nevertheless, the blocked of Kaolinite was progressively decrease with the increase of the presence of other particles, either alumina or cathode powder. This could be explained, because despite kaolinite forms a matrix that imbibes the other particles blocking them to be reached by the gas phase, when this matrix is saturated by

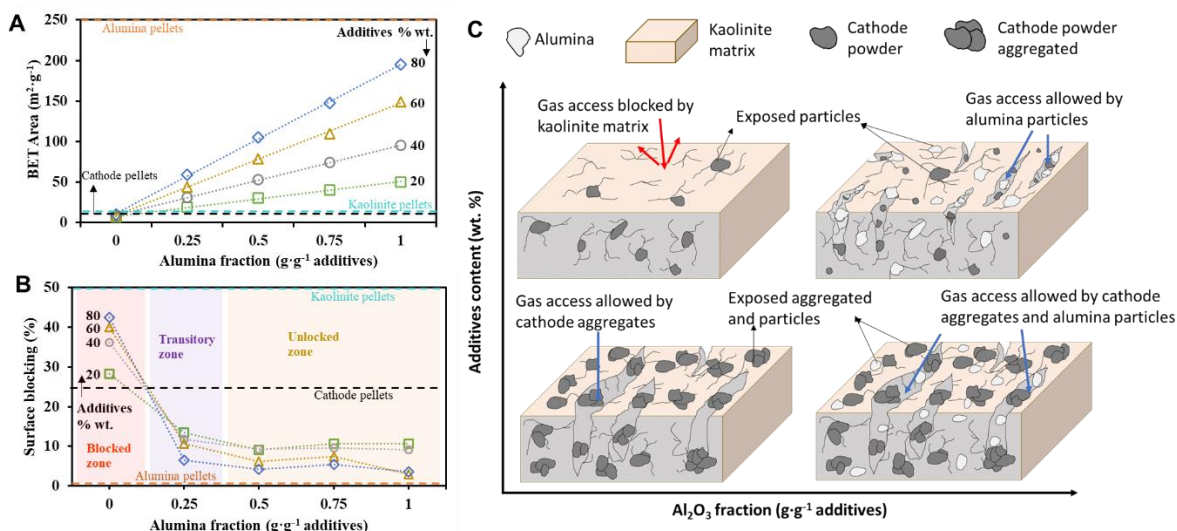
other particles it is cracked allowing the access of the gas phase. As commented, the cracked pellets had a higher exposition of its internal mass to the gas phase. The aggregation of cathode powder was also analyzed by SEM-EDS and by blocked surface area. For the pellets of the cathode powder without additives a blocking was observed. Since the cathode powder is not known by its cross-linking properties, it is expected that during the extrusion it suffered an aggregation. That means that the aggregation of the particles is another cause for the blocking of the internal mass. The behavior of the surface area is coherent with density results, that were characterized by their increase with the additives content and alumina content. In this case, the measured volume was higher when the pellet was blocked which implicated a decrease in the density. The scheme presented in Fig. 3C illustrates the particles and aggregates accommodation on the pellets. In this scheme, it is proposed that the accommodation and aggregation of the particles can influence the access of a gas phase into the pellets.

Figure 10.*Morphologic and semiquantitative analysis of the pellets.*

Note: SEM images of the pellets composed by 20 % wt. additives with a alumina fraction of (A) 0 and (B) $0.25 \text{ g}\cdot\text{g}^{-1}$ of additives, and by 80 % wt. additives with a alumina fraction of (C) 0 and (D) $0.5 \text{ g}\cdot\text{g}^{-1}$ of additives. EDS analysis for Mn, Zn, Si and Al of the pellets composed by 20 % wt. additives with a alumina fraction of (E) 0 and (F) $0.25 \text{ g}\cdot\text{g}^{-1}$ of additives, and by 80 % wt. additives with a alumina fraction of (G) 0 and (H) $0.5 \text{ g}\cdot\text{g}^{-1}$ of additives.

Figure 11.

Specific surface area (*A*) and the percentage of surface blocking (*B*) on the pellets as a function of % wt. of additives and the alumina fraction.



Note: The dotted lines correspond to the linear trend of the experimental data. The dashed horizontal lines represent the density of raw pellets. Scheme (C) of cracks and particles/aggregates distribution on the pellets.

3.2.3 Mechanical performance of the pellets

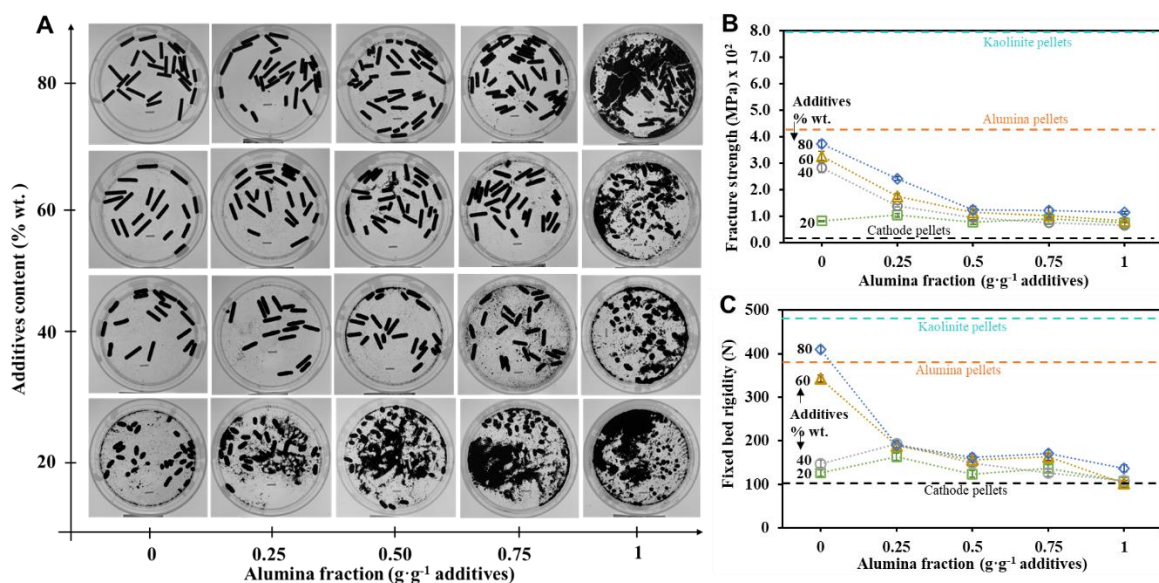
The synthesized pellets were exposed to preliminary mechanical tests in order to qualitatively characterize their crushing and impact properties. Only pellets with an additives content > 40 % wt maintained their integrity after the 1meter drop and finger compression, which means that the use of additives improves the mechanical properties of the pellets. However, that improving can vary with the nature and concentration of the additives. From attrition test results (Fig. 4A), it is observed that the pellet erosion was decreased with the increase in the additives % wt. Likewise, this effect is promoted with the increase in the alumina content. Such a finding was

corroborated by the particle size distribution after attrition test. According to that, the cross-linking and cohesion properties of the kaolinite, resalted above, made the external surface of the pellets more stable to the abrasion. On the contrast, the lower cohesion of alumina and cathode powder placed in the external surface of the pellets promoted the particles erosion. On the other hand, a similar influence of the additives in the mechanical behavior of the pellets in the three-point cutting test (Fig.4B) was observed. The increase in the additives % wt. apparently enhances the mechanical resistance to the fracture of the pellets; however, this effect is attenuated by the increase in the alumina content in the pellets. Analogous results were observed in the results of the radial bed rigidity (Fig. 4C). An apparent stabilization in the mechanical behavior of the bed is observed above of an alumina fraction of $0.5 \text{ g}\cdot\text{g}^{-1}$ of additives. This tendency on the mechanical resistance results is coherent with the trend of the surface access blocking results (Fig. 3, B and C), which suggest that the pellets breaks, fissures or holes generated by alumina and cathode particles (as those observed by SEM analysis shown in Fig. 2, A to D) influences the mechanical failure. In contrast, pellets with the highest content of kaolinite presented the better mechanical behavior as a consequence of a rigid body formation. The aggregation of cathode powder observed by SEM-EDS also can promote the rupture of the pellets with low additives content. It is known that the increase in the size of the particles inside a rigid body can generates internal forces that increase the probability of failure (Jaya, Firdaus Omar, Md Akil, Arifin Ahmad, & Noriman Zulkepli, 2016). The results of pellets bed crushing strength were compared with those results from industrial alumina-based catalyst in pellets (Yongdan Li et al., 2004; Staub et al., 2015; Ying et al., 1998; Zakeri, Samimi, Shafiee Afarani, & Salehirad, 2018), finding the same order results around 5-25 MPa. This implicates that some of the pellets synthesized presented expected mechanical properties for the industrial catalyst. In addition, the mechanical test results were

compared with a benchmark based on alumina pellets which was placed in that strength range. By comparing, the pellets synthesized presented the 20-60 % of the mechanical resistance of the benchmark, while the kaolinite 80 % wt. pellets were as resistant as the alumina benchmark.

Figure 12.

Mechanical analysis of the pellets.



Note: Images of pellets after attrition test (A), cutting strength (B) and fixed bed rigidity (C) as a function of wt. % of additives and alumina fraction on the pellets. The dashed horizontal lines represent the properties of raw pellets.

3.2.4 Study of the catalytic activity

The activity of the catalytic materials either powder or pellets was tested in the methane combustion reaction. It was found that the cathode powder, used as pellets active phase, converted methane into CO₂ with 100 % selectivity at 500 °C. This activity was associated primarily with

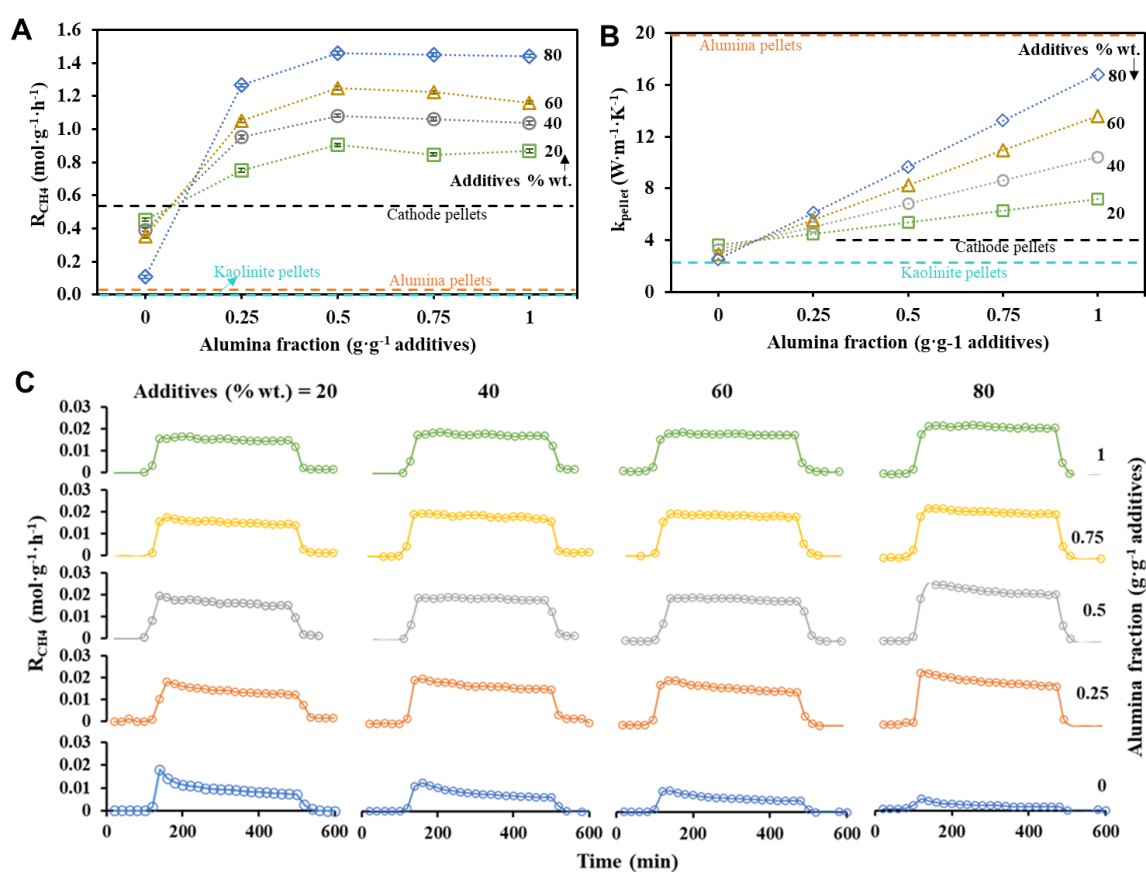
the manganese oxides that compose the cathode, especially with the residual MnO_2 (16.8 %) (C. He et al., 2019; Park, Song, et al., 2021). Specifically, it was found a direct relationship of the reaction rate with the amount of reducible oxygen in the surface lattice of the material and with the surface average oxidation state (S. C. Kim & Shim, 2010; Xiuyun Wang et al., 2018). In contrast, the specific surface area, the surface concentration of Mn or O, and the bulk concentration of Mn were not associated with the catalytic activity of the cathode powder. The activity of the cathode powder was compared to a benchmark of $\gamma\text{-MnO}_2$ (Baldovino-Medrano et al., 2019a). The cathode powder showed a lower reaction rate but similar turnover frequency as the benchmark. These results can be interpreted to mean that the cathode powder has a lower density of active sites, but each active site has a catalytic performance similar to that of the benchmark. Furthermore, that is consistent with the fact that the cathode powder has a lower MnO_2 concentration than the benchmark and with the assumption that MnO_2 is the most relevant active phase in the cathode powder.

The pellets synthesized from the cathode powder extrusion were also active in the catalytic combustion of methane (Fig. 5A). Since alumina and kaolinite were found to be inactive, such activity was only associated with the MnO_2 of the cathode powder. However, it was observed that the activity of pellets varied with the additives content (Fig. 5A). To assure that this variation was not a consequence of a change in the reactants flow, the pressure drop in the bed was discarded and the ideal flow was verified by using theoretic criteria proposed by Dautzenberg (Dautzenberg, 1989). Particularly, it is observed that the increase in the additives content increases the specific reaction rate except for the pellets that have only kaolinite as additive, where that trend is opposite. In addition, it can be analyzed that the increase in alumina content promotes an increase in the activity which trends to stabilize after 0.5 g alumina per gram of additives. The fact that the trend

shown in the reaction rate results (Fig. 5A) is opposite to the blocked surface area (Fig. 3B) indicates that there are two structural aspects in the pellets that influence their activity: first, methane access inside the pellet can be blocked by the kaolinite matrix, but this blockage decreases with decreasing kaolinite mass fraction; second, the formation of cathode powder aggregates decreases the density of active sites exposed to methane adsorption. Both phenomena were previously described and analyzed in Fig. 3C.

Figure 13.

Specific reaction rate (R_{CH_4}) (A), theoretic thermal conductivity (k_{pellet}) (B), reaction rate monitoring through the reactions (C) of the pellets as a function of additives content and the alumina mass fraction. The dashed horizontal lines represent the value of raw pellets.



On the other hand, the reaction rate through the catalytic test was analyzed (Fig. 5B). It is observed that the pellets with lower contents of alumina presented a peak in the first minutes of the reaction, which goes decreasing and stabilizing posteriorly. Moreover, these peaks tend to attenuate themselves when the content of alumina in the pellets is increased. These results were compared with the bed and oven temperature profiles in the reaction system, presenting the same trend. According to that, it can be supposed that the heat released by the reaction generates hot spots on the pellets with low content of alumina. In order to show the relation between that behavior and the thermal conductivity of pellets, Fig. 5C presents the results of theoretic calculation of that parameter as a function of their composition using Eq. 11. As it is expected, given that the alumina has a higher conductivity (~ 20 W/mK) than the kaolinite (~ 0.8 W/mK) and the cathode powder (~ 4 W/mK), the results of thermal conductivity of the pellets increase linearly with the alumina content (Gregorová, Pabst, Smith, & Zivcová, 2009; Hedden, Francis, Haraldsen, Ahmed, & Constantin, 2015; Michot, Smith, Degot, & Gault, 2008). Moreover, it was found that the trend in the results of thermal conductivity was very close to the reaction rate results in the range of 0 and 0.25 alumina mass fraction. So that, it can be concluded that the lower thermal conductivity of kaolinite promotes heat transport limitations in the pellets, and this negative effect tends to decrease with increasing the alumina content. Nevertheless, to corroborate that the thermal conductivity promotes some kind of limitations to the heat transport, the theoretic criteria proposed by Mears (Mears, 1971b, 1971a) to evaluate limitations of intraparticle, surface and interparticle heat transport were evaluated for two selected pellets with both lowest and highest reaction rate, which were those composed by 80 % wt. additives with 0 and 1 alumina mass fraction, respectively. It was found that according to results of Mears's criteria, in coherence with discussed,

only the pellets without alumina presented limitations in the heat transport in both intraparticle and interparticle.

$$k_p^{\text{cal}} = \sum_i^n k_i * \omega_i \quad \text{Eq. 11}$$

Where k_p^{cal} is the theoretic thermal conductivity of the pellets, and k_i and ω_i are the thermal conductivity and the mass fraction of the powder i in the pellet.

3.2.5 Relation between mechanical resistance, activity and stability of the pellets

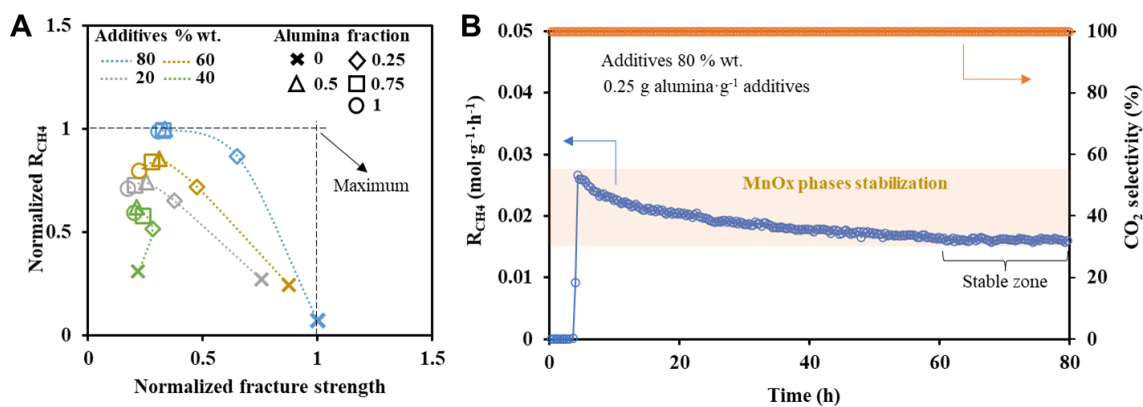
The mechanical strength and catalytic activity of the pellets were correlated by matching the normalized fracture strength and reaction rate (Fig. 6A). In all profiles, an increase in the reaction rate promotes a decrease in mechanical resistance. It can be explained from the scheme presented in Fig. 3C, which indicates that the cracks in the pellet improve the access of the reactants inside the pellets, but at the same time, these cracks promote mechanical failure. A particular behavior observed in Fig. 6A, is that for each concentration of additives, the pellets that present greater mechanical resistance and reaction rate are those based on an alumina mass fraction of 0.25. Those pellets were previously cataloged to be in a transition zone (Fig. 3C), where the gas access inside the pellet was unlocked by the formation of cracks in the kaolinite matrix after the addition of alumina particles. Moreover, the pellet that presented the highest mechanical resistance and reaction rate (these placed closer to the maximum point in Fig. 6A), was that composed by additives 80 % wt. and an alumina mass fraction of 0.25.

On the other hand, the stability of the pellets in the methane combustion was studied. For this, an 80 h reaction was carried out using the best formulation of the pellets (additives 80 % wt.

and an alumina mass fraction of 0.25) in terms of mechanical and catalytic behavior. It was found that the reaction rate presented two zones: one characterized by a decrease in the reaction rate that showed a duration of 60 h, and other where the reaction rate was stabilized. This behavior may be associated with the thermodynamic stabilization of the active phase, which means the transformation of the MnO_2 in a more stable phase. Since this behavior was only observed for the pellets with low thermal conductivity, it is possible to propose that the increase in the pellet temperature due to the hot spots formation transformed the MnO_2 . According to results reported by Baldovino et al. (Baldovino-Medrano et al., 2019a), the increase in temperature (from 300 to 500 °C) completely modified the crystalline phase from MnO_2 to Mn_2O_3 . Moreover, the activity of the cathode powder and benchmark was analyzed by increasing the reaction temperature in light-off experiments. In this case, it was confirmed that after exposing manganese oxides to a temperature of 600 °C, their catalytic activity at lower temperatures decreases.

Figure 14.

Comparison of the normalized reaction rate and fracture strength of the pellets (A), and the analysis of stability for a specific pellet formulation (B).



3.3 Conclusion

Pellet catalysts active for methane abatement were synthesized based on a circular synthesis process due to it was used a toxic residue as active phase source and based on green chemistry since no residues were generated, nor used chemical substances as dissolvents, peptizes or leaching agents. Such pellets consisted of a cylindrical-like shape formed by extrusion of a paste composed by recovered cathode powder as active phase, and kaolinite and alumina powder as plasticizer and binder additives, respectively, and water as lubricant. Both mechanical and catalytic properties of the pellets were influenced by their composition. On the one hand, the kaolinite improves the mechanical resistance of the pellets in terms of attrition, bed rigidity and fracture strength, but sacrifices the catalytic activity due to, blocking the access to the reactants inside the pellet decreasing the exposition of bulk active phase. In this sense, an excess of kaolinite must be avoided if the intrapellet catalytic activity is expected. The alumina, on the other hand, decreased the mechanical resistance of the pellets due to disrupt the continuity of the kaolinite matrix, generating cracks that increasing the internal forces in the rigid body promoting the mechanical failure. However, these cracks also allow the access of the gas on the pellet, improving the catalytic activity. Due to the contribution of the alumina to the pellet thermal conductivity, the formulations based on an alumina mass fraction greater than 0.5, do not show catalytic instability. On the contrast, low alumina content pellets present an initial peak in the reaction rate due to an intraparticle and interparticle heat transport limitations. For all the pellets formulations studied it was observed that an increase in the catalytic activity entails a detriment of the mechanical resistance. However, we selected as the pellets best formulation those composed by additives 80 % wt. and an alumina mass fraction in the additives of 0.25.

4. General conclusions

Different formulations of catalysts, both powder, and pellets, were obtained from the cathode of spent batteries. On the one hand, the acid treatment of the recovered cathode from a spent battery is an easy alternative to obtaining MnO_x-based nanorods. It consists in a one-step synthesis method in which occurs two simultaneous chemical processes: the dissolution of MnO_x from the recovered cathode and the crystallization of nanorods, both equilibrated by the solubility of manganese at pH close to zero. By this route, two types of nanorods can be synthesized, one elongated and thin-like based on ϵ -MnO₂ and the other sea urchin-like based on Mn₂O₃. To control the nature of nanorods, varying from MnO₂ to Mn₂O₃, was enough a NaOH-washed of the recovered cathode. In this sense, the degree of reduction of MnO_x in the precursor cathode powder directly affects the degree of reduction of MnO_x-based nanorods. The key element in the nano-formation was the residual graphite present in the cathode. Properties such as specific surface area, crystalline composition, or the surface Mn oxidation state, are sensible to the one-step synthesis. Particularly, MnO₂-based nanorods were found as an active catalyst for methane combustion, showing a specific reaction rate close to a benchmark catalyst based on γ -MnO₂. Convincingly, the activity of those materials was associated with crystalline phase content, the MnO₂-based the most active, due to higher reducibility at lower temperatures, and the higher amount of adsorbed and lattice oxygen. In contrast, Mn₂O₃ was the less active crystalline phase due to its low content of adsorbed and lattice oxygen. An activity factor proposed in this work served to discriminate the individual effect of those crystalline phases, despising possible synergistic effects. In prospective, seeing waste in an integral way, not as a set of contaminants, but as a mixture of possible active

phases or structuring agents, can change the current way of valuing electronic waste, which is based on several hydrometallurgical and electrochemical steps. A change in this traditional methodology represents an advance not only in terms of a circular economy but also in the sustainability of the process.

On the other hand, a set of cylindrical-like shape formed catalysts was developed by extrusion of a paste composed of recovered cathode powder as active phase, and Al_2O_3 and Kaolinite powder as binder and plasticizer additives, respectively. The mechanical behavior of this type of catalyst is influenced by composition. The increment in the concentration of additives is associated with an increase in the attrition and fracture toughness, due to the additives generated a more compact body decreasing defects in the structure. The increase in the fraction of Al_2O_3 in the additives decreases especially the fracture toughness. In the same way, the additives affect the catalytic activity, however, contrary to the mechanical results, Al_2O_3 appears as a promotor of the activity of MnO_x from the recovered cathode, having its higher activity from an Al_2O_3 fraction of 0.5 with respect to the mass of the additives.

References Bibliographical

- Abbasi, R., Wu, L., Wanke, S. E., & Hayes, R. E. (2012). Kinetics of methane combustion over Pt and Pt-Pd catalysts. *Chemical Engineering Research and Design*, 90(11), 1930–1942. <https://doi.org/10.1016/j.cherd.2012.03.003>
- Abid Charef, S., Affoune, A. M., Caballero, A., Cruz-Yusta, M., & Morales, J. (2017a). Simultaneous recovery of Zn and Mn from used batteries in acidic and alkaline mediums: A comparative study. *Waste Management*, 68, 518–526. <https://doi.org/10.1016/j.wasman.2017.06.048>
- Abid Charef, S., Affoune, A. M., Caballero, A., Cruz-Yusta, M., & Morales, J. (2017b). Simultaneous recovery of Zn and Mn from used batteries in acidic and alkaline mediums: A comparative study. *Waste Management*, 68, 518–526. <https://doi.org/10.1016/j.wasman.2017.06.048>
- Akbari, E., Alavi, S. M., Rezaei, M., & Larimi, A. (2021). Catalytic Methane Combustion on the Hydrothermally Synthesized MnO₂Nanowire Catalysts. *Industrial and Engineering Chemistry Research*, 60(20), 7572–7587. <https://doi.org/10.1021/acs.iecr.1c00881>
- Akhtar, F., Andersson, L., Ogunwumi, S., Hedin, N., & Bergström, L. (2014). Structuring adsorbents and catalysts by processing of porous powders. *Journal of the European Ceramic Society*, 34(7), 1643–1666. <https://doi.org/10.1016/j.jeurceramsoc.2014.01.008>
- Almeida, M. F., Xará, S. M., Delgado, J., & Costa, C. A. (2006). Characterization of spent AA household alkaline batteries. *Waste Management*, 26(5), 466–476. <https://doi.org/10.1016/j.wasman.2005.04.005>

Analysis, G., Analysis, T., & Analysis, R. G. (n.d.). *Software for Hiden Mass Spectrometers*.

Retrieved from <https://www.hidenanalytical.com/wp-content/uploads/2020/06/MASsoft-PC-Win-10-Software.pdf>

Andak, B., Özduğan, E., Türdü, S., & Bulutcu, A. N. (2019). Recovery of zinc and manganese from spent zinc-carbon and alkaline battery mixtures via selective leaching and crystallization processes. *Journal of Environmental Chemical Engineering*, 7(5), 103372. <https://doi.org/10.1016/j.jece.2019.103372>

Andersson, R., Boutonnet, M., & Järås, S. (2012). On-line gas chromatographic analysis of higher alcohol synthesis products from syngas. *Journal of Chromatography A*, 1247, 134–145. <https://doi.org/10.1016/j.chroma.2012.05.060>

Anejionu, O. C. D., Whyatt, J. D., Blackburn, G. A., & Price, C. S. (2015). Contributions of gas flaring to a global air pollution hotspot: Spatial and temporal variations, impacts and alleviation. *Atmospheric Environment*, 118, 184–193. <https://doi.org/10.1016/j.atmosenv.2015.08.006>

Anthony, J. W., Bideaux, R. A., Bladh, K. W., & Nichols, M. C. (2006). Handbook of Mineralogy. In *Mineralogical Society of America* (Vol. 11). Retrieved from <http://www.handbookofmineralogy.org/>

Arai, H., & Machida, M. (1991). Recent progress in high-temperature catalytic combustion. *Catalysis Today*, 10(1), 81–94. [https://doi.org/10.1016/0920-5861\(91\)80076-L](https://doi.org/10.1016/0920-5861(91)80076-L)

Bach, S., Henry, M., Baffier, N., & Livage, J. (1990). Sol-gel synthesis of manganese oxides. *Journal of Solid State Chemistry*, 88(2), 325–333. [https://doi.org/10.1016/0022-4596\(90\)90228-P](https://doi.org/10.1016/0022-4596(90)90228-P)

- Baldovino-Medrano, V. G., Kartheuser, B., & Gaigneaux, E. M. (2019a). Production and testing of technical catalysts based on MnO₂ for the abatement of aromatic volatile compounds at the laboratory and pilot plant scales. *Catalysis Today*, 338(February), 81–92. <https://doi.org/10.1016/j.cattod.2019.03.029>
- Baldovino-Medrano, V. G., Kartheuser, B., & Gaigneaux, E. M. (2019b). Production and testing of technical catalysts based on MnO₂ for the abatement of aromatic volatile compounds at the laboratory and pilot plant scales. *Catalysis Today*, 338, 81–92. <https://doi.org/10.1016/j.cattod.2019.03.029>
- Barrett, E. P., Joyner, L. G., & Halenda, P. P. (1951). The Determination of Pore Volume and Area Distributions in Porous Substances. I. Computations from Nitrogen Isotherms. *Journal of the American Chemical Society*, 73(1), 373–380. <https://doi.org/10.1021/ja01145a126>
- Batey, J. H. (2014). The physics and technology of quadrupole mass spectrometers. *Vacuum*, 101(i), 410–415. <https://doi.org/10.1016/j.vacuum.2013.05.005>
- Baynham, A., Randall, D., & Hancy, C. (2017). Incinerators and Oxidizers. *EPA Air Pollution Control Cost Manual*, (November), 1–70. Retrieved from https://www.epa.gov/sites/production/files/2017-12/documents/oxidizersincinerators_chapter2_7theditionfinal.pdf
- Belardi, G., Lavecchia, R., Medici, F., & Piga, L. (2012). Thermal treatment for recovery of manganese and zinc from zinc-carbon and alkaline spent batteries. *Waste Management*, 32(10), 1945–1951. <https://doi.org/10.1016/j.wasman.2012.05.008>
- Belardi, G., Medici, F., & Piga, L. (2014). Influence of gaseous atmosphere during a thermal process for recovery of manganese and zinc from spent batteries. *Journal of Power Sources*, 248, 1290–1298. <https://doi.org/10.1016/j.jpowsour.2013.10.064>

- Bernardes, A. M., Espinosa, D. C. R., & Tenório, J. A. S. (2004). Recycling of batteries: A review of current processes and technologies. *Journal of Power Sources*, 130(1–2), 291–298. <https://doi.org/10.1016/j.jpowsour.2003.12.026>
- Biesinger, M. C., Payne, B. P., Grosvenor, A. P., Lau, L. W. M., Gerson, A. R., & Smart, R. S. C. (2011). Resolving surface chemical states in XPS analysis of first row transition metals, oxides and hydroxides: Cr, Mn, Fe, Co and Ni. *Applied Surface Science*, 257(7), 2717–2730. <https://doi.org/10.1016/j.apsusc.2010.10.051>
- Bischoff, C. F., Fitz, O. S., Burns, J., Bauer, M., Gentischer, H., Birke, K. P., ... Biro, D. (2020). Revealing the Local pH Value Changes of Acidic Aqueous Zinc Ion Batteries with a Manganese Dioxide Electrode during Cycling. *Journal of The Electrochemical Society*, 167(2), 020545. <https://doi.org/10.1149/1945-7111/ab6c57>
- Biswal, A., Mahakud, S., Bhuyan, S., Dash, B., Sarangi, C. K., Sanjay, K., ... Park, K. H. (2015). Recovery of Co metal and Electrolytic Manganese Dioxide (EMD) from Co-Mn sludge. *Hydrometallurgy*, 152, 159–168. <https://doi.org/10.1016/j.hydromet.2015.01.006>
- Blackburn, S., & Wilson, D. I. (2008). Shaping ceramics by plastic processing. *Journal of the European Ceramic Society*, 28(7), 1341–1351. <https://doi.org/10.1016/j.jeurceramsoc.2007.12.013>
- Blake, G. R. (2015). Particle density. *Methods of Soil Analysis, Part 1: Physical and Mineralogical Properties, Including Statistics of Measurement and Sampling*, 9(11121), 371–373. <https://doi.org/10.2134/agronmonogr9.1.c29>
- Blight, G. (2011). Mine Waste: A Brief Overview of Origins, Quantities, and Methods of Storage. *Waste*, 77–88. <https://doi.org/10.1016/B978-0-12-381475-3.10005-1>

- Buzatu, M., Săceanu, S., Ghica, V. G., Iacob, G., & Buzatu, T. (2013). Simultaneous recovery of Zn and MnO₂ from used batteries, as raw materials, by electrolysis. *Waste Management*, 33(8), 1764–1769. <https://doi.org/10.1016/j.wasman.2013.04.010>
- Buzatu, T., Popescu, G., Birloaga, I., & Săceanu, S. (2013). Study concerning the recovery of zinc and manganese from spent batteries by hydrometallurgical processes. *Waste Management*, 33(3), 699–705. <https://doi.org/10.1016/j.wasman.2012.10.005>
- Cabral, M., Pedrosa, F., Margarido, F., & Nogueira, C. A. (2013). End-of-life Zn-MnO₂ batteries: Electrode materials characterization. *Environmental Technology (United Kingdom)*, 34(10), 1283–1295. <https://doi.org/10.1080/09593330.2012.745621>
- Cai, X., Zhang, Y., Hu, H., Huang, Z., Yin, Y., Liang, X., ... Liang, J. (2020). Valorization of manganese residue to prepare a highly stable and active Fe₃O₄@SiO₂/starch-derived carbon composite for catalytic degradation of dye waste water. *Journal of Cleaner Production*, 258, 120741. <https://doi.org/10.1016/j.jclepro.2020.120741>
- Canda, L., Heput, T., & Ardelean, E. (2016). Methods for recovering precious metals from industrial waste. *IOP Conference Series: Materials Science and Engineering*, 106(1). <https://doi.org/10.1088/1757-899X/106/1/012020>
- Cano, R., Mackey, K., & McGlacken, G. P. (2018). Recent advances in manganese-catalysed C-H activation: Scope and mechanism. *Catalysis Science and Technology*, 8(5), 1251–1266. <https://doi.org/10.1039/c7cy02514a>
- Carrero, C. A., Schloegl, R., Wachs, I. E., & Schomaecker, R. (2014). Critical Literature Review of the Kinetics for the Oxidative Dehydrogenation of Propane over Well-Defined Supported Vanadium Oxide Catalysts. *ACS Catalysis*, 4(10), 3357–3380. <https://doi.org/10.1021/cs5003417>

- Castellanos-Beltran, I. J., Assima, G. P., & Lavoie, J. M. (2018). Effect of temperature in the conversion of methanol to olefins (MTO) using an extruded SAPO-34 catalyst. *Frontiers of Chemical Science and Engineering*, 12(2), 226–238. <https://doi.org/10.1007/s11705-018-1709-8>
- Chai, W. S., Cheun, J. Y., Kumar, P. S., Mubashir, M., Majeed, Z., Banat, F., ... Show, P. L. (2021). A review on conventional and novel materials towards heavy metal adsorption in wastewater treatment application. *Journal of Cleaner Production*, 296, 126589. <https://doi.org/10.1016/j.jclepro.2021.126589>
- Chen, B. R., Sun, W., Kitchaev, D. A., Mangum, J. S., Thampy, V., Garten, L. M., ... Schelhas, L. T. (2018). Understanding crystallization pathways leading to manganese oxide polymorph formation. *Nature Communications*, 9(1). <https://doi.org/10.1038/s41467-018-04917-y>
- Chen, H., Liu, R., Shu, J., & Li, W. (2015). Simultaneous stripping recovery of ammonia-nitrogen and precipitation of manganese from electrolytic manganese residue by air under calcium oxide assist. *Journal of Environmental Science and Health - Part A Toxic/Hazardous Substances and Environmental Engineering*, 50(12), 1282–1290. <https://doi.org/10.1080/10934529.2015.1055157>
- Chen, J., Arandiyan, H., Gao, X., & Li, J. (2015). Recent Advances in Catalysts for Methane Combustion. *Catalysis Surveys from Asia*, 19(3), 140–171. <https://doi.org/10.1007/s10563-015-9191-5>
- Cheng, G., Yu, L., He, B., Sun, M., Zhang, B., Ye, W., & Lan, B. (2017). Catalytic combustion of dimethyl ether over α -MnO₂ nanostructures with different morphologies. *Applied Surface Science*, 409, 223–231. <https://doi.org/10.1016/j.apsusc.2017.02.218>

- Cheng, Z., Mozammel, T., Patel, J., Lee, W. J., Huang, S., Lim, S., ... Li, C. (2018). A method for the quantitative analysis of gaseous mixtures by online mass spectrometry. *International Journal of Mass Spectrometry*, 434, 23–28. <https://doi.org/10.1016/j.ijms.2018.09.002>
- Christensen, K. A. (2007). Chapter 11 Design of industrial catalysts. In *Computer Aided Chemical Engineering* (Vol. 23). [https://doi.org/10.1016/S1570-7946\(07\)80014-9](https://doi.org/10.1016/S1570-7946(07)80014-9)
- Cook, K. D., Bennett, K. H., & Haddix, M. L. (1999). On-line mass spectrometry: A faster route to process monitoring and control. *Industrial and Engineering Chemistry Research*, 38(4), 1192–1204. <https://doi.org/10.1021/ie9707984>
- Das, A. P., Ghosh, S., Mohanty, S., & Sukla, L. B. (2014a). Consequences of manganese compounds: a review. *Toxicological and Environmental Chemistry*, 96(7), 981–997. <https://doi.org/10.1080/02772248.2015.1005428>
- Das, A. P., Ghosh, S., Mohanty, S., & Sukla, L. B. (2014b). Consequences of manganese compounds: a review. *Toxicological and Environmental Chemistry*, 96(7), 981–997. <https://doi.org/10.1080/02772248.2015.1005428>
- Das, A. P., Sukla, L. B., Pradhan, N., & Nayak, S. (2011). Manganese biomining: A review. *Bioresource Technology*, 102(16), 7381–7387. <https://doi.org/10.1016/j.biortech.2011.05.018>
- Dash, S. S., & Parida, K. M. (2007). Esterification of acetic acid with n-butanol over manganese nodule leached residue. *Journal of Molecular Catalysis A: Chemical*, 266(1–2), 88–92. <https://doi.org/10.1016/j.molcata.2006.10.031>
- Dautzenberg, F. M. (1989). *Ten Guidelines for Catalyst Testing*. 99–119. <https://doi.org/10.1021/bk-1989-0411.ch011>

- de Oliveira Demarco, J., Stefanello Cadore, J., da Silveira de Oliveira, F., Hiromitsu Tanabe, E., & Assumpção Bertuol, D. (2019). Recovery of metals from spent lithium-ion batteries using organic acids. *Hydrometallurgy*, 190(December 2018), 105169. <https://doi.org/10.1016/j.hydromet.2019.105169>
- Desai, B. D., Fernandes, J. B., & Dalal, V. N. K. (1985). Manganese dioxide - a review of a battery chemical Part II. Solid state and electrochemical properties of manganese dioxides. *Journal of Power Sources*, 16(1), 1–43. [https://doi.org/10.1016/0378-7753\(85\)80001-X](https://doi.org/10.1016/0378-7753(85)80001-X)
- Dey, S., & Praveen Kumar, V. V. (2020). The performance of highly active manganese oxide catalysts for ambient conditions carbon monoxide oxidation. *Current Research in Green and Sustainable Chemistry*, 3(May), 100012. <https://doi.org/10.1016/j.crgsc.2020.100012>
- Du, B., Zhou, C. bo, & Duan, N. (2014). Recycling of electrolytic manganese solid waste in autoclaved bricks preparation in China. *Journal of Material Cycles and Waste Management*, 16(2), 258–269. <https://doi.org/10.1007/s10163-013-0181-2>
- Du, B., Zhou, C., Li, X., Guo, T., & Wang, Z. (2015). A kinetic study of Mn(II) precipitation of leached aqueous solution from electrolytic manganese residues. *Toxicological and Environmental Chemistry*, 97(3–4), 349–357. <https://doi.org/10.1080/02772248.2015.1050188>
- Duan, N., Fan, W., Changbo, Z., Chunlei, Z., & Hongbing, Y. (2010). Analysis of pollution materials generated from electrolytic manganese industries in China. *Resources, Conservation and Recycling*, 54(8), 506–511. <https://doi.org/10.1016/j.resconrec.2009.10.007>

- Duan, N., Zhou, C., Chen, B., Jiang, W., & Xin, B. (2011). Bioleaching of Mn from manganese residues by the mixed culture of *Acidithiobacillus* and mechanism. *Journal of Chemical Technology and Biotechnology*, *86*(6), 832–837. <https://doi.org/10.1002/jctb.2596>
- Dunlop, J. R., & Tully, F. P. (1993). A kinetic study of OH radical reactions with methane and perdeuterated methane. *Journal of Physical Chemistry*, *97*(43), 11148–11150. <https://doi.org/10.1021/j100145a003>
- Dwivedi, D., Randhawa, N. S., Saroj, S., & Jana, R. K. (2017). An Overview of Manganese Recovery by Hydro and Pyro-Metallurgical Routes. *Journal of The Institution of Engineers (India): Series D*, *98*(1), 147–154. <https://doi.org/10.1007/s40033-016-0119-7>
- Ebin, B., Petranikova, M., Steenari, B. M., & Ekberg, C. (2016). Production of zinc and manganese oxide particles by pyrolysis of alkaline and Zn-C battery waste. *Waste Management*, *51*, 157–167. <https://doi.org/10.1016/j.wasman.2015.10.029>
- Ebin, B., Petranikova, M., Steenari, B. M., & Ekberg, C. (2019). Recovery of industrial valuable metals from household battery waste. *Waste Management and Research*, *37*(2), 168–175. <https://doi.org/10.1177/0734242X18815966>
- Ellefson, R. E., Cain, D., & Lindsay, C. N. (1987). Calibration of mass spectrometers for quantitative gas mixture analysis. *Journal of Vacuum Science & Technology A: Vacuum, Surfaces, and Films*, *5*(1), 134–139. <https://doi.org/10.1116/1.574126>
- Elvidge, C. D., Bazilian, M. D., Zhizhin, M., Ghosh, T., Baugh, K., & Hsu, F. C. (2018). The potential role of natural gas flaring in meeting greenhouse gas mitigation targets. *Energy Strategy Reviews*, *20*, 156–162. <https://doi.org/10.1016/j.esr.2017.12.012>
- Energizer Brands, L. (2018). *Alkaline Manganese Dioxide Handbook and Application Manual*. 1–15.

- Falco, L., Quina, M. J., Gando-Ferreira, L. M., Thomas, H., & Curutchet, G. (2014). Solvent Extraction Studies for Separation of Zn(II) and Mn(II) from Spent Batteries Leach Solutions. *Separation Science and Technology (Philadelphia)*, 49(3), 398–409. <https://doi.org/10.1080/01496395.2013.850510>
- Farzana, R., Rajarao, R., Hassan, K., Behera, P. R., & Sahajwalla, V. (2018). Thermal nanosizing: Novel route to synthesize manganese oxide and zinc oxide nanoparticles simultaneously from spent Zn–C battery. *Journal of Cleaner Production*, 196, 478–488. <https://doi.org/10.1016/j.jclepro.2018.06.055>
- Farzana, R., Sayeed, M. A., Joseph, J., Ostrikov, K., O'Mullane, A. P., & Sahajwalla, V. (2020). Manganese Oxide Derived from a Spent Zn–C Battery as a Catalyst for the Oxygen Evolution Reaction. *ChemElectroChem*, 7(9), 2073–2080. <https://doi.org/10.1002/celec.202000422>
- Fawole, O. G., Cai, X. M., & Mackenzie, A. R. (2016). Gas flaring and resultant air pollution: A review focusing on black carbon. *Environmental Pollution*, 216, 182–197. <https://doi.org/10.1016/j.envpol.2016.05.075>
- Ferella, F., De Michelis, I., Beolchini, F., Innocenzi, V., & Vegliò, F. (2010). Extraction of zinc and manganese from alkaline and zinc-carbon spent batteries by citric-sulphuric acid solution. *International Journal of Chemical Engineering*, 2010. <https://doi.org/10.1155/2010/659434>
- Ferella, F., De Michelis, I., & Vegliò, F. (2008). Process for the recycling of alkaline and zinc-carbon spent batteries. *Journal of Power Sources*, 183(2), 805–811. <https://doi.org/10.1016/j.jpowsour.2008.05.043>

- Ferreira, B. S., Van Keulen, F., & Da Fonseca, M. M. R. (1998). Novel calibration method for mass spectrometers for on-line gas analysis. Set-up for the monitoring of a bacterial fermentation. *Bioprocess Engineering*, 19(4), 289–296.
<https://doi.org/10.1007/s004490050522>
- Fu, J., He, Z., Wang, H., Liang, W., & Guo, C. (2010). Preparation of chemical manganese dioxide from manganese sulfate. *Mining Science and Technology*, 20(6), 877–881.
[https://doi.org/10.1016/S1674-5264\(09\)60299-4](https://doi.org/10.1016/S1674-5264(09)60299-4)
- Gallegos, M. V., Falco, L. R., Peluso, M. A., Sambeth, J. E., & Thomas, H. J. (2013). Recovery of manganese oxides from spent alkaline and zinc-carbon batteries. An application as catalysts for VOCs elimination. *Waste Management*, 33(6), 1483–1490.
<https://doi.org/10.1016/j.wasman.2013.03.006>
- Gallegos, M. V., Peluso, M. A., Finocchio, E., Thomas, H. J., Busca, G., & Sambeth, J. E. (2017). Removal of VOCs by catalytic process. A study of MnZnO composites synthesized from waste alkaline and Zn/C batteries. *Chemical Engineering Journal*, 313, 1099–1111.
<https://doi.org/10.1016/j.cej.2016.11.001>
- Gancarczyk, A., Iwaniszyn, M., Piątek, M., Korpyś, M., Sinder, K., Jodłowski, P. J., ... Kołodziej, A. (2018). Catalytic Combustion of Low-Concentration Methane on Structured Catalyst Supports. *Industrial & Engineering Chemistry Research*, 57(31), 10281–10291.
<https://doi.org/10.1021/acs.iecr.8b01987>
- Gangwar, D., & Rath, C. (2021). *Structural , optical and magnetic properties of α - and β -MnO₂ nanorods*. 557(April).

- Gao, J., Wang, Y., Ping, Y., Hu, D., Xu, G., Gu, F., & Su, F. (2012). A thermodynamic analysis of methanation reactions of carbon oxides for the production of synthetic natural gas. *RSC Advances*, 2(6), 2358. <https://doi.org/10.1039/c2ra00632d>
- Gao, Y., Wang, Z., Cui, C., Wang, B., Liu, W., Liu, W., & Wang, L. (2020). Amorphous manganese oxide as highly active catalyst for soot oxidation. *Environmental Science and Pollution Research*, 27(12), 13488–13500. <https://doi.org/10.1007/s11356-020-07909-y>
- Ghosh, S., & Das, A. P. (2017). Bioleaching of manganese from mining waste residues using *Acinetobacter* sp. *Geology, Ecology, and Landscapes*, 1(2), 77–83. <https://doi.org/10.1080/24749508.2017.1332847>
- Ghosh, S., Mohanty, S., Akcil, A., Sukla, L. B., & Das, A. P. (2016). A greener approach for resource recycling: Manganese bioleaching. *Chemosphere*, 154, 628–639. <https://doi.org/10.1016/j.chemosphere.2016.04.028>
- Gregorová, E., Pabst, W., Smith, D. S., & Zivcová, Z. (2009). *Thermal conductivity of porous alumina ceramics prepared using starch as a pore-forming agent*. 29, 347–353. <https://doi.org/10.1016/j.jeurceramsoc.2008.06.018>
- Gunarathne, V., Rajapaksha, A. U., Vithanage, M., Alessi, D. S., Selvasembian, R., Naushad, M., ... Ok, Y. S. (2020). Hydrometallurgical processes for heavy metals recovery from industrial sludges. *Critical Reviews in Environmental Science and Technology*, 0(0), 1–41. <https://doi.org/10.1080/10643389.2020.1847949>
- Guo, M., Li, K., Liu, L., Zhang, H., Guo, W., Hu, X., ... Sun, T. (2019). Manganese-based multi-oxide derived from spent ternary lithium-ions batteries as high-efficient catalyst for VOCs oxidation. *Journal of Hazardous Materials*, 380, 120905. <https://doi.org/10.1016/j.jhazmat.2019.120905>

- Guo, M., Li, K., Liu, L., Zhang, H., Hu, X., Min, X., ... Sun, T. (2019). Resource utilization of spent ternary lithium-ions batteries: Synthesis of highly active manganese-based perovskite catalyst for toluene oxidation. *Journal of the Taiwan Institute of Chemical Engineers*, *102*, 268–275. <https://doi.org/10.1016/j.jtice.2019.06.012>
- Guo, M., Li, K., Zhang, H., Min, X., Liang, J., Hu, X., ... Sun, T. (2020). Promotional removal of oxygenated VOC over manganese-based multi oxides from spent lithium-ions manganate batteries: Modification with Fe, Bi and Ce dopants. *Science of the Total Environment*, *740*, 139951. <https://doi.org/10.1016/j.scitotenv.2020.139951>
- Guo, M., Liu, L., Gu, J. nan, Zhang, H., Min, X., Liang, J., ... Sun, T. (2021). Catalytic performance improvement of volatile organic compounds oxidation over MnOx and GdMnO3 composite oxides from spent lithium-ion batteries: Effect of acid treatment. *Chinese Journal of Chemical Engineering*. <https://doi.org/10.1016/j.cjche.2020.08.015>
- Guo, N., Wei, X. Q., Deng, X. L., & Xu, X. J. (2015). Synthesis and property of spinel porous ZnMn₂O₄ microspheres. *Applied Surface Science*, *356*, 1127–1134. <https://doi.org/10.1016/j.apsusc.2015.08.185>
- Haber, J. (1991). Manual on catalyst characterization (Recommendations 1991). *Pure and Applied Chemistry*, *63*(9), 1227–1246. <https://doi.org/10.1351/pac199163091227>
- Hagelstein, K. (2009). Globally sustainable manganese metal production and use. *Journal of Environmental Management*, *90*(12), 3736–3740. <https://doi.org/10.1016/j.jenvman.2008.05.025>
- Hammond, J. P. (2018). Quality Assurance: Spectroscopic Standards. In *Reference Module in Chemistry, Molecular Sciences and Chemical Engineering* (pp. 426–432). <https://doi.org/10.1016/B978-0-12-409547-2.00455-8>

- Han, Y. F., Chen, F., Zhong, Z., Ramesh, K., Chen, L., & Widjaja, E. (2006). Controlled synthesis, characterization, and catalytic properties of Mn₂O₃ and Mn₃O₄ nanoparticles supported on mesoporous silica SBA-15. *Journal of Physical Chemistry B*, *110*(48), 24450–24456. <https://doi.org/10.1021/jp064941v>
- Hanf, L., Henschel, J., Diehl, M., Winter, M., & Nowak, S. (2020). Mn²⁺ or Mn³⁺? Investigating transition metal dissolution of manganese species in lithium ion battery electrolytes by capillary electrophoresis. *Electrophoresis*, *41*(9), 697–704. <https://doi.org/10.1002/elps.201900443>
- He, C., Cheng, J., Zhang, X., Douthwaite, M., Pattison, S., & Hao, Z. (2019). Recent Advances in the Catalytic Oxidation of Volatile Organic Compounds: A Review Based on Pollutant Sorts and Sources [Review-article]. *Chemical Reviews*, *119*(7), 4471–4568. <https://doi.org/10.1021/acs.chemrev.8b00408>
- He, L., Fan, Y., Bellettre, J., Yue, J., & Luo, L. (2020). A review on catalytic methane combustion at low temperatures: Catalysts, mechanisms, reaction conditions and reactor designs. *Renewable and Sustainable Energy Reviews*, *119*(November 2019). <https://doi.org/10.1016/j.rser.2019.109589>
- He, L., Fan, Y., Luo, L., Bellettre, J., & Yue, J. (2020). Preparation of Pt/γ-Al₂O₃ catalyst coating in microreactors for catalytic methane combustion. *Chemical Engineering Journal*, *380*(August 2019). <https://doi.org/10.1016/j.cej.2019.122424>
- He, S., Jiang, D., Hong, M., & Liu, Z. (2021). Hazard-free treatment and resource utilisation of electrolytic manganese residue: A review. *Journal of Cleaner Production*, *306*. <https://doi.org/10.1016/j.jclepro.2021.127224>

- He, S., Wilson, B. P., Lundström, M., & Liu, Z. (2021). Hazard-free treatment of electrolytic manganese residue and recovery of manganese using low temperature roasting-water washing process. *Journal of Hazardous Materials*, 402(July 2020). <https://doi.org/10.1016/j.jhazmat.2020.123561>
- Hedden, M., Francis, N., Haraldsen, J. T., Ahmed, T., & Constantin, C. (2015). Thermoelectric properties of nano-meso-micro β -MnO₂ powders as a function of electrical resistance. *Nanoscale Research Letters*, 10(1). <https://doi.org/10.1186/s11671-015-1000-6>
- Heinzle, E., Moes, J., Griot, M., Kramer, H., Dunn, I. J., & Bourne, J. R. (1984). On-line mass spectrometry in fermentation. *Analytica Chimica Acta*, 163(C), 219–229. [https://doi.org/10.1016/S0003-2670\(00\)81510-X](https://doi.org/10.1016/S0003-2670(00)81510-X)
- Heinzle, E., Oeggerli, A., & Dettwiler, B. (1990). On-line fermentation gas analysis: Error analysis and application of mass spectrometry. *Analytica Chimica Acta*, 238(C), 101–115. [https://doi.org/10.1016/S0003-2670\(00\)80528-0](https://doi.org/10.1016/S0003-2670(00)80528-0)
- Helmus, R., ter Laak, T. L., van Wezel, A. P., de Voogt, P., & Schymanski, E. L. (2021). patRoom: open source software platform for environmental mass spectrometry based non-target screening. *Journal of Cheminformatics*, 13(1), 1–25. <https://doi.org/10.1186/s13321-020-00477-w>
- Herndon, E. M., & Brantley, S. L. (2011). Movement of manganese contamination through the Critical Zone. *Applied Geochemistry*, 26(SUPPL.), S40–S43. <https://doi.org/10.1016/j.apgeochem.2011.03.024>
- Hoffmann, E. De, & Stroobant, V. (2007). Mass Spectrometry Principles and Applications Third Edition. In *Mass spectrometry reviews* (Vol. 29). Retrieved from <https://www.wiley.com/en->

- us/Mass+Spectrometry%3A+Principles+and+Applications%2C+3rd+Edition-p-9780470033111
- Hohrenk, L. L., Itzel, F., Baetz, N., Tuerk, J., Vosough, M., & Schmidt, T. C. (2020). Comparison of Software Tools for Liquid Chromatography-High-Resolution Mass Spectrometry Data Processing in Nontarget Screening of Environmental Samples. *Analytical Chemistry*, 92(2), 1898–1907. <https://doi.org/10.1021/acs.analchem.9b04095>
- Holmes, N., Akien, G. R., Savage, R. J. D., Stanetty, C., Baxendale, I. R., Blacker, A. J., ... Bourne, R. A. (2016). Online quantitative mass spectrometry for the rapid adaptive optimisation of automated flow reactors. *Reaction Chemistry and Engineering*, 1(1), 96–100. <https://doi.org/10.1039/c5re00083a>
- Hoseini, S., Rahemi, N., Allahyari, S., & Tasbihi, M. (2019). Application of plasma technology in the removal of volatile organic compounds (BTX) using manganese oxide nano-catalysts synthesized from spent batteries. *Journal of Cleaner Production*, 232, 1134–1147. <https://doi.org/10.1016/j.jclepro.2019.05.227>
- Hoseini, S., Rahemi, N., Allahyari, S., Tasbihi, M., & Gharehabani, E. (2020). Effect of hydrometallurgical process parameters on the Mn₂O₃ nano catalysts derived from spent batteries used in the plasma catalytic oxidation of BTX. *Advanced Powder Technology*, 31(10), 4187–4196. <https://doi.org/10.1016/j.apt.2020.08.026>
- Ippolito, N. M., Belardi, G., Medici, F., & Piga, L. (2016). Utilization of automotive shredder residues in a thermal process for recovery of manganese and zinc from zinc-carbon and alkaline spent batteries. *Waste Management*, 51, 182–189. <https://doi.org/10.1016/j.wasman.2015.12.033>

- Işildar, A., Rene, E. R., van Hullebusch, E. D., & Lens, P. N. L. (2018). Electronic waste as a secondary source of critical metals: Management and recovery technologies. *Resources, Conservation and Recycling*, 135(December 2016), 296–312. <https://doi.org/10.1016/j.resconrec.2017.07.031>
- Ismail, O. S., & Umukoro, G. E. (2016). Modelling combustion reactions for gas flaring and its resulting emissions. *Journal of King Saud University - Engineering Sciences*, 28(2), 130–140. <https://doi.org/10.1016/j.jksues.2014.02.003>
- Jahan, M., Tominaka, S., & Henzie, J. (2016). Phase pure α -Mn₂O₃ prisms and their bifunctional electrocatalytic activity in oxygen evolution and reduction reactions. *Dalton Transactions*, 45(46), 18494–18501. <https://doi.org/10.1039/c6dt03158g>
- Jampaiah, D., Velisoju, V. K., Venkataswamy, P., Coyle, V. E., Nafady, A., Reddy, B. M., & Bhargava, S. K. (2017). Nanowire Morphology of Mono- and Bidoped α -MnO₂ Catalysts for Remarkable Enhancement in Soot Oxidation. *ACS Applied Materials and Interfaces*, 9(38), 32652–32666. <https://doi.org/10.1021/acsami.7b07656>
- Jaya, H., Firdaus Omar, M., Md Akil, H., Arifin Ahmad, Z., & Noriman Zulkepli, N. (2016). Sawdust polyethylene composites. *BioResources*, 11(3), 6489–6504. Retrieved from https://bioresources.cnr.ncsu.edu/wp-content/uploads/2016/07/BioRes_11_3_6489_Jaya_OAAZ_Effect_Particle_Size_Mecha_Prop_Sawdust_HDPE_Comp_9342.pdf
- Jee, J. E., Pestovsky, O., & Bakac, A. (2010). Preparation and characterization of manganese(IV) in aqueous acetic acid. *Dalton Transactions*, 39(48), 11636–11642. <https://doi.org/10.1039/c0dt00476f>

- Ji, F., Men, Y., Wang, J., Sun, Y., Wang, Z., Zhao, B., ... Xu, G. (2019). Promoting diesel soot combustion efficiency by tailoring the shapes and crystal facets of nanoscale Mn₃O₄. *Applied Catalysis B: Environmental*, 242(October 2018), 227–237. <https://doi.org/10.1016/j.apcatb.2018.09.092>
- Kaiser, R. I., Jansen, P., Petersen, K., & Roessler, K. (1995). On line and in situ quantification of gas mixtures by matrix interval algebra assisted quadrupole mass spectrometry. *Review of Scientific Instruments*, 66(11), 5226–5231. <https://doi.org/10.1063/1.1146089>
- Kim, B. S., Lee, J. C., Jeong, S. B., Lee, H. I., & Kim, C. W. (2010). Kinetics of the volatilization removal of zinc from manganese dust. *Materials Transactions*, 51(7), 1313–1318. <https://doi.org/10.2320/matertrans.M2010108>
- Kim, S. C., & Shim, W. G. (2010). Catalytic combustion of VOCs over a series of manganese oxide catalysts. *Applied Catalysis B: Environmental*, 98(3–4), 180–185. <https://doi.org/10.1016/j.apcatb.2010.05.027>
- Kloprogge, J. T., Ponce, C. P., & Loomis, T. A. (2020). The Periodic Table: Nature's Building Blocks. In *The Periodic Table: Nature's Building Blocks*. <https://doi.org/10.1016/C2019-0-03114-7>
- Klusacek, K., & Schneider, P. (1981). Effect of size and shape of catalyst on pellet pore structure and effectiveness. *Chemical Engineering Science*, 36, 523–527.
- Koivula, R., Pakarinen, J., Sivenius, M., Sirola, K., Harjula, R., & Paatero, E. (2009). Use of hydrometallurgical wastewater as a precursor for the synthesis of cryptomelane-type manganese dioxide ion exchange material. *Separation and Purification Technology*, 70(1), 53–57. <https://doi.org/10.1016/j.seppur.2009.08.014>

- Kononov, R., Ostrovski, O., & Ganguly, S. (2008). Carbothermal reduction of manganese oxide in different gas atmospheres. *Metallurgical and Materials Transactions B: Process Metallurgy and Materials Processing Science*, 39(5), 662–668. <https://doi.org/10.1007/s11663-008-9191-1>
- Kreutzer, M. T., Kapteijn, F., & Moulijn, J. A. (2006). Shouldn't catalysts shape up? Structured reactors in general and gas-liquid monolith reactors in particular. *Catalysis Today*, 111(1–2), 111–118. <https://doi.org/10.1016/j.cattod.2005.10.014>
- Kularatne, R. K. A., Kasturiarachchi, J. C., Manatunge, J. M. A., & Wijeyekoon, S. L. J. (2009). Mechanisms of Manganese Removal from Wastewaters in Constructed Wetlands Comprising Water Hyacinth (*Eichhornia crassipes* (Mart.) Solms) Grown under Different Nutrient Conditions . *Water Environment Research*, 81(2), 165–172. <https://doi.org/10.2175/106143008x370403>
- Kumar, S., García-Triñanes, P., Teixeira-Pinto, A., & Bao, M. (2013). Development of alkali activated cement from mechanically activated silico-manganese (SiMn) slag. *Cement and Concrete Composites*, 40, 7–13. <https://doi.org/10.1016/j.cemconcomp.2013.03.026>
- Lahousse, C., Bernier, A., Grange, P., Delmon, B., Papaefthimiou, P., Ioannides, T., & Verykios, X. (1998). Evaluation of γ -MnO₂ as a VOC removal catalyst: Comparison with a noble metal catalyst. *Journal of Catalysis*, 178(1), 214–225. <https://doi.org/10.1006/jcat.1998.2148>
- Lamaita, L., Peluso, M. A., Sambeth, J. E., & Thomas, H. J. (2005). Synthesis and characterization of manganese oxides employed in VOCs abatement. *Applied Catalysis B: Environmental*, 61(1–2), 114–119. <https://doi.org/10.1016/j.apcatb.2005.03.014>

- Lan, J., Sun, Y., Guo, L., Li, Z., Du, D., & Zhang, T. C. (2019). A novel method to recover ammonia, manganese and sulfate from electrolytic manganese residues by bio-leaching. *Journal of Cleaner Production*, 223, 499–507. <https://doi.org/10.1016/j.jclepro.2019.03.098>
- Lan, J., Sun, Y., Huang, P., Du, Y., Zhan, W., Zhang, T. C., & Du, D. (2020). Using Electrolytic Manganese Residue to prepare novel nanocomposite catalysts for efficient degradation of Azo Dyes in Fenton-like processes. *Chemosphere*, 252, 126487. <https://doi.org/10.1016/j.chemosphere.2020.126487>
- Lannoo, S., Vilas-Boas, A., Sadeghi, S. M., Jesus, J., & Soares, H. M. V. M. (2019). An environmentally friendly closed loop process to recycle raw materials from spent alkaline batteries. *Journal of Cleaner Production*, 236, 117612. <https://doi.org/10.1016/j.jclepro.2019.117612>
- Larsen, D., & Mann, R. (2005). Origin of high manganese concentrations in coal mine drainage, eastern Tennessee. *Journal of Geochemical Exploration*, 86(3), 143–163. <https://doi.org/10.1016/j.gexplo.2005.06.001>
- Le Bourre, B., Neculita, C. M., Coudert, L., & Rosa, E. (2020). Manganese removal processes and geochemical behavior in residues from passive treatment of mine drainage. *Chemosphere*, 259, 127424. <https://doi.org/10.1016/j.chemosphere.2020.127424>
- Lee, S. A., Lee, J. J., You, G. R., Choi, Y. W., & Kim, C. (2015). Distinction between Mn(III) and Mn(II) by using a colorimetric chemosensor in aqueous solution. *RSC Advances*, 5(116), 95618–95630. <https://doi.org/10.1039/c5ra20396a>
- Leite, D. da S., Carvalho, P. L. G., de Lemos, L. R., Mageste, A. B., & Rodrigues, G. D. (2019). Hydrometallurgical recovery of Zn(II) and Mn(II) from alkaline batteries waste employing

- aqueous two-phase system. *Separation and Purification Technology*, 210(July 2018), 327–334. <https://doi.org/10.1016/j.seppur.2018.07.038>
- Li, H., Zhang, Z., Tang, S., Li, Y., & Zhang, Y. (2008). Ultrasonically assisted acid extraction of manganese from slag. *Ultrasonics Sonochemistry*, 15(4), 339–343. <https://doi.org/10.1016/j.ultsonch.2007.07.010>
- Li, K., Chen, C., Zhang, H., Hu, X., Sun, T., & Jia, J. (2019). Effects of phase structure of MnO₂ and morphology of δ -MnO₂ on toluene catalytic oxidation. *Applied Surface Science*, 496(July). <https://doi.org/10.1016/j.apsusc.2019.143662>
- Li, M., Hu, L., Zhong, H., He, Z., Sun, W., & Xiong, D. (2021). Efficient removal of diethyl dithiocarbamate with EDTA functionalized electrolytic manganese residue and mechanism exploration. *Journal of Hazardous Materials*, 410(November), 124582. <https://doi.org/10.1016/j.jhazmat.2020.124582>
- Li, M., Huang, F., Hu, L., Sun, W., Li, E., Xiong, D. L., ... He, Z. (2020). Efficient activation of peroxymonosulfate by a novel catalyst prepared directly from electrolytic manganese slag for degradation of recalcitrant organic pollutants. *Chemical Engineering Journal*, 401, 126085. <https://doi.org/10.1016/j.cej.2020.126085>
- Li, M., Zhong, H., He, Z., Hu, L., Sun, W., Loganathan, P., & Xiong, D. (2021). Degradation of various thiol collectors in simulated and real mineral processing wastewater of sulfide ore in heterogeneous modified manganese slag/PMS system. *Chemical Engineering Journal*, 413, 127478. <https://doi.org/10.1016/j.cej.2020.127478>
- Li, Yongchao, Huang, H., Xu, Z., Ma, H., & Guo, Y. (2020). Mechanism study on manganese(II) removal from acid mine wastewater using red mud and its application to a lab-scale

- column. *Journal of Cleaner Production*, 253, 119955.
<https://doi.org/10.1016/j.jclepro.2020.119955>
- Li, Yongchao, Xu, Z., Ma, H., & Hursthouse, A. S. (2019). Removal of Manganese (II) from Acid Mine Wastewater : A Review of the Challenges and Opportunities with Special Emphasis on. *Water*, (Ii).
- Li, Yongdan, Wu, D., & Lin, Y. S. (2004). Mechanical strength and reliability of solid catalysts. *China Particuology*, 2(2), 53–62. [https://doi.org/10.1016/s1672-2515\(07\)60024-4](https://doi.org/10.1016/s1672-2515(07)60024-4)
- Li, Yunqing, & Xi, G. (2005). The dissolution mechanism of cathodic active materials of spent Zn-Mn batteries in HCl. *Journal of Hazardous Materials*, 127(1–3), 244–248.
<https://doi.org/10.1016/j.jhazmat.2005.07.024>
- Liang, S., Teng, F., Bulgan, G., Zong, R., & Zhu, Y. (2008). Effect of phase structure of MnO₂ nanorod catalyst on the activity for CO oxidation. *Journal of Physical Chemistry C*, 112(14), 5307–5315. <https://doi.org/10.1021/jp0774995>
- Lin, T., Yu, L., Sun, M., Cheng, G., Lan, B., & Fu, Z. (2016). Mesoporous α -MnO₂ microspheres with high specific surface area: Controlled synthesis and catalytic activities. *Chemical Engineering Journal*, 286, 114–121. <https://doi.org/10.1016/j.cej.2015.09.024>
- Liu, C., Han, Q., Chen, Y., Zhu, S., Su, T., Qu, Z., ... Huo, M. (2021). Resource Recycling of Mn-Rich Sludge: Effective Separation of Impure Fe/Al and Recovery of High-Purity Hausmannite. *ACS Omega*, 6(11), 7351–7359. <https://doi.org/10.1021/acsomega.0c05487>
- Liu, P. (2018). Recycling Waste Batteries: Recovery of Valuable Resources or Reutilization as Functional Materials. *ACS Sustainable Chemistry and Engineering*, 6(9), 11176–11185.
<https://doi.org/10.1021/acssuschemeng.8b03495>

- Liu, X., Shi, L., Jiang, W., Zhang, J., & Huang, L. (2018). Taking full advantage of KMnO₄ in simplified Hummers method: A green and one pot process for the fabrication of alpha MnO₂ nanorods on graphene oxide. *Chemical Engineering Science*, *192*, 414–421. <https://doi.org/10.1016/j.ces.2018.07.044>
- López, E., Gígola, C., Borio, D. O., & Bucalá, V. (2001). Catalytic combustion of methane over Pd/γ-Al₂O₃ in a monolithic reactor: Kinetic study. *Studies in Surface Science and Catalysis*, *133*(1961), 625–630. [https://doi.org/10.1016/s0167-2991\(01\)82023-1](https://doi.org/10.1016/s0167-2991(01)82023-1)
- Lu, J., Dreisinger, D., & Glück, T. (2014). Manganese electrodeposition — A literature review. *Hydrometallurgy*, *141*, 105–116. <https://doi.org/10.1016/j.hydromet.2013.11.002>
- Lyu, Y., Li, C., Du, X., Zhu, Y., Zhang, Y., & Li, S. (2020a). Catalytic oxidation of toluene over MnO₂ catalysts with different Mn (II) precursors and the study of reaction pathway. *Fuel*, *262*(August), 116610. <https://doi.org/10.1016/j.fuel.2019.116610>
- Lyu, Y., Li, C., Du, X., Zhu, Y., Zhang, Y., & Li, S. (2020b). Catalytic removal of toluene over manganese oxide-based catalysts: a review. *Environmental Science and Pollution Research*, *27*(3), 2482–2501. <https://doi.org/10.1007/s11356-019-07037-2>
- Malcolm, H. M., Wood, M., & Kingdom, U. (2004). IPCS Concise International Chemical Assessment Documents. Manganese and its compounds: Environmental aspects. *IPCS Concise International Chemical Assessment Documents*, (63), 1–37.
- Maryam Sadeghi, S., Vanpeteghem, G., Neto, I. F. F., & Soares, H. M. V. M. (2017). Selective leaching of Zn from spent alkaline batteries using environmentally friendly approaches. *Waste Management*, *60*, 696–705. <https://doi.org/10.1016/j.wasman.2016.12.002>

- Maynard, J. B. (2010). The chemistry of manganese ores through time: A signal of increasing diversity of earth-surface environments. *Economic Geology*, *105*(3), 535–552. <https://doi.org/10.2113/gsecongeo.105.3.535>
- Mears, D. E. (1971a). Diagnostic criteria for heat transport limitations in fixed bed reactors. *Journal of Catalysis*, *20*(2), 127–131. [https://doi.org/10.1016/0021-9517\(71\)90073-X](https://doi.org/10.1016/0021-9517(71)90073-X)
- Mears, D. E. (1971b). Tests for Transport Limitations in Experimental Catalytic Reactors. *Industrial and Engineering Chemistry Process Design and Development*, *10*(4), 541–547. <https://doi.org/10.1021/i260040a020>
- Melchor-Martínez, E. M., Macias-Garbett, R., Malacara-Becerra, A., Iqbal, H. M. N., Sosa-Hernández, J. E., & Parra-Saldívar, R. (2021). Environmental impact of emerging contaminants from battery waste: A mini review. *Case Studies in Chemical and Environmental Engineering*, *3*(April). <https://doi.org/10.1016/j.cscee.2021.100104>
- Menezes, P. W., Indra, A., Gutkin, V., & Driess, M. (2017). Boosting electrochemical water oxidation through replacement of Oh Co sites in cobalt oxide spinel with manganese. *Chemical Communications*, *53*(57), 8018–8021. <https://doi.org/10.1039/c7cc03749j>
- Michot, A., Smith, D. S., Degot, S., & Gault, C. (2008). Thermal conductivity and specific heat of kaolinite: Evolution with thermal treatment. *Journal of the European Ceramic Society*, *28*(14), 2639–2644. <https://doi.org/10.1016/j.jeurceramsoc.2008.04.007>
- Minette, F., Lugo-Pimentel, M., Modroukas, D., Davis, A. W., Gill, R., Castaldi, M. J., & De Wilde, J. (2018). Intrinsic kinetics of steam methane reforming on a thin, nanostructured and adherent Ni coating. *Applied Catalysis B: Environmental*, *238*, 184–197. <https://doi.org/10.1016/j.apcatb.2018.07.015>

- Mitchell, S., Michels, N. L., & Pérez-Ramírez, J. (2013). From powder to technical body: The undervalued science of catalyst scale up. *Chemical Society Reviews*, 42(14), 6094–6112. <https://doi.org/10.1039/c3cs60076a>
- Mocellin, J., Mercier, G., Morel, J. L., Blais, J. F., & Simonnot, M. O. (2015). Factors influencing the Zn and Mn extraction from pyrometallurgical sludge in the steel manufacturing industry. *Journal of Environmental Management*, 158, 48–54. <https://doi.org/10.1016/j.jenvman.2015.04.039>
- Mocellin, J., Mercier, G., Morel, J. L., Charbonnier, P., Blais, J. F., & Simonnot, M. O. (2017). Recovery of zinc and manganese from pyrometallurgy sludge by hydrometallurgical processing. *Journal of Cleaner Production*, 168, 311–321. <https://doi.org/10.1016/j.jclepro.2017.09.003>
- Mohammadzadeh, J. S. S., & Zamaniyan, A. (2002). Catalyst Shape As a Design Parameter — Optimum Shape for. *Transport*, 80(May), Part A.
- Mohanty, S., Ghosh, S., Bal, B., & Das, A. P. (2018). A review of biotechnology processes applied for manganese recovery from wastes. *Reviews in Environmental Science and Biotechnology*, 17(4), 791–811. <https://doi.org/10.1007/s11157-018-9482-1>
- Morais, V. S., Barrada, R. V., Moura, M. N., Almeida, J. R., Moreira, T. F. M., Gonçalves, G. R., ... Freitas, M. B. J. G. (2020). Synthesis of manganese ferrite from spent Zn-MnO₂ batteries and its application as a catalyst in heterogeneous photo-Fenton processes. *Journal of Environmental Chemical Engineering*, 8(3), 103716. <https://doi.org/10.1016/j.jece.2020.103716>

- Neculita, C. M., & Rosa, E. (2019). A review of the implications and challenges of manganese removal from mine drainage. *Chemosphere*, *214*, 491–510. <https://doi.org/10.1016/j.chemosphere.2018.09.106>
- Nogueira, C. A., & Margarido, F. (2015). Selective process of zinc extraction from spent Zn-MnO₂ batteries by ammonium chloride leaching. *Hydrometallurgy*, *157*, 13–21. <https://doi.org/10.1016/j.hydromet.2015.07.004>
- Okal, J., Zawadzki, M., & Baranowska, K. (2016). Methane combustion over bimetallic Ru-Re/ γ -Al₂O₃ catalysts: Effect of Re and pretreatments. *Applied Catalysis B: Environmental*, *194*, 22–31. <https://doi.org/10.1016/j.apcatb.2016.04.038>
- Olivares, J. A. (2006). Mass Spectrometry in Process Analysis. In *Encyclopedia of Analytical Chemistry* (pp. 1–16). <https://doi.org/10.1002/9780470027318.a2109>
- Ong, D. C., de Luna, M. D. G., Pingul-Ong, S. M. B., & Kan, C. C. (2018). Manganese and iron recovery from groundwater treatment sludge by reductive acid leaching and hydroxide precipitation. *Journal of Environmental Management*, *223*(January), 723–730. <https://doi.org/10.1016/j.jenvman.2018.06.052>
- Ong, D. C., Tumampos, S. B., Kan, C. C., Pingul-Ong, S. M. B., Ensano, B. M. B., & De Luna, M. D. G. (2021a). Optimization of manganese recovery from groundwater treatment sludge for the production of highly-efficient Cu(II) and Pb(II) adsorbents. *Journal of Environmental Chemical Engineering*, *9*(1), 104705. <https://doi.org/10.1016/j.jece.2020.104705>
- Ong, D. C., Tumampos, S. B., Kan, C. C., Pingul-Ong, S. M. B., Ensano, B. M. B., & De Luna, M. D. G. (2021b). Optimization of manganese recovery from groundwater treatment sludge

- for the production of highly-efficient Cu(II) and Pb(II) adsorbents. *Journal of Environmental Chemical Engineering*, 9(1). <https://doi.org/10.1016/j.jece.2020.104705>
- Park, Y. K., Kim, M. K., Jung, S. C., Shim, W. G., Jang, S. H., & Kim, S. C. (2021a). Effect of calcination temperature on properties of waste alkaline battery-based catalysts for deep oxidation of toluene and o-xylene. *Energy and Environment*, 32(3), 367–379. <https://doi.org/10.1177/0958305X20932551>
- Park, Y. K., Kim, M. K., Jung, S. C., Shim, W. G., Jang, S. H., & Kim, S. C. (2021b). Effect of calcination temperature on properties of waste alkaline battery-based catalysts for deep oxidation of toluene and o-xylene. *Energy and Environment*, 32(3), 367–379. <https://doi.org/10.1177/0958305X20932551>
- Park, Y. K., Song, H., Kim, M. K., Jung, S. C., Jung, H. Y., & Kim, S. C. (2021). Recycling of a spent alkaline battery as a catalyst for the total oxidation of hydrocarbons. *Journal of Hazardous Materials*, 403(September 2020), 123929. <https://doi.org/10.1016/j.jhazmat.2020.123929>
- Patil, D. S., Chavan, S. M., & Oubagaranadin, J. U. K. (2016). A review of technologies for manganese removal from wastewaters. *Journal of Environmental Chemical Engineering*, 4(1), 468–487. <https://doi.org/10.1016/j.jece.2015.11.028>
- Peng, N., Pan, Q., Liu, H., Yang, Z., & Wang, G. (2018). Recovery of iron and manganese from iron-bearing manganese residues by multi-step roasting and magnetic separation. *Minerals Engineering*, 126(May), 177–183. <https://doi.org/10.1016/j.mineng.2018.07.002>
- Piumetti, M., Fino, D., & Russo, N. (2015). Mesoporous manganese oxides prepared by solution combustion synthesis as catalysts for the total oxidation of VOCs. *Applied Catalysis B: Environmental*, 163, 277–287. <https://doi.org/10.1016/j.apcatb.2014.08.012>

- Post, J. E. (1999). Manganese oxide minerals: Crystal structures and economic and environmental significance. *Proceedings of the National Academy of Sciences of the United States of America*, 96(7), 3447–3454. <https://doi.org/10.1073/pnas.96.7.3447>
- Pulleri, J. K., Singh, S. K., Yearwar, D., Saravanan, G., Al-Fatesh, A. S., & Labhasetwar, N. K. (2021). Morphology Dependent Catalytic Activity of Mn₃O₄ for Complete Oxidation of Toluene and Carbon Monoxide. *Catalysis Letters*, 151(1), 172–183. <https://doi.org/10.1007/s10562-020-03278-w>
- Qi, W., Ran, J., Wang, R., Du, X., Shi, J., Niu, J., ... Ran, M. (2016). Kinetic consequences of methane combustion on Pd, Pt and Pd-Pt catalysts. *RSC Advances*, 6(111), 109834–109845. <https://doi.org/10.1039/c6ra21150j>
- Quintanilha, C. L., Afonso, J. C., Vianna, C. A., Gante, V., & Mantovano, J. L. (2014). Recovery of manganese and zinc via sequential precipitation from spent zinc-MnO₂ dry cells after fusion with potassium hydrogensulfate. *Journal of Power Sources*, 248, 596–603. <https://doi.org/10.1016/j.jpowsour.2013.09.111>
- R.D.W. Kemmitt and R.D. Peacock. (1973). *The Chemistry of Manganese, Technetium and Rhenium* (First). <https://doi.org/10.1016/C2013-0-05702-7>
- Rácz, R., & Ilea, P. (2013). Electrolytic recovery of Mn₃O₄ and Zn from sulphuric acid leach liquors of spent zinc-carbon-MnO₂ battery powder. *Hydrometallurgy*, 139, 116–123. <https://doi.org/10.1016/j.hydromet.2013.08.006>
- Rashid, R., Shafiq, I., Akhter, P., Iqbal, M. J., & Hussain, M. (2021). A state-of-the-art review on wastewater treatment techniques: the effectiveness of adsorption method. *Environmental Science and Pollution Research*, 28(8), 9050–9066. <https://doi.org/10.1007/s11356-021-12395-x>

- Ray, A., Bristow, T., Whitmore, C., & Mosely, J. (2018). On-line reaction monitoring by mass spectrometry, modern approaches for the analysis of chemical reactions. *Mass Spectrometry Reviews*, Vol. 37, pp. 565–579. <https://doi.org/10.1002/mas.21539>
- Reidies, A. H. (2000). Manganese Compounds. In *Ullmann's Encyclopedia of Industrial Chemistry* (Vol. 16, pp. 13–15). https://doi.org/10.1002/14356007.a16_123
- Ren, T., An, M., Hu, X., Ma, J., & Guo, Q. (2021). Development of inexpensive perovskite Mn-based oxygen carriers using the waste manganese sand for chemical looping gasification. *International Journal of Energy Research*, 45(2), 2416–2431. <https://doi.org/10.1002/er.5936>
- Rezaei, R., Moradi, G., & Sharifnia, S. (2019). Dry Reforming of Methane over Ni-Cu/Al₂O₃ Catalyst Coatings in a Microchannel Reactor: Modeling and Optimization Using Design of Experiments [Research-article]. *Energy & Fuels*, 33(7), 6689–6706. <https://doi.org/10.1021/acs.energyfuels.9b00692>
- Rubel, O., Nguyen, T., Tran, T., Gourley, S., Anand, S., Bommel, A. Van, ... Ivey, D. G. (n.d.). *Electrochemical Stability of ZnMn₂O₄: Understanding Zn-ion Rechargeable Battery*. 1–33.
- Sadeghabad, M. S., Bahaloo-Horeh, N., & Mousavi, S. M. (2019). Using bacterial culture supernatant for extraction of manganese and zinc from waste alkaline button-cell batteries. *Hydrometallurgy*, 188(December 2018), 81–91. <https://doi.org/10.1016/j.hydromet.2019.06.003>
- Sandoval-Bohorquez, V. S., Rozo, E. A. V., & Baldovino-Medrano, V. G. (2020). A method for the highly accurate quantification of gas streams by on-line chromatography. *Journal of Chromatography A*, 1626, 461355. <https://doi.org/10.1016/j.chroma.2020.461355>

- Satterfield, C. N. (1991). Acid and Zeolite Catalysts. *Heterogeneous Catalysis in Industrial Practice*, pp. 209–266.
- Sayilgan, E., Kukrer, T., Civelekoglu, G., Ferella, F., Akcil, A., Veglio, F., & Kitis, M. (2009). A review of technologies for the recovery of metals from spent alkaline and zinc-carbon batteries. *Hydrometallurgy*, 97(3–4), 158–166. <https://doi.org/10.1016/j.hydromet.2009.02.008>
- Scott Fogler, H. (1987). Elements of chemical reaction engineering. *Chemical Engineering Science*, 42(10), 2493. [https://doi.org/10.1016/0009-2509\(87\)80130-6](https://doi.org/10.1016/0009-2509(87)80130-6)
- Shen, B., Zhou, P., Chen, S., Yuan, H., Zhu, N., Sun, T., & Lou, Z. (2019). Manganese-based catalysts recovered from spent ternary lithium-ion batteries and its catalytic activity enhanced by a mechanical method. *Journal of Cleaner Production*, 213, 1346–1352. <https://doi.org/10.1016/j.jclepro.2018.12.248>
- Sher Shah, M. S. A., Oh, C., Park, H., Hwang, Y. J., Ma, M., & Park, J. H. (2020). Catalytic Oxidation of Methane to Oxygenated Products: Recent Advancements and Prospects for Electrocatalytic and Photocatalytic Conversion at Low Temperatures. *Advanced Science*, 7(23), 1–24. <https://doi.org/10.1002/advs.202001946>
- Shi, F., Wang, F., Dai, H., Dai, J., Deng, J., Liu, Y., ... Au, C. T. (2012). Rod-, flower-, and dumbbell-like MnO₂: Highly active catalysts for the combustion of toluene. *Applied Catalysis A: General*, 433–434, 206–213. <https://doi.org/10.1016/j.apcata.2012.05.016>
- Shu, J., Li, B., Chen, M., Sun, D., Wei, L., Wang, Y., & Wang, J. (2020). An innovative method for manganese (Mn²⁺) and ammonia nitrogen (NH₄⁺-N) stabilization/solidification in electrolytic manganese residue by basic burning raw material. *Chemosphere*, 253, 126896. <https://doi.org/10.1016/j.chemosphere.2020.126896>

- Shu, J., Liu, R., Liu, Z., Chen, H., & Tao, C. (2016a). Enhanced extraction of manganese from electrolytic manganese residue by electrochemical. *Journal of Electroanalytical Chemistry*, *780*, 32–37. <https://doi.org/10.1016/j.jelechem.2016.08.033>
- Shu, J., Liu, R., Liu, Z., Chen, H., & Tao, C. (2016b). Simultaneous removal of ammonia and manganese from electrolytic metal manganese residue leachate using phosphate salt. *Journal of Cleaner Production*, *135*, 468–475. <https://doi.org/10.1016/j.jclepro.2016.06.141>
- Shu, J., Wu, H., Chen, M., Peng, H., Li, B., Liu, R., ... Hu, Z. (2019). Fractional removal of manganese and ammonia nitrogen from electrolytic metal manganese residue leachate using carbonate and struvite precipitation. *Water Research*, *153*, 229–238. <https://doi.org/10.1016/j.watres.2018.12.044>
- Sie, S. T., & Krishna, R. (1998). Process development and scale up: II. Catalyst design strategy. *Reviews in Chemical Engineering*, *14*(3), 159–202. <https://doi.org/10.1515/REVCE.1998.14.3.159>
- Sihaib, Z., Puleo, F., Garcia-Vargas, J. M., Retailleau, L., Descorme, C., Liotta, L. F., ... Giroir-Fendler, A. (2017). Manganese oxide-based catalysts for toluene oxidation. *Applied Catalysis B: Environmental*, *209*, 689–700. <https://doi.org/10.1016/j.apcatb.2017.03.042>
- Sobianowska-Turek, A., Szczepaniak, W., Maciejewski, P., & Gawlik-Kobylińska, M. (2016). Recovery of zinc and manganese, and other metals (Fe, Cu, Ni, Co, Cd, Cr, Na, K) from Zn-MnO₂ and Zn-C waste batteries: Hydroxyl and carbonate co-precipitation from solution after reducing acidic leaching with use of oxalic acid. *Journal of Power Sources*, *325*(79), 220–228. <https://doi.org/10.1016/j.jpowsour.2016.06.042>

- Sobianowska-Turek, Agnieszka. (2018). Hydrometallurgical recovery of metals: Ce, La, Co, Fe, Mn, Ni and Zn from the stream of used Ni-MH cells. *Waste Management*, 77, 213–219. <https://doi.org/10.1016/j.wasman.2018.03.046>
- Sobianowska-Turek, Agnieszka, Szczepaniak, W., & Zabłocka-Malicka, M. (2014). Electrochemical evaluation of manganese reducers - Recovery of Mn from Zn-Mn and Zn-C battery waste. *Journal of Power Sources*, 270, 668–674. <https://doi.org/10.1016/j.jpowsour.2014.07.136>
- Soltanieh, M., Zohrabian, A., Gholipour, M. J., & Kalnay, E. (2016). A review of global gas flaring and venting and impact on the environment: Case study of Iran. *International Journal of Greenhouse Gas Control*, 49, 488–509. <https://doi.org/10.1016/j.ijggc.2016.02.010>
- Sotudeh-Gharebagh, R., & Chaouki, J. (2008). The Heterogeneous and Homogeneous Combustion of Methane Over Inert Particles. *The Canadian Journal of Chemical Engineering*, 81(6), 1182–1191. <https://doi.org/10.1002/cjce.5450810607>
- Staub, D., Meille, S., Le Corre, V., Chevalier, J., & Rouleau, L. (2015). Revisiting the Side Crushing Test Using the Three-Point Bending Test for the Strength Measurement of Catalyst Supports. *Oil & Gas Science and Technology – Revue d'IFP Energies Nouvelles*, 70(3), 475–486. <https://doi.org/10.2516/ogst/2013214>
- Stegarescu, A., Lung, I., Leoștean, C., Kacso, I., Opreș, O., Lazăr, M. D., ... Soran, M. L. (2020). Green Synthesis, Characterization and Test of MnO₂ Nanoparticles as Catalyst in Biofuel Production from Grape Residue and Seeds Oil. *Waste and Biomass Valorization*, 11(9), 5003–5013. <https://doi.org/10.1007/s12649-019-00805-8>
- Stranick, M. A. (1999). Mn₂O₃ by XPS. *Surface Science Spectra*, 6(1), 39–46. <https://doi.org/10.1116/1.1247889>

- Sun, L., Zhao, P., Liu, Y., Tan, B., Yu, C., Feng, N., ... Guan, G. (2021). Enhancing the catalytic activity of MnO₂ via structural phase transition for propane combustion: Promotional role of ionic liquid. *Journal of Environmental Chemical Engineering*, 9(6), 106453. <https://doi.org/10.1016/j.jece.2021.106453>
- Sun, Z., Cao, H., Xiao, Y., Sietsma, J., Jin, W., Agterhuis, H., & Yang, Y. (2017). Toward Sustainability for Recovery of Critical Metals from Electronic Waste: The Hydrochemistry Processes. *ACS Sustainable Chemistry and Engineering*, 5(1), 21–40. <https://doi.org/10.1021/acssuschemeng.6b00841>
- Survey, U. S. G. (2020). Mineral commodity summaries 2020. In *U.S Department OF The Interior, U.S Geological Survey*. Retrieved from <https://pubs.usgs.gov/periodicals/mcs2020/mcs2020.pdf>
- Takeda, A. (2003). Manganese action in brain function. *Brain Research Reviews*, 41(1), 79–87. [https://doi.org/10.1016/S0165-0173\(02\)00234-5](https://doi.org/10.1016/S0165-0173(02)00234-5)
- Thüne, P. C., & Niemantsverdriet, J. W. (Hans. (2009). Surface science models of industrial catalysts. *Surface Science*, 603(10–12), 1756–1762. <https://doi.org/10.1016/j.susc.2008.10.061>
- Tian, Y., Shu, J., Chen, M., Wang, J., Wang, Y., Luo, Z., ... Sun, Z. (2019). Manganese and ammonia nitrogen recovery from electrolytic manganese residue by electric field enhanced leaching. *Journal of Cleaner Production*, 236. <https://doi.org/10.1016/j.jclepro.2019.117708>
- Todorova, S., Stefanov, P., Naydenov, A., & Kolev, H. (2014). Catalytic oxidation of methane over Pd-MeO_x (Me = Mn, Co, Ni, Ce) catalysts - influence of metal oxides. *Revue Roumaine de Chimie*, 59(3–4), 251–257.

- Tomašić, V., & Jović, F. (2006). State-of-the-art in the monolithic catalysts/reactors. *Applied Catalysis A: General*, 311(1–2), 112–121. <https://doi.org/10.1016/j.apcata.2006.06.013>
- Toro, N., Jeldres, R. I., Órdenes, J. A., Robles, P., & Navarra, A. (2020). Manganese nodules in Chile, an alternative for the production of Co and Mn in the future—A review. *Minerals*, 10(8), 1–19. <https://doi.org/10.3390/min10080674>
- U.S. Geological Survey. (2021). *Manganese Commodity Summary 2021*. (703). Retrieved from <https://www.usgs.gov/centers/national-minerals-information-center/manganese-statistics-and-information>
- US EPA, O. (2021). *Recycling Basics*. 1–8. Retrieved from <https://www.epa.gov/recycle/recycling-basics>
- Vaudano, Pierre; Plattner, Eric; Comninellis, C. (1995). The Industrial Electrolytic Regeneration of $Mn_2(SO_4)_3$ for the Oxidation of Substituted Toluene to the Corresponding Benzaldehyde. *Chimia*, 49(1–2), 12. <https://doi.org/10.2533/chimia.1995.12>
- Velasco-Rozo, E. A., Ballesteros-Rueda, L. M., & Baldovino-Medrano, V. G. (2021). A Method for the Accurate Quantification of Gas Streams by Online Mass Spectrometry. *Journal of the American Society for Mass Spectrometry*, 32(8), 2135–2143. <https://doi.org/10.1021/jasms.1c00090>
- Walton, J., Alexander, M. R., Fairley, N., Roach, P., & Shard, A. G. (2016). Film thickness measurement and contamination layer correction for quantitative XPS. *Surface and Interface Analysis*, 48(3), 164–172. <https://doi.org/10.1002/sia.5934>
- Wang, C., Rosenfeldt, E., Li, Y., & Hofmann, R. (2020). External standard calibration method to measure the hydroxyl radical scavenging capacity of water samples. *Environmental Science and Technology*, 54(3), 1929–1937. <https://doi.org/10.1021/acs.est.9b06273>

- Wang, G., Zhang, J., Liu, L., Zhou, J. Z., Liu, Q., Qian, G., ... Richards, R. M. (2018). Novel multi-metal containing MnCr catalyst made from manganese slag and chromium wastewater for effective selective catalytic reduction of nitric oxide at low temperature. *Journal of Cleaner Production*, 183, 917–924. <https://doi.org/10.1016/j.jclepro.2018.02.207>
- Wang, G., Zhang, J., Zhou, J., & Qian, G. (2019). Production of an effective catalyst with increased oxygen vacancies from manganese slag for selective catalytic reduction of nitric oxide. *Journal of Environmental Management*, 239(February), 90–95. <https://doi.org/10.1016/j.jenvman.2019.03.056>
- Wang, N., Fang, Z., Peng, S., Cheng, D., Du, B., & Zhou, C. (2016). Recovery of soluble manganese from electrolyte manganese residue using a combination of ammonia and CO₂. *Hydrometallurgy*, 164, 288–294. <https://doi.org/10.1016/j.hydromet.2016.06.019>
- Wang, Xiuyun, Liu, Y., Zhang, Y., Zhang, T., Chang, H., Zhang, Y., & Jiang, L. (2018). Structural requirements of manganese oxides for methane oxidation: XAS spectroscopy and transition-state studies. *Applied Catalysis B: Environmental*, 229, 52–62. <https://doi.org/10.1016/j.apcatb.2018.02.007>
- Wang, Xu, Qiu, H., Liu, H., Shi, P., Fan, J., Min, Y., & Xu, Q. (2018). Recycling application of waste Li-MnO₂ batteries as efficient catalysts based on electrochemical lithiation to improve catalytic activity. *Green Chemistry*, 20(21), 4901–4910. <https://doi.org/10.1039/c8gc02183j>
- Wang, Y., Liu, Y., Cao, Q., Wang, C. A., & Che, D. (2011). Homogeneous combustion of fuel ultra-lean methane-air mixtures: Experimental study and simplified reaction mechanism. *Energy and Fuels*, 25(8), 3437–3445. <https://doi.org/10.1021/ef200484c>

- Watson, J. T., & Sparkman, O. D. (2007). *Introduction to Mass Spectrometry* (Fourth Edi).
<https://doi.org/10.1002/9780470516898>
- Wei, Y., Ni, L., Li, M., & Zhao, J. (2017). A template-free method for preparation of MnO₂ catalysts with high surface areas. *Catalysis Today*, 297, 188–192.
<https://doi.org/10.1016/j.cattod.2016.12.044>
- Whelpton, R. (2019). Quality assurance | internal standards. In *Encyclopedia of Analytical Science* (3rd ed.). <https://doi.org/10.1016/B978-0-12-409547-2.14399-9>
- Winiarska, K., Klimkiewicz, R., Tylus, W., Sobianowska-Turek, A., Winiarski, J., Szczygieł, B., & Szczygieł, I. (2019). Study of the catalytic activity and surface properties of manganese-zinc ferrite prepared from used batteries. *Journal of Chemistry*, 2019.
<https://doi.org/10.1155/2019/5430904>
- Wu, F. F., Li, X. P., Zhong, H., & Wang, S. (2016). Utilization of Electrolytic Manganese Residues in Production of Porous Ceramics. *International Journal of Applied Ceramic Technology*, 13(3), 511–521. <https://doi.org/10.1111/ijac.12502>
- Xin, B., Chen, B., Duan, N., & Zhou, C. (2011). Extraction of manganese from electrolytic manganese residue by bioleaching. *Bioresource Technology*, 102(2), 1683–1687.
<https://doi.org/10.1016/j.biortech.2010.09.107>
- Xin, B., Jiang, W., Aslam, H., Zhang, K., Liu, C., Wang, R., & Wang, Y. (2012). Bioleaching of zinc and manganese from spent Zn-Mn batteries and mechanism exploration. *Bioresource Technology*, 106, 147–153. <https://doi.org/10.1016/j.biortech.2011.12.013>
- Xin, B., Jiang, W., Li, X., Zhang, K., Liu, C., Wang, R., & Wang, Y. (2012). Analysis of reasons for decline of bioleaching efficiency of spent Zn-Mn batteries at high pulp densities and

- exploration measure for improving performance. *Bioresource Technology*, *112*, 186–192.
<https://doi.org/10.1016/j.biortech.2012.02.133>
- Xu, F., Jiang, L., Dan, Z., Gao, X., Duan, N., Han, G., & Zhu, H. (2014). Water balance analysis and wastewater recycling investigation in electrolytic manganese industry of China - A case study. *Hydrometallurgy*, *149*, 12–22. <https://doi.org/10.1016/j.hydromet.2014.05.002>
- Xu, H., Yan, N., Qu, Z., Liu, W., Mei, J., Huang, W., & Zhao, S. (2017). Gaseous Heterogeneous Catalytic Reactions over Mn-Based Oxides for Environmental Applications: A Critical Review. *Environmental Science and Technology*, *51*(16), 8879–8892.
<https://doi.org/10.1021/acs.est.6b06079>
- Yang, Renchun, Ren, C., Teng, X., Chen, Z., Wu, S., & Zhang, W. (2017). Study of the Surface Oxygen Vacancies Evolvement on the Single and Bi-Components Manganese Oxide Precursors and their Catalytic Performance. *Catalysis Letters*, *147*(3), 727–737.
<https://doi.org/10.1007/s10562-017-1973-0>
- Yang, Ruizhi, Wang, Z., Dai, L., & Chen, L. (2005). Synthesis and characterization of single-crystalline nanorods of α -MnO₂ and γ -MnOOH. *Materials Chemistry and Physics*, *93*(1), 149–153. <https://doi.org/10.1016/j.matchemphys.2005.03.006>
- Ying, A. Y., Lu, Z., & Abdou, M. A. (1998). Mechanical behavior and design database of packed beds for blanket designs. *Fusion Engineering and Design*, *39–40*, 759–764.
[https://doi.org/10.1016/S0920-3796\(97\)00157-9](https://doi.org/10.1016/S0920-3796(97)00157-9)
- Yuan, A., Wang, X., Wang, Y., & Hu, J. (2009). Textural and capacitive characteristics of MnO₂ nanocrystals derived from a novel solid-reaction route. *Electrochimica Acta*, *54*(3), 1021–1026. <https://doi.org/10.1016/j.electacta.2008.08.057>

- Zakeri, M., Samimi, A., Shafiee Afarani, M., & Salehirad, A. (2018). Effects of porosity and pore size distribution on mechanical strength reliability of industrial-scale catalyst during preparation and catalytic test steps. *Particulate Science and Technology*, *36*(1), 96–103. <https://doi.org/10.1080/02726351.2016.1220437>
- Zeng, F., Pan, Y., Yang, Y., Li, Q., Li, G., Hou, Z., & Gu, G. (2016). Facile construction of Mn₃O₄-MnO₂ hetero-nanorods/graphene nanocomposite for highly sensitive electrochemical detection of hydrogen peroxide. *Electrochimica Acta*, *196*, 587–596. <https://doi.org/10.1016/j.electacta.2016.03.031>
- Zhang, K., Peng, X., Cao, Y., Yang, H., Wang, X., Zhang, Y., ... Jiang, L. (2019a). Effect of MnO₂ morphology on its catalytic performance in lean methane combustion. *Materials Research Bulletin*, *111*, 338–341. <https://doi.org/10.1016/j.materresbull.2018.11.023>
- Zhang, K., Peng, X., Cao, Y., Yang, H., Wang, X., Zhang, Y., ... Jiang, L. (2019b). Effect of MnO₂ morphology on its catalytic performance in lean methane combustion. *Materials Research Bulletin*, *111*(January 2018), 338–341. <https://doi.org/10.1016/j.materresbull.2018.11.023>
- Zhang, L., Wang, S., Lv, L., Ding, Y., Tian, D., & Wang, S. (2021). Insights into the Reactive and Deactivation Mechanisms of Manganese Oxides for Ozone Elimination: The Roles of Surface Oxygen Species. *Langmuir*, *37*(4), 1410–1419. <https://doi.org/10.1021/acs.langmuir.0c02841>
- Zhang, W., & Cheng, C. Y. (2007a). Manganese metallurgy review. Part I: Leaching of ores/secondary materials and recovery of electrolytic/chemical manganese dioxide. *Hydrometallurgy*, *89*(3–4), 137–159. <https://doi.org/10.1016/j.hydromet.2007.08.010>

- Zhang, W., & Cheng, C. Y. (2007b). Manganese metallurgy review. Part II: Manganese separation and recovery from solution. *Hydrometallurgy*, 89(3–4), 160–177. <https://doi.org/10.1016/j.hydromet.2007.08.009>
- Zhang, W., & Cheng, C. Y. (2007c). Manganese metallurgy review. Part III: Manganese control in zinc and copper electrolytes. *Hydrometallurgy*, 89(3–4), 178–188. <https://doi.org/10.1016/j.hydromet.2007.08.011>
- Zhou, C., Wang, J., Liu, X., Chen, F., Di, Y., Gao, S., & Shi, Q. (2018). Magnetic and thermodynamic properties of α , β , γ and δ -MnO₂. *New Journal of Chemistry*, 42(11), 8400–8407. <https://doi.org/10.1039/c8nj00896e>
- Zhou, X., Luo, C., Wang, J., Wang, H., Chen, Z., Wang, S., & Chen, Z. (2021). Recycling application of modified waste electrolytic manganese anode slag as efficient catalyst for PMS activation. *Science of the Total Environment*, 762, 143120. <https://doi.org/10.1016/j.scitotenv.2020.143120>
- Zimmerman, J. B., Anastas, P. T., Erythropel, H. C., & Leitner, W. (2020). Designing for a green chemistry future. *Science*, 367(6476), 397–400. <https://doi.org/10.1126/science.aay3060>

Appendices

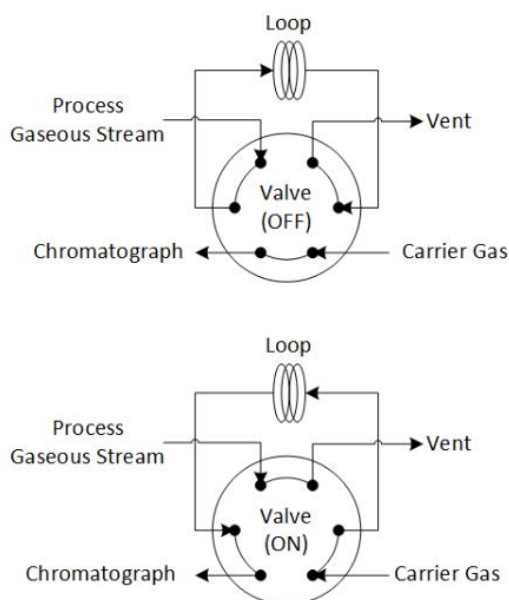
Appendix A. Method for the highly accurate quantification of gas streams by on-line chromatography

On-line chromatography is the most used technique to quantitatively characterize the gaseous streams from chemical reactors and certain unit operations [1–3]. By “on-line,” it is implied that the gas chromatograph (GC) is connected to the outlet stream of the corresponding process unit. The gaseous samples must be introduced into the GC by intricate arrangements of valves. Fig. 1 sketches a basic six-way valve system that allows the automatic injection of the samples into the instrument. In a typical run, the outlet gas stream from the given process continuously passes through a loop, placed in the injection port of the chromatograph, and discharges in a vent (Fig. 1 top). When a sample is to be analyzed, the valve is switched to a position in which the gas flowing by the loop is injected to the GC by passing the carrier gas of the instrument through the loop in order to carry the analyte into the chromatograph (Fig. 1 bottom). In most conventional on-line GC systems, the atmospheric conditions, namely, temperature and pressure, can affect the quantity of analyte collected by the loop to a degree where reproducibility between runs becomes a stringent constraint of the analysis [4]. To correct this issue, internal standards are added to the gaseous samples during each sample injection.[2]; alternatively, some researchers have opted for implementing statistical methods for assessing the uncertainty in the quantity of analyte that is injected in the runs of their on-line GC systems [4,5].

After accomplishing the automatized injection of the sample, the carrier gas carries the analyte through the separation columns, where each gaseous compound is partially retained and separated and further eluted before reaching the detection system of the instrument.

Figure 1.

Scheme of the injection mechanism in on-line gas chromatography, in the normal position (top) and the injection position (bottom).



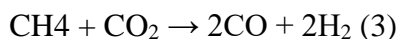
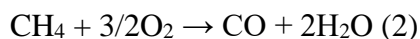
Most on-line GC detection systems used for the analysis of gaseous streams from hydrocarbon or biomass related processes are typically configured with one or several detectors such as: i) one Thermal Conductivity Detector (TCD) able to detect gaseous compounds as a function of their differences in thermal conductivity and whose concentration is higher than ~100ppm; ii) one Flame Ionization Detector (FID) that detects hydrocarbons in concentrations higher than ~0.5ppm, but cannot detect permanent gases like O₂, N₂, CO, CO₂, and H₂O [2]. Due to this limitation, most GC systems are provided by iii) a serial TCD-FID arrangement that allows

detecting permanent gases with the TCD and hydrocarbons with the FID; and iv) TCD-methanizer-FID arrangements that allow detecting concentrations of CO₂ and CO below the 100ppm limit of the TCD, by hydrogenating CO₂ and CO to methane after passing a fraction of the analyte through a small catalytic reactor; called the methanizer, and further submitting the outlet of the methanizer to the FID [6]. Despite the implementation of TCD-methanizer-FID arrangements, on-line GC systems still have other drawbacks when aiming to make a complete characterization of a gaseous stream containing both hydrocarbons and non-hydrocarbon gases.

On-line GC systems are fundamental for the study and monitoring of gaseous catalytic reaction units. Within this context, very accurate and reliable quantification of the concentration of each reactant is a must when assessing the performance of either the reaction unit or of the catalyst itself. Within this context, achieving closed mass balances from the input and output gaseous streams of the reaction systems is a necessary condition for process de-sign and monitoring. Mass balances must be calculated from the relative concentrations quantified by the TCD and FID detectors of the on-line GC. However, such a task can be challenging up to a point where many process operators and even researchers either consider it helpless or tend to ignore it. The problem of achieving closed mass balances is associated with the inherent limitations of each type of detector as described before and with the fact that one needs to devise a reliable method for relating the concentrations of the different compounds from more than one detector at the same time.

As particular examples of the hurdles of measuring concentrations and closing mass balances from data read from more than one detector in an on-line GC, it may be cite processes in which relatively simple reactions such as the total (Eq. 1) or partial (Eq. 2) combustion of methane,

and the reforming of methane with carbon dioxide, a.k.a. dry re-forming, (Eq. 3), must be followed by on-line GC.



To do so, the instrument must be at least provided with both one TCD and one FID since the outlet gas stream is composed by CH₄, O₂, H₂, CO₂, CO, and H₂O [7–10]. These reactions are traditionally studied as alternatives for the abatement or valorization of methane which is a 21 times more potent greenhouse gas than carbon dioxide [11–13]. At the research level, many scientists devote efforts towards the development of low-cost stable catalysts able to activate methane at the lowest possible temperature [11,12,14–17]. For this purpose, the studies are most often carried out in fixed bed catalytic micro-reactors whose output is monitored by on-line GC with input streams whose composition is about 0.1-10 vol. % of methane, 2-50 vol. % oxygen diluted in nitrogen, argon or helium [11]. Let us consider the lower concentration of reactants and assume 80% conversion of methane to CO₂ (Eq. 1), and 10% conversion to CO (Eq. 2); the output stream would be composed for ~100 ppm CH₄, ~800ppm CO₂, and ~100ppm CO. If only a TCD is employed for quantification, the results would be 100% conversion of methane to CO₂, i.e., an overestimation of 10% in conversion and selectivity, which is due to such hydrocarbon together the CO are in concentrations hardly detected by the TCD.

For the above, it is usually preferred a GC with at least a serial TCD-FID arrangement for detection. However, most investigators report quantification either by only the TCD or the FID or from an uncorrelated combination of both detectors. Furthermore, they seldom neither report statistics on the reliability of their measurements nor the mass balances for the analyzed gaseous

streams of their catalytic setups [18–22]. Besides the complications inherent to handle quantification with more than one detector, on-line GC analyses of the products from these reaction systems is complicated by the selection of an adequate internal standard. For example, the internal standard to be added must be more stable than the reactants under the usually harsh reaction conditions employed to test the catalysts [23,24]. Consequently, only gases such as N₂, He, and Ar are suitable as internal standards for methane combustion and dry reforming. However, none of these gases is detected by the FID hence hampering the analysis of the fluctuations in the amount of analyte injected after taken each sample. Under such circumstances, the analysis must rely on the response from the TCD even if the GC is also provided with a methanizer. As already mentioned, a TCD is two orders of magnitude less sensible as compared to an FID; hence relying solely on the former also harms product quantification.

This contribution presents an alternative method for quantifying the composition of gaseous streams by on-line GC. Particularly, it was successfully implemented a method that, using N₂ as an internal standard, allows correlating the responses from a serial TCD-FID arrangement for compounds quantification while checking for mass balance closure during the analysis of the gaseous effluents from a catalytic reactor. As an example, it is shown how this method was implemented to monitor the effluents from a lab-scale reaction setup performing the catalytic combustion of methane. The mathematical deduction of a parameter called sensitivity factor allowed for the combined use of both the signals from the TCD and the FID for quantification despite their strong differences in sensibility. In general, the developed method can be applied to the on-line GC monitoring of any gaseous stream.

1. Analysis of the performance of catalytic systems from the GC quantification of gaseous streams.

Before presenting the mathematical fundamentals of the method, it is detailed how the performance of catalytic systems is assessed by GC quantification of gas effluents.

According to IUPAC recommendations [25], the catalytic performance of a catalytic system can be assessed by calculating the conversion of reactants (X_r) and the selectivity toward the products from the reaction. For continuous reactors; which are those most often monitored by on-line GC, the conversion of reactants is calculated in terms of the molar flow of the feed (reactants) that inlet (F_r^0) and outlet (F_r) the reactor following Eq. 4. Conversion is thus defined as a parameter that describes the fraction of a given reactant that has reacted. Therefore, conversion is the first metric for analyzing the catalytic activity of a given material. On the other hand, the selectivity to any given reaction product (S_p) is calculated as a function of the molar flow of products detected at the inlet (F_p^0) and outlet (F_p) of the reactor multiplied by the ratio between the stoichiometric coefficients of the reactants and products (ν), as shown in Eq. 5. Selectivity is a critical metric for the assessment of the catalytic properties of a material since it is directly related to the cost-benefit ratio of the process.

$$X_r = \frac{F_r^0 - F_r}{F_r^0} \quad (4)$$

$$S_p = \nu \frac{F_p - F_p^0}{F_r^0 - F_r} \quad (5)$$

Within this context, the challenge when quantifying conversion and selectivity by on-line GC thus consists of measuring the molar flow of all species that participate in the reaction as a function of the detector signal with the highest precision possible. There are two possible methods

for a high accurate quantification of molar flows with GC. They are the so called external and internal standard methods.

2.1 External standard method

In the case of chromatographic analysis, the concentration of the i -th compound (reactant, r , or product, p) in a gaseous sample (e.g., the ratio between the molar flow of the i -th compound, F_i , and the total molar flow, F_T) can be related to the area of its peak (A_i) in the corresponding chromatogram by way of a proportionality constant named response factor (γ_i), as shown in Eq. 6. The value of this constant must be calculated for each species by a calibration curve obtained from plotting different known molar flows and their respective signal. By replacing the Eq. 6 in Eqs. 4 and 5, and assuming that the total molar flow is constant ($F_T^0 = F_T$), the conversion and selectivity in terms of the chromatograph response can be obtained as shown in Eq. 7 and 8. By correlating the F_i/F_T ratio with the chromatographic peak areas, the fluctuations of the gas flows, mostly caused by the contraction of the gases due to thermal gradients, can be normalized.

$$\frac{F_i}{F_T} = \gamma_i * A_i \quad (6)$$

$$X_r = \frac{A_r^0 - A_r}{A_r^0} \quad (7)$$

$$S_p = v \frac{\gamma_p}{\gamma_r} \frac{A_p}{(A_r^0 - A_r)} \quad (8)$$

Closure of the mass balance in the reaction system allows validating the calculated conversion and selectivity. Herein, it was defined mass balances, B_z , as the ratio between the total mass of the atomic species z (i.e., carbon, oxygen or hydrogen) at the outlet and the inlet of the reactor, as shown in Eq. 9.

$$B_z = \frac{\sum_i (\gamma_i A_i N_{z,i})}{\sum_i (\gamma_i A_i^0 N_{z,i})} \quad (9)$$

Where, $N_{z,i}$ is the number of atoms of the z species present in compound i -th.

2.2 Internal standard method

The methodology featured in the precedent section is commonly known as the external standard method. One of the problems of this method is the change in the total molar flow of gas stream after passage through the catalytic reactor. Under such circumstances, the installation of a detection system able to measure the F_T^0 and F_T molar flows would be a must. Another problem is that the natural fluctuations of the atmospheric conditions (pressure, P , and temperature, T) can vary the total amount of injected moles (n_T) into the GC, although the instrument has an injection loop of constant volume (V_{loop}), see Eq. 10. Because of this, variations of the recorded peak areas which are due to random errors, introduce uncertainty in the quantification.

$$n_T = \frac{P V_{loop}}{R T} \quad (10)$$

A means to control the fluctuations in both the total amount of moles injected by the loop of the GC and the total molar flow of the gaseous stream is to add an internal standard. Therefore, Eq. 6 is modified as shown in Eq. 11. In this case, the ratio between A_i and the chromatographic peak area for the standard (A_s) can be related to the ratio between F_i and the respective molar flow of the standard (F_s), using a response factor (β_i). This normalization procedure counteracts the fluctuations in the amount of sample injected to the GC.

$$\frac{F_i}{F_s} = \beta_i * \frac{A_i}{A_s} \quad (11)$$

For the method to be successful, the standard must remain inert under the reaction conditions employed in the corresponding catalytic tests. If this condition is fulfilled, the molar flow of the standard is constant. Therefore, using the internal standard method, it can be calculated the conversion of the reactants with Eq. 12, which is obtained by replacing Eq. 11 into Eq. 4 and making $\omega = A_s^0/A_s$. Likewise, the selectivity, Eq. 13, is calculated by replacing Eq. 11 into Eq. 5 while the mass balance can be calculated with Eq. 14.

$$X_r = \frac{A_r^0 - A_r \omega}{A_r^0} \quad (12)$$

$$S_p = v \frac{\beta_p}{\beta_r} \frac{A_p \omega}{(A_r^0 - A_r \omega)} \quad (13)$$

$$B_z = \frac{\omega \sum_i^n (\beta_i A_i N_{z,i})}{\sum_i^n (\beta_i A_i^0 N_{z,i})} \quad (14)$$

3. Experimental

3.1 Catalytic tests

The GC quantification of the gaseous streams from a catalytic reactor for the combustion of methane was used to test the analytical methods presented herein. The catalytic tests were carried out in a continuous flow fixed bed reactor made of stainless steel with an inner diameter of 10.4 mm. The bed was made of 100 mg of MnO₂, supplied by Erachem Comilog (LOT 622) (Baldovino-Medrano et al., 2019a), diluted with 500 mg of SiO₂, both with a particle size of 75-180 μ m. The amount of diluent and the bed particle size were selected in order to satisfy the criteria presented in Table 1. Plugs made of quartz wool were placed before and after the catalytic bed to ensure isothermal conditions and plug flow.

Table 1.

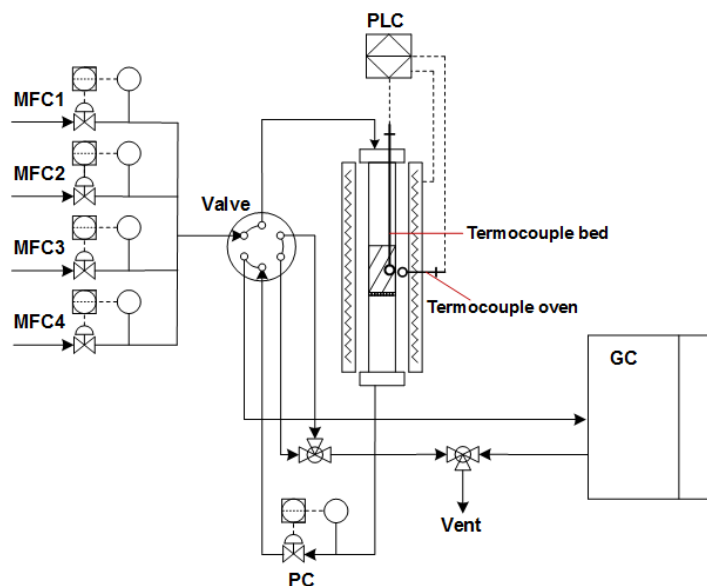
Analytical criteria used to reduce intra-reactor limitations. L is the length of the bed, d_p is the particle diameter, d_t is the internal diameter of the tube, b_{max} is the maximum volumetric dilution ratio (inert volume/total volume of solids), Δx_{rel} is the acceptable relative deviation of the conversion (e.g., 0.05), and x_{dil} is the conversion obtained with the diluted bed (Minette et al., 2018).

Criteria	Expression
Negligible axial dispersion	$\frac{L}{d_p} > 20 - 50$
Negligible radial dispersion	$\frac{d_t}{d_p} > 8 - 10$
Maximum volumetric dilution of the bed	$b_{max} = \frac{\Delta x_{rel}}{\Delta x_{rel} + 0.5x_{dil} \frac{d_p}{L}}$

The reaction feed was a mixture of 7.7 vol. % of methane and 15.4 vol. % of oxygen diluted in nitrogen. The space velocity was 78000 mL g⁻¹ min⁻¹. It was used mass flow controllers (MFC, Alicat Scientific) with an accuracy of ±0.1 % of full scale to feed the reactor. The outlet pressure of the reaction system was set at 110.3 kPa using a back-pressure controller (PC, Alicat Scientific) with an accuracy of ± 0.3 % of full scale. The catalytic reactor was heated to the reaction temperature, 500 °C, by placing it inside a concentric tubular furnace controlled by a programmable logic controller (PLC, Rockwell Automation) with a heating ramp of 5 °C min⁻¹. The temperature of the catalytic bed was measured by inserting a Type K thermocouple provided with stainless steel sheath and an external diameter of 3.2 mm in the middle of it. Before the tests, the catalyst was dried at 120 °C with a flow of 100 mL min⁻¹ of N₂ for 1 h. Fig 2 shows a scheme of the reaction system.

Figure 2.

Schematic representation of the reaction system. MFC: mass flow controller; PC: pressure controller; PLC: programmable logic controller; GC: gas chromatograph.



The feed and reaction products were analyzed by on-line chromatography using a GC-2014 instrument (Shimadzu Corporation). The internal configuration of the detectors and the set of packed columns used for the chromatographic analyses is presented in Fig. 3. The reactor outlet gases flowed continuously during the reaction by the 1 mL chromatograph injection loop. Every so often, the ten-way valve named valve 1 (Valco Instruments) switched its position to inject the sample from the gas stream of the reactor passing by the loop. Simultaneously, the carrier gas, argon, 20 mL min^{-1} , flowed through the loop and carried the sample to column 1 (80/100 Hayesep N, $1.5 \text{ m} \times 2.1 \text{ mm ID}$) where heavy hydrocarbons and water were retained and evacuated by backflushing. The remaining gases passed to column 2 (80/100 Hayesep Q, $3 \text{ m} \times 2.1 \text{ mm ID}$) that retains CH_4 and CO_2 , and then sent to the detectors by changing the position of the six-way valve (valve 2, Valco Instruments). The lighter gases: O_2 , N_2 , H_2 , and CO flowed to column 3 (60/80

Molecular Sieve 5A, 3 m × 2.1 mm ID) for further separation and subsequent detection. Table 2 summarizes the position of the valves during a typical GC run, and Fig 4 shows a typically recorded chromatogram from a catalytic run.

Figure 3.

Schematic representation of the GC-2014 instrument used in this work. The instrument has a serial TCD-methanizer-FID system.

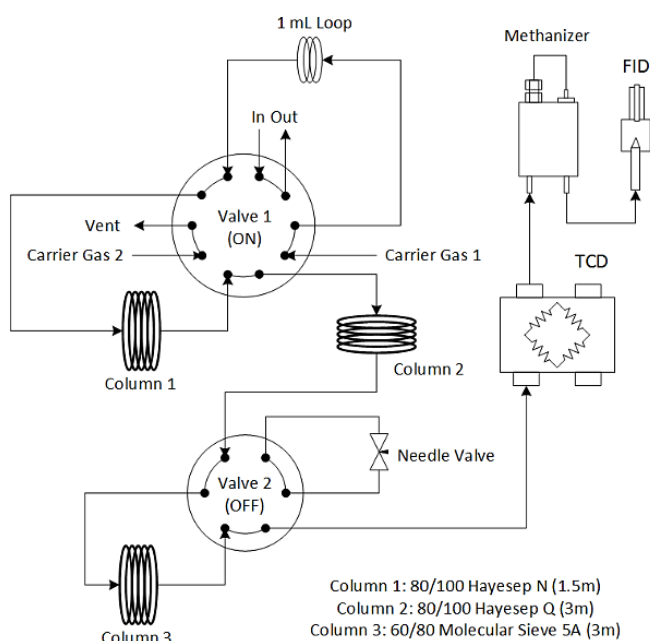


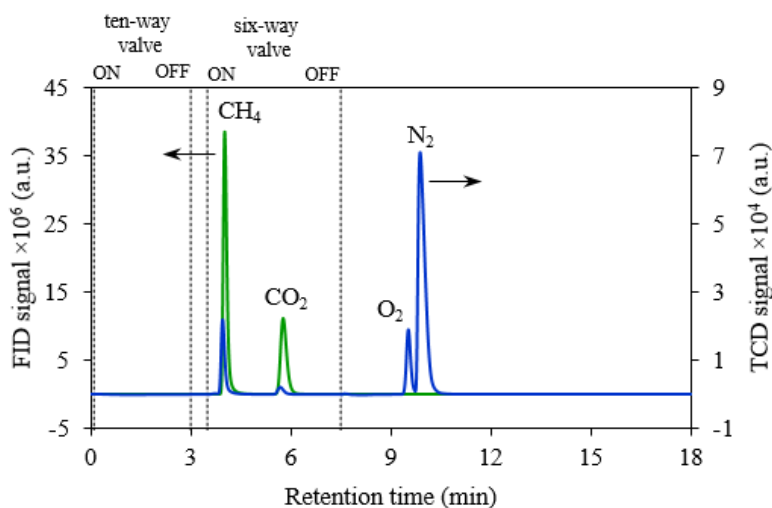
Table 2.

Summary of valve position during the GC analysis.

Time (min)	Position	
	Valve 1	Valve 2
0.0	OFF	OFF
0.1	ON	OFF
3.0	OFF	OFF
3.5	OFF	ON
7.5	OFF	OFF

Figure 4.

Chromatograms collected for the FID (green) and TCD (blue) in the analysis of CH₄ combustion products. Dashed vertical lines indicate switching in the position of the valves.



The temperature of the oven of the GC was kept constant at 100 °C. A TCD and an FID connected in series were used for measurements. The TCD was heated at 160 °C using argon as a reference gas (20 mL min⁻¹). The FID was operated at 200 °C and fed with hydrogen (45 mL min⁻¹) and air (400 mL min⁻¹). Before entering the FID, the gaseous analytes passed through a methanizer formed by a catalytic bed of metallic Ni. The methanizer converts CO and CO₂ into methane (according to Eqs. 15 and 16) at 375 °C, hence allowing the indirect quantification of the former with the methane signal detected in the FID. The TCD-methanizer-FID configuration was implemented to validate the measurements of CO and CO₂ in the TCD detector.



3.2 Catalyst performance calculation by different configurations of the detection system

The expressions developed previously for calculating the conversion, selectivity, and the mass balances were adjusted considering three configurations of the detection system: TCD, TCD-FID, TCD-Methanizer-FID, as is shown in Table 3. Only for the TCD, equations 7-9 and 12-14 were rewritten as a function of the areas of the signals read with the TCD ($A_{i,TCD}$).

Table 3.

Equations set to follow the methane combustion reaction in different detection systems, using both the external and the internal standard method.

Parameter	Method	Detection system		
		TCD	TCD-FID	TCD-Methanizer-FID
Conversion of CH ₄	External Standard	$X_{CH_4} = \frac{A_{CH_4,TCD}^0 - A_{CH_4,TCD}}{A_{CH_4,TCD}^0}$	$X_{CH_4} = \frac{A_{CH_4,FID}^0 - A_{CH_4,FID}}{A_{CH_4,FID}^0}$	
	Internal Standard	$X_{CH_4} = \frac{A_{CH_4,TCD}^0 - A_{CH_4,TCD} \omega}{A_{CH_4,TCD}^0}$	$X_{CH_4} = \frac{A_{CH_4,FID}^0 - A_{CH_4,FID} \omega}{A_{CH_4,FID}^0}$	
Conversion of O ₂	External Standard		$X_{O_2} = \frac{A_{O_2,TCD}^0 - A_{O_2,TCD}}{A_{O_2,TCD}^0}$	
	Internal Standard		$X_{O_2} = \frac{A_{O_2,TCD}^0 - A_{O_2,TCD} \omega}{A_{O_2,TCD}^0}$	
Selectivity to CO ₂	External Standard	$S_{CO_2} = \frac{Y_{CO_2,TCD} A_{CO_2,TCD}}{Y_{CH_4,TCD} (A_{CH_4,TCD}^0 - A_{CH_4,TCD})}$	$S_{CO_2} = \frac{Y_{CO_2,TCD} \alpha_{CH_4} A_{CO_2,TCD}}{Y_{CH_4,TCD} (A_{CH_4,FID}^0 - A_{CH_4,FID})}$	$S_{CO_2} = \frac{Y_{CO_2,TCD} \alpha_{CH_4} A_{CO_2,FID}}{Y_{CH_4,TCD} \alpha_{CO_2} (A_{CH_4,FID}^0 - A_{CH_4,FID})}$
	Internal Standard	$S_{CO_2} = \frac{\beta_{CO_2} A_{CO_2,TCD} \omega}{\beta_{CH_4} (A_{CH_4,TCD}^0 - A_{CH_4,TCD} \omega)}$	$S_{CO_2} = \frac{\beta_{CO_2} \alpha_{CH_4} A_{CO_2,TCD} \omega}{\beta_{CH_4} (A_{CH_4,FID}^0 - A_{CH_4,FID} \omega)}$	$S_{CO_2} = \frac{\beta_{CO_2} \alpha_{CH_4} A_{CO_2,FID} \omega}{\beta_{CH_4} \alpha_{CO_2} (A_{CH_4,FID}^0 - A_{CH_4,FID} \omega)}$
Carbon Mass Balance	External Standard	$B_C = \frac{Y_{CH_4,TCD} A_{CH_4,TCD} + Y_{CO_2,TCD} A_{CO_2,TCD} + Y_{CO_2,TCD} A_{CO_2,TCD}}{Y_{CH_4} A_{CH_4,TCD}^0}$	$B_C = \frac{Y_{CH_4,TCD} A_{CH_4,FID} + Y_{CO_2,TCD} A_{CO_2,TCD} + Y_{CO_2,TCD} A_{CO_2,TCD}}{\frac{Y_{CH_4} A_{CH_4,FID}^0}{\alpha_{CH_4}}}$	$B_C = \frac{Y_{CH_4,TCD} A_{CH_4,FID} + Y_{CO_2,TCD} A_{CO_2,FID} + Y_{CO_2,TCD} A_{CO_2,FID}}{\frac{Y_{CH_4} A_{CH_4,FID}^0}{\alpha_{CH_4}}}$
	Internal Standard	$B_C = \frac{\beta_{CH_4,TCD} A_{CH_4,TCD} + \beta_{CO_2,TCD} A_{CO_2,TCD} + \beta_{CO_2,TCD} A_{CO_2,TCD}}{\beta_{CH_4} A_{CH_4,TCD}^0 \omega}$	$B_C = \frac{\beta_{CH_4,TCD} A_{CH_4,FID} + \beta_{CO_2,TCD} A_{CO_2,TCD} + \beta_{CO_2,TCD} A_{CO_2,TCD}}{\frac{\beta_{CH_4} A_{CH_4,FID}^0}{\omega \alpha_{CH_4}}}$	$B_C = \frac{\beta_{CH_4,TCD} A_{CH_4,FID} + \beta_{CO_2,TCD} A_{CO_2,FID} + \beta_{CO_2,TCD} A_{CO_2,FID}}{\frac{\beta_{CH_4} A_{CH_4,FID}^0}{\omega \alpha_{CH_4}}}$
Other	Internal Standard		$\omega = \frac{A_{O_2,TCD}^0}{A_{O_2,TCD}}$	

For the TCD-FID system, the term $A_{i,TCD}$ from the equations developed for the single TCD was put as a function of $A_{i,FID}$, hence allowing to integrate the signal from the FID. In this last case, it was postulated the hypothesis that the signals from the FID ($A_{i,FID}$) and the TCD ($A_{i,TCD}$) are proportional given that there is no flow split between the TCD and the FID. Such a

proportionality was expressed by a coefficient named sensitivity factor (α_i), as it is described by Eq. 17. α_i can be calculated after comparing the TCD and FID peak areas of an i-th compound from different molar flows. For the TCD-FID system, α_i was calculated for CH₄, whereas for the TCD-methanizer-FID configuration, α_i can also be calculated for CO₂ and CO.

$$A_{i,FID} = \alpha_i A_{i,TCD} \quad (17)$$

Besides the expressions summarized in Table 3, estimations of the production of water can be made via the hydrogen and oxygen mass balances. For the combustion of methane, the hydrogen from the methane fed to the reactor forms water in stoichiometric proportions. Meanwhile, a mass balance for oxygen follows the stoichiometry of the reactions producing CO₂, CO, and water. Considering a closed mass balance, the ratio of the water production calculated by hydrogen and oxygen ($B_{H_2O} = F_{H_2O,BH}/F_{H_2O,BO}$) must equal 1. Therefore, B_{H_2O} for the external and internal standard method using the TCD, TCD-FID, and TCD-methanizer-FID configurations was written as presented in Eqs. 18-23.

$$B_{H_2O} = \frac{2\gamma_{CH_4}(A_{CH_4,TCD}^0 - A_{CH_4,TCD})}{2\gamma_{O_2}(A_{O_2,TCD}^0 - A_{O_2,TCD}) - 2\gamma_{CO_2}A_{CO_2,TCD} - \gamma_{CO}A_{CO,TCD}} \quad (18)$$

$$B_{H_2O} = \frac{\frac{2\gamma_{CH_4}}{\alpha_{CH_4}}(A_{CH_4,FID}^0 - A_{CH_4,FID})}{2\gamma_{O_2}(A_{O_2,TCD}^0 - A_{O_2,TCD}) - 2\gamma_{CO_2}A_{CO_2,TCD} - \gamma_{CO}A_{CO,TCD}} \quad (19)$$

$$B_{H_2O} = \frac{\frac{2\gamma_{CH_4}}{\alpha_{CH_4}}(A_{CH_4,FID}^0 - A_{CH_4,FID})}{2\gamma_{O_2}(A_{O_2,TCD}^0 - A_{O_2,TCD}) - \frac{2\gamma_{CO_2}A_{CO_2,FID}}{\alpha_{CO_2}} - \frac{\gamma_{CO}A_{CO,FID}}{\alpha_{CO}}} \quad (20)$$

$$B_{H_2O} = \frac{2\beta_{CH_4}(A_{CH_4,TCD}^0 - \omega A_{CH_4,TCD})}{2\beta_{O_2}(A_{O_2,TCD}^0 - \omega A_{O_2,TCD}) - 2\omega\beta_{CO_2}A_{CO_2,TCD} - \omega\beta_{CO}A_{CO,TCD}} \quad (21)$$

$$B_{H_2O} = \frac{\frac{2\beta_{CH_4}}{\alpha_{CH_4}} (A_{CH_4,FID}^0 - \omega A_{CH_4,FID})}{2\beta_{O_2} (A_{O_2,TCD}^0 - \omega A_{O_2,TCD}) - 2\omega\beta_{CO_2} A_{CO_2,TCD} - \omega\beta_{CO} A_{CO,TCD}} \quad (22)$$

$$B_{H_2O} = \frac{\frac{2\beta_{CH_4}}{\alpha_{CH_4}} (A_{CH_4,FID}^0 - \omega A_{CH_4,FID})}{2\beta_{O_2} (A_{O_2,TCD}^0 - \omega A_{O_2,TCD}) - \frac{2\omega\beta_{CO_2} A_{CO_2,FID}}{\alpha_{CO_2}} - \frac{\omega\beta_{CO} A_{CO,FID}}{\alpha_{CO}}} \quad (23)$$

Considering the mathematics of the method, the accuracy of the detection systems can be monitored by assessing the closure of the mass balances.

For implementing the analytic method developed above, calibration curves for each one of the compounds resulting from the methane combustion reaction were made. Calibration was made according to the following steps:

i) It was prepared four gaseous mixtures of the reaction products and analyzed them with the different configurations of the detection system of the GC. Readings for CH₄, CO₂, and CO were taken from both the FID and the TCD detectors, whereas the readings for O₂ and N₂ were done with the TCD. Such readings were used to calculate the corresponding areas $A_{i,FID}$ and/or $A_{i,TCD}$ in the calibration curves.

ii) It was calculated α_i values from the slope of plots of $A_{i,FID}$ vs $A_{i,TCD}$.

iii) For making calculations with the external standard method, it was plotted $\frac{F_i}{F_T}$ vs $A_{i,FID}$ or $A_{i,TCD}$ and estimated $\gamma_{i,FID}$ or $\gamma_{i,TCD}$ from the slopes of the produced curves. Notice that, according to the mathematics of the method, $\gamma_{i,TCD} = \alpha_i \gamma_{i,FID}$.

For the internal standard method, the slopes from the curves were obtained after plotting $\frac{F_i}{F_s}$ vs $\frac{A_{i,FID}}{A_{s,TCD}}$ and/or $\frac{A_{i,TCD}}{A_{s,TCD}}$ correspond to $\beta_{i,FID}$ and/or $\beta_{i,TCD}$, respectively. Herein, $\beta_{i,TCD} = \alpha_i \beta_{i,FID}$.

After calibration, the following procedure was implemented for quantifying the composition of the gaseous streams from the catalytic reactor on-line:

i) At least five samples from the reactor feed to the GC were injected and it was calculated the average $A_{i,FID}^0$ and/or $A_{i,TCD}^0$. Periodic injections of samples from the outlet stream of the catalytic reactor were made after starting to run the reaction. Therefore, $A_{i,FID}$ and/or $A_{i,TCD}$ were calculated as a function of time on stream. Finally, the average $A_{s,TCD}^0$ for the internal standard method from the signal for N_2 was calculated.

ii) It was calculated the concentration for each compound after replacing the values of $A_{i,FID}^0$ and/or $A_{i,TCD}^0$, $A_{i,FID}$ and/or $A_{i,TCD}$, $\gamma_{i,FID}$ and/or $\gamma_{i,TCD}$, $\beta_{i,FID}$ and/or $\beta_{i,TCD}$, and α_i in the corresponding equations presented in Table 3.

4. Results and discussion

4.1 Assessment of the sensitivity and response factors

A working hypothesis for the developed method is that there is a linear correlation between the responses of a given compound in the TCD and FID detectors. Fig. 5 plots the areas calculated for the FID signals of CH_4 , CO , and CO_2 as a function of the corresponding areas calculated from the signals of the TCD when different molar flows were injected to the GC. The linearity of the featured curves had $R^2 \sim 0.999$ in all instances. This validates the working hypothesis within the concentration ranges for the compounds studied herein, 0.8-7.7 vol % of CH_4 , CO_2 , and CO , 7.7-38.5 vol. % of O_2 , and 46.2-90.8 vol. % of N_2 at a total flow of 130 mL min^{-1} that was kept constant during the calibration procedure. According to the proposed mathematical model, the slopes of these curves are the sensitivity factors of each compound. Table 4 summarizes the calculated sensitivity factors for CH_4 , CO , and CO_2 . To ensure that the accuracy of the sensitivity factors for

CO and CO₂ were not affected by the methanizer, the CH₄, CO₂, and CO were calibrated at equivalent molar flows to obtain equivalent FID areas. Fig. 5 shows the results (axis of ordinates). This strategy was based on two facts. (1) The stoichiometry factor between methane and CO₂ or CO is 1.0; see Eq. 15-16. (2) Methanation reactions are exothermic and spontaneous (i.e., negative free energy) below 500 °C. Therefore, the criterion of having conversions for both CO₂ and CO around close to 100 % (J. Gao et al., 2012) when using a methanizer was fulfilled and this was further supported by the similarity found for the values of $\gamma_{i,FID}$ and $\beta_{i,FID}$ for these molecules, Table 4.

Figure 5.

*Correlation between the FID and TCD areas through the sensitivity factor. $R^2 > 0.999$. Error bars correspond to *t*-Student confidence intervals for the mean built with $\alpha = 0.05$.*

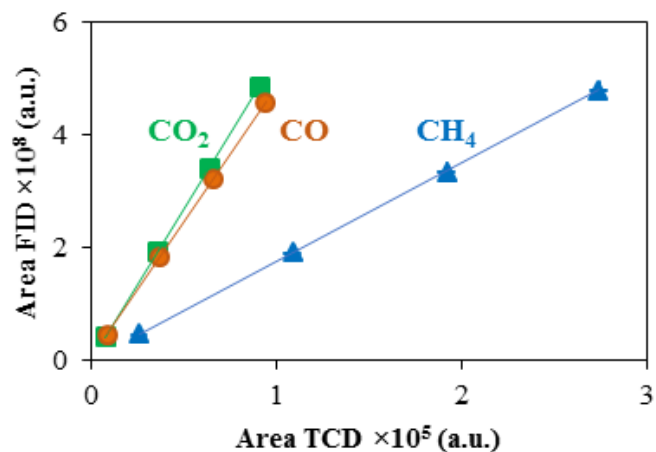


Table 4.

Summary of sensitivity and response factors. The R^2 for all calibration graphs was greater than 0.998.

Factor*	CH ₄	O ₂	N ₂	CO	CO ₂
α_i	1752.6	-	-	4863.5	5318.9
$\beta_{i,TCD}$	0.3631	0.7461	1.0000	1.0543	1.0770
$\beta_{i,FID}(\times 10^3)$	0.2072			0.2168	0.2025
$\gamma_{i,TCD}(\times 10^7)$	2.8117	5.7699	7.8273	8.1625	8.4298
$\gamma_{i,FID}(\times 10^{10})$	1.6043	-	-	1.6783	1.5849

The calibration data also served to calculate the response factors β_i and γ_i for all the analyzed compounds. The results are also summarized in Table 4. When the response factors were calculated from the areas derived from the TCD, their values decreased in the order: CH₄ < O₂ < CO < CO₂. This tendency is correlated to the decrease in the difference of thermal conductivities of these gases and argon; namely, 32, 12, 11 and 4 mW m⁻¹ K⁻¹ for CH₄, O₂, CO, and CO₂, at 160°C, respectively. The tendencies found for the calibration curves attest for the adequateness of the proposed method.

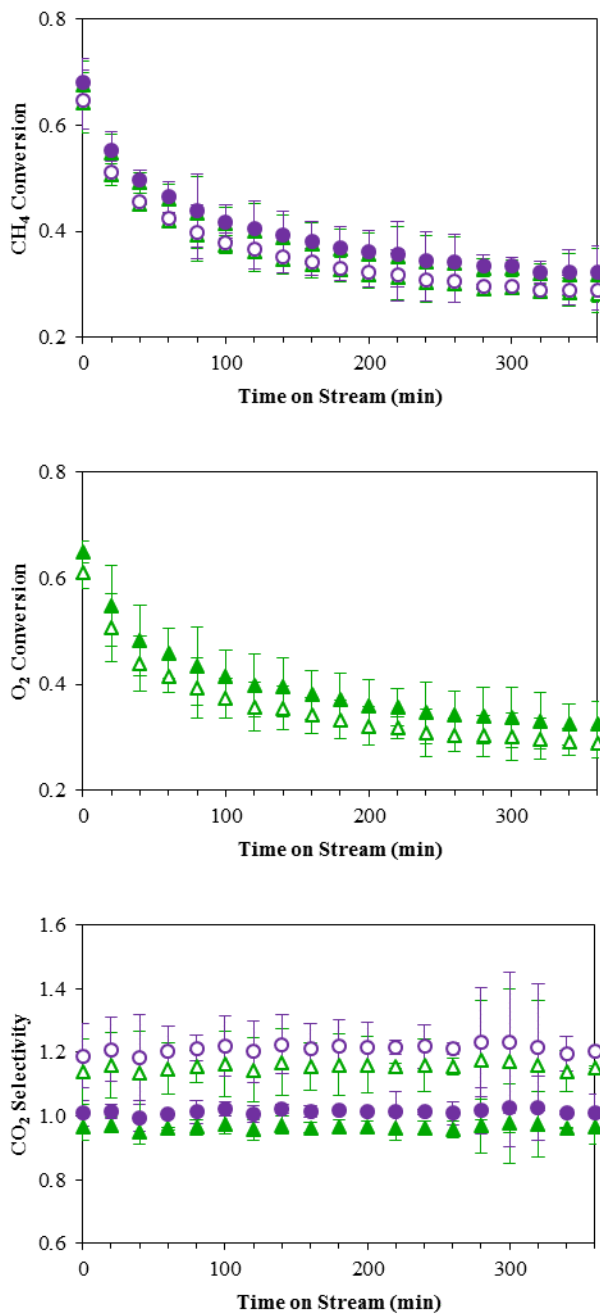
4.2 Validation of the developed method

To validate the proposed method, the products stream from a catalytic reactor performing the catalytic combustion of methane were quantified. Table 3 shows the definitions of conversion, selectivity, and mass balance that were employed. Fig. 6 shows the conversions of CH₄ and O₂, and the selectivity to CO₂ as calculated from the expressions developed for both the FID and the TCD. Fig 5 (unfilled marks) shows the results for these catalytic parameters when applying the external standard method while Fig. 6 (filled marks) does the same for the internal standard

method. For the external standard method, the trends observed for the conversion of CH_4 calculated from the signals of both detectors are the same, but the conversions calculated from the TCD were ca. 1% lower to those calculated from the FID. The conversion of O_2 calculated from the TCD was also plotted to corroborate the consistency of the quantification. It was observed that both the CH_4 and O_2 conversions were very similar which is consistent with the stoichiometry of the reaction, Eq. 1, since the reaction feed had a 1:2 CH_4 to O_2 molar ratio. Concerning the selectivity to CO_2 , values around 1.20 during the experiments were found, which does not seem to have physical meaning. On the other hand, the results for conversion calculated from the internal standard method, Fig. 6 top-middle, were ca. 4% higher to those found with the external standard method. On the other hand, the curves for the selectivity to CO_2 displayed a constant value of 1.00. Therefore, the internal standard method suppressed the artifact of a selectivity higher than 1.00. One takeaway message is thus that carefully devised analytical methods are required for drawing meaningful conclusions about the performance of reaction systems when using on-line chromatography.

Figure 6.

Results of methane (top) and oxygen (middle) conversion and selectivity towards CO₂ (bottom) using TCD (triangles) and FID (circles) detectors. The calculations were based on the external (unfilled marks) and the internal standard (filled marks) methods. Error bars correspond to *t*-Student confidence intervals for the mean built with $\alpha = 0.05$.

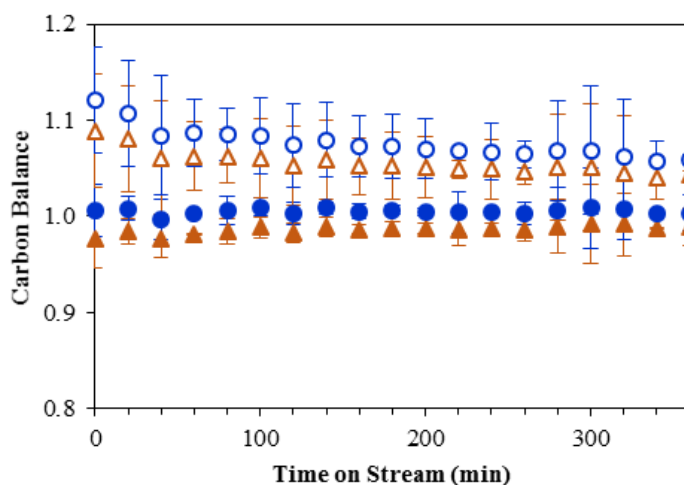


Computing elemental mass balances from the performed quantification is a reliable way of validating the developed methods. However, it is somehow surprising that, as highlighted by Carrero et al. (Carrero, Schloegl, Wachs, & Schomaecker, 2014), scores of papers from the catalytic community do not report elemental mass balances. In contrast, Fig. 7 shows the evolution of the carbon mass balance in the catalytic system as a function of time on stream. The carbon balances computed from the external standard method showed a decrease from 1.12 to 1.05, Fig. 7 (unfilled marks). In other words, according to this method, there was more mass leaving the reactor than entering it. And, also, the quantity of mass decreased with time on stream despite maintaining the same mass flow to the system. Somehow, such a result is actually in agreement with the nonrealistic values of selectivity calculated with the external standard method further strengthening the conclusion that this method is unreliable for the kind of analysis developed herein. On the other hand, there was a difference of ca. 2% between the carbon balance for both detectors. For example, at 2h time on stream, the carbon balance value for the FID was 1.07 whereas for the TCD was 1.05. Such a difference is a consequence of the higher sensitivity of the FID [2]. The accuracy and stability of the carbon mass balance was strongly improved with the internal standard method. Fig. 7 (filled marks) shows that the carbon mass balances calculated from both the TCD and the FID were always closer and not above 1.00 while remaining stable during the duration of the tests. Particularly, the carbon balance calculated from the FID was closer to 1.00 and higher than the one calculated from the TCD. Once again, the accuracy of the FID was superior than the one of the TCD.

Results in Fig. 7 (filled marks) are consistent with those presented in Fig. 6 bottom (filled marks), where no changes in selectivity were observed. These results hence validate the proposed method in this work.

Figure 7.

Carbon mass balances using TCD (triangles) and FID (circles). The calculations were based on methods of external standard (unfilled marks) and internal standard (filled marks). Error bars correspond to *t*-Student confidence intervals for the mean built with $\alpha = 0.05$.

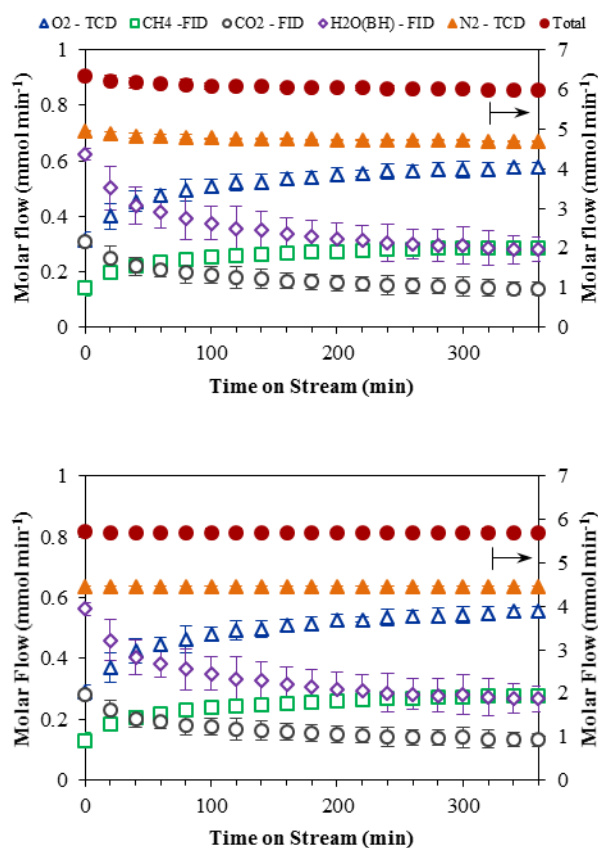


Finally, the calculated molar flows for the products exiting the catalytic reactor were analyzed. Fig. 8 shows the molar flows of the compounds involved in the reaction calculated from both the external (Fig. 8 top) and the internal (Fig. 8 bottom) standard methods. The results suggest that the external standard method tends to overestimate the molar flows from the reactor due to its inherent limitations. This is the reason why conversions were lower than those of the internal standard method. The calculations from the external standard method did not fulfill the restriction for a constant total molar flow, Fig. 8 top. According to the stoichiometry of Eq. 1, the total number of moles of the products are equal to those of the reactants, so the total molar flow of the system should be constant. However, the calculations from the external standard method indicated that the total molar flow at the inlet of the reactor (i.e., $5.69 \pm 0.10 \text{ mmol min}^{-1}$) was lower than those estimated in the outlet stream of the reactor during the catalytic experiments. Namely, this method

indicated that at the beginning of the reaction, the total molar flow was $6.34 \text{ mmol min}^{-1}$ and decreased during the reaction to $5.98 \text{ mmol min}^{-1}$. This explains the pattern of the carbon balance when this method was applied, Fig. 7 (unfilled marks).

Figure 8.

The molar flow of the gaseous stream compounds at the outlet of the reactor during a combustion test, calculated by external (top) and internal (bottom) standard method. Error bars correspond to t -Student confidence intervals for the mean built with $\alpha = 0.05$.



On the other hand, with the internal standard method, the total molar flow during the duration of the tests was constant, at ca. $5.70 \text{ mmol min}^{-1}$, and equal to that of the reaction system

inlet. Accordingly, this method produced a physically meaningful closed carbon balance, Fig 7 bottom. For both methods, the ratio of the water production calculated by hydrogen and oxygen (B_{H_2O}) was equal to 1.00, and the molar flow ratio CO_2 to water calculated from the hydrogen balance was 2.00, which demonstrates that the calculated value for water production was reasonable.

5. Conclusions

An analytical method for the highly accurate quantification of gaseous streams by on-line chromatography provided with multiple detectors was developed. Particularly, the method considered the use of an on-line gas chromatograph provided with thermal conductivity and flame ionization detectors and a methanizer and applied both the so-called external and internal standard methods of analysis. It was found that the external standard method, that actually is the most used by the chemical community, leads to inaccurate quantification which in turn leads to physically meaningless conclusions when applied to the analysis of the gaseous streams in catalytic reaction systems. Conversely, the internal standard method was highly accurate, and its results had physical meaning. These facts are also a call to action from analysts on how crucial it is avoiding oversimplification during gas chromatography for drawing meaningful conclusions in studies that apply the technique for studying diverse gaseous systems.

6. Acknowledgements

This work was funded by Agencia Nacional de Hidrocarburos -ANH- and Minciencias, Colombia, within the frame of the Project 1102-721-50962: “*Desarrollo de alternativas catalíticas para la reducción y valorización de emisiones de gases de efecto invernadero típicas de pozos y refinerías petroleras por combustión catalítica de VOCs y transformación de CO₂ y CH₄ en gas de síntesis*”

7. References

- Abbasi, R., Wu, L., Wanke, S. E., & Hayes, R. E. (2012). Kinetics of methane combustion over Pt and Pt-Pd catalysts. *Chemical Engineering Research and Design*, 90(11), 1930–1942. <https://doi.org/10.1016/j.cherd.2012.03.003>
- Abid Charef, S., Affoune, A. M., Caballero, A., Cruz-Yusta, M., & Morales, J. (2017a). Simultaneous recovery of Zn and Mn from used batteries in acidic and alkaline mediums: A comparative study. *Waste Management*, 68, 518–526. <https://doi.org/10.1016/j.wasman.2017.06.048>
- Abid Charef, S., Affoune, A. M., Caballero, A., Cruz-Yusta, M., & Morales, J. (2017b). Simultaneous recovery of Zn and Mn from used batteries in acidic and alkaline mediums: A comparative study. *Waste Management*, 68, 518–526. <https://doi.org/10.1016/j.wasman.2017.06.048>

- Akbari, E., Alavi, S. M., Rezaei, M., & Larimi, A. (2021). Catalytic Methane Combustion on the Hydrothermally Synthesized MnO₂Nanowire Catalysts. *Industrial and Engineering Chemistry Research*, 60(20), 7572–7587. <https://doi.org/10.1021/acs.iecr.1c00881>
- Akhtar, F., Andersson, L., Ogunwumi, S., Hedin, N., & Bergström, L. (2014). Structuring adsorbents and catalysts by processing of porous powders. *Journal of the European Ceramic Society*, 34(7), 1643–1666. <https://doi.org/10.1016/j.jeurceramsoc.2014.01.008>
- Almeida, M. F., Xará, S. M., Delgado, J., & Costa, C. A. (2006). Characterization of spent AA household alkaline batteries. *Waste Management*, 26(5), 466–476. <https://doi.org/10.1016/j.wasman.2005.04.005>
- Analysis, G., Analysis, T., & Analysis, R. G. (n.d.). *Software for Hiden Mass Spectrometers*. Retrieved from <https://www.hidenanalytical.com/wp-content/uploads/2020/06/MASsoft-PC-Win-10-Software.pdf>
- Andak, B., Özduğan, E., Türdü, S., & Bulutcu, A. N. (2019). Recovery of zinc and manganese from spent zinc-carbon and alkaline battery mixtures via selective leaching and crystallization processes. *Journal of Environmental Chemical Engineering*, 7(5), 103372. <https://doi.org/10.1016/j.jece.2019.103372>
- Andersson, R., Boutonnet, M., & Järås, S. (2012). On-line gas chromatographic analysis of higher alcohol synthesis products from syngas. *Journal of Chromatography A*, 1247, 134–145. <https://doi.org/10.1016/j.chroma.2012.05.060>
- Anejionu, O. C. D., Whyatt, J. D., Blackburn, G. A., & Price, C. S. (2015). Contributions of gas flaring to a global air pollution hotspot: Spatial and temporal variations, impacts and alleviation. *Atmospheric Environment*, 118, 184–193. <https://doi.org/10.1016/j.atmosenv.2015.08.006>

- Anthony, J. W., Bideaux, R. A., Bladh, K. W., & Nichols, M. C. (2006). Handbook of Mineralogy. In *Mineralogical Society of America* (Vol. 11). Retrieved from <http://www.handbookofmineralogy.org/>
- Arai, H., & Machida, M. (1991). Recent progress in high-temperature catalytic combustion. *Catalysis Today*, *10*(1), 81–94. [https://doi.org/10.1016/0920-5861\(91\)80076-L](https://doi.org/10.1016/0920-5861(91)80076-L)
- Bach, S., Henry, M., Baffier, N., & Livage, J. (1990). Sol-gel synthesis of manganese oxides. *Journal of Solid State Chemistry*, *88*(2), 325–333. [https://doi.org/10.1016/0022-4596\(90\)90228-P](https://doi.org/10.1016/0022-4596(90)90228-P)
- Baldovino-Medrano, V. G., Kartheuser, B., & Gaigneaux, E. M. (2019a). Production and testing of technical catalysts based on MnO₂ for the abatement of aromatic volatile compounds at the laboratory and pilot plant scales. *Catalysis Today*, *338*(February), 81–92. <https://doi.org/10.1016/j.cattod.2019.03.029>
- Baldovino-Medrano, V. G., Kartheuser, B., & Gaigneaux, E. M. (2019b). Production and testing of technical catalysts based on MnO₂ for the abatement of aromatic volatile compounds at the laboratory and pilot plant scales. *Catalysis Today*, *338*, 81–92. <https://doi.org/10.1016/j.cattod.2019.03.029>
- Barrett, E. P., Joyner, L. G., & Halenda, P. P. (1951). The Determination of Pore Volume and Area Distributions in Porous Substances. I. Computations from Nitrogen Isotherms. *Journal of the American Chemical Society*, *73*(1), 373–380. <https://doi.org/10.1021/ja01145a126>
- Batey, J. H. (2014). The physics and technology of quadrupole mass spectrometers. *Vacuum*, *101*(i), 410–415. <https://doi.org/10.1016/j.vacuum.2013.05.005>
- Baynham, A., Randall, D., & Hancy, C. (2017). Incinerators and Oxidizers. *EPA Air Pollution Control Cost Manual*, (November), 1–70. Retrieved from

- https://www.epa.gov/sites/production/files/2017-12/documents/oxidizersincinerators_chapter2_7theditionfinal.pdf
- Belardi, G., Lavecchia, R., Medici, F., & Piga, L. (2012). Thermal treatment for recovery of manganese and zinc from zinc-carbon and alkaline spent batteries. *Waste Management*, 32(10), 1945–1951. <https://doi.org/10.1016/j.wasman.2012.05.008>
- Belardi, G., Medici, F., & Piga, L. (2014). Influence of gaseous atmosphere during a thermal process for recovery of manganese and zinc from spent batteries. *Journal of Power Sources*, 248, 1290–1298. <https://doi.org/10.1016/j.jpowsour.2013.10.064>
- Bernardes, A. M., Espinosa, D. C. R., & Tenório, J. A. S. (2004). Recycling of batteries: A review of current processes and technologies. *Journal of Power Sources*, 130(1–2), 291–298. <https://doi.org/10.1016/j.jpowsour.2003.12.026>
- Biesinger, M. C., Payne, B. P., Grosvenor, A. P., Lau, L. W. M., Gerson, A. R., & Smart, R. S. C. (2011). Resolving surface chemical states in XPS analysis of first row transition metals, oxides and hydroxides: Cr, Mn, Fe, Co and Ni. *Applied Surface Science*, 257(7), 2717–2730. <https://doi.org/10.1016/j.apsusc.2010.10.051>
- Bischoff, C. F., Fitz, O. S., Burns, J., Bauer, M., Gentischer, H., Birke, K. P., ... Biro, D. (2020). Revealing the Local pH Value Changes of Acidic Aqueous Zinc Ion Batteries with a Manganese Dioxide Electrode during Cycling. *Journal of The Electrochemical Society*, 167(2), 020545. <https://doi.org/10.1149/1945-7111/ab6c57>
- Biswal, A., Mahakud, S., Bhuyan, S., Dash, B., Sarangi, C. K., Sanjay, K., ... Park, K. H. (2015). Recovery of Co metal and Electrolytic Manganese Dioxide (EMD) from Co-Mn sludge. *Hydrometallurgy*, 152, 159–168. <https://doi.org/10.1016/j.hydromet.2015.01.006>

- Blackburn, S., & Wilson, D. I. (2008). Shaping ceramics by plastic processing. *Journal of the European Ceramic Society*, 28(7), 1341–1351. <https://doi.org/10.1016/j.jeurceramsoc.2007.12.013>
- Blake, G. R. (2015). Particle density. *Methods of Soil Analysis, Part 1: Physical and Mineralogical Properties, Including Statistics of Measurement and Sampling*, 9(11121), 371–373. <https://doi.org/10.2134/agronmonogr9.1.c29>
- Blight, G. (2011). Mine Waste: A Brief Overview of Origins, Quantities, and Methods of Storage. *Waste*, 77–88. <https://doi.org/10.1016/B978-0-12-381475-3.10005-1>
- Buzatu, M., Săceanu, S., Ghica, V. G., Iacob, G., & Buzatu, T. (2013). Simultaneous recovery of Zn and MnO₂ from used batteries, as raw materials, by electrolysis. *Waste Management*, 33(8), 1764–1769. <https://doi.org/10.1016/j.wasman.2013.04.010>
- Buzatu, T., Popescu, G., Birloaga, I., & Săceanu, S. (2013). Study concerning the recovery of zinc and manganese from spent batteries by hydrometallurgical processes. *Waste Management*, 33(3), 699–705. <https://doi.org/10.1016/j.wasman.2012.10.005>
- Cabral, M., Pedrosa, F., Margarido, F., & Nogueira, C. A. (2013). End-of-life Zn-MnO₂ batteries: Electrode materials characterization. *Environmental Technology (United Kingdom)*, 34(10), 1283–1295. <https://doi.org/10.1080/09593330.2012.745621>
- Cai, X., Zhang, Y., Hu, H., Huang, Z., Yin, Y., Liang, X., ... Liang, J. (2020). Valorization of manganese residue to prepare a highly stable and active Fe₃O₄@SiO₂/starch-derived carbon composite for catalytic degradation of dye waste water. *Journal of Cleaner Production*, 258, 120741. <https://doi.org/10.1016/j.jclepro.2020.120741>

- Canda, L., Heput, T., & Ardelean, E. (2016). Methods for recovering precious metals from industrial waste. *IOP Conference Series: Materials Science and Engineering*, 106(1). <https://doi.org/10.1088/1757-899X/106/1/012020>
- Cano, R., Mackey, K., & McGlacken, G. P. (2018). Recent advances in manganese-catalysed C-H activation: Scope and mechanism. *Catalysis Science and Technology*, 8(5), 1251–1266. <https://doi.org/10.1039/c7cy02514a>
- Carrero, C. A., Schloegl, R., Wachs, I. E., & Schomaecker, R. (2014). Critical Literature Review of the Kinetics for the Oxidative Dehydrogenation of Propane over Well-Defined Supported Vanadium Oxide Catalysts. *ACS Catalysis*, 4(10), 3357–3380. <https://doi.org/10.1021/cs5003417>
- Castellanos-Beltran, I. J., Assima, G. P., & Lavoie, J. M. (2018). Effect of temperature in the conversion of methanol to olefins (MTO) using an extruded SAPO-34 catalyst. *Frontiers of Chemical Science and Engineering*, 12(2), 226–238. <https://doi.org/10.1007/s11705-018-1709-8>
- Chai, W. S., Cheun, J. Y., Kumar, P. S., Mubashir, M., Majeed, Z., Banat, F., ... Show, P. L. (2021). A review on conventional and novel materials towards heavy metal adsorption in wastewater treatment application. *Journal of Cleaner Production*, 296, 126589. <https://doi.org/10.1016/j.jclepro.2021.126589>
- Chen, B. R., Sun, W., Kitchaev, D. A., Mangum, J. S., Thampy, V., Garten, L. M., ... Schelhas, L. T. (2018). Understanding crystallization pathways leading to manganese oxide polymorph formation. *Nature Communications*, 9(1). <https://doi.org/10.1038/s41467-018-04917-y>

- Chen, H., Liu, R., Shu, J., & Li, W. (2015). Simultaneous stripping recovery of ammonia-nitrogen and precipitation of manganese from electrolytic manganese residue by air under calcium oxide assist. *Journal of Environmental Science and Health - Part A Toxic/Hazardous Substances and Environmental Engineering*, 50(12), 1282–1290. <https://doi.org/10.1080/10934529.2015.1055157>
- Chen, J., Arandiyana, H., Gao, X., & Li, J. (2015). Recent Advances in Catalysts for Methane Combustion. *Catalysis Surveys from Asia*, 19(3), 140–171. <https://doi.org/10.1007/s10563-015-9191-5>
- Cheng, G., Yu, L., He, B., Sun, M., Zhang, B., Ye, W., & Lan, B. (2017). Catalytic combustion of dimethyl ether over α -MnO₂ nanostructures with different morphologies. *Applied Surface Science*, 409, 223–231. <https://doi.org/10.1016/j.apsusc.2017.02.218>
- Cheng, Z., Mozammel, T., Patel, J., Lee, W. J., Huang, S., Lim, S., ... Li, C. (2018). A method for the quantitative analysis of gaseous mixtures by online mass spectrometry. *International Journal of Mass Spectrometry*, 434, 23–28. <https://doi.org/10.1016/j.ijms.2018.09.002>
- Christensen, K. A. (2007). Chapter 11 Design of industrial catalysts. In *Computer Aided Chemical Engineering* (Vol. 23). [https://doi.org/10.1016/S1570-7946\(07\)80014-9](https://doi.org/10.1016/S1570-7946(07)80014-9)
- Cook, K. D., Bennett, K. H., & Haddix, M. L. (1999). On-line mass spectrometry: A faster route to process monitoring and control. *Industrial and Engineering Chemistry Research*, 38(4), 1192–1204. <https://doi.org/10.1021/ie9707984>
- Das, A. P., Ghosh, S., Mohanty, S., & Sukla, L. B. (2014a). Consequences of manganese compounds: a review. *Toxicological and Environmental Chemistry*, 96(7), 981–997. <https://doi.org/10.1080/02772248.2015.1005428>

- Das, A. P., Ghosh, S., Mohanty, S., & Sukla, L. B. (2014b). Consequences of manganese compounds: a review. *Toxicological and Environmental Chemistry*, 96(7), 981–997. <https://doi.org/10.1080/02772248.2015.1005428>
- Das, A. P., Sukla, L. B., Pradhan, N., & Nayak, S. (2011). Manganese biomining: A review. *Bioresource Technology*, 102(16), 7381–7387. <https://doi.org/10.1016/j.biortech.2011.05.018>
- Dash, S. S., & Parida, K. M. (2007). Esterification of acetic acid with n-butanol over manganese nodule leached residue. *Journal of Molecular Catalysis A: Chemical*, 266(1–2), 88–92. <https://doi.org/10.1016/j.molcata.2006.10.031>
- Dautzenberg, F. M. (1989). *Ten Guidelines for Catalyst Testing*. 99–119. <https://doi.org/10.1021/bk-1989-0411.ch011>
- de Oliveira Demarco, J., Stefanello Cadore, J., da Silveira de Oliveira, F., Hiromitsu Tanabe, E., & Assumpção Bertuol, D. (2019). Recovery of metals from spent lithium-ion batteries using organic acids. *Hydrometallurgy*, 190(December 2018), 105169. <https://doi.org/10.1016/j.hydromet.2019.105169>
- Desai, B. D., Fernandes, J. B., & Dalal, V. N. K. (1985). Manganese dioxide - a review of a battery chemical Part II. Solid state and electrochemical properties of manganese dioxides. *Journal of Power Sources*, 16(1), 1–43. [https://doi.org/10.1016/0378-7753\(85\)80001-X](https://doi.org/10.1016/0378-7753(85)80001-X)
- Dey, S., & Praveen Kumar, V. V. (2020). The performance of highly active manganese oxide catalysts for ambient conditions carbon monoxide oxidation. *Current Research in Green and Sustainable Chemistry*, 3(May), 100012. <https://doi.org/10.1016/j.crgsc.2020.100012>

- Du, B., Zhou, C. bo, & Duan, N. (2014). Recycling of electrolytic manganese solid waste in autoclaved bricks preparation in China. *Journal of Material Cycles and Waste Management*, 16(2), 258–269. <https://doi.org/10.1007/s10163-013-0181-2>
- Du, B., Zhou, C., Li, X., Guo, T., & Wang, Z. (2015). A kinetic study of Mn(II) precipitation of leached aqueous solution from electrolytic manganese residues. *Toxicological and Environmental Chemistry*, 97(3–4), 349–357. <https://doi.org/10.1080/02772248.2015.1050188>
- Duan, N., Fan, W., Changbo, Z., Chunlei, Z., & Hongbing, Y. (2010). Analysis of pollution materials generated from electrolytic manganese industries in China. *Resources, Conservation and Recycling*, 54(8), 506–511. <https://doi.org/10.1016/j.resconrec.2009.10.007>
- Duan, N., Zhou, C., Chen, B., Jiang, W., & Xin, B. (2011). Bioleaching of Mn from manganese residues by the mixed culture of Acidithiobacillus and mechanism. *Journal of Chemical Technology and Biotechnology*, 86(6), 832–837. <https://doi.org/10.1002/jctb.2596>
- Dunlop, J. R., & Tully, F. P. (1993). A kinetic study of OH radical reactions with methane and perdeuterated methane. *Journal of Physical Chemistry*, 97(43), 11148–11150. <https://doi.org/10.1021/j100145a003>
- Dwivedi, D., Randhawa, N. S., Saroj, S., & Jana, R. K. (2017). An Overview of Manganese Recovery by Hydro and Pyro-Metallurgical Routes. *Journal of The Institution of Engineers (India): Series D*, 98(1), 147–154. <https://doi.org/10.1007/s40033-016-0119-7>
- Ebin, B., Petranikova, M., Steenari, B. M., & Ekberg, C. (2016). Production of zinc and manganese oxide particles by pyrolysis of alkaline and Zn-C battery waste. *Waste Management*, 51, 157–167. <https://doi.org/10.1016/j.wasman.2015.10.029>

- Ebin, B., Petranikova, M., Steenari, B. M., & Ekberg, C. (2019). Recovery of industrial valuable metals from household battery waste. *Waste Management and Research*, 37(2), 168–175. <https://doi.org/10.1177/0734242X18815966>
- Ellefson, R. E., Cain, D., & Lindsay, C. N. (1987). Calibration of mass spectrometers for quantitative gas mixture analysis. *Journal of Vacuum Science & Technology A: Vacuum, Surfaces, and Films*, 5(1), 134–139. <https://doi.org/10.1116/1.574126>
- Elvidge, C. D., Bazilian, M. D., Zhizhin, M., Ghosh, T., Baugh, K., & Hsu, F. C. (2018). The potential role of natural gas flaring in meeting greenhouse gas mitigation targets. *Energy Strategy Reviews*, 20, 156–162. <https://doi.org/10.1016/j.esr.2017.12.012>
- Energizer Brands, L. (2018). *Alkaline Manganese Dioxide Handbook and Application Manual*. 1–15.
- Falco, L., Quina, M. J., Gando-Ferreira, L. M., Thomas, H., & Curutchet, G. (2014). Solvent Extraction Studies for Separation of Zn(II) and Mn(II) from Spent Batteries Leach Solutions. *Separation Science and Technology (Philadelphia)*, 49(3), 398–409. <https://doi.org/10.1080/01496395.2013.850510>
- Farzana, R., Rajarao, R., Hassan, K., Behera, P. R., & Sahajwalla, V. (2018). Thermal nanosizing: Novel route to synthesize manganese oxide and zinc oxide nanoparticles simultaneously from spent Zn–C battery. *Journal of Cleaner Production*, 196, 478–488. <https://doi.org/10.1016/j.jclepro.2018.06.055>
- Farzana, R., Sayeed, M. A., Joseph, J., Ostrikov, K., O’Mullane, A. P., & Sahajwalla, V. (2020). Manganese Oxide Derived from a Spent Zn–C Battery as a Catalyst for the Oxygen Evolution Reaction. *ChemElectroChem*, 7(9), 2073–2080. <https://doi.org/10.1002/celec.202000422>

- Fawole, O. G., Cai, X. M., & Mackenzie, A. R. (2016). Gas flaring and resultant air pollution: A review focusing on black carbon. *Environmental Pollution*, 216, 182–197.
<https://doi.org/10.1016/j.envpol.2016.05.075>
- Ferella, F., De Michelis, I., Beolchini, F., Innocenzi, V., & Vegliò, F. (2010). Extraction of zinc and manganese from alkaline and zinc-carbon spent batteries by citric-sulphuric acid solution. *International Journal of Chemical Engineering*, 2010.
<https://doi.org/10.1155/2010/659434>
- Ferella, F., De Michelis, I., & Vegliò, F. (2008). Process for the recycling of alkaline and zinc-carbon spent batteries. *Journal of Power Sources*, 183(2), 805–811.
<https://doi.org/10.1016/j.jpowsour.2008.05.043>
- Ferreira, B. S., Van Keulen, F., & Da Fonseca, M. M. R. (1998). Novel calibration method for mass spectrometers for on-line gas analysis. Set-up for the monitoring of a bacterial fermentation. *Bioprocess Engineering*, 19(4), 289–296.
<https://doi.org/10.1007/s004490050522>
- Fu, J., He, Z., Wang, H., Liang, W., & Guo, C. (2010). Preparation of chemical manganese dioxide from manganese sulfate. *Mining Science and Technology*, 20(6), 877–881.
[https://doi.org/10.1016/S1674-5264\(09\)60299-4](https://doi.org/10.1016/S1674-5264(09)60299-4)
- Gallegos, M. V., Falco, L. R., Peluso, M. A., Sambeth, J. E., & Thomas, H. J. (2013). Recovery of manganese oxides from spent alkaline and zinc-carbon batteries. An application as catalysts for VOCs elimination. *Waste Management*, 33(6), 1483–1490.
<https://doi.org/10.1016/j.wasman.2013.03.006>
- Gallegos, M. V., Peluso, M. A., Finocchio, E., Thomas, H. J., Busca, G., & Sambeth, J. E. (2017). Removal of VOCs by catalytic process. A study of MnZnO composites synthesized from

- waste alkaline and Zn/C batteries. *Chemical Engineering Journal*, 313, 1099–1111.
<https://doi.org/10.1016/j.cej.2016.11.001>
- Gancarczyk, A., Iwaniszyn, M., Piątek, M., Korpyś, M., Sintera, K., Jodłowski, P. J., ... Kołodziej, A. (2018). Catalytic Combustion of Low-Concentration Methane on Structured Catalyst Supports. *Industrial & Engineering Chemistry Research*, 57(31), 10281–10291.
<https://doi.org/10.1021/acs.iecr.8b01987>
- Gangwar, D., & Rath, C. (2021). *Structural , optical and magnetic properties of α - and β -MnO₂ nanorods*. 557(April).
- Gao, J., Wang, Y., Ping, Y., Hu, D., Xu, G., Gu, F., & Su, F. (2012). A thermodynamic analysis of methanation reactions of carbon oxides for the production of synthetic natural gas. *RSC Advances*, 2(6), 2358. <https://doi.org/10.1039/c2ra00632d>
- Gao, Y., Wang, Z., Cui, C., Wang, B., Liu, W., Liu, W., & Wang, L. (2020). Amorphous manganese oxide as highly active catalyst for soot oxidation. *Environmental Science and Pollution Research*, 27(12), 13488–13500. <https://doi.org/10.1007/s11356-020-07909-y>
- Ghosh, S., & Das, A. P. (2017). Bioleaching of manganese from mining waste residues using *Acinetobacter* sp. *Geology, Ecology, and Landscapes*, 1(2), 77–83.
<https://doi.org/10.1080/24749508.2017.1332847>
- Ghosh, S., Mohanty, S., Akcil, A., Sukla, L. B., & Das, A. P. (2016). A greener approach for resource recycling: Manganese bioleaching. *Chemosphere*, 154, 628–639.
<https://doi.org/10.1016/j.chemosphere.2016.04.028>
- Gregorová, E., Pabst, W., Smith, D. S., & Zivcová, Z. (2009). *Thermal conductivity of porous alumina ceramics prepared using starch as a pore-forming agent*. 29, 347–353.
<https://doi.org/10.1016/j.jeurceramsoc.2008.06.018>

- Gunarathne, V., Rajapaksha, A. U., Vithanage, M., Alessi, D. S., Selvasembian, R., Naushad, M., ... Ok, Y. S. (2020). Hydrometallurgical processes for heavy metals recovery from industrial sludges. *Critical Reviews in Environmental Science and Technology*, 0(0), 1–41. <https://doi.org/10.1080/10643389.2020.1847949>
- Guo, M., Li, K., Liu, L., Zhang, H., Guo, W., Hu, X., ... Sun, T. (2019). Manganese-based multi-oxide derived from spent ternary lithium-ions batteries as high-efficient catalyst for VOCs oxidation. *Journal of Hazardous Materials*, 380, 120905. <https://doi.org/10.1016/j.jhazmat.2019.120905>
- Guo, M., Li, K., Liu, L., Zhang, H., Hu, X., Min, X., ... Sun, T. (2019). Resource utilization of spent ternary lithium-ions batteries: Synthesis of highly active manganese-based perovskite catalyst for toluene oxidation. *Journal of the Taiwan Institute of Chemical Engineers*, 102, 268–275. <https://doi.org/10.1016/j.jtice.2019.06.012>
- Guo, M., Li, K., Zhang, H., Min, X., Liang, J., Hu, X., ... Sun, T. (2020). Promotional removal of oxygenated VOC over manganese-based multi oxides from spent lithium-ions manganate batteries: Modification with Fe, Bi and Ce dopants. *Science of the Total Environment*, 740, 139951. <https://doi.org/10.1016/j.scitotenv.2020.139951>
- Guo, M., Liu, L., Gu, J. nan, Zhang, H., Min, X., Liang, J., ... Sun, T. (2021). Catalytic performance improvement of volatile organic compounds oxidation over MnO_x and GdMnO₃ composite oxides from spent lithium-ion batteries: Effect of acid treatment. *Chinese Journal of Chemical Engineering*. <https://doi.org/10.1016/j.cjche.2020.08.015>
- Guo, N., Wei, X. Q., Deng, X. L., & Xu, X. J. (2015). Synthesis and property of spinel porous ZnMn₂O₄ microspheres. *Applied Surface Science*, 356, 1127–1134. <https://doi.org/10.1016/j.apsusc.2015.08.185>

- Haber, J. (1991). Manual on catalyst characterization (Recommendations 1991). *Pure and Applied Chemistry*, 63(9), 1227–1246. <https://doi.org/10.1351/pac199163091227>
- Hagelstein, K. (2009). Globally sustainable manganese metal production and use. *Journal of Environmental Management*, 90(12), 3736–3740. <https://doi.org/10.1016/j.jenvman.2008.05.025>
- Hammond, J. P. (2018). Quality Assurance: Spectroscopic Standards. In *Reference Module in Chemistry, Molecular Sciences and Chemical Engineering* (pp. 426–432). <https://doi.org/10.1016/B978-0-12-409547-2.00455-8>
- Han, Y. F., Chen, F., Zhong, Z., Ramesh, K., Chen, L., & Widjaja, E. (2006). Controlled synthesis, characterization, and catalytic properties of Mn₂O₃ and Mn₃O₄ nanoparticles supported on mesoporous silica SBA-15. *Journal of Physical Chemistry B*, 110(48), 24450–24456. <https://doi.org/10.1021/jp064941v>
- Hanf, L., Henschel, J., Diehl, M., Winter, M., & Nowak, S. (2020). Mn²⁺ or Mn³⁺? Investigating transition metal dissolution of manganese species in lithium ion battery electrolytes by capillary electrophoresis. *Electrophoresis*, 41(9), 697–704. <https://doi.org/10.1002/elps.201900443>
- He, C., Cheng, J., Zhang, X., Douthwaite, M., Pattison, S., & Hao, Z. (2019). Recent Advances in the Catalytic Oxidation of Volatile Organic Compounds: A Review Based on Pollutant Sorts and Sources [Review-article]. *Chemical Reviews*, 119(7), 4471–4568. <https://doi.org/10.1021/acs.chemrev.8b00408>
- He, L., Fan, Y., Bellettre, J., Yue, J., & Luo, L. (2020). A review on catalytic methane combustion at low temperatures: Catalysts, mechanisms, reaction conditions and reactor designs.

- Renewable and Sustainable Energy Reviews*, 119(November 2019).
<https://doi.org/10.1016/j.rser.2019.109589>
- He, L., Fan, Y., Luo, L., Bellettre, J., & Yue, J. (2020). Preparation of Pt/Ti-Al₂O₃ catalyst coating in microreactors for catalytic methane combustion. *Chemical Engineering Journal*, 380(August 2019). <https://doi.org/10.1016/j.cej.2019.122424>
- He, S., Jiang, D., Hong, M., & Liu, Z. (2021). Hazard-free treatment and resource utilisation of electrolytic manganese residue: A review. *Journal of Cleaner Production*, 306. <https://doi.org/10.1016/j.jclepro.2021.127224>
- He, S., Wilson, B. P., Lundström, M., & Liu, Z. (2021). Hazard-free treatment of electrolytic manganese residue and recovery of manganese using low temperature roasting-water washing process. *Journal of Hazardous Materials*, 402(July 2020). <https://doi.org/10.1016/j.jhazmat.2020.123561>
- Hedden, M., Francis, N., Haraldsen, J. T., Ahmed, T., & Constantin, C. (2015). Thermoelectric properties of nano-meso-micro β -MnO₂ powders as a function of electrical resistance. *Nanoscale Research Letters*, 10(1). <https://doi.org/10.1186/s11671-015-1000-6>
- Heinzle, E., Moes, J., Griot, M., Kramer, H., Dunn, I. J., & Bourne, J. R. (1984). On-line mass spectrometry in fermentation. *Analytica Chimica Acta*, 163(C), 219–229. [https://doi.org/10.1016/S0003-2670\(00\)81510-X](https://doi.org/10.1016/S0003-2670(00)81510-X)
- Heinzle, E., Oeggerli, A., & Dettwiler, B. (1990). On-line fermentation gas analysis: Error analysis and application of mass spectrometry. *Analytica Chimica Acta*, 238(C), 101–115. [https://doi.org/10.1016/S0003-2670\(00\)80528-0](https://doi.org/10.1016/S0003-2670(00)80528-0)
- Helmus, R., ter Laak, T. L., van Wezel, A. P., de Voogt, P., & Schymanski, E. L. (2021). patRoom: open source software platform for environmental mass spectrometry based non-target

- screening. *Journal of Cheminformatics*, 13(1), 1–25. <https://doi.org/10.1186/s13321-020-00477-w>
- Herndon, E. M., & Brantley, S. L. (2011). Movement of manganese contamination through the Critical Zone. *Applied Geochemistry*, 26(SUPPL.), S40–S43. <https://doi.org/10.1016/j.apgeochem.2011.03.024>
- Hoffmann, E. De, & Stroobant, V. (2007). Mass Spectrometry Principles and Applications Third Edition. In *Mass spectrometry reviews* (Vol. 29). Retrieved from <https://www.wiley.com/en-us/Mass+Spectrometry%3A+Principles+and+Applications%2C+3rd+Edition-p-9780470033111>
- Hohrenk, L. L., Itzel, F., Baetz, N., Tuerk, J., Vosough, M., & Schmidt, T. C. (2020). Comparison of Software Tools for Liquid Chromatography-High-Resolution Mass Spectrometry Data Processing in Nontarget Screening of Environmental Samples. *Analytical Chemistry*, 92(2), 1898–1907. <https://doi.org/10.1021/acs.analchem.9b04095>
- Holmes, N., Akien, G. R., Savage, R. J. D., Stanetty, C., Baxendale, I. R., Blacker, A. J., ... Bourne, R. A. (2016). Online quantitative mass spectrometry for the rapid adaptive optimisation of automated flow reactors. *Reaction Chemistry and Engineering*, 1(1), 96–100. <https://doi.org/10.1039/c5re00083a>
- Hoseini, S., Rahemi, N., Allahyari, S., & Tasbihi, M. (2019). Application of plasma technology in the removal of volatile organic compounds (BTX) using manganese oxide nano-catalysts synthesized from spent batteries. *Journal of Cleaner Production*, 232, 1134–1147. <https://doi.org/10.1016/j.jclepro.2019.05.227>

- Hoseini, S., Rahemi, N., Allahyari, S., Tasbihi, M., & Gharehabani, E. (2020). Effect of hydrometallurgical process parameters on the Mn₂O₃ nano catalysts derived from spent batteries used in the plasma catalytic oxidation of BTX. *Advanced Powder Technology*, 31(10), 4187–4196. <https://doi.org/10.1016/j.appt.2020.08.026>
- Ippolito, N. M., Belardi, G., Medici, F., & Piga, L. (2016). Utilization of automotive shredder residues in a thermal process for recovery of manganese and zinc from zinc-carbon and alkaline spent batteries. *Waste Management*, 51, 182–189. <https://doi.org/10.1016/j.wasman.2015.12.033>
- Işıldar, A., Rene, E. R., van Hullebusch, E. D., & Lens, P. N. L. (2018). Electronic waste as a secondary source of critical metals: Management and recovery technologies. *Resources, Conservation and Recycling*, 135(December 2016), 296–312. <https://doi.org/10.1016/j.resconrec.2017.07.031>
- Ismail, O. S., & Umukoro, G. E. (2016). Modelling combustion reactions for gas flaring and its resulting emissions. *Journal of King Saud University - Engineering Sciences*, 28(2), 130–140. <https://doi.org/10.1016/j.jksues.2014.02.003>
- Jahan, M., Tominaka, S., & Henzie, J. (2016). Phase pure α -Mn₂O₃ prisms and their bifunctional electrocatalytic activity in oxygen evolution and reduction reactions. *Dalton Transactions*, 45(46), 18494–18501. <https://doi.org/10.1039/c6dt03158g>
- Jampaiah, D., Velisoju, V. K., Venkataswamy, P., Coyle, V. E., Nafady, A., Reddy, B. M., & Bhargava, S. K. (2017). Nanowire Morphology of Mono- and Bidoped α -MnO₂ Catalysts for Remarkable Enhancement in Soot Oxidation. *ACS Applied Materials and Interfaces*, 9(38), 32652–32666. <https://doi.org/10.1021/acsami.7b07656>

- Jaya, H., Firdaus Omar, M., Md Akil, H., Arifin Ahmad, Z., & Noriman Zulkepli, N. (2016). Sawdust polyethylene composites. *BioResources*, *11*(3), 6489–6504. Retrieved from https://bioresources.cnr.ncsu.edu/wp-content/uploads/2016/07/BioRes_11_3_6489_Jaya_OAAZ_Effect_Particle_Size_Mecha_Prop_Sawdust_HDPE_Comp_9342.pdf
- Jee, J. E., Pestovsky, O., & Bakac, A. (2010). Preparation and characterization of manganese(IV) in aqueous acetic acid. *Dalton Transactions*, *39*(48), 11636–11642. <https://doi.org/10.1039/c0dt00476f>
- Ji, F., Men, Y., Wang, J., Sun, Y., Wang, Z., Zhao, B., ... Xu, G. (2019). Promoting diesel soot combustion efficiency by tailoring the shapes and crystal facets of nanoscale Mn₃O₄. *Applied Catalysis B: Environmental*, *242*(October 2018), 227–237. <https://doi.org/10.1016/j.apcatb.2018.09.092>
- Kaiser, R. I., Jansen, P., Petersen, K., & Roessler, K. (1995). On line and in situ quantification of gas mixtures by matrix interval algebra assisted quadrupole mass spectrometry. *Review of Scientific Instruments*, *66*(11), 5226–5231. <https://doi.org/10.1063/1.1146089>
- Kim, B. S., Lee, J. C., Jeong, S. B., Lee, H. I., & Kim, C. W. (2010). Kinetics of the volatilization removal of zinc from manganese dust. *Materials Transactions*, *51*(7), 1313–1318. <https://doi.org/10.2320/matertrans.M2010108>
- Kim, S. C., & Shim, W. G. (2010). Catalytic combustion of VOCs over a series of manganese oxide catalysts. *Applied Catalysis B: Environmental*, *98*(3–4), 180–185. <https://doi.org/10.1016/j.apcatb.2010.05.027>

- Kloprogge, J. T., Ponce, C. P., & Loomis, T. A. (2020). The Periodic Table: Nature's Building Blocks. In *The Periodic Table: Nature's Building Blocks*. <https://doi.org/10.1016/C2019-0-03114-7>
- Klusacek, K., & Schneider, P. (1981). Effect of size and shape of catalyst on pellet pore structure and effectiveness. *Chemical Engineering Science*, *36*, 523–527.
- Koivula, R., Pakarinen, J., Sivenius, M., Sirola, K., Harjula, R., & Paatero, E. (2009). Use of hydrometallurgical wastewater as a precursor for the synthesis of cryptomelane-type manganese dioxide ion exchange material. *Separation and Purification Technology*, *70*(1), 53–57. <https://doi.org/10.1016/j.seppur.2009.08.014>
- Kononov, R., Ostrovski, O., & Ganguly, S. (2008). Carbothermal reduction of manganese oxide in different gas atmospheres. *Metallurgical and Materials Transactions B: Process Metallurgy and Materials Processing Science*, *39*(5), 662–668. <https://doi.org/10.1007/s11663-008-9191-1>
- Kreutzer, M. T., Kapteijn, F., & Moulijn, J. A. (2006). Shouldn't catalysts shape up? Structured reactors in general and gas-liquid monolith reactors in particular. *Catalysis Today*, *111*(1–2), 111–118. <https://doi.org/10.1016/j.cattod.2005.10.014>
- Kularatne, R. K. A., Kasturiarachchi, J. C., Manatunge, J. M. A., & Wijeyekoon, S. L. J. (2009). Mechanisms of Manganese Removal from Wastewaters in Constructed Wetlands Comprising Water Hyacinth (*Eichhornia crassipes* (Mart.) Solms) Grown under Different Nutrient Conditions . *Water Environment Research*, *81*(2), 165–172. <https://doi.org/10.2175/106143008x370403>

- Kumar, S., García-Triñanes, P., Teixeira-Pinto, A., & Bao, M. (2013). Development of alkali activated cement from mechanically activated silico-manganese (SiMn) slag. *Cement and Concrete Composites*, *40*, 7–13. <https://doi.org/10.1016/j.cemconcomp.2013.03.026>
- Lahousse, C., Bernier, A., Grange, P., Delmon, B., Papaefthimiou, P., Ioannides, T., & Verykios, X. (1998). Evaluation of γ -MnO₂ as a VOC removal catalyst: Comparison with a noble metal catalyst. *Journal of Catalysis*, *178*(1), 214–225. <https://doi.org/10.1006/jcat.1998.2148>
- Lamaita, L., Peluso, M. A., Sambeth, J. E., & Thomas, H. J. (2005). Synthesis and characterization of manganese oxides employed in VOCs abatement. *Applied Catalysis B: Environmental*, *61*(1–2), 114–119. <https://doi.org/10.1016/j.apcatb.2005.03.014>
- Lan, J., Sun, Y., Guo, L., Li, Z., Du, D., & Zhang, T. C. (2019). A novel method to recover ammonia, manganese and sulfate from electrolytic manganese residues by bio-leaching. *Journal of Cleaner Production*, *223*, 499–507. <https://doi.org/10.1016/j.jclepro.2019.03.098>
- Lan, J., Sun, Y., Huang, P., Du, Y., Zhan, W., Zhang, T. C., & Du, D. (2020). Using Electrolytic Manganese Residue to prepare novel nanocomposite catalysts for efficient degradation of Azo Dyes in Fenton-like processes. *Chemosphere*, *252*, 126487. <https://doi.org/10.1016/j.chemosphere.2020.126487>
- Lannoo, S., Vilas-Boas, A., Sadeghi, S. M., Jesus, J., & Soares, H. M. V. M. (2019). An environmentally friendly closed loop process to recycle raw materials from spent alkaline batteries. *Journal of Cleaner Production*, *236*, 117612. <https://doi.org/10.1016/j.jclepro.2019.117612>

- Larsen, D., & Mann, R. (2005). Origin of high manganese concentrations in coal mine drainage, eastern Tennessee. *Journal of Geochemical Exploration*, 86(3), 143–163. <https://doi.org/10.1016/j.gexplo.2005.06.001>
- Le Bourre, B., Neculita, C. M., Coudert, L., & Rosa, E. (2020). Manganese removal processes and geochemical behavior in residues from passive treatment of mine drainage. *Chemosphere*, 259, 127424. <https://doi.org/10.1016/j.chemosphere.2020.127424>
- Lee, S. A., Lee, J. J., You, G. R., Choi, Y. W., & Kim, C. (2015). Distinction between Mn(III) and Mn(II) by using a colorimetric chemosensor in aqueous solution. *RSC Advances*, 5(116), 95618–95630. <https://doi.org/10.1039/c5ra20396a>
- Leite, D. da S., Carvalho, P. L. G., de Lemos, L. R., Mageste, A. B., & Rodrigues, G. D. (2019). Hydrometallurgical recovery of Zn(II) and Mn(II) from alkaline batteries waste employing aqueous two-phase system. *Separation and Purification Technology*, 210(July 2018), 327–334. <https://doi.org/10.1016/j.seppur.2018.07.038>
- Li, H., Zhang, Z., Tang, S., Li, Y., & Zhang, Y. (2008). Ultrasonically assisted acid extraction of manganese from slag. *Ultrasonics Sonochemistry*, 15(4), 339–343. <https://doi.org/10.1016/j.ultsonch.2007.07.010>
- Li, K., Chen, C., Zhang, H., Hu, X., Sun, T., & Jia, J. (2019). Effects of phase structure of MnO₂ and morphology of δ -MnO₂ on toluene catalytic oxidation. *Applied Surface Science*, 496(July). <https://doi.org/10.1016/j.apsusc.2019.143662>
- Li, M., Hu, L., Zhong, H., He, Z., Sun, W., & Xiong, D. (2021). Efficient removal of diethyl dithiocarbamate with EDTA functionalized electrolytic manganese residue and mechanism exploration. *Journal of Hazardous Materials*, 410(November), 124582. <https://doi.org/10.1016/j.jhazmat.2020.124582>

- Li, M., Huang, F., Hu, L., Sun, W., Li, E., Xiong, D. L., ... He, Z. (2020). Efficient activation of peroxymonosulfate by a novel catalyst prepared directly from electrolytic manganese slag for degradation of recalcitrant organic pollutants. *Chemical Engineering Journal*, 401, 126085. <https://doi.org/10.1016/j.cej.2020.126085>
- Li, M., Zhong, H., He, Z., Hu, L., Sun, W., Loganathan, P., & Xiong, D. (2021). Degradation of various thiol collectors in simulated and real mineral processing wastewater of sulfide ore in heterogeneous modified manganese slag/PMS system. *Chemical Engineering Journal*, 413, 127478. <https://doi.org/10.1016/j.cej.2020.127478>
- Li, Yongchao, Huang, H., Xu, Z., Ma, H., & Guo, Y. (2020). Mechanism study on manganese(II) removal from acid mine wastewater using red mud and its application to a lab-scale column. *Journal of Cleaner Production*, 253, 119955. <https://doi.org/10.1016/j.jclepro.2020.119955>
- Li, Yongchao, Xu, Z., Ma, H., & Hursthouse, A. S. (2019). Removal of Manganese (II) from Acid Mine Wastewater : A Review of the Challenges and Opportunities with Special Emphasis on. *Water*, (1i).
- Li, Yongdan, Wu, D., & Lin, Y. S. (2004). Mechanical strength and reliability of solid catalysts. *China Particuology*, 2(2), 53–62. [https://doi.org/10.1016/s1672-2515\(07\)60024-4](https://doi.org/10.1016/s1672-2515(07)60024-4)
- Li, Yunqing, & Xi, G. (2005). The dissolution mechanism of cathodic active materials of spent Zn-Mn batteries in HCl. *Journal of Hazardous Materials*, 127(1–3), 244–248. <https://doi.org/10.1016/j.jhazmat.2005.07.024>
- Liang, S., Teng, F., Bulgan, G., Zong, R., & Zhu, Y. (2008). Effect of phase structure of MnO₂ nanorod catalyst on the activity for CO oxidation. *Journal of Physical Chemistry C*, 112(14), 5307–5315. <https://doi.org/10.1021/jp0774995>

- Lin, T., Yu, L., Sun, M., Cheng, G., Lan, B., & Fu, Z. (2016). Mesoporous α -MnO₂ microspheres with high specific surface area: Controlled synthesis and catalytic activities. *Chemical Engineering Journal*, 286, 114–121. <https://doi.org/10.1016/j.cej.2015.09.024>
- Liu, C., Han, Q., Chen, Y., Zhu, S., Su, T., Qu, Z., ... Huo, M. (2021). Resource Recycling of Mn-Rich Sludge: Effective Separation of Impure Fe/Al and Recovery of High-Purity Hausmannite. *ACS Omega*, 6(11), 7351–7359. <https://doi.org/10.1021/acsomega.0c05487>
- Liu, P. (2018). Recycling Waste Batteries: Recovery of Valuable Resources or Reutilization as Functional Materials. *ACS Sustainable Chemistry and Engineering*, 6(9), 11176–11185. <https://doi.org/10.1021/acssuschemeng.8b03495>
- Liu, X., Shi, L., Jiang, W., Zhang, J., & Huang, L. (2018). Taking full advantage of KMnO₄ in simplified Hummers method: A green and one pot process for the fabrication of alpha MnO₂ nanorods on graphene oxide. *Chemical Engineering Science*, 192, 414–421. <https://doi.org/10.1016/j.ces.2018.07.044>
- López, E., Gígola, C., Borio, D. O., & Bucalá, V. (2001). Catalytic combustion of methane over Pd/ γ -Al₂O₃ in a monolithic reactor: Kinetic study. *Studies in Surface Science and Catalysis*, 133(1961), 625–630. [https://doi.org/10.1016/s0167-2991\(01\)82023-1](https://doi.org/10.1016/s0167-2991(01)82023-1)
- Lu, J., Dreisinger, D., & Glück, T. (2014). Manganese electrodeposition — A literature review. *Hydrometallurgy*, 141, 105–116. <https://doi.org/10.1016/j.hydromet.2013.11.002>
- Lyu, Y., Li, C., Du, X., Zhu, Y., Zhang, Y., & Li, S. (2020a). Catalytic oxidation of toluene over MnO₂ catalysts with different Mn (II) precursors and the study of reaction pathway. *Fuel*, 262(August), 116610. <https://doi.org/10.1016/j.fuel.2019.116610>

- Lyu, Y., Li, C., Du, X., Zhu, Y., Zhang, Y., & Li, S. (2020b). Catalytic removal of toluene over manganese oxide-based catalysts: a review. *Environmental Science and Pollution Research*, 27(3), 2482–2501. <https://doi.org/10.1007/s11356-019-07037-2>
- Malcolm, H. M., Wood, M., & Kingdom, U. (2004). IPCS Concise International Chemical Assessment Documents. Manganese and its compounds: Environmental aspects. *IPCS Concise International Chemical Assessment Documents*, (63), 1–37.
- Maryam Sadeghi, S., Vanpeteghem, G., Neto, I. F. F., & Soares, H. M. V. M. (2017). Selective leaching of Zn from spent alkaline batteries using environmentally friendly approaches. *Waste Management*, 60, 696–705. <https://doi.org/10.1016/j.wasman.2016.12.002>
- Maynard, J. B. (2010). The chemistry of manganese ores through time: A signal of increasing diversity of earth-surface environments. *Economic Geology*, 105(3), 535–552. <https://doi.org/10.2113/gsecongeo.105.3.535>
- Mears, D. E. (1971a). Diagnostic criteria for heat transport limitations in fixed bed reactors. *Journal of Catalysis*, 20(2), 127–131. [https://doi.org/10.1016/0021-9517\(71\)90073-X](https://doi.org/10.1016/0021-9517(71)90073-X)
- Mears, D. E. (1971b). Tests for Transport Limitations in Experimental Catalytic Reactors. *Industrial and Engineering Chemistry Process Design and Development*, 10(4), 541–547. <https://doi.org/10.1021/i260040a020>
- Melchor-Martínez, E. M., Macias-Garbett, R., Malacara-Becerra, A., Iqbal, H. M. N., Sosa-Hernández, J. E., & Parra-Saldívar, R. (2021). Environmental impact of emerging contaminants from battery waste: A mini review. *Case Studies in Chemical and Environmental Engineering*, 3(April). <https://doi.org/10.1016/j.cscee.2021.100104>

- Menezes, P. W., Indra, A., Gutkin, V., & Driess, M. (2017). Boosting electrochemical water oxidation through replacement of Oh Co sites in cobalt oxide spinel with manganese. *Chemical Communications*, 53(57), 8018–8021. <https://doi.org/10.1039/c7cc03749j>
- Michot, A., Smith, D. S., Degot, S., & Gault, C. (2008). Thermal conductivity and specific heat of kaolinite: Evolution with thermal treatment. *Journal of the European Ceramic Society*, 28(14), 2639–2644. <https://doi.org/10.1016/j.jeurceramsoc.2008.04.007>
- Minette, F., Lugo-Pimentel, M., Modroukas, D., Davis, A. W., Gill, R., Castaldi, M. J., & De Wilde, J. (2018). Intrinsic kinetics of steam methane reforming on a thin, nanostructured and adherent Ni coating. *Applied Catalysis B: Environmental*, 238, 184–197. <https://doi.org/10.1016/j.apcatb.2018.07.015>
- Mitchell, S., Michels, N. L., & Pérez-Ramírez, J. (2013). From powder to technical body: The undervalued science of catalyst scale up. *Chemical Society Reviews*, 42(14), 6094–6112. <https://doi.org/10.1039/c3cs60076a>
- Mocellin, J., Mercier, G., Morel, J. L., Blais, J. F., & Simonnot, M. O. (2015). Factors influencing the Zn and Mn extraction from pyrometallurgical sludge in the steel manufacturing industry. *Journal of Environmental Management*, 158, 48–54. <https://doi.org/10.1016/j.jenvman.2015.04.039>
- Mocellin, J., Mercier, G., Morel, J. L., Charbonnier, P., Blais, J. F., & Simonnot, M. O. (2017). Recovery of zinc and manganese from pyrometallurgy sludge by hydrometallurgical processing. *Journal of Cleaner Production*, 168, 311–321. <https://doi.org/10.1016/j.jclepro.2017.09.003>
- Mohammadzadeh, J. S. S., & Zamaniyan, A. (2002). Catalyst Shape As a Design Parameter — Optimum Shape for. *Transport*, 80(May), Part A.

- Mohanty, S., Ghosh, S., Bal, B., & Das, A. P. (2018). A review of biotechnology processes applied for manganese recovery from wastes. *Reviews in Environmental Science and Biotechnology*, 17(4), 791–811. <https://doi.org/10.1007/s11157-018-9482-1>
- Morais, V. S., Barrada, R. V., Moura, M. N., Almeida, J. R., Moreira, T. F. M., Gonçalves, G. R., ... Freitas, M. B. J. G. (2020). Synthesis of manganese ferrite from spent Zn-MnO₂ batteries and its application as a catalyst in heterogeneous photo-Fenton processes. *Journal of Environmental Chemical Engineering*, 8(3), 103716. <https://doi.org/10.1016/j.jece.2020.103716>
- Neculita, C. M., & Rosa, E. (2019). A review of the implications and challenges of manganese removal from mine drainage. *Chemosphere*, 214, 491–510. <https://doi.org/10.1016/j.chemosphere.2018.09.106>
- Nogueira, C. A., & Margarido, F. (2015). Selective process of zinc extraction from spent Zn-MnO₂ batteries by ammonium chloride leaching. *Hydrometallurgy*, 157, 13–21. <https://doi.org/10.1016/j.hydromet.2015.07.004>
- Okal, J., Zawadzki, M., & Baranowska, K. (2016). Methane combustion over bimetallic Ru-Re/ γ -Al₂O₃ catalysts: Effect of Re and pretreatments. *Applied Catalysis B: Environmental*, 194, 22–31. <https://doi.org/10.1016/j.apcatb.2016.04.038>
- Olivares, J. A. (2006). Mass Spectrometry in Process Analysis. In *Encyclopedia of Analytical Chemistry* (pp. 1–16). <https://doi.org/10.1002/9780470027318.a2109>
- Ong, D. C., de Luna, M. D. G., Pingul-Ong, S. M. B., & Kan, C. C. (2018). Manganese and iron recovery from groundwater treatment sludge by reductive acid leaching and hydroxide precipitation. *Journal of Environmental Management*, 223(January), 723–730. <https://doi.org/10.1016/j.jenvman.2018.06.052>

- Ong, D. C., Tumamos, S. B., Kan, C. C., Pingul-Ong, S. M. B., Ensano, B. M. B., & De Luna, M. D. G. (2021a). Optimization of manganese recovery from groundwater treatment sludge for the production of highly-efficient Cu(II) and Pb(II) adsorbents. *Journal of Environmental Chemical Engineering*, 9(1), 104705. <https://doi.org/10.1016/j.jece.2020.104705>
- Ong, D. C., Tumamos, S. B., Kan, C. C., Pingul-Ong, S. M. B., Ensano, B. M. B., & De Luna, M. D. G. (2021b). Optimization of manganese recovery from groundwater treatment sludge for the production of highly-efficient Cu(II) and Pb(II) adsorbents. *Journal of Environmental Chemical Engineering*, 9(1). <https://doi.org/10.1016/j.jece.2020.104705>
- Park, Y. K., Kim, M. K., Jung, S. C., Shim, W. G., Jang, S. H., & Kim, S. C. (2021a). Effect of calcination temperature on properties of waste alkaline battery-based catalysts for deep oxidation of toluene and o-xylene. *Energy and Environment*, 32(3), 367–379. <https://doi.org/10.1177/0958305X20932551>
- Park, Y. K., Kim, M. K., Jung, S. C., Shim, W. G., Jang, S. H., & Kim, S. C. (2021b). Effect of calcination temperature on properties of waste alkaline battery-based catalysts for deep oxidation of toluene and o-xylene. *Energy and Environment*, 32(3), 367–379. <https://doi.org/10.1177/0958305X20932551>
- Park, Y. K., Song, H., Kim, M. K., Jung, S. C., Jung, H. Y., & Kim, S. C. (2021). Recycling of a spent alkaline battery as a catalyst for the total oxidation of hydrocarbons. *Journal of Hazardous Materials*, 403(September 2020), 123929. <https://doi.org/10.1016/j.jhazmat.2020.123929>

- Patil, D. S., Chavan, S. M., & Oubagaranadin, J. U. K. (2016). A review of technologies for manganese removal from wastewaters. *Journal of Environmental Chemical Engineering*, 4(1), 468–487. <https://doi.org/10.1016/j.jece.2015.11.028>
- Peng, N., Pan, Q., Liu, H., Yang, Z., & Wang, G. (2018). Recovery of iron and manganese from iron-bearing manganese residues by multi-step roasting and magnetic separation. *Minerals Engineering*, 126(May), 177–183. <https://doi.org/10.1016/j.mineng.2018.07.002>
- Piumetti, M., Fino, D., & Russo, N. (2015). Mesoporous manganese oxides prepared by solution combustion synthesis as catalysts for the total oxidation of VOCs. *Applied Catalysis B: Environmental*, 163, 277–287. <https://doi.org/10.1016/j.apcatb.2014.08.012>
- Post, J. E. (1999). Manganese oxide minerals: Crystal structures and economic and environmental significance. *Proceedings of the National Academy of Sciences of the United States of America*, 96(7), 3447–3454. <https://doi.org/10.1073/pnas.96.7.3447>
- Pulleri, J. K., Singh, S. K., Yearwar, D., Saravanan, G., Al-Fatesh, A. S., & Labhasetwar, N. K. (2021). Morphology Dependent Catalytic Activity of Mn₃O₄ for Complete Oxidation of Toluene and Carbon Monoxide. *Catalysis Letters*, 151(1), 172–183. <https://doi.org/10.1007/s10562-020-03278-w>
- Qi, W., Ran, J., Wang, R., Du, X., Shi, J., Niu, J., ... Ran, M. (2016). Kinetic consequences of methane combustion on Pd, Pt and Pd-Pt catalysts. *RSC Advances*, 6(111), 109834–109845. <https://doi.org/10.1039/c6ra21150j>
- Quintanilha, C. L., Afonso, J. C., Vianna, C. A., Gante, V., & Mantovano, J. L. (2014). Recovery of manganese and zinc via sequential precipitation from spent zinc-MnO₂ dry cells after fusion with potassium hydrogensulfate. *Journal of Power Sources*, 248, 596–603. <https://doi.org/10.1016/j.jpowsour.2013.09.111>

- R.D.W. Kemmitt and R.D. Peacock. (1973). *The Chemistry of Manganese, Technetium and Rhenium* (First). <https://doi.org/10.1016/C2013-0-05702-7>
- Rącz, R., & Ilea, P. (2013). Electrolytic recovery of Mn₃O₄ and Zn from sulphuric acid leach liquors of spent zinc-carbon-MnO₂ battery powder. *Hydrometallurgy*, 139, 116–123. <https://doi.org/10.1016/j.hydromet.2013.08.006>
- Rashid, R., Shafiq, I., Akhter, P., Iqbal, M. J., & Hussain, M. (2021). A state-of-the-art review on wastewater treatment techniques: the effectiveness of adsorption method. *Environmental Science and Pollution Research*, 28(8), 9050–9066. <https://doi.org/10.1007/s11356-021-12395-x>
- Ray, A., Bristow, T., Whitmore, C., & Mosely, J. (2018). On-line reaction monitoring by mass spectrometry, modern approaches for the analysis of chemical reactions. *Mass Spectrometry Reviews*, Vol. 37, pp. 565–579. <https://doi.org/10.1002/mas.21539>
- Reidies, A. H. (2000). Manganese Compounds. In *Ullmann's Encyclopedia of Industrial Chemistry* (Vol. 16, pp. 13–15). https://doi.org/10.1002/14356007.a16_123
- Ren, T., An, M., Hu, X., Ma, J., & Guo, Q. (2021). Development of inexpensive perovskite Mn-based oxygen carriers using the waste manganese sand for chemical looping gasification. *International Journal of Energy Research*, 45(2), 2416–2431. <https://doi.org/10.1002/er.5936>
- Rezaei, R., Moradi, G., & Sharifnia, S. (2019). Dry Reforming of Methane over Ni-Cu/Al₂O₃ Catalyst Coatings in a Microchannel Reactor: Modeling and Optimization Using Design of Experiments [Research-article]. *Energy & Fuels*, 33(7), 6689–6706. <https://doi.org/10.1021/acs.energyfuels.9b00692>

Rubel, O., Nguyen, T., Tran, T., Gourley, S., Anand, S., Bommel, A. Van, ... Ivey, D. G. (n.d.).

Electrochemical Stability of ZnMn₂O₄ : Understanding Zn-ion Rechargeable Battery. 1–33.

Sadeghabad, M. S., Bahaloo-Horeh, N., & Mousavi, S. M. (2019). Using bacterial culture supernatant for extraction of manganese and zinc from waste alkaline button-cell batteries.

Hydrometallurgy, 188(December 2018), 81–91.

<https://doi.org/10.1016/j.hydromet.2019.06.003>

Sandoval-Bohorquez, V. S., Rozo, E. A. V., & Baldovino-Medrano, V. G. (2020). A method for the highly accurate quantification of gas streams by on-line chromatography. *Journal of Chromatography A*, 1626, 461355. <https://doi.org/10.1016/j.chroma.2020.461355>

Satterfield, C. N. (1991). Acid and Zeolite Catalysts. *Heterogeneous Catalysis in Industrial Practice*, pp. 209–266.

Sayilgan, E., Kukrer, T., Civelekoglu, G., Ferella, F., Akcil, A., Veglio, F., & Kitis, M. (2009). A review of technologies for the recovery of metals from spent alkaline and zinc-carbon batteries. *Hydrometallurgy*, 97(3–4), 158–166.

<https://doi.org/10.1016/j.hydromet.2009.02.008>

Scott Fogler, H. (1987). Elements of chemical reaction engineering. *Chemical Engineering Science*, 42(10), 2493. [https://doi.org/10.1016/0009-2509\(87\)80130-6](https://doi.org/10.1016/0009-2509(87)80130-6)

Shen, B., Zhou, P., Chen, S., Yuan, H., Zhu, N., Sun, T., & Lou, Z. (2019). Manganese-based catalysts recovered from spent ternary lithium-ion batteries and its catalytic activity enhanced by a mechanical method. *Journal of Cleaner Production*, 213, 1346–1352.

<https://doi.org/10.1016/j.jclepro.2018.12.248>

- Sher Shah, M. S. A., Oh, C., Park, H., Hwang, Y. J., Ma, M., & Park, J. H. (2020). Catalytic Oxidation of Methane to Oxygenated Products: Recent Advancements and Prospects for Electrocatalytic and Photocatalytic Conversion at Low Temperatures. *Advanced Science*, 7(23), 1–24. <https://doi.org/10.1002/advs.202001946>
- Shi, F., Wang, F., Dai, H., Dai, J., Deng, J., Liu, Y., ... Au, C. T. (2012). Rod-, flower-, and dumbbell-like MnO₂: Highly active catalysts for the combustion of toluene. *Applied Catalysis A: General*, 433–434, 206–213. <https://doi.org/10.1016/j.apcata.2012.05.016>
- Shu, J., Li, B., Chen, M., Sun, D., Wei, L., Wang, Y., & Wang, J. (2020). An innovative method for manganese (Mn²⁺) and ammonia nitrogen (NH₄⁺-N) stabilization/solidification in electrolytic manganese residue by basic burning raw material. *Chemosphere*, 253, 126896. <https://doi.org/10.1016/j.chemosphere.2020.126896>
- Shu, J., Liu, R., Liu, Z., Chen, H., & Tao, C. (2016a). Enhanced extraction of manganese from electrolytic manganese residue by electrochemical. *Journal of Electroanalytical Chemistry*, 780, 32–37. <https://doi.org/10.1016/j.jelechem.2016.08.033>
- Shu, J., Liu, R., Liu, Z., Chen, H., & Tao, C. (2016b). Simultaneous removal of ammonia and manganese from electrolytic metal manganese residue leachate using phosphate salt. *Journal of Cleaner Production*, 135, 468–475. <https://doi.org/10.1016/j.jclepro.2016.06.141>
- Shu, J., Wu, H., Chen, M., Peng, H., Li, B., Liu, R., ... Hu, Z. (2019). Fractional removal of manganese and ammonia nitrogen from electrolytic metal manganese residue leachate using carbonate and struvite precipitation. *Water Research*, 153, 229–238. <https://doi.org/10.1016/j.watres.2018.12.044>

- Sie, S. T., & Krishna, R. (1998). Process development and scale up: II. Catalyst design strategy. *Reviews in Chemical Engineering*, 14(3), 159–202. <https://doi.org/10.1515/REVCE.1998.14.3.159>
- Sihaib, Z., Puleo, F., Garcia-Vargas, J. M., Retailleau, L., Descorme, C., Liotta, L. F., ... Giroir-Fendler, A. (2017). Manganese oxide-based catalysts for toluene oxidation. *Applied Catalysis B: Environmental*, 209, 689–700. <https://doi.org/10.1016/j.apcatb.2017.03.042>
- Sobianowska-Turek, A., Szczepaniak, W., Maciejewski, P., & Gawlik-Kobylińska, M. (2016). Recovery of zinc and manganese, and other metals (Fe, Cu, Ni, Co, Cd, Cr, Na, K) from Zn-MnO₂ and Zn-C waste batteries: Hydroxyl and carbonate co-precipitation from solution after reducing acidic leaching with use of oxalic acid. *Journal of Power Sources*, 325(79), 220–228. <https://doi.org/10.1016/j.jpowsour.2016.06.042>
- Sobianowska-Turek, Agnieszka. (2018). Hydrometallurgical recovery of metals: Ce, La, Co, Fe, Mn, Ni and Zn from the stream of used Ni-MH cells. *Waste Management*, 77, 213–219. <https://doi.org/10.1016/j.wasman.2018.03.046>
- Sobianowska-Turek, Agnieszka, Szczepaniak, W., & Zabłocka-Malicka, M. (2014). Electrochemical evaluation of manganese reducers - Recovery of Mn from Zn-Mn and Zn-C battery waste. *Journal of Power Sources*, 270, 668–674. <https://doi.org/10.1016/j.jpowsour.2014.07.136>
- Soltanieh, M., Zohrabian, A., Gholipour, M. J., & Kalnay, E. (2016). A review of global gas flaring and venting and impact on the environment: Case study of Iran. *International Journal of Greenhouse Gas Control*, 49, 488–509. <https://doi.org/10.1016/j.ijggc.2016.02.010>

- Sotudeh-Gharebagh, R., & Chaouki, J. (2008). The Heterogeneous and Homogeneous Combustion of Methane Over Inert Particles. *The Canadian Journal of Chemical Engineering*, 81(6), 1182–1191. <https://doi.org/10.1002/cjce.5450810607>
- Staub, D., Meille, S., Le Corre, V., Chevalier, J., & Rouleau, L. (2015). Revisiting the Side Crushing Test Using the Three-Point Bending Test for the Strength Measurement of Catalyst Supports. *Oil & Gas Science and Technology – Revue d'IFP Energies Nouvelles*, 70(3), 475–486. <https://doi.org/10.2516/ogst/2013214>
- Stegarescu, A., Lung, I., Leoștean, C., Kacso, I., Opriș, O., Lazăr, M. D., ... Soran, M. L. (2020). Green Synthesis, Characterization and Test of MnO₂ Nanoparticles as Catalyst in Biofuel Production from Grape Residue and Seeds Oil. *Waste and Biomass Valorization*, 11(9), 5003–5013. <https://doi.org/10.1007/s12649-019-00805-8>
- Stranick, M. A. (1999). Mn₂O₃ by XPS. *Surface Science Spectra*, 6(1), 39–46. <https://doi.org/10.1116/1.1247889>
- Sun, L., Zhao, P., Liu, Y., Tan, B., Yu, C., Feng, N., ... Guan, G. (2021). Enhancing the catalytic activity of MnO₂ via structural phase transition for propane combustion: Promotional role of ionic liquid. *Journal of Environmental Chemical Engineering*, 9(6), 106453. <https://doi.org/10.1016/j.jece.2021.106453>
- Sun, Z., Cao, H., Xiao, Y., Sietsma, J., Jin, W., Agterhuis, H., & Yang, Y. (2017). Toward Sustainability for Recovery of Critical Metals from Electronic Waste: The Hydrochemistry Processes. *ACS Sustainable Chemistry and Engineering*, 5(1), 21–40. <https://doi.org/10.1021/acssuschemeng.6b00841>

- Survey, U. S. G. (2020). Mineral commodity summaries 2020. In *U.S Department OF The Interior, U.S Geological Survey*. Retrieved from <https://pubs.usgs.gov/periodicals/mcs2020/mcs2020.pdf>
- Takeda, A. (2003). Manganese action in brain function. *Brain Research Reviews*, 41(1), 79–87. [https://doi.org/10.1016/S0165-0173\(02\)00234-5](https://doi.org/10.1016/S0165-0173(02)00234-5)
- Thüne, P. C., & Niemantsverdriet, J. W. (Hans. (2009). Surface science models of industrial catalysts. *Surface Science*, 603(10–12), 1756–1762. <https://doi.org/10.1016/j.susc.2008.10.061>
- Tian, Y., Shu, J., Chen, M., Wang, J., Wang, Y., Luo, Z., ... Sun, Z. (2019). Manganese and ammonia nitrogen recovery from electrolytic manganese residue by electric field enhanced leaching. *Journal of Cleaner Production*, 236. <https://doi.org/10.1016/j.jclepro.2019.117708>
- Todorova, S., Stefanov, P., Naydenov, A., & Kolev, H. (2014). Catalytic oxidation of methane over Pd-MeOx (Me = Mn, Co, Ni, Ce) catalysts - influence of metal oxides. *Revue Roumaine de Chimie*, 59(3–4), 251–257.
- Tomašić, V., & Jović, F. (2006). State-of-the-art in the monolithic catalysts/reactors. *Applied Catalysis A: General*, 311(1–2), 112–121. <https://doi.org/10.1016/j.apcata.2006.06.013>
- Toro, N., Jeldres, R. I., Órdenes, J. A., Robles, P., & Navarra, A. (2020). Manganese nodules in Chile, an alternative for the production of Co and Mn in the future—A review. *Minerals*, 10(8), 1–19. <https://doi.org/10.3390/min10080674>
- U.S. Geological Survey. (2021). *Manganese Commodity Summary 2021*. (703). Retrieved from <https://www.usgs.gov/centers/national-minerals-information-center/manganese-statistics-and-information>

- US EPA, O. (2021). *Recycling Basics*. 1–8. Retrieved from <https://www.epa.gov/recycle/recycling-basics>
- Vaudano, Pierre; Plattner, Eric; Comninellis, C. (1995). The Industrial Electrolytic Regeneration of $\text{Mn}_2(\text{SO}_4)_3$ for the Oxidation of Substituted Toluene to the Corresponding Benzaldehyde. *Chimia*, 49(1–2), 12. <https://doi.org/10.2533/chimia.1995.12>
- Velasco-Rozo, E. A., Ballesteros-Rueda, L. M., & Baldovino-Medrano, V. G. (2021). A Method for the Accurate Quantification of Gas Streams by Online Mass Spectrometry. *Journal of the American Society for Mass Spectrometry*, 32(8), 2135–2143. <https://doi.org/10.1021/jasms.1c00090>
- Walton, J., Alexander, M. R., Fairley, N., Roach, P., & Shard, A. G. (2016). Film thickness measurement and contamination layer correction for quantitative XPS. *Surface and Interface Analysis*, 48(3), 164–172. <https://doi.org/10.1002/sia.5934>
- Wang, C., Rosenfeldt, E., Li, Y., & Hofmann, R. (2020). External standard calibration method to measure the hydroxyl radical scavenging capacity of water samples. *Environmental Science and Technology*, 54(3), 1929–1937. <https://doi.org/10.1021/acs.est.9b06273>
- Wang, G., Zhang, J., Liu, L., Zhou, J. Z., Liu, Q., Qian, G., ... Richards, R. M. (2018). Novel multi-metal containing MnCr catalyst made from manganese slag and chromium wastewater for effective selective catalytic reduction of nitric oxide at low temperature. *Journal of Cleaner Production*, 183, 917–924. <https://doi.org/10.1016/j.jclepro.2018.02.207>
- Wang, G., Zhang, J., Zhou, J., & Qian, G. (2019). Production of an effective catalyst with increased oxygen vacancies from manganese slag for selective catalytic reduction of nitric oxide.

- Journal of Environmental Management*, 239(February), 90–95.
<https://doi.org/10.1016/j.jenvman.2019.03.056>
- Wang, N., Fang, Z., Peng, S., Cheng, D., Du, B., & Zhou, C. (2016). Recovery of soluble manganese from electrolyte manganese residue using a combination of ammonia and CO₂. *Hydrometallurgy*, 164, 288–294. <https://doi.org/10.1016/j.hydromet.2016.06.019>
- Wang, Xiuyun, Liu, Y., Zhang, Y., Zhang, T., Chang, H., Zhang, Y., & Jiang, L. (2018). Structural requirements of manganese oxides for methane oxidation: XAS spectroscopy and transition-state studies. *Applied Catalysis B: Environmental*, 229, 52–62. <https://doi.org/10.1016/j.apcatb.2018.02.007>
- Wang, Xu, Qiu, H., Liu, H., Shi, P., Fan, J., Min, Y., & Xu, Q. (2018). Recycling application of waste Li-MnO₂ batteries as efficient catalysts based on electrochemical lithiation to improve catalytic activity. *Green Chemistry*, 20(21), 4901–4910. <https://doi.org/10.1039/c8gc02183j>
- Wang, Y., Liu, Y., Cao, Q., Wang, C. A., & Che, D. (2011). Homogeneous combustion of fuel ultra-lean methane-air mixtures: Experimental study and simplified reaction mechanism. *Energy and Fuels*, 25(8), 3437–3445. <https://doi.org/10.1021/ef200484c>
- Watson, J. T., & Sparkman, O. D. (2007). *Introduction to Mass Spectrometry* (Fourth Ed.). <https://doi.org/10.1002/9780470516898>
- Wei, Y., Ni, L., Li, M., & Zhao, J. (2017). A template-free method for preparation of MnO₂ catalysts with high surface areas. *Catalysis Today*, 297, 188–192. <https://doi.org/10.1016/j.cattod.2016.12.044>
- Whelpton, R. (2019). Quality assurance | internal standards. In *Encyclopedia of Analytical Science* (3rd ed.). <https://doi.org/10.1016/B978-0-12-409547-2.14399-9>

- Winiarska, K., Klimkiewicz, R., Tylus, W., Sobianowska-Turek, A., Winiarski, J., Szczygieł, B., & Szczygieł, I. (2019). Study of the catalytic activity and surface properties of manganese-zinc ferrite prepared from used batteries. *Journal of Chemistry*, 2019. <https://doi.org/10.1155/2019/5430904>
- Wu, F. F., Li, X. P., Zhong, H., & Wang, S. (2016). Utilization of Electrolytic Manganese Residues in Production of Porous Ceramics. *International Journal of Applied Ceramic Technology*, 13(3), 511–521. <https://doi.org/10.1111/ijac.12502>
- Xin, B., Chen, B., Duan, N., & Zhou, C. (2011). Extraction of manganese from electrolytic manganese residue by bioleaching. *Bioresource Technology*, 102(2), 1683–1687. <https://doi.org/10.1016/j.biortech.2010.09.107>
- Xin, B., Jiang, W., Aslam, H., Zhang, K., Liu, C., Wang, R., & Wang, Y. (2012). Bioleaching of zinc and manganese from spent Zn-Mn batteries and mechanism exploration. *Bioresource Technology*, 106, 147–153. <https://doi.org/10.1016/j.biortech.2011.12.013>
- Xin, B., Jiang, W., Li, X., Zhang, K., Liu, C., Wang, R., & Wang, Y. (2012). Analysis of reasons for decline of bioleaching efficiency of spent Zn-Mn batteries at high pulp densities and exploration measure for improving performance. *Bioresource Technology*, 112, 186–192. <https://doi.org/10.1016/j.biortech.2012.02.133>
- Xu, F., Jiang, L., Dan, Z., Gao, X., Duan, N., Han, G., & Zhu, H. (2014). Water balance analysis and wastewater recycling investigation in electrolytic manganese industry of China - A case study. *Hydrometallurgy*, 149, 12–22. <https://doi.org/10.1016/j.hydromet.2014.05.002>
- Xu, H., Yan, N., Qu, Z., Liu, W., Mei, J., Huang, W., & Zhao, S. (2017). Gaseous Heterogeneous Catalytic Reactions over Mn-Based Oxides for Environmental Applications: A Critical

- Review. *Environmental Science and Technology*, 51(16), 8879–8892.
<https://doi.org/10.1021/acs.est.6b06079>
- Yang, Renchun, Ren, C., Teng, X., Chen, Z., Wu, S., & Zhang, W. (2017). Study of the Surface Oxygen Vacancies Evolvement on the Single and Bi-Components Manganese Oxide Precursors and their Catalytic Performance. *Catalysis Letters*, 147(3), 727–737.
<https://doi.org/10.1007/s10562-017-1973-0>
- Yang, Ruizhi, Wang, Z., Dai, L., & Chen, L. (2005). Synthesis and characterization of single-crystalline nanorods of α -MnO₂ and γ -MnOOH. *Materials Chemistry and Physics*, 93(1), 149–153. <https://doi.org/10.1016/j.matchemphys.2005.03.006>
- Ying, A. Y., Lu, Z., & Abdou, M. A. (1998). Mechanical behavior and design database of packed beds for blanket designs. *Fusion Engineering and Design*, 39–40, 759–764.
[https://doi.org/10.1016/S0920-3796\(97\)00157-9](https://doi.org/10.1016/S0920-3796(97)00157-9)
- Yuan, A., Wang, X., Wang, Y., & Hu, J. (2009). Textural and capacitive characteristics of MnO₂ nanocrystals derived from a novel solid-reaction route. *Electrochimica Acta*, 54(3), 1021–1026. <https://doi.org/10.1016/j.electacta.2008.08.057>
- Zakeri, M., Samimi, A., Shafiee Afarani, M., & Salehirad, A. (2018). Effects of porosity and pore size distribution on mechanical strength reliability of industrial-scale catalyst during preparation and catalytic test steps. *Particulate Science and Technology*, 36(1), 96–103.
<https://doi.org/10.1080/02726351.2016.1220437>
- Zeng, F., Pan, Y., Yang, Y., Li, Q., Li, G., Hou, Z., & Gu, G. (2016). Facile construction of Mn₃O₄-MnO₂ hetero-nanorods/graphene nanocomposite for highly sensitive electrochemical detection of hydrogen peroxide. *Electrochimica Acta*, 196, 587–596.
<https://doi.org/10.1016/j.electacta.2016.03.031>

- Zhang, K., Peng, X., Cao, Y., Yang, H., Wang, X., Zhang, Y., ... Jiang, L. (2019a). Effect of MnO₂ morphology on its catalytic performance in lean methane combustion. *Materials Research Bulletin*, *111*, 338–341. <https://doi.org/10.1016/j.materresbull.2018.11.023>
- Zhang, K., Peng, X., Cao, Y., Yang, H., Wang, X., Zhang, Y., ... Jiang, L. (2019b). Effect of MnO₂ morphology on its catalytic performance in lean methane combustion. *Materials Research Bulletin*, *111*(January 2018), 338–341. <https://doi.org/10.1016/j.materresbull.2018.11.023>
- Zhang, L., Wang, S., Lv, L., Ding, Y., Tian, D., & Wang, S. (2021). Insights into the Reactive and Deactivation Mechanisms of Manganese Oxides for Ozone Elimination: The Roles of Surface Oxygen Species. *Langmuir*, *37*(4), 1410–1419. <https://doi.org/10.1021/acs.langmuir.0c02841>
- Zhang, W., & Cheng, C. Y. (2007a). Manganese metallurgy review. Part I: Leaching of ores/secondary materials and recovery of electrolytic/chemical manganese dioxide. *Hydrometallurgy*, *89*(3–4), 137–159. <https://doi.org/10.1016/j.hydromet.2007.08.010>
- Zhang, W., & Cheng, C. Y. (2007b). Manganese metallurgy review. Part II: Manganese separation and recovery from solution. *Hydrometallurgy*, *89*(3–4), 160–177. <https://doi.org/10.1016/j.hydromet.2007.08.009>
- Zhang, W., & Cheng, C. Y. (2007c). Manganese metallurgy review. Part III: Manganese control in zinc and copper electrolytes. *Hydrometallurgy*, *89*(3–4), 178–188. <https://doi.org/10.1016/j.hydromet.2007.08.011>
- Zhou, C., Wang, J., Liu, X., Chen, F., Di, Y., Gao, S., & Shi, Q. (2018). Magnetic and thermodynamic properties of α , β , γ and δ -MnO₂. *New Journal of Chemistry*, *42*(11), 8400–8407. <https://doi.org/10.1039/c8nj00896e>

- Zhou, X., Luo, C., Wang, J., Wang, H., Chen, Z., Wang, S., & Chen, Z. (2021). Recycling application of modified waste electrolytic manganese anode slag as efficient catalyst for PMS activation. *Science of the Total Environment*, 762, 143120. <https://doi.org/10.1016/j.scitotenv.2020.143120>
- Zimmerman, J. B., Anastas, P. T., Erythropel, H. C., & Leitner, W. (2020). Designing for a green chemistry future. *Science*, 367(6476), 397–400. <https://doi.org/10.1126/science.aay3060>

Appendix B. A Method for the Accurate Quantification of Gas Streams by Online Mass Spectrometry

Further fundamental and technological developments on catalytic gaseous phase reactions such as hydrocarbon reforming and partial or total oxidation of organic volatile compounds are environmentally strategic to cope with climate change and for controlling the emission of hazard compounds.(C. He et al., 2019; Rezaei, Moradi, & Sharifnia, 2019) Basic research on this field aims at understanding the effects of the reaction conditions; temperature, composition, and space velocity, over the catalytic performance and over the designs of both the reactor and the catalysts themselves. The most common metrics for assessing the catalytic performance are the conversion of reactants and the yields and selectivities to the reaction products(Haber, 1991; L. He, Fan, Belletre, et al., 2020; Scott Fogler, 1987). These metrics are normally the base for assessing the thermodynamics, transport phenomena, and kinetics of the system and their further correlation with the physicochemical properties of the catalyst and with their evolution with time on stream. The calculation of the former is rather straightforward given that the composition of the gaseous effluents from the reactor is determined. Therefore, the accuracy of the instrumental set-up implemented for their quantification defines the accuracy of the metrics used to evaluate the catalytic performance.

On-line techniques such as gas chromatography (GC) and mass spectrometry (MS) are common for quantifying gaseous streams (Andersson, Boutonnet, & Järås, 2012; Ray, Bristow, Whitmore, & Mosely, 2018). In general, gas chromatography is highly versatile but conventional instruments require methods whose analysis time may range between minutes and a short couple

of hours. Furthermore, multiple detectors arranged in special configurations may be required for the analysis of all the components in a multicomponent effluent. On the other hand, on-line mass spectrometry can potentially overcome the above problems thanks to its capacity to provide structural information and product composition of multicomponent systems in analysis times on the order of seconds to minutes. Indeed, mass spectrometry is currently used in industries such as ethylene oxide plants but the specifics of these applications are often kept as industrial secrets.

A given analyte studied by conventional mass spectrometers undergoes three basic processes inside the instrument. First, the analyte is submitted to fragmentation/ionization by the impact of high energy electrons. Second, the produced ions are filtered according to the scanning of a predefined mass to charge, m/z , range. And, third, the selected ions are detected. (Batey, 2014) In general, the software developed for data acquisition and analysis plays a key role in the detection and identification of the compounds from the gaseous stream being analyzed. For quantification, Olivares (Olivares, 2006) states that the analysis can be based on the proportionality between the partial pressures of the components from the analyzed mixture and the intensity of the signals for the ions read in the MS spectrum. However, phenomena such as overlapping of signals coming from two or more compounds totally or partially sharing fragmentation patterns, and the dependence of signal intensities on the temperature and pressure of the monitored system and on the evolution of the internal parts of the mass spectrometer; e.g. the filament, may make quantification so difficult that often researchers opt for interpreting MS data only from a qualitative standpoint.

To overcome the issues of MS quantification, some authors (Z. Cheng et al., 2018; Kaiser, Jansen, Petersen, & Roessler, 1995; Olivares, 2006) have proposed methods that allow to calculate the individual contribution of each compound to the MS spectrum. The methods comprise the

solution of an algebraic interval matrix formed by all the analytes of the effluent and their detected ions by assuming that there is a proportionality between the concentration of the former and the non-overlapping spectra of the latter. The proportionality factors; also named as sensitivity or calibration factors, can be calculated using defined calibration routines. There are two known calibration methods: namely, the external and the internal standard methods. (C. Wang, Rosenfeldt, Li, & Hofmann, 2020; Whelpton, 2019) The external standard method estimates the sensitivity factors by correlating MS signals to known gas concentrations via least-squares regressions. The internal standard method not only does the latter but also uses the signal from a given inert compound whose concentration remain constant and know during the performed tests to normalize the intensities of the other analytes. For on-line MS systems aimed at monitoring catalytic systems or related experimental set-ups, the internal standard method is recommended.

The aim of this contribution was to develop a reliable method for accurately quantifying of the composition of gaseous reaction effluents by online mass spectrometry. A particular challenge for this kind of applications is that both the concentration and nature of the components of effluent change over time due to the catalytic reaction. To tackle the effect that these changes have on the MS spectra, a mathematical model integrating the variables inherent to the evolution of the catalytic reaction and those comprised in the instrumental analysis was developed. Particularly, the analysis of mass balances was implemented as a control tool for checking both the accuracy and physical meaning of the developed method. This strategy has proved successful for improving the accuracy of on-line GC analysis(Sandoval-Bohorquez et al., 2020) but, as far as the authors of this paper know, it had not been used as part of a method for accurately quantifying gaseous streams from catalytic systems by mass spectrometry. Herein, the catalytic combustion of methane over a continuous plug-flow bed reactor was used as a model reaction to test the accuracy of the

mathematical methods developed from both the internal and the external standard methods of calibration. In general, the internal standard method produced the most accurate and physically meaningful MS quantification for the studied gaseous streams. To validate the results of the method, catalytic tests were also made in a different reaction set-up operated under identical reaction conditions but whose effluent was monitored by on-line gas chromatography.

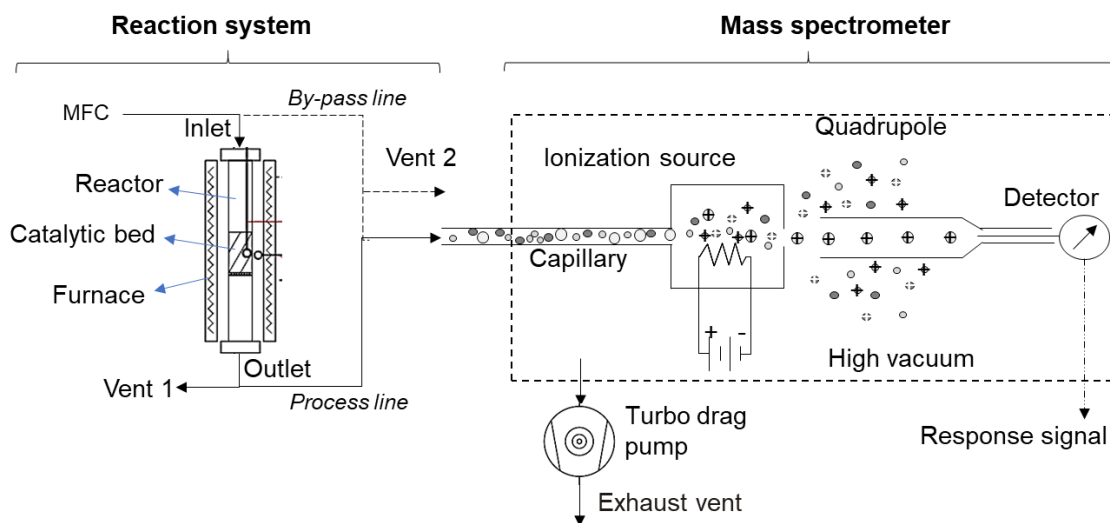
1. Theoretical background

The response of a mass spectrometer in front of a gaseous stream is a distribution of current intensities for each one of the ions formed after the partition of each one of the components of the stream. The registered signals are showed in a software interface in the form of a distribution of m/z ratios. When the instrument is coupled to the outlet of a continuous reactor, i.e. online analysis, its response is a function of the time on stream (TOS) of the catalytic system.(Holmes et al., 2016) This implies that for each molecule or atom composing the outlet stream of the catalytic system and entering the spectrometer a variety of m/z signals are found. These signals may overlap, but state of the art software (Analysis, Analysis, & Analysis, n.d.; Helmus, ter Laak, van Wezel, de Voogt, & Schymanski, 2021; Hohrenk et al., 2020) has allowed accurate compound identification. Furthermore, there are highly efficient instrumentation and software allowing completely automatized reactors coupled to online mass spectrometers. However, quantification from on-line mass spectrometry and satisfactory correlations for accurately determining the composition of gaseous streams from catalytic reactors remains mostly as niche developments. In what follows, we discuss some aspects related to the challenges that are generally present in this kind of coupled online systems.

Online mass spectrometry. Online mass spectrometers are generally provided with a capillary connected directly to the outlet stream of the reactor set-up, as outlined in Figure 1. The internal diameter of the capillary is in the scale of microns and its length should be long enough to reduce the amount of matter entering the instrument while keeping its vacuum level. This item is the bridge between the reactor and the detection system. Normally, at the end of the capillary, the analyte, herein a sample of the gaseous stream from the reactor outlet, passes to the low-pressure ion source via a ferrule-sealed vacuum feedthrough. Once the sample is inside the mass spectrometer, it is ionized and fragmented by the bombardment of high energy electrons emitted by a hot wire filament. The latter is the most common and maybe the oldest method for ionization, but it is not unique (Hoffmann & Stroobant, 2007; Watson & Sparkman, 2007). After that, the ions are directed to the quadrupole mass analyzer. This consists of four parallel rods placed at the corner of a square. The principal function of the mass analyzer is to filter and to accelerate the ions. This is done by quickly modifying the direct current and radiofrequency voltages in a way in which only a selected mass to charge ratio (m/z) goes through the quadrupole while other ions collide with the rods or are accelerated out of the array. The process is repeated for a wide range of m/z in a very short time thus allowing the ions passing to the detector once at a time.

Figure 1.

Scheme of the catalytic reaction system coupled online to a mass spectrometer. MFC: Mass Flow Controllers.



Typically, there are two types of detectors at the end of the instrument: the Faraday cup and the Secondary Electron Multiplier (SEM). The Faraday cup works with high accuracy in concentrations above the parts per millions of gas at atmospheric pressure. Low cost, simplicity, accuracy, and low noise are among its most representative characteristics. Its functioning is simple; when the accelerated ions beam collides with a metallic electrode it generates a current that after passing through a grounded high impedance resistor then generates a voltage that is read as the signal by the instrument. On the other hand, SEM detectors are sensitive to concentrations of parts per billion. The larger sensitivity of these detectors is due to the use of dynodes that successively amplify secondary electrons generated by the collision of the ions beam with an electron emissive surface. The multiplied electrons cascade is finally guided to a receptor electrode where a response signal is generated. In systems provided with coupled Faraday cup and SEM detectors, generally the SEM is used when the Faraday detection sensibility is not enough. Overall, detectors generate

an ion current response (I_{ij}) for the i^{th} m/z of the j^{th} gaseous compound analyzed, Equation 1:(Ellefson, Cain, & Lindsay, 1987; Hoffmann & Stroobant, 2007)

$$I_{ij} = G_i I_e \sigma_i n_i \quad (1)$$

Where, G_i is the transmission efficiency for a given ion, I_e is the electron beam current, σ_i is the cross-section for ionization, and n_j is the number density of target molecules (or atoms). Equation. 1 relates the current detected for a specific ion with the number of molecules (or atoms) that generated these ions in the ionization source. At conditions of ionization, n_i can be related to the total pressure in the ionization source ($P_{T,IS}$), Equation 2.

$$n_i = P_{j,IS}/T_{IS}a \quad (2)$$

Where, a is a constant and T_{IS} is the effective temperature in the ionization region. Equations 1 and 2 can be rewritten to relate linearly the ion current response with the partial pressure, Equation 3. Notice that this expression assumed a constant transmission efficiency, an electron beam current for a specified m/z , and a constant temperature in the ionization region.

$$I_{ij} = L_{ij} P_{j,IS} \quad (3)$$

Where, L_{ij} , is an integrated calibration factor commonly named as instrument sensitivity. In a multicomponent gaseous mixture, the measured ion current (I_i) of each i^{th} m/z can be described as the sum of the individual contributions of each j^{th} gaseous compound fragmented at this mass to charge, Equation 4:

$$I_i = \sum_j I_{ij} = \sum_j L_{ij} P_{j,IS} \quad (4)$$

According to Ellefson et al.(Ellefson et al., 1987), $P_{j,IS}$ is proportional to the pressure of j^{th} gaseous compound in the gaseous stream source (P_j), such as P_j is equivalent to the pressure on the outlet of the reactor in online systems, see Figure 1. Hence, Equation 4 can be rewritten as

Equation 5. By assuming the above and an ideal gas behavior, Equation 4 can also be rewritten in terms of the molar flow of a j^{th} gaseous compound (F_j):

$$I_i = \sum_j I_{ij} = \sum_j L_{ij}P_j \quad \text{or} \quad I_i = \sum_j I_{ij} = \sum_j l_{ij}F_j \quad (5)$$

Where, l_{ij} is the sensitivity factor affected by the proportionality between the pressure and the molar flow. On the other hand, since usually the initial mass spectrometer responses are always different to zero, and, since Equation 1 does not include an initial value, it is necessary to apply a correction to Equation 5, by including the real mass spectrometer response, $I_{i,j}^{real}$, and its background response, $I_{i,j}^{BG}$, Equation 6.

$$I_{i,j} = I_{i,j}^{real} - I_{i,j}^{BG} \quad (6)$$

The above analysis is a mathematical treatment that relates the molar flow at the outlet of the reactor with the mass spectrometer signal. Other authors(Cook, Bennett, & Haddix, 1999; Hammond, 2018; Heinzle, Oeggerli, & Dettwiler, 1990) have presented analogous procedures in the literature

Online mass spectrometer calibration. Calibration routines are carried out to estimate sensitivity factors relating the mass spectrometer response signal for a given j component with its molar flow (pressure or concentration). According to Equation 5, there are ixj sensitivity factors; that is, one for each fragment of each gas in the multicomponent mixture. To avoid the excessive experimentation and cost of implementing a calibration routine for determining all sensitivity factors, it is possible to use the following expression to calculate the minor fragments starting from the main fragment, i.e. the highest m/z detected for each gas, Equation 7:

$$l_{ij} = I_{R,ij} l_{ij}^{main} \quad (7)$$

Where, l_{ij}^{main} is the sensitivity factor for the main fragment, and $I_{R,ij}$ is the relative intensity of the i^{th} fragment from the main fragment for compound j which can be gotten from the database provided by the manufacturer of each particular instrument. Besides this, there are two known ways to calculate the sensitivity factor: namely, the external standard and internal standard methods.

In the external standard method, sensitivity factors are calculated by the determination of the slope of a linear regression of the molar flow (partial pressure or concentration) from the gas stream as a function of the intensity of the signal of each fragment of each gas in the multicomponent mixture. (Ferreira, Van Keulen, & Da Fonseca, 1998) For this purpose, gaseous mixtures of different and known compositions are analyzed by the mass spectrometer. After calibration, the sensitivity factors are replaced in Equation 5. With the latter, an algebraic expression to calculate the molar flow from a detected response signal of a gas compound is obtained.

On the other hand, in the internal standard method, the mass spectrometer response signal for a compound j is normalized in terms of the response signal of a given standard compound (I_{std}). Of course, the standard must remain inert under the studied experimental conditions. (Whelpton, 2019) Normalization allows compensating the effects generated by the chemical transformation occurring in the catalytic reactor on the flow entering the mass spectrometer (Heinzle et al., 1984). Therefore, the sensitivity factors are calculated with the slope of the linear regression of the normalized data of the molar flow (partial pressure or concentration), $(\frac{I_{ij}}{I_{std}})$ as a function of the response signal of the main fragment $(\frac{F_j}{F_{std}})$ for each gas in the mixture. After calibration, sensitivity factors are replaced in Equation 8 to obtain an algebraic expression to calculate the molar flow from a detected response signal of a gas compound.

$$\frac{I_{i,j}}{I_{std}} = l_{ij} \frac{F_j}{F_{std}} \quad (8)$$

Characterization of the behavior of a catalytic reactor with online mass spectrometry. The performance of a catalytic reactor is rather straightforwardly assessed by two metrics: namely, conversion (X_r) and overall selectivity (S_p). (Haber, 1991; Satterfield, 1991; Scott Fogler, 1987) Conversion refers to the change in the amount of a determined reactant due to its transformation during a chemical reaction. It may be calculated as the difference between the molar flow at the inlet and at the outlet of the reactor, Equation 9:

$$X_r = \frac{F_r^0 - F_r}{F_r^0} \quad (9)$$

On the other hand, the overall selectivity expresses the relative amount of a given product as referred to the other products, Equation 10:

$$S_p = v \frac{F_p - F_p^0}{F_r^0 - F_r} \quad (10)$$

In Equations 9 and 10, F_r^0 and F_r are the molar flows of the reactants at the inlet and at the outlet of the reactor, respectively, F_p^0 and F_p are the molar flows of products at the inlet and at the outlet of the reactor, respectively, and v is the ratio between the stoichiometric coefficients of the reactants and products. Conveniently, conversion and selectivity can be rewritten in terms of the mass spectrometer response signal. For the reactor effluents, considering that there is no overlap between the fragments generated for each gas, the external and internal standard methods produce the following relationships:

External standard:

$$I_r = l_r F_r \quad \text{or} \quad I_p = l_p F_p \quad (11)$$

Internal standard:

$$\frac{I_r}{I_{std}} = l_r \frac{F_r}{F_{std}} \quad \text{or} \quad \frac{I_p}{I_{std}} = l_p \frac{F_p}{F_{std}} \quad (12)$$

Where, the nomenclature for the gaseous compounds is now referred to reactants, r , and products, p . Replacing equations 11 and 12 in equations 9 and 10 leads to the following:

External standard:

$$X_r = \frac{I_r^0 - I_r}{I_r^0} \quad (13)$$

$$S_p = v \frac{l_p (I_p - I_p^0)}{l_r (I_r^0 - I_r)} \quad (14)$$

Internal standard:

$$X_r = \frac{\frac{I_r^0}{I_{std}^0} - I_r/I_{std}}{\frac{I_r^0}{I_{std}^0}} \quad (15)$$

$$S_p = v \frac{l_p \left(\frac{I_p}{I_{std}} - \frac{I_p^0}{I_{std}^0} \right)}{l_r \left(\frac{I_r^0}{I_{std}^0} - \frac{I_r}{I_{std}} \right)} \quad (16)$$

Where, I_r^0 and I_p^0 are the mass spectrometer response signals for the reactants and products, respectively. For these expressions, I_r^0 and I_p^0 are referred to samples takes downstream of the reaction set-up, Figure 1.

On the other hand, when there is overlap between the fragments generated for each gas, it is necessary to solve the equation systems stemming from the Matrixes 1 or 2, according to the selected calibration method, to calculate the molar flows of reactants and products:

External standard:

$$\begin{pmatrix} l_{ij} & l_{ij+1} & \dots & l_{in} \\ l_{i+1j} & l_{i+1j+1} & \dots & l_{i+1n} \\ \dots & \dots & \dots & \dots \\ l_{mj} & l_{mj+1} & \dots & l_{mn} \end{pmatrix} x \begin{pmatrix} F_j \\ F_{j+1} \\ \dots \\ F_n \end{pmatrix} = \begin{pmatrix} I_i \\ I_{i+1} \\ \dots \\ I_m \end{pmatrix} \quad \text{(Matrix 1)}$$

Internal standard:

$$\begin{pmatrix} l_{ij} & l_{ij+1} & \dots & l_{in} \\ l_{i+1j} & l_{i+1j+1} & \dots & l_{i+1n} \\ \dots & \dots & \dots & \dots \\ l_{mj} & l_{mj+1} & \dots & l_{mn} \end{pmatrix} x \begin{pmatrix} \frac{F_j}{F_{std}} \\ \frac{F_{j+1}}{F_{std}} \\ \dots \\ \frac{F_n}{F_{std}} \end{pmatrix} = \begin{pmatrix} \frac{I_i}{I_{std}} \\ \frac{I_{i+1}}{I_{std}} \\ \dots \\ \frac{I_m}{I_{std}} \end{pmatrix} \quad \text{(Matrix 2)}$$

Where, **m** and **n** are the total *m/z* fragments and the total gaseous compounds in the multicomponent mixture, respectively. To avoid including terms for the component used as the internal standard in matrix 2, the fragments from the internal standard must not overlap the fragments from any other compound.

Application of mass balances to improve the accuracy of the quantification of gaseous streams with online mass spectrometry. In principle, online mass spectrometry is ideal for monitoring catalytic reactions because all the compounds that inlet and outlet the reactor can be detected. This allows implementing mass balances as a tool for improving the accuracy of the quantification made by the technique. A mass balance is based on the principle of mass conservation (that is always true if nuclear reactions are not involved). Therefore, the mass of the reactants entering the reactor equals the mass of the products at its outlet. Herein, this principle is applied by means of a metric called the mass balance coefficient (**θ**) that relates the masses of the gases that inlet and outlet the reactor, Equation 17:(Sandoval-Bohorquez et al., 2020)

$$\frac{\sum[F_j^0 \overline{PM}_j]}{\sum[F_j \overline{PM}_j]} = \theta \quad (17)$$

Where \overline{PM}_j is the molar weight of compound j. Of course, the maximum value of θ is 1 for this value corresponds to a full closure of the mass balance. In this sense, when θ diverts from 1 a decrease in the accuracy of the quantification method is suggested when all other factors are considered equal. Equation 17 can be conveniently expressed in terms of the factors related to the mass spectrometer response signal by making adequate substitutions of Equations 11, or 12. One may notice that θ is a function of time and hence can provide information about the reliability and accuracy of the quantification process at all times and under all conditions of flow and temperature of the reaction test. On the other hand, Equation 17 could also be applied to each element that participate in the reaction; carbon balance, oxygen balance, among others. Further details on how to apply mass balances to improve the accuracy of online quantification systems is presented elsewhere. (Sandoval-Bohorquez et al., 2020).

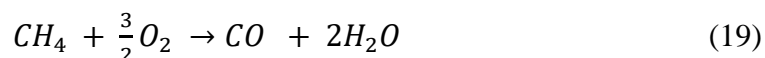
2. Experimental

The methods described above were used for the online quantification of the products from the catalytic combustion of methane, Equations 18 and 19. Catalytic tests were carried out using an automated microreactor system, CATLAB - PCS module 1 type 303230 (Hidden Analytical). The microreactor was coupled to a QGA mass spectrometer system type 305110

Table 1.*Parameters set for the QGA spectrometer.*

Gas	Argon	Methane	Oxygen	Carbon dioxide	Carbon monoxide	Water
Detector	Faraday	Faraday	Faraday	SEM	SEM	SEM
Electron Energy	70	70	70	70	70	70
Emission Current	400	350	400	300	400	400
Start Range	1×10^{-7}	1×10^{-9}	1×10^{-7}	1×10^{-9}	1×10^{-9}	1×10^{-5}
Auto Range Low	1×10^{-8}	1×10^{-12}	1×10^{-8}	1×10^{-12}	1×10^{-12}	1×10^{-1}
Auto Range High	1×10^{-5}	1×10^{-7}	1×10^{-5}	1×10^{-7}	1×10^{-7}	1×10^{-1}

(Hidden Analytical). For comparison purposes, a set of reaction tests were done in another reaction set-up coupled online to a gas chromatograph. The specific details and the methods for quantification in the latter system are presented elsewhere. (Sandoval-Bohorquez et al., 2020)



2.1 Materials.

Methane (CH₄, Linde, purity of 99.99%), oxygen (O₂, Linde, purity of 99.994%), argon (Ar, Linde, Purity 99.998%); used as a diluent, and helium (He, Linde, purity of 99.99%); used as an internal standard, were used for the catalytic tests. For some experiments, nitrogen (N₂, Linde, Purity 99.998%) was used as both diluent and internal standard. Commercial MnO₂ (Erachem Comilog, LOT 622) was used as catalyst. The catalyst was diluted with inert quartz particles (Merck). Both the catalyst and the quartz particles were sifted to obtain particles of ~75 μm. Glass wool, used to support the catalyst in the reactor, was provided by Merck.

2.2 Description of the CATLAB set-up.

The microreactor module of the CATLAB (Hiden Analytical-United Kingdom) set-up is provided with a quartz fixed-bed tubular microreactor of internal diameter equal to 0.6 cm placed inside of a tubular low thermal mass furnace controlled by a Eurotherm controller connected to a -in bed- sentry K-type thermocouple (with Cold Junction Compensation, Accuracy +/-1 °C, and Response 0.05 s). The gases fed to the reactor are controlled by independent thermal mass flow controllers (Bronkhorst®) with an accuracy of ± 0.1 % of full scale at ambient temperature, repeatability $< \pm 0.04$ % of full scale, a turndown of 1:150 and a temperature sensitivity of < 0.02 % of full scale/°C. At the outlet of the reactor, a sample of the reaction products is drawn down to a 2 m heated inert quartz capillary (1.58 mm of diameter) with heater supply operating up to 200 °C by the action of a sample bypass pumping line connected to a 60 liter per second turbomolecular pump. The capillary connects the reactor with an ultra-high vacuum (4.7×10^{-7} mbar) QGA mass spectrometer for the online analysis. The mass spectrometer is provided with an ion source, a quadrupole filter with a 300 amu mass range capability, and a dual Faraday/SEM detector having a detection limit around 100 ppb. Table 1 presents the parameters set for the QGA spectrometer in this work.

For the catalytic tests, the catalytic bed was composed of a 1:10 weight ratio mixture of catalyst and quartz particles. The use of quartz as a diluent avoids artifacts due to temperature gradients. Further homogenization of the temperature of the reactor as well as reaching plug-flow in the system was achieved by placing a glass wool plug on top of the catalytic bed. The catalyst was dried in situ at 120 °C (5 °C min^{-1}) for 90 min with a flow of argon at a space velocity of $78000 \text{ ml g}^{-1} \text{ h}^{-1}$. Then, still under argon flow, the reactor was allowed to cool down to 50 °C and

then fed with a mixture of CH₄ (7.7 % vol.), O₂ (15.4 % vol.), He (6 % vol.), and argon as gas balance, keeping the same space velocity mentioned above. The temperature of the reactor was raised to 500 °C (5 °C min⁻¹) either after 30 min or until complete stabilization of the flow fed to reactor. In a typical test, reaction products started to appear from 300 °C. The reaction tests at 500°C were typically done for 6 h after which the reactor was again cooled to 50°C while keeping the flow of reactants. Finally, the reactor was kept at 50°C for 30 min to ensure the stability of the gas flowing to the mass spectrometer.

The analysis conditions for online mass spectrometry are shown in Table 1. Data acquisition was made by the CATLAB software. The following m/z signals were followed: 44, 40, 32, 28, 18, 4 and 15, which were associated to the main fragments of Ar, CO₂, O₂, CO, H₂O, He, and a minor fragment of CH₄, respectively. The latter m/z was chosen over the main m/z line for CH₄ at 16 to avoid overlap with the other lines such as O⁺. Before the catalytic test, calibration runs were performed at 50 °C. These runs consisted of the analysis of gaseous mixtures with known compositions fed through the charged reactor in order to calculate sensitivity factors. Both the external and the internal standard calibration methods were applied using Equations 11 and 12. The recorded response signals and the calculated sensitivity factors were used to calculate reaction conversions and selectivities using Equations 13-16. Mass balance coefficients were calculated for the carbon mass balance using Equation 17.

2.3 Description of the OXIDATEST-online GC system set up.

Catalytic tests were also done in an automated reaction system, OXIDATEST, for validating the MS quantification method proposed herein. The OXIDATEST consists of a

continuous flow stainless steel fixed bed reactor with an inner diameter of 10.4 mm. The feed of the reactor was controlled by a set of independent mass flow controllers (Alicat Scientific) with an accuracy of ± 0.1 % of full scale, repeatability of ± 0.08 % of full Scale, a turndown of 1:200 and a temperature sensitivity of 0.02% of full Scale / °C. The reactor temperature was controlled by a programmable logic controller (PLC, Rockwell Automation) coupled to a concentric tubular furnace and a thermocouple placed inside the catalytic bed. The outlet pressure of the reaction system was set at 110.3 kPa using a back-pressure controller (PC, Alicat Scientific) with an accuracy of ± 0.3 % of full scale. The outlet of the reactor was connected online to a Gas Chromatograph (GC-2014 instrument, Shimadzu Corporation) to make the online analysis of the reaction products. The instrument was provided with a set of packed columns and with a TCD-Methanizer-FID array for detection and quantification. Samples from the gaseous stream from the reactor outlet, were analyzed every ~20 min. The catalytic reactor of the OXIDATEST was loaded and operated keeping the same conditions used for the tests made in CATLAB reactor, except for the use of N₂ as both internal standard and balance gas instead of He and Ar. Further details on the OXIDATEST set-up and on the GC quantification method are provided by Sandoval-Bohorquez et al. (Sandoval-Bohorquez et al., 2020).

3. Results and discussion

3.1 Mass spectrometer calibration.

Table 2 shows the sensitivity factor determined in calibration tests using external and internal standard method, for CH₄, O₂, CO₂, and CO. In all instances, the coefficient of

determination (R^2) was higher than 0.995, even when linear regression was forced to zero. Therefore, Equations 11 and 12 are proved to be adequate for quantification with mass spectrometry. Overall, there was no obvious influence of the calibration method on the coefficient of determination. Thus, the flow of the gases entering the mass spectrometer was only affected by the setting of the automated flow controllers.

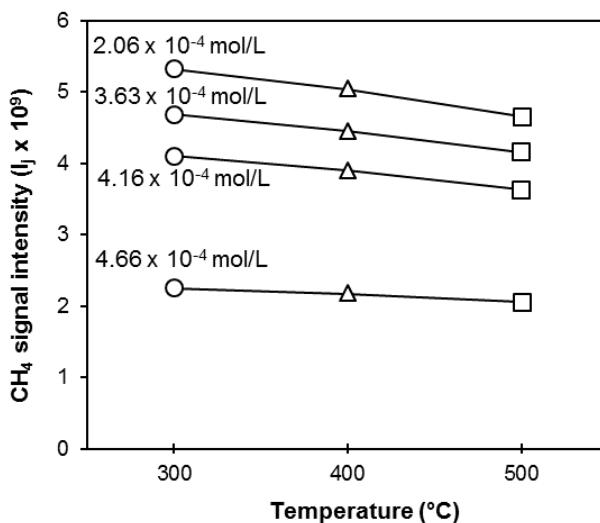
Table 2.

Calibration parameters from internal and external standard method. l_j correspond to sensitivity factor and R^2 is the coefficient of determination of linear regression.

Gas	External standard		Internal standard	
	$l_j \times 10^8$	R^2	l_j	R^2
CH ₄	0.474	0.9991	0.6424	0.9997
O ₂	0.8344	0.9997	0.8344	0.9997
CO ₂	0.6731	0.9984	0.909	0.9991
CO	0.6693	0.9953	0.9067	0.9967

Figure 2.

Intensity of the mass spectrometer response signal for methane as a function of temperature for different flows of CH₄. Tests were made by passing the flow through an empty reactor.

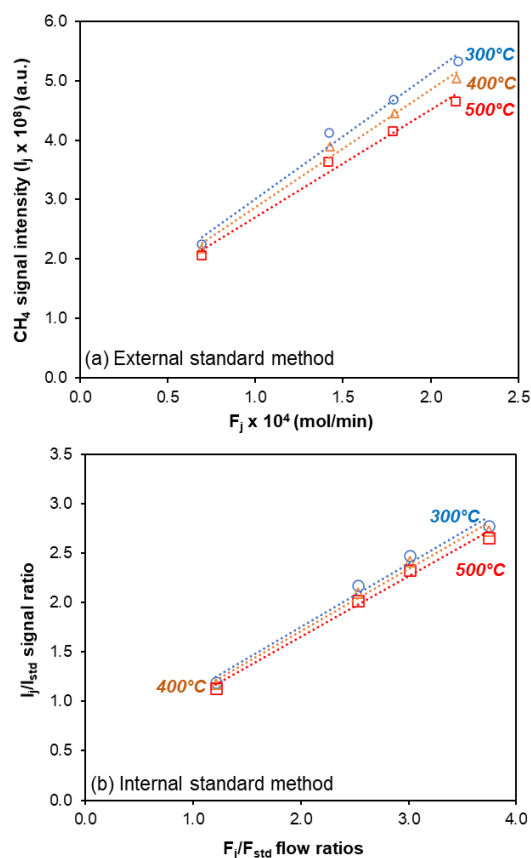


3.2 Effect of temperature on the calibration methods.

Additional tests were made for assessing the effect of temperature on both the external and internal standard calibration routines. These tests consisted on passing different flows of the gas stream fed to the reactor at 300, 400, and 500°C. The results of these tests are presented in Figures 2 and 3. Figure 2 showed that the intensity of the signal for methane decreased with the increase in the temperature of the empty reactor. As observed in Figure 3, the changes found for the intensity of the signal of methane affected the calibration made with the external standard method, Figure 3a, but not the one made with the internal standard method, Figure 3b.

Figure 3.

Calibration curves at different temperatures for methane with the external, Figure 3a, and internal, Figure 3b, methods, respectively. Tests were made by passing the flow through an empty reactor.



3.3 On-line mass spectrometry characterization of the catalytic behavior.

Figure 4 shows the mass spectrometer analysis of reactants and products of the catalytic combustion of methane. About the profiles generated by plotting the response signal, it is observed a trough between 100 and 360 min for the signals assigned to O₂ and CH₄ which is due to their consumption in the catalytic reaction. This trough coincided with a crest in the signals assigned to

CO₂ and CO due to their production in the catalytic reactor. All the signals assigned to the reaction gases decreased with time on stream. This behavior has also been reported by other authors. (Z. Cheng et al., 2018) An analysis of Equations 1 and 2 suggests that this trend is due to a decrease of the pressure of the ion source due to the compensation made-up by the vacuum pump for allowing the gas stream entering the instrument. As it is showed in Figure 4, this trend was corrected after applying the normalization of the signals with the internal standard signal.

Figure 4.

Detection of reaction reactants and products by mass spectrometry in terms of response signal (I_j) and response signal normalized with internal standard (I_j/I_{std}), during pre-reaction (40 °C), reaction (500 °C), and post-reaction (40 °C) stages.

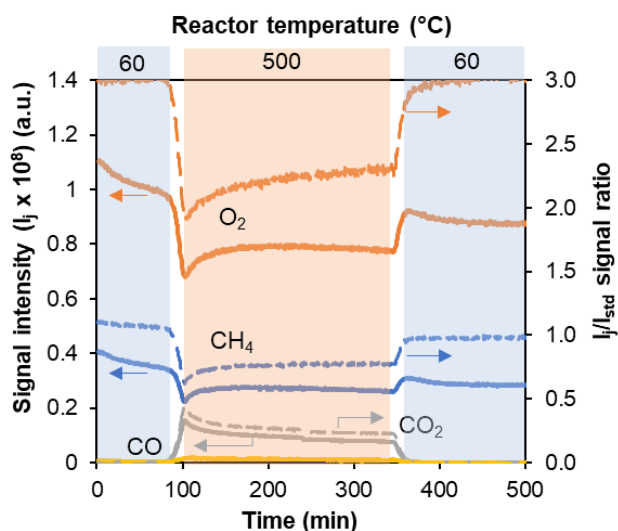
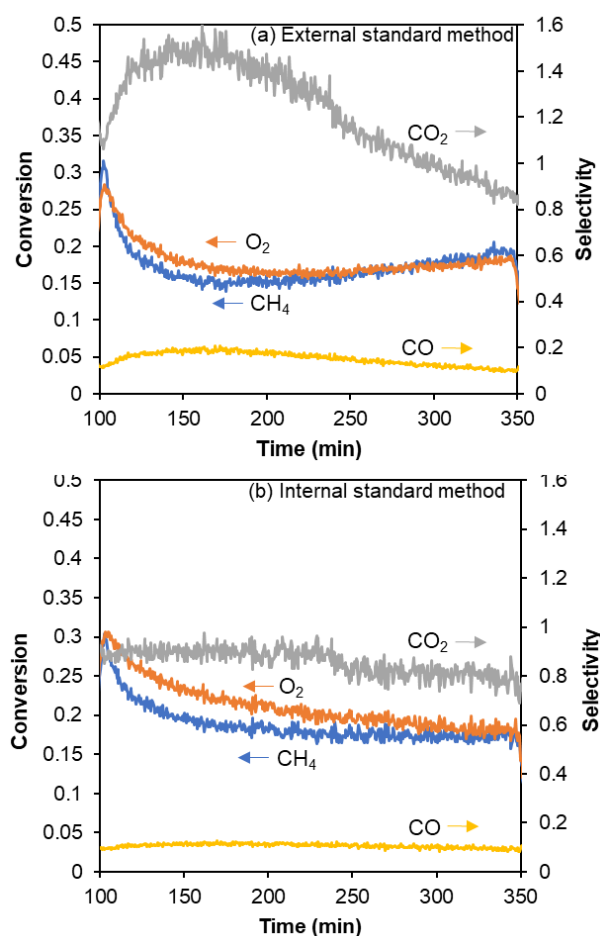


Figure 5 shows the results of conversion of CH₄ and O₂, and the selectivities to CO₂ and CO, calculated using both the external, Figure 5a, and the internal, Figure 5b, standard methods. For the external standard method some inconsistent trends were observed. First, an apparent steady increase in the conversions of both reactants after 200 min was observed. When interpreting the

data, catalytic researchers may be led to think that this shows that the catalyst was “activated” during the test. Second, the selectivity to CO_2 was larger than 1 at the beginning of the test. The inconsistencies found for the external standard method were not found with the internal standard method. Indeed, the conversions of CH_4 and O_2 remained stable after an initial period of deactivation of the catalyst, while the sum of the selectivities to CO_2 and CO remained very close to 1 at all instances.

Figure 5.

Conversion of CH_4 and O_2 , and selectivity to CO_2 and CO in the combustion reaction, calculated by external (a) and internal (b) standard method.



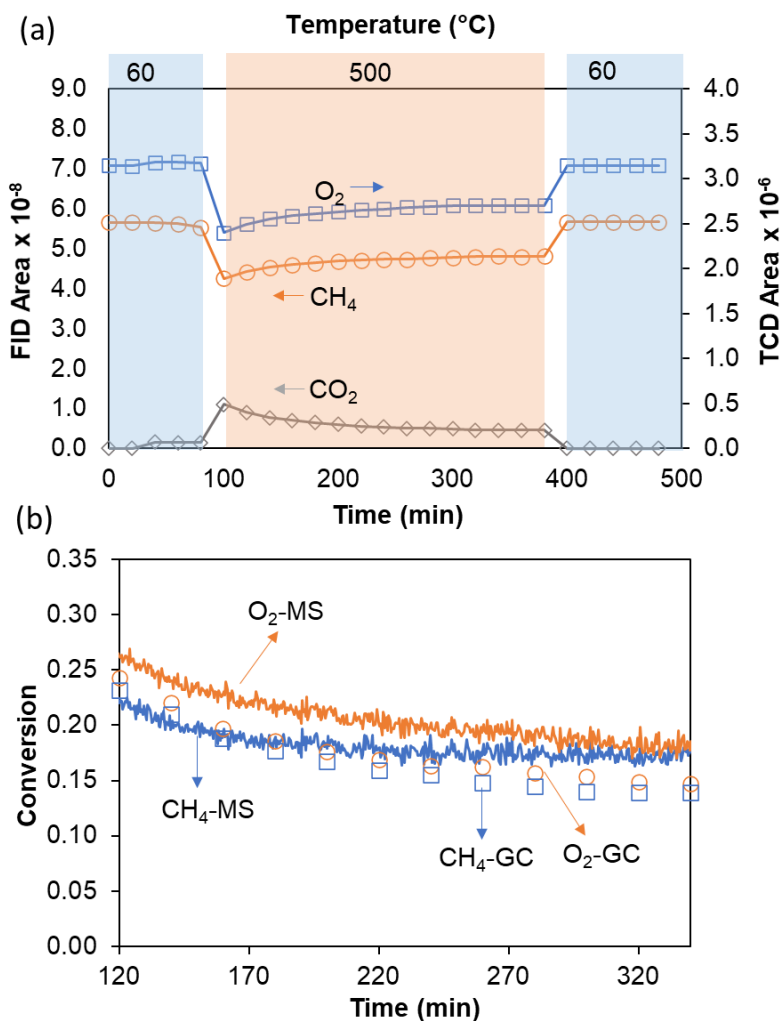
The carbon mass balance coefficient was calculated as a strategy to verify the reliability of the analysis method. It was found that for the external standard method this coefficient presented an average of 1.39 with a standard deviation of 0.24. Conversely, the quantification by the internal standard method had an average in of the carbon mass balance coefficient of 0.97, with a standard deviation of 0.06. Therefore, while the internal standard method appears highly reliable for the on-line characterization of catalytic experiments, the external standard method is highly unreliable for such a purpose. Furthermore, the conclusions drawn from the latter method are misleading for the interpretation of catalytic experiments.

3.4 Validation of the internal standard method.

The results from the on-line mass spectrometry quantification of the products from the catalytic combustion of methane were validated by comparing them with those obtained by on-line gas chromatography in the OXIDATEST set-up. Results from on-line gas chromatography in terms of FID and TCD areas of the reactants and products are presented in Figure 6. The similarity between both sets of results, conversions differed less than 3 % between both types of measurements, validates the internal standard method for on-line mass spectrometry proposed in this work.

Figure 6.

FID Areas of CH₄ and CO₂, and TCD Area of O₂ detected by gas chromatography (GC) during the catalytic combustion of methane carried out in OXIDATEST (a), and comparison between conversions of CH₄ (blue) and O₂ (orange) obtained by GC and mass spectrometry (MS) (b).



4. Conclusions

Though on-line mass spectrometry is often used for the characterization of catalytic reactors, the quantification of the components of the products streams is still used in qualitative

terms. Indeed, conventional data analysis in mass spectrometry to estimate key metrics such as conversion and selectivity is considered unreliable because of flow disturbances generated by changes in temperature or pressure in the coupled reactor-detector systems which in turn affect the intensity of the detected signal for the analyzed molecules. The results of this work demonstrated that such a behavior is present when quantification with mass spectrometry is made using the so-called external standard method of calibration. Conversely, the application of the internal standard method for quantification developed in this work produced a reliable characterization of the catalytic behavior for an experimental set-up consisting on an automated continuous fixed-bed flow reactor coupled on-line to a mass spectrometer detection system. For developing this method, mathematical expressions coupling the fundamentals of mass spectrometry detection and material balances were developed. The method was further validated with data obtained via the on-line gas chromatography characterization of a parent catalytic set-up. In general, the results of this work help provide a reliable and accurate basis for extending the use of on-line mass spectrometry in reaction process research.

7. Acknowledgments

This work was funded by Agencia Nacional de Hidrocarburos -ANH- and Minciencias, Colombia, within the frame of the projects 1102-721-50962: “*Desarrollo de alternativas catalíticas para la reducción y valorización de emisiones de gases de efecto invernadero típicas de pozos y refinerías petroleras por combustión catalítica de VOCs y transformación de CO₂ y CH₄ en gas de síntesis*” and 365-2018: “*Preparación de nanomateriales basados en metales de*

transición para procesos ligados al recobro térmico de crudos colombianos y análisis de su comportamiento catalítico en procesos de combustión in-situ.”.

7. References

- Abbasi, R., Wu, L., Wanke, S. E., & Hayes, R. E. (2012). Kinetics of methane combustion over Pt and Pt-Pd catalysts. *Chemical Engineering Research and Design*, 90(11), 1930–1942. <https://doi.org/10.1016/j.cherd.2012.03.003>
- Abid Charef, S., Affoune, A. M., Caballero, A., Cruz-Yusta, M., & Morales, J. (2017a). Simultaneous recovery of Zn and Mn from used batteries in acidic and alkaline mediums: A comparative study. *Waste Management*, 68, 518–526. <https://doi.org/10.1016/j.wasman.2017.06.048>
- Abid Charef, S., Affoune, A. M., Caballero, A., Cruz-Yusta, M., & Morales, J. (2017b). Simultaneous recovery of Zn and Mn from used batteries in acidic and alkaline mediums: A comparative study. *Waste Management*, 68, 518–526. <https://doi.org/10.1016/j.wasman.2017.06.048>
- Akbari, E., Alavi, S. M., Rezaei, M., & Larimi, A. (2021). Catalytic Methane Combustion on the Hydrothermally Synthesized MnO₂Nanowire Catalysts. *Industrial and Engineering Chemistry Research*, 60(20), 7572–7587. <https://doi.org/10.1021/acs.iecr.1c00881>
- Akhtar, F., Andersson, L., Ogunwumi, S., Hedin, N., & Bergström, L. (2014). Structuring adsorbents and catalysts by processing of porous powders. *Journal of the European Ceramic Society*, 34(7), 1643–1666. <https://doi.org/10.1016/j.jeurceramsoc.2014.01.008>

- Almeida, M. F., Xará, S. M., Delgado, J., & Costa, C. A. (2006). Characterization of spent AA household alkaline batteries. *Waste Management*, 26(5), 466–476. <https://doi.org/10.1016/j.wasman.2005.04.005>
- Analysis, G., Analysis, T., & Analysis, R. G. (n.d.). *Software for Hiden Mass Spectrometers*. Retrieved from <https://www.hidenanalytical.com/wp-content/uploads/2020/06/MASsoft-PC-Win-10-Software.pdf>
- Andak, B., Özduğan, E., Türdü, S., & Bulutcu, A. N. (2019). Recovery of zinc and manganese from spent zinc-carbon and alkaline battery mixtures via selective leaching and crystallization processes. *Journal of Environmental Chemical Engineering*, 7(5), 103372. <https://doi.org/10.1016/j.jece.2019.103372>
- Andersson, R., Boutonnet, M., & Järås, S. (2012). On-line gas chromatographic analysis of higher alcohol synthesis products from syngas. *Journal of Chromatography A*, 1247, 134–145. <https://doi.org/10.1016/j.chroma.2012.05.060>
- Anejionu, O. C. D., Whyatt, J. D., Blackburn, G. A., & Price, C. S. (2015). Contributions of gas flaring to a global air pollution hotspot: Spatial and temporal variations, impacts and alleviation. *Atmospheric Environment*, 118, 184–193. <https://doi.org/10.1016/j.atmosenv.2015.08.006>
- Anthony, J. W., Bideaux, R. A., Bladh, K. W., & Nichols, M. C. (2006). Handbook of Mineralogy. In *Mineralogical Society of America* (Vol. 11). Retrieved from <http://www.handbookofmineralogy.org/>
- Arai, H., & Machida, M. (1991). Recent progress in high-temperature catalytic combustion. *Catalysis Today*, 10(1), 81–94. [https://doi.org/10.1016/0920-5861\(91\)80076-L](https://doi.org/10.1016/0920-5861(91)80076-L)

- Bach, S., Henry, M., Baffier, N., & Livage, J. (1990). Sol-gel synthesis of manganese oxides. *Journal of Solid State Chemistry*, 88(2), 325–333. [https://doi.org/10.1016/0022-4596\(90\)90228-P](https://doi.org/10.1016/0022-4596(90)90228-P)
- Baldovino-Medrano, V. G., Kartheuser, B., & Gaigneaux, E. M. (2019a). Production and testing of technical catalysts based on MnO₂ for the abatement of aromatic volatile compounds at the laboratory and pilot plant scales. *Catalysis Today*, 338(February), 81–92. <https://doi.org/10.1016/j.cattod.2019.03.029>
- Baldovino-Medrano, V. G., Kartheuser, B., & Gaigneaux, E. M. (2019b). Production and testing of technical catalysts based on MnO₂ for the abatement of aromatic volatile compounds at the laboratory and pilot plant scales. *Catalysis Today*, 338, 81–92. <https://doi.org/10.1016/j.cattod.2019.03.029>
- Barrett, E. P., Joyner, L. G., & Halenda, P. P. (1951). The Determination of Pore Volume and Area Distributions in Porous Substances. I. Computations from Nitrogen Isotherms. *Journal of the American Chemical Society*, 73(1), 373–380. <https://doi.org/10.1021/ja01145a126>
- Batey, J. H. (2014). The physics and technology of quadrupole mass spectrometers. *Vacuum*, 101(i), 410–415. <https://doi.org/10.1016/j.vacuum.2013.05.005>
- Baynham, A., Randall, D., & Hancy, C. (2017). Incinerators and Oxidizers. *EPA Air Pollution Control Cost Manual*, (November), 1–70. Retrieved from https://www.epa.gov/sites/production/files/2017-12/documents/oxidizersincinerators_chapter2_7theditionfinal.pdf
- Belardi, G., Lavecchia, R., Medici, F., & Piga, L. (2012). Thermal treatment for recovery of manganese and zinc from zinc-carbon and alkaline spent batteries. *Waste Management*, 32(10), 1945–1951. <https://doi.org/10.1016/j.wasman.2012.05.008>

- Belardi, G., Medici, F., & Piga, L. (2014). Influence of gaseous atmosphere during a thermal process for recovery of manganese and zinc from spent batteries. *Journal of Power Sources*, 248, 1290–1298. <https://doi.org/10.1016/j.jpowsour.2013.10.064>
- Bernardes, A. M., Espinosa, D. C. R., & Tenório, J. A. S. (2004). Recycling of batteries: A review of current processes and technologies. *Journal of Power Sources*, 130(1–2), 291–298. <https://doi.org/10.1016/j.jpowsour.2003.12.026>
- Biesinger, M. C., Payne, B. P., Grosvenor, A. P., Lau, L. W. M., Gerson, A. R., & Smart, R. S. C. (2011). Resolving surface chemical states in XPS analysis of first row transition metals, oxides and hydroxides: Cr, Mn, Fe, Co and Ni. *Applied Surface Science*, 257(7), 2717–2730. <https://doi.org/10.1016/j.apsusc.2010.10.051>
- Bischoff, C. F., Fitz, O. S., Burns, J., Bauer, M., Gentischer, H., Birke, K. P., ... Biro, D. (2020). Revealing the Local pH Value Changes of Acidic Aqueous Zinc Ion Batteries with a Manganese Dioxide Electrode during Cycling. *Journal of The Electrochemical Society*, 167(2), 020545. <https://doi.org/10.1149/1945-7111/ab6c57>
- Biswal, A., Mahakud, S., Bhuyan, S., Dash, B., Sarangi, C. K., Sanjay, K., ... Park, K. H. (2015). Recovery of Co metal and Electrolytic Manganese Dioxide (EMD) from Co-Mn sludge. *Hydrometallurgy*, 152, 159–168. <https://doi.org/10.1016/j.hydromet.2015.01.006>
- Blackburn, S., & Wilson, D. I. (2008). Shaping ceramics by plastic processing. *Journal of the European Ceramic Society*, 28(7), 1341–1351. <https://doi.org/10.1016/j.jeurceramsoc.2007.12.013>
- Blake, G. R. (2015). Particle density. *Methods of Soil Analysis, Part 1: Physical and Mineralogical Properties, Including Statistics of Measurement and Sampling*, 9(11121), 371–373. <https://doi.org/10.2134/agronmonogr9.1.c29>

- Blight, G. (2011). Mine Waste: A Brief Overview of Origins, Quantities, and Methods of Storage. *Waste*, 77–88. <https://doi.org/10.1016/B978-0-12-381475-3.10005-1>
- Buzatu, M., Săceanu, S., Ghica, V. G., Iacob, G., & Buzatu, T. (2013). Simultaneous recovery of Zn and MnO₂ from used batteries, as raw materials, by electrolysis. *Waste Management*, 33(8), 1764–1769. <https://doi.org/10.1016/j.wasman.2013.04.010>
- Buzatu, T., Popescu, G., Birloaga, I., & Săceanu, S. (2013). Study concerning the recovery of zinc and manganese from spent batteries by hydrometallurgical processes. *Waste Management*, 33(3), 699–705. <https://doi.org/10.1016/j.wasman.2012.10.005>
- Cabral, M., Pedrosa, F., Margarido, F., & Nogueira, C. A. (2013). End-of-life Zn-MnO₂ batteries: Electrode materials characterization. *Environmental Technology (United Kingdom)*, 34(10), 1283–1295. <https://doi.org/10.1080/09593330.2012.745621>
- Cai, X., Zhang, Y., Hu, H., Huang, Z., Yin, Y., Liang, X., ... Liang, J. (2020). Valorization of manganese residue to prepare a highly stable and active Fe₃O₄@SiO₂/starch-derived carbon composite for catalytic degradation of dye waste water. *Journal of Cleaner Production*, 258, 120741. <https://doi.org/10.1016/j.jclepro.2020.120741>
- Canda, L., Heput, T., & Ardelean, E. (2016). Methods for recovering precious metals from industrial waste. *IOP Conference Series: Materials Science and Engineering*, 106(1). <https://doi.org/10.1088/1757-899X/106/1/012020>
- Cano, R., Mackey, K., & McGlacken, G. P. (2018). Recent advances in manganese-catalysed C-H activation: Scope and mechanism. *Catalysis Science and Technology*, 8(5), 1251–1266. <https://doi.org/10.1039/c7cy02514a>
- Carrero, C. A., Schloegl, R., Wachs, I. E., & Schomaecker, R. (2014). Critical Literature Review of the Kinetics for the Oxidative Dehydrogenation of Propane over Well-Defined

- Supported Vanadium Oxide Catalysts. *ACS Catalysis*, 4(10), 3357–3380.
<https://doi.org/10.1021/cs5003417>
- Castellanos-Beltran, I. J., Assima, G. P., & Lavoie, J. M. (2018). Effect of temperature in the conversion of methanol to olefins (MTO) using an extruded SAPO-34 catalyst. *Frontiers of Chemical Science and Engineering*, 12(2), 226–238. <https://doi.org/10.1007/s11705-018-1709-8>
- Chai, W. S., Cheun, J. Y., Kumar, P. S., Mubashir, M., Majeed, Z., Banat, F., ... Show, P. L. (2021). A review on conventional and novel materials towards heavy metal adsorption in wastewater treatment application. *Journal of Cleaner Production*, 296, 126589. <https://doi.org/10.1016/j.jclepro.2021.126589>
- Chen, B. R., Sun, W., Kitchaev, D. A., Mangum, J. S., Thamby, V., Garten, L. M., ... Schelhas, L. T. (2018). Understanding crystallization pathways leading to manganese oxide polymorph formation. *Nature Communications*, 9(1). <https://doi.org/10.1038/s41467-018-04917-y>
- Chen, H., Liu, R., Shu, J., & Li, W. (2015). Simultaneous stripping recovery of ammonia-nitrogen and precipitation of manganese from electrolytic manganese residue by air under calcium oxide assist. *Journal of Environmental Science and Health - Part A Toxic/Hazardous Substances and Environmental Engineering*, 50(12), 1282–1290. <https://doi.org/10.1080/10934529.2015.1055157>
- Chen, J., Arandiyana, H., Gao, X., & Li, J. (2015). Recent Advances in Catalysts for Methane Combustion. *Catalysis Surveys from Asia*, 19(3), 140–171. <https://doi.org/10.1007/s10563-015-9191-5>

- Cheng, G., Yu, L., He, B., Sun, M., Zhang, B., Ye, W., & Lan, B. (2017). Catalytic combustion of dimethyl ether over α -MnO₂ nanostructures with different morphologies. *Applied Surface Science*, *409*, 223–231. <https://doi.org/10.1016/j.apsusc.2017.02.218>
- Cheng, Z., Mozammel, T., Patel, J., Lee, W. J., Huang, S., Lim, S., ... Li, C. (2018). A method for the quantitative analysis of gaseous mixtures by online mass spectrometry. *International Journal of Mass Spectrometry*, *434*, 23–28. <https://doi.org/10.1016/j.ijms.2018.09.002>
- Christensen, K. A. (2007). Chapter 11 Design of industrial catalysts. In *Computer Aided Chemical Engineering* (Vol. 23). [https://doi.org/10.1016/S1570-7946\(07\)80014-9](https://doi.org/10.1016/S1570-7946(07)80014-9)
- Cook, K. D., Bennett, K. H., & Haddix, M. L. (1999). On-line mass spectrometry: A faster route to process monitoring and control. *Industrial and Engineering Chemistry Research*, *38*(4), 1192–1204. <https://doi.org/10.1021/ie9707984>
- Das, A. P., Ghosh, S., Mohanty, S., & Sukla, L. B. (2014a). Consequences of manganese compounds: a review. *Toxicological and Environmental Chemistry*, *96*(7), 981–997. <https://doi.org/10.1080/02772248.2015.1005428>
- Das, A. P., Ghosh, S., Mohanty, S., & Sukla, L. B. (2014b). Consequences of manganese compounds: a review. *Toxicological and Environmental Chemistry*, *96*(7), 981–997. <https://doi.org/10.1080/02772248.2015.1005428>
- Das, A. P., Sukla, L. B., Pradhan, N., & Nayak, S. (2011). Manganese biomining: A review. *Bioresource Technology*, *102*(16), 7381–7387. <https://doi.org/10.1016/j.biortech.2011.05.018>
- Dash, S. S., & Parida, K. M. (2007). Esterification of acetic acid with n-butanol over manganese nodule leached residue. *Journal of Molecular Catalysis A: Chemical*, *266*(1–2), 88–92. <https://doi.org/10.1016/j.molcata.2006.10.031>

- Dautzenberg, F. M. (1989). *Ten Guidelines for Catalyst Testing*. 99–119.
<https://doi.org/10.1021/bk-1989-0411.ch011>
- de Oliveira Demarco, J., Stefanello Cadore, J., da Silveira de Oliveira, F., Hiromitsu Tanabe, E., & Assumpção Bertuol, D. (2019). Recovery of metals from spent lithium-ion batteries using organic acids. *Hydrometallurgy*, *190*(December 2018), 105169.
<https://doi.org/10.1016/j.hydromet.2019.105169>
- Desai, B. D., Fernandes, J. B., & Dalal, V. N. K. (1985). Manganese dioxide - a review of a battery chemical Part II. Solid state and electrochemical properties of manganese dioxides. *Journal of Power Sources*, *16*(1), 1–43. [https://doi.org/10.1016/0378-7753\(85\)80001-X](https://doi.org/10.1016/0378-7753(85)80001-X)
- Dey, S., & Praveen Kumar, V. V. (2020). The performance of highly active manganese oxide catalysts for ambient conditions carbon monoxide oxidation. *Current Research in Green and Sustainable Chemistry*, *3*(May), 100012. <https://doi.org/10.1016/j.crgsc.2020.100012>
- Du, B., Zhou, C. bo, & Duan, N. (2014). Recycling of electrolytic manganese solid waste in autoclaved bricks preparation in China. *Journal of Material Cycles and Waste Management*, *16*(2), 258–269. <https://doi.org/10.1007/s10163-013-0181-2>
- Du, B., Zhou, C., Li, X., Guo, T., & Wang, Z. (2015). A kinetic study of Mn(II) precipitation of leached aqueous solution from electrolytic manganese residues. *Toxicological and Environmental Chemistry*, *97*(3–4), 349–357.
<https://doi.org/10.1080/02772248.2015.1050188>
- Duan, N., Fan, W., Changbo, Z., Chunlei, Z., & Hongbing, Y. (2010). Analysis of pollution materials generated from electrolytic manganese industries in China. *Resources, Conservation and Recycling*, *54*(8), 506–511.
<https://doi.org/10.1016/j.resconrec.2009.10.007>

- Duan, N., Zhou, C., Chen, B., Jiang, W., & Xin, B. (2011). Bioleaching of Mn from manganese residues by the mixed culture of *Acidithiobacillus* and mechanism. *Journal of Chemical Technology and Biotechnology*, *86*(6), 832–837. <https://doi.org/10.1002/jctb.2596>
- Dunlop, J. R., & Tully, F. P. (1993). A kinetic study of OH radical reactions with methane and perdeuterated methane. *Journal of Physical Chemistry*, *97*(43), 11148–11150. <https://doi.org/10.1021/j100145a003>
- Dwivedi, D., Randhawa, N. S., Saroj, S., & Jana, R. K. (2017). An Overview of Manganese Recovery by Hydro and Pyro-Metallurgical Routes. *Journal of The Institution of Engineers (India): Series D*, *98*(1), 147–154. <https://doi.org/10.1007/s40033-016-0119-7>
- Ebin, B., Petranikova, M., Steenari, B. M., & Ekberg, C. (2016). Production of zinc and manganese oxide particles by pyrolysis of alkaline and Zn-C battery waste. *Waste Management*, *51*, 157–167. <https://doi.org/10.1016/j.wasman.2015.10.029>
- Ebin, B., Petranikova, M., Steenari, B. M., & Ekberg, C. (2019). Recovery of industrial valuable metals from household battery waste. *Waste Management and Research*, *37*(2), 168–175. <https://doi.org/10.1177/0734242X18815966>
- Ellefson, R. E., Cain, D., & Lindsay, C. N. (1987). Calibration of mass spectrometers for quantitative gas mixture analysis. *Journal of Vacuum Science & Technology A: Vacuum, Surfaces, and Films*, *5*(1), 134–139. <https://doi.org/10.1116/1.574126>
- Elvidge, C. D., Bazilian, M. D., Zhizhin, M., Ghosh, T., Baugh, K., & Hsu, F. C. (2018). The potential role of natural gas flaring in meeting greenhouse gas mitigation targets. *Energy Strategy Reviews*, *20*, 156–162. <https://doi.org/10.1016/j.esr.2017.12.012>
- Energizer Brands, L. (2018). *Alkaline Manganese Dioxide Handbook and Application Manual*. 1–15.

- Falco, L., Quina, M. J., Gando-Ferreira, L. M., Thomas, H., & Curutchet, G. (2014). Solvent Extraction Studies for Separation of Zn(II) and Mn(II) from Spent Batteries Leach Solutions. *Separation Science and Technology (Philadelphia)*, 49(3), 398–409. <https://doi.org/10.1080/01496395.2013.850510>
- Farzana, R., Rajarao, R., Hassan, K., Behera, P. R., & Sahajwalla, V. (2018). Thermal nanosizing: Novel route to synthesize manganese oxide and zinc oxide nanoparticles simultaneously from spent Zn–C battery. *Journal of Cleaner Production*, 196, 478–488. <https://doi.org/10.1016/j.jclepro.2018.06.055>
- Farzana, R., Sayeed, M. A., Joseph, J., Ostrikov, K., O'Mullane, A. P., & Sahajwalla, V. (2020). Manganese Oxide Derived from a Spent Zn–C Battery as a Catalyst for the Oxygen Evolution Reaction. *ChemElectroChem*, 7(9), 2073–2080. <https://doi.org/10.1002/celec.202000422>
- Fawole, O. G., Cai, X. M., & Mackenzie, A. R. (2016). Gas flaring and resultant air pollution: A review focusing on black carbon. *Environmental Pollution*, 216, 182–197. <https://doi.org/10.1016/j.envpol.2016.05.075>
- Ferella, F., De Michelis, I., Beolchini, F., Innocenzi, V., & Vegliò, F. (2010). Extraction of zinc and manganese from alkaline and zinc-carbon spent batteries by citric-sulphuric acid solution. *International Journal of Chemical Engineering*, 2010. <https://doi.org/10.1155/2010/659434>
- Ferella, F., De Michelis, I., & Vegliò, F. (2008). Process for the recycling of alkaline and zinc-carbon spent batteries. *Journal of Power Sources*, 183(2), 805–811. <https://doi.org/10.1016/j.jpowsour.2008.05.043>

- Ferreira, B. S., Van Keulen, F., & Da Fonseca, M. M. R. (1998). Novel calibration method for mass spectrometers for on-line gas analysis. Set-up for the monitoring of a bacterial fermentation. *Bioprocess Engineering*, 19(4), 289–296.
<https://doi.org/10.1007/s004490050522>
- Fu, J., He, Z., Wang, H., Liang, W., & Guo, C. (2010). Preparation of chemical manganese dioxide from manganese sulfate. *Mining Science and Technology*, 20(6), 877–881.
[https://doi.org/10.1016/S1674-5264\(09\)60299-4](https://doi.org/10.1016/S1674-5264(09)60299-4)
- Gallegos, M. V., Falco, L. R., Peluso, M. A., Sambeth, J. E., & Thomas, H. J. (2013). Recovery of manganese oxides from spent alkaline and zinc-carbon batteries. An application as catalysts for VOCs elimination. *Waste Management*, 33(6), 1483–1490.
<https://doi.org/10.1016/j.wasman.2013.03.006>
- Gallegos, M. V., Peluso, M. A., Finocchio, E., Thomas, H. J., Busca, G., & Sambeth, J. E. (2017). Removal of VOCs by catalytic process. A study of MnZnO composites synthesized from waste alkaline and Zn/C batteries. *Chemical Engineering Journal*, 313, 1099–1111.
<https://doi.org/10.1016/j.cej.2016.11.001>
- Gancarczyk, A., Iwaniszyn, M., Piątek, M., Korpyś, M., Sinder, K., Jodłowski, P. J., ... Kołodziej, A. (2018). Catalytic Combustion of Low-Concentration Methane on Structured Catalyst Supports. *Industrial & Engineering Chemistry Research*, 57(31), 10281–10291.
<https://doi.org/10.1021/acs.iecr.8b01987>
- Gangwar, D., & Rath, C. (2021). *Structural , optical and magnetic properties of α - and β -MnO₂ nanorods*. 557(April).

- Gao, J., Wang, Y., Ping, Y., Hu, D., Xu, G., Gu, F., & Su, F. (2012). A thermodynamic analysis of methanation reactions of carbon oxides for the production of synthetic natural gas. *RSC Advances*, 2(6), 2358. <https://doi.org/10.1039/c2ra00632d>
- Gao, Y., Wang, Z., Cui, C., Wang, B., Liu, W., Liu, W., & Wang, L. (2020). Amorphous manganese oxide as highly active catalyst for soot oxidation. *Environmental Science and Pollution Research*, 27(12), 13488–13500. <https://doi.org/10.1007/s11356-020-07909-y>
- Ghosh, S., & Das, A. P. (2017). Bioleaching of manganese from mining waste residues using *Acinetobacter* sp. *Geology, Ecology, and Landscapes*, 1(2), 77–83. <https://doi.org/10.1080/24749508.2017.1332847>
- Ghosh, S., Mohanty, S., Akcil, A., Sukla, L. B., & Das, A. P. (2016). A greener approach for resource recycling: Manganese bioleaching. *Chemosphere*, 154, 628–639. <https://doi.org/10.1016/j.chemosphere.2016.04.028>
- Gregorová, E., Pabst, W., Smith, D. S., & Zivcová, Z. (2009). *Thermal conductivity of porous alumina ceramics prepared using starch as a pore-forming agent*. 29, 347–353. <https://doi.org/10.1016/j.jeurceramsoc.2008.06.018>
- Gunarathne, V., Rajapaksha, A. U., Vithanage, M., Alessi, D. S., Selvasembian, R., Naushad, M., ... Ok, Y. S. (2020). Hydrometallurgical processes for heavy metals recovery from industrial sludges. *Critical Reviews in Environmental Science and Technology*, 0(0), 1–41. <https://doi.org/10.1080/10643389.2020.1847949>
- Guo, M., Li, K., Liu, L., Zhang, H., Guo, W., Hu, X., ... Sun, T. (2019). Manganese-based multi-oxide derived from spent ternary lithium-ions batteries as high-efficient catalyst for VOCs oxidation. *Journal of Hazardous Materials*, 380, 120905. <https://doi.org/10.1016/j.jhazmat.2019.120905>

- Guo, M., Li, K., Liu, L., Zhang, H., Hu, X., Min, X., ... Sun, T. (2019). Resource utilization of spent ternary lithium-ions batteries: Synthesis of highly active manganese-based perovskite catalyst for toluene oxidation. *Journal of the Taiwan Institute of Chemical Engineers*, *102*, 268–275. <https://doi.org/10.1016/j.jtice.2019.06.012>
- Guo, M., Li, K., Zhang, H., Min, X., Liang, J., Hu, X., ... Sun, T. (2020). Promotional removal of oxygenated VOC over manganese-based multi oxides from spent lithium-ions manganate batteries: Modification with Fe, Bi and Ce dopants. *Science of the Total Environment*, *740*, 139951. <https://doi.org/10.1016/j.scitotenv.2020.139951>
- Guo, M., Liu, L., Gu, J. nan, Zhang, H., Min, X., Liang, J., ... Sun, T. (2021). Catalytic performance improvement of volatile organic compounds oxidation over MnOx and GdMnO3 composite oxides from spent lithium-ion batteries: Effect of acid treatment. *Chinese Journal of Chemical Engineering*. <https://doi.org/10.1016/j.cjche.2020.08.015>
- Guo, N., Wei, X. Q., Deng, X. L., & Xu, X. J. (2015). Synthesis and property of spinel porous ZnMn₂O₄ microspheres. *Applied Surface Science*, *356*, 1127–1134. <https://doi.org/10.1016/j.apsusc.2015.08.185>
- Haber, J. (1991). Manual on catalyst characterization (Recommendations 1991). *Pure and Applied Chemistry*, *63*(9), 1227–1246. <https://doi.org/10.1351/pac199163091227>
- Hagelstein, K. (2009). Globally sustainable manganese metal production and use. *Journal of Environmental Management*, *90*(12), 3736–3740. <https://doi.org/10.1016/j.jenvman.2008.05.025>
- Hammond, J. P. (2018). Quality Assurance: Spectroscopic Standards. In *Reference Module in Chemistry, Molecular Sciences and Chemical Engineering* (pp. 426–432). <https://doi.org/10.1016/B978-0-12-409547-2.00455-8>

- Han, Y. F., Chen, F., Zhong, Z., Ramesh, K., Chen, L., & Widjaja, E. (2006). Controlled synthesis, characterization, and catalytic properties of Mn₂O₃ and Mn₃O₄ nanoparticles supported on mesoporous silica SBA-15. *Journal of Physical Chemistry B*, *110*(48), 24450–24456. <https://doi.org/10.1021/jp064941v>
- Hanf, L., Henschel, J., Diehl, M., Winter, M., & Nowak, S. (2020). Mn²⁺ or Mn³⁺? Investigating transition metal dissolution of manganese species in lithium ion battery electrolytes by capillary electrophoresis. *Electrophoresis*, *41*(9), 697–704. <https://doi.org/10.1002/elps.201900443>
- He, C., Cheng, J., Zhang, X., Douthwaite, M., Pattison, S., & Hao, Z. (2019). Recent Advances in the Catalytic Oxidation of Volatile Organic Compounds: A Review Based on Pollutant Sorts and Sources [Review-article]. *Chemical Reviews*, *119*(7), 4471–4568. <https://doi.org/10.1021/acs.chemrev.8b00408>
- He, L., Fan, Y., Bellettre, J., Yue, J., & Luo, L. (2020). A review on catalytic methane combustion at low temperatures: Catalysts, mechanisms, reaction conditions and reactor designs. *Renewable and Sustainable Energy Reviews*, *119*(November 2019). <https://doi.org/10.1016/j.rser.2019.109589>
- He, L., Fan, Y., Luo, L., Bellettre, J., & Yue, J. (2020). Preparation of Pt/γ-Al₂O₃ catalyst coating in microreactors for catalytic methane combustion. *Chemical Engineering Journal*, *380*(August 2019). <https://doi.org/10.1016/j.cej.2019.122424>
- He, S., Jiang, D., Hong, M., & Liu, Z. (2021). Hazard-free treatment and resource utilisation of electrolytic manganese residue: A review. *Journal of Cleaner Production*, *306*. <https://doi.org/10.1016/j.jclepro.2021.127224>

- He, S., Wilson, B. P., Lundström, M., & Liu, Z. (2021). Hazard-free treatment of electrolytic manganese residue and recovery of manganese using low temperature roasting-water washing process. *Journal of Hazardous Materials*, 402(July 2020). <https://doi.org/10.1016/j.jhazmat.2020.123561>
- Hedden, M., Francis, N., Haraldsen, J. T., Ahmed, T., & Constantin, C. (2015). Thermoelectric properties of nano-meso-micro β -MnO₂ powders as a function of electrical resistance. *Nanoscale Research Letters*, 10(1). <https://doi.org/10.1186/s11671-015-1000-6>
- Heinzle, E., Moes, J., Griot, M., Kramer, H., Dunn, I. J., & Bourne, J. R. (1984). On-line mass spectrometry in fermentation. *Analytica Chimica Acta*, 163(C), 219–229. [https://doi.org/10.1016/S0003-2670\(00\)81510-X](https://doi.org/10.1016/S0003-2670(00)81510-X)
- Heinzle, E., Oeggerli, A., & Dettwiler, B. (1990). On-line fermentation gas analysis: Error analysis and application of mass spectrometry. *Analytica Chimica Acta*, 238(C), 101–115. [https://doi.org/10.1016/S0003-2670\(00\)80528-0](https://doi.org/10.1016/S0003-2670(00)80528-0)
- Helmus, R., ter Laak, T. L., van Wezel, A. P., de Voogt, P., & Schymanski, E. L. (2021). patRoom: open source software platform for environmental mass spectrometry based non-target screening. *Journal of Cheminformatics*, 13(1), 1–25. <https://doi.org/10.1186/s13321-020-00477-w>
- Herndon, E. M., & Brantley, S. L. (2011). Movement of manganese contamination through the Critical Zone. *Applied Geochemistry*, 26(SUPPL.), S40–S43. <https://doi.org/10.1016/j.apgeochem.2011.03.024>
- Hoffmann, E. De, & Stroobant, V. (2007). Mass Spectrometry Principles and Applications Third Edition. In *Mass spectrometry reviews* (Vol. 29). Retrieved from <https://www.wiley.com/en->

- us/Mass+Spectrometry%3A+Principles+and+Applications%2C+3rd+Edition-p-9780470033111
- Hohrenk, L. L., Itzel, F., Baetz, N., Tuerk, J., Vosough, M., & Schmidt, T. C. (2020). Comparison of Software Tools for Liquid Chromatography-High-Resolution Mass Spectrometry Data Processing in Nontarget Screening of Environmental Samples. *Analytical Chemistry*, 92(2), 1898–1907. <https://doi.org/10.1021/acs.analchem.9b04095>
- Holmes, N., Akien, G. R., Savage, R. J. D., Stanetty, C., Baxendale, I. R., Blacker, A. J., ... Bourne, R. A. (2016). Online quantitative mass spectrometry for the rapid adaptive optimisation of automated flow reactors. *Reaction Chemistry and Engineering*, 1(1), 96–100. <https://doi.org/10.1039/c5re00083a>
- Hoseini, S., Rahemi, N., Allahyari, S., & Tasbihi, M. (2019). Application of plasma technology in the removal of volatile organic compounds (BTX) using manganese oxide nano-catalysts synthesized from spent batteries. *Journal of Cleaner Production*, 232, 1134–1147. <https://doi.org/10.1016/j.jclepro.2019.05.227>
- Hoseini, S., Rahemi, N., Allahyari, S., Tasbihi, M., & Gharehabani, E. (2020). Effect of hydrometallurgical process parameters on the Mn₂O₃ nano catalysts derived from spent batteries used in the plasma catalytic oxidation of BTX. *Advanced Powder Technology*, 31(10), 4187–4196. <https://doi.org/10.1016/j.apt.2020.08.026>
- Ippolito, N. M., Belardi, G., Medici, F., & Piga, L. (2016). Utilization of automotive shredder residues in a thermal process for recovery of manganese and zinc from zinc-carbon and alkaline spent batteries. *Waste Management*, 51, 182–189. <https://doi.org/10.1016/j.wasman.2015.12.033>

- Işildar, A., Rene, E. R., van Hullebusch, E. D., & Lens, P. N. L. (2018). Electronic waste as a secondary source of critical metals: Management and recovery technologies. *Resources, Conservation and Recycling*, 135(December 2016), 296–312. <https://doi.org/10.1016/j.resconrec.2017.07.031>
- Ismail, O. S., & Umukoro, G. E. (2016). Modelling combustion reactions for gas flaring and its resulting emissions. *Journal of King Saud University - Engineering Sciences*, 28(2), 130–140. <https://doi.org/10.1016/j.jksues.2014.02.003>
- Jahan, M., Tominaka, S., & Henzie, J. (2016). Phase pure α -Mn₂O₃ prisms and their bifunctional electrocatalytic activity in oxygen evolution and reduction reactions. *Dalton Transactions*, 45(46), 18494–18501. <https://doi.org/10.1039/c6dt03158g>
- Jampaiah, D., Velisoju, V. K., Venkataswamy, P., Coyle, V. E., Nafady, A., Reddy, B. M., & Bhargava, S. K. (2017). Nanowire Morphology of Mono- and Bidoped α -MnO₂ Catalysts for Remarkable Enhancement in Soot Oxidation. *ACS Applied Materials and Interfaces*, 9(38), 32652–32666. <https://doi.org/10.1021/acsami.7b07656>
- Jaya, H., Firdaus Omar, M., Md Akil, H., Arifin Ahmad, Z., & Noriman Zulkepli, N. (2016). Sawdust polyethylene composites. *BioResources*, 11(3), 6489–6504. Retrieved from https://bioresources.cnr.ncsu.edu/wp-content/uploads/2016/07/BioRes_11_3_6489_Jaya_OAAZ_Effect_Particle_Size_Mecha_Prop_Sawdust_HDPE_Comp_9342.pdf
- Jee, J. E., Pestovsky, O., & Bakac, A. (2010). Preparation and characterization of manganese(IV) in aqueous acetic acid. *Dalton Transactions*, 39(48), 11636–11642. <https://doi.org/10.1039/c0dt00476f>

- Ji, F., Men, Y., Wang, J., Sun, Y., Wang, Z., Zhao, B., ... Xu, G. (2019). Promoting diesel soot combustion efficiency by tailoring the shapes and crystal facets of nanoscale Mn₃O₄. *Applied Catalysis B: Environmental*, 242(October 2018), 227–237. <https://doi.org/10.1016/j.apcatb.2018.09.092>
- Kaiser, R. I., Jansen, P., Petersen, K., & Roessler, K. (1995). On line and in situ quantification of gas mixtures by matrix interval algebra assisted quadrupole mass spectrometry. *Review of Scientific Instruments*, 66(11), 5226–5231. <https://doi.org/10.1063/1.1146089>
- Kim, B. S., Lee, J. C., Jeong, S. B., Lee, H. I., & Kim, C. W. (2010). Kinetics of the volatilization removal of zinc from manganese dust. *Materials Transactions*, 51(7), 1313–1318. <https://doi.org/10.2320/matertrans.M2010108>
- Kim, S. C., & Shim, W. G. (2010). Catalytic combustion of VOCs over a series of manganese oxide catalysts. *Applied Catalysis B: Environmental*, 98(3–4), 180–185. <https://doi.org/10.1016/j.apcatb.2010.05.027>
- Kloprogge, J. T., Ponce, C. P., & Loomis, T. A. (2020). The Periodic Table: Nature's Building Blocks. In *The Periodic Table: Nature's Building Blocks*. <https://doi.org/10.1016/C2019-0-03114-7>
- Klusacek, K., & Schneider, P. (1981). Effect of size and shape of catalyst on pellet pore structure and effectiveness. *Chemical Engineering Science*, 36, 523–527.
- Koivula, R., Pakarinen, J., Sivenius, M., Sirola, K., Harjula, R., & Paatero, E. (2009). Use of hydrometallurgical wastewater as a precursor for the synthesis of cryptomelane-type manganese dioxide ion exchange material. *Separation and Purification Technology*, 70(1), 53–57. <https://doi.org/10.1016/j.seppur.2009.08.014>

- Kononov, R., Ostrovski, O., & Ganguly, S. (2008). Carbothermal reduction of manganese oxide in different gas atmospheres. *Metallurgical and Materials Transactions B: Process Metallurgy and Materials Processing Science*, 39(5), 662–668. <https://doi.org/10.1007/s11663-008-9191-1>
- Kreutzer, M. T., Kapteijn, F., & Moulijn, J. A. (2006). Shouldn't catalysts shape up? Structured reactors in general and gas-liquid monolith reactors in particular. *Catalysis Today*, 111(1–2), 111–118. <https://doi.org/10.1016/j.cattod.2005.10.014>
- Kularatne, R. K. A., Kasturiarachchi, J. C., Manatunge, J. M. A., & Wijeyekoon, S. L. J. (2009). Mechanisms of Manganese Removal from Wastewaters in Constructed Wetlands Comprising Water Hyacinth (*Eichhornia crassipes* (Mart.) Solms) Grown under Different Nutrient Conditions . *Water Environment Research*, 81(2), 165–172. <https://doi.org/10.2175/106143008x370403>
- Kumar, S., García-Triñanes, P., Teixeira-Pinto, A., & Bao, M. (2013). Development of alkali activated cement from mechanically activated silico-manganese (SiMn) slag. *Cement and Concrete Composites*, 40, 7–13. <https://doi.org/10.1016/j.cemconcomp.2013.03.026>
- Lahousse, C., Bernier, A., Grange, P., Delmon, B., Papaefthimiou, P., Ioannides, T., & Verykios, X. (1998). Evaluation of γ -MnO₂ as a VOC removal catalyst: Comparison with a noble metal catalyst. *Journal of Catalysis*, 178(1), 214–225. <https://doi.org/10.1006/jcat.1998.2148>
- Lamaita, L., Peluso, M. A., Sambeth, J. E., & Thomas, H. J. (2005). Synthesis and characterization of manganese oxides employed in VOCs abatement. *Applied Catalysis B: Environmental*, 61(1–2), 114–119. <https://doi.org/10.1016/j.apcatb.2005.03.014>

- Lan, J., Sun, Y., Guo, L., Li, Z., Du, D., & Zhang, T. C. (2019). A novel method to recover ammonia, manganese and sulfate from electrolytic manganese residues by bio-leaching. *Journal of Cleaner Production*, 223, 499–507. <https://doi.org/10.1016/j.jclepro.2019.03.098>
- Lan, J., Sun, Y., Huang, P., Du, Y., Zhan, W., Zhang, T. C., & Du, D. (2020). Using Electrolytic Manganese Residue to prepare novel nanocomposite catalysts for efficient degradation of Azo Dyes in Fenton-like processes. *Chemosphere*, 252, 126487. <https://doi.org/10.1016/j.chemosphere.2020.126487>
- Lannoo, S., Vilas-Boas, A., Sadeghi, S. M., Jesus, J., & Soares, H. M. V. M. (2019). An environmentally friendly closed loop process to recycle raw materials from spent alkaline batteries. *Journal of Cleaner Production*, 236, 117612. <https://doi.org/10.1016/j.jclepro.2019.117612>
- Larsen, D., & Mann, R. (2005). Origin of high manganese concentrations in coal mine drainage, eastern Tennessee. *Journal of Geochemical Exploration*, 86(3), 143–163. <https://doi.org/10.1016/j.gexplo.2005.06.001>
- Le Bourre, B., Neculita, C. M., Coudert, L., & Rosa, E. (2020). Manganese removal processes and geochemical behavior in residues from passive treatment of mine drainage. *Chemosphere*, 259, 127424. <https://doi.org/10.1016/j.chemosphere.2020.127424>
- Lee, S. A., Lee, J. J., You, G. R., Choi, Y. W., & Kim, C. (2015). Distinction between Mn(III) and Mn(II) by using a colorimetric chemosensor in aqueous solution. *RSC Advances*, 5(116), 95618–95630. <https://doi.org/10.1039/c5ra20396a>
- Leite, D. da S., Carvalho, P. L. G., de Lemos, L. R., Mageste, A. B., & Rodrigues, G. D. (2019). Hydrometallurgical recovery of Zn(II) and Mn(II) from alkaline batteries waste employing

- aqueous two-phase system. *Separation and Purification Technology*, 210(July 2018), 327–334. <https://doi.org/10.1016/j.seppur.2018.07.038>
- Li, H., Zhang, Z., Tang, S., Li, Y., & Zhang, Y. (2008). Ultrasonically assisted acid extraction of manganese from slag. *Ultrasonics Sonochemistry*, 15(4), 339–343. <https://doi.org/10.1016/j.ultsonch.2007.07.010>
- Li, K., Chen, C., Zhang, H., Hu, X., Sun, T., & Jia, J. (2019). Effects of phase structure of MnO₂ and morphology of δ -MnO₂ on toluene catalytic oxidation. *Applied Surface Science*, 496(July). <https://doi.org/10.1016/j.apsusc.2019.143662>
- Li, M., Hu, L., Zhong, H., He, Z., Sun, W., & Xiong, D. (2021). Efficient removal of diethyl dithiocarbamate with EDTA functionalized electrolytic manganese residue and mechanism exploration. *Journal of Hazardous Materials*, 410(November), 124582. <https://doi.org/10.1016/j.jhazmat.2020.124582>
- Li, M., Huang, F., Hu, L., Sun, W., Li, E., Xiong, D. L., ... He, Z. (2020). Efficient activation of peroxymonosulfate by a novel catalyst prepared directly from electrolytic manganese slag for degradation of recalcitrant organic pollutants. *Chemical Engineering Journal*, 401, 126085. <https://doi.org/10.1016/j.cej.2020.126085>
- Li, M., Zhong, H., He, Z., Hu, L., Sun, W., Loganathan, P., & Xiong, D. (2021). Degradation of various thiol collectors in simulated and real mineral processing wastewater of sulfide ore in heterogeneous modified manganese slag/PMS system. *Chemical Engineering Journal*, 413, 127478. <https://doi.org/10.1016/j.cej.2020.127478>
- Li, Yongchao, Huang, H., Xu, Z., Ma, H., & Guo, Y. (2020). Mechanism study on manganese(II) removal from acid mine wastewater using red mud and its application to a lab-scale

- column. *Journal of Cleaner Production*, 253, 119955.
<https://doi.org/10.1016/j.jclepro.2020.119955>
- Li, Yongchao, Xu, Z., Ma, H., & Hursthouse, A. S. (2019). Removal of Manganese (II) from Acid Mine Wastewater : A Review of the Challenges and Opportunities with Special Emphasis on. *Water*, (Ii).
- Li, Yongdan, Wu, D., & Lin, Y. S. (2004). Mechanical strength and reliability of solid catalysts. *China Particuology*, 2(2), 53–62. [https://doi.org/10.1016/s1672-2515\(07\)60024-4](https://doi.org/10.1016/s1672-2515(07)60024-4)
- Li, Yunqing, & Xi, G. (2005). The dissolution mechanism of cathodic active materials of spent Zn-Mn batteries in HCl. *Journal of Hazardous Materials*, 127(1–3), 244–248.
<https://doi.org/10.1016/j.jhazmat.2005.07.024>
- Liang, S., Teng, F., Bulgan, G., Zong, R., & Zhu, Y. (2008). Effect of phase structure of MnO₂ nanorod catalyst on the activity for CO oxidation. *Journal of Physical Chemistry C*, 112(14), 5307–5315. <https://doi.org/10.1021/jp0774995>
- Lin, T., Yu, L., Sun, M., Cheng, G., Lan, B., & Fu, Z. (2016). Mesoporous α -MnO₂ microspheres with high specific surface area: Controlled synthesis and catalytic activities. *Chemical Engineering Journal*, 286, 114–121. <https://doi.org/10.1016/j.cej.2015.09.024>
- Liu, C., Han, Q., Chen, Y., Zhu, S., Su, T., Qu, Z., ... Huo, M. (2021). Resource Recycling of Mn-Rich Sludge: Effective Separation of Impure Fe/Al and Recovery of High-Purity Hausmannite. *ACS Omega*, 6(11), 7351–7359. <https://doi.org/10.1021/acsomega.0c05487>
- Liu, P. (2018). Recycling Waste Batteries: Recovery of Valuable Resources or Reutilization as Functional Materials. *ACS Sustainable Chemistry and Engineering*, 6(9), 11176–11185.
<https://doi.org/10.1021/acssuschemeng.8b03495>

- Liu, X., Shi, L., Jiang, W., Zhang, J., & Huang, L. (2018). Taking full advantage of KMnO₄ in simplified Hummers method: A green and one pot process for the fabrication of alpha MnO₂ nanorods on graphene oxide. *Chemical Engineering Science*, *192*, 414–421. <https://doi.org/10.1016/j.ces.2018.07.044>
- López, E., Gígola, C., Borio, D. O., & Bucalá, V. (2001). Catalytic combustion of methane over Pd/γ-Al₂O₃ in a monolithic reactor: Kinetic study. *Studies in Surface Science and Catalysis*, *133*(1961), 625–630. [https://doi.org/10.1016/s0167-2991\(01\)82023-1](https://doi.org/10.1016/s0167-2991(01)82023-1)
- Lu, J., Dreisinger, D., & Glück, T. (2014). Manganese electrodeposition — A literature review. *Hydrometallurgy*, *141*, 105–116. <https://doi.org/10.1016/j.hydromet.2013.11.002>
- Lyu, Y., Li, C., Du, X., Zhu, Y., Zhang, Y., & Li, S. (2020a). Catalytic oxidation of toluene over MnO₂ catalysts with different Mn (II) precursors and the study of reaction pathway. *Fuel*, *262*(August), 116610. <https://doi.org/10.1016/j.fuel.2019.116610>
- Lyu, Y., Li, C., Du, X., Zhu, Y., Zhang, Y., & Li, S. (2020b). Catalytic removal of toluene over manganese oxide-based catalysts: a review. *Environmental Science and Pollution Research*, *27*(3), 2482–2501. <https://doi.org/10.1007/s11356-019-07037-2>
- Malcolm, H. M., Wood, M., & Kingdom, U. (2004). IPCS Concise International Chemical Assessment Documents. Manganese and its compounds: Environmental aspects. *IPCS Concise International Chemical Assessment Documents*, (63), 1–37.
- Maryam Sadeghi, S., Vanpeteghem, G., Neto, I. F. F., & Soares, H. M. V. M. (2017). Selective leaching of Zn from spent alkaline batteries using environmentally friendly approaches. *Waste Management*, *60*, 696–705. <https://doi.org/10.1016/j.wasman.2016.12.002>

- Maynard, J. B. (2010). The chemistry of manganese ores through time: A signal of increasing diversity of earth-surface environments. *Economic Geology*, 105(3), 535–552. <https://doi.org/10.2113/gsecongeo.105.3.535>
- Mears, D. E. (1971a). Diagnostic criteria for heat transport limitations in fixed bed reactors. *Journal of Catalysis*, 20(2), 127–131. [https://doi.org/10.1016/0021-9517\(71\)90073-X](https://doi.org/10.1016/0021-9517(71)90073-X)
- Mears, D. E. (1971b). Tests for Transport Limitations in Experimental Catalytic Reactors. *Industrial and Engineering Chemistry Process Design and Development*, 10(4), 541–547. <https://doi.org/10.1021/i260040a020>
- Melchor-Martínez, E. M., Macias-Garbett, R., Malacara-Becerra, A., Iqbal, H. M. N., Sosa-Hernández, J. E., & Parra-Saldívar, R. (2021). Environmental impact of emerging contaminants from battery waste: A mini review. *Case Studies in Chemical and Environmental Engineering*, 3(April). <https://doi.org/10.1016/j.cscee.2021.100104>
- Menezes, P. W., Indra, A., Gutkin, V., & Driess, M. (2017). Boosting electrochemical water oxidation through replacement of Oh Co sites in cobalt oxide spinel with manganese. *Chemical Communications*, 53(57), 8018–8021. <https://doi.org/10.1039/c7cc03749j>
- Michot, A., Smith, D. S., Degot, S., & Gault, C. (2008). Thermal conductivity and specific heat of kaolinite: Evolution with thermal treatment. *Journal of the European Ceramic Society*, 28(14), 2639–2644. <https://doi.org/10.1016/j.jeurceramsoc.2008.04.007>
- Minette, F., Lugo-Pimentel, M., Modroukas, D., Davis, A. W., Gill, R., Castaldi, M. J., & De Wilde, J. (2018). Intrinsic kinetics of steam methane reforming on a thin, nanostructured and adherent Ni coating. *Applied Catalysis B: Environmental*, 238, 184–197. <https://doi.org/10.1016/j.apcatb.2018.07.015>

- Mitchell, S., Michels, N. L., & Pérez-Ramírez, J. (2013). From powder to technical body: The undervalued science of catalyst scale up. *Chemical Society Reviews*, 42(14), 6094–6112. <https://doi.org/10.1039/c3cs60076a>
- Mocellin, J., Mercier, G., Morel, J. L., Blais, J. F., & Simonnot, M. O. (2015). Factors influencing the Zn and Mn extraction from pyrometallurgical sludge in the steel manufacturing industry. *Journal of Environmental Management*, 158, 48–54. <https://doi.org/10.1016/j.jenvman.2015.04.039>
- Mocellin, J., Mercier, G., Morel, J. L., Charbonnier, P., Blais, J. F., & Simonnot, M. O. (2017). Recovery of zinc and manganese from pyrometallurgy sludge by hydrometallurgical processing. *Journal of Cleaner Production*, 168, 311–321. <https://doi.org/10.1016/j.jclepro.2017.09.003>
- Mohammadzadeh, J. S. S., & Zamaniyan, A. (2002). Catalyst Shape As a Design Parameter — Optimum Shape for. *Transport*, 80(May), Part A.
- Mohanty, S., Ghosh, S., Bal, B., & Das, A. P. (2018). A review of biotechnology processes applied for manganese recovery from wastes. *Reviews in Environmental Science and Biotechnology*, 17(4), 791–811. <https://doi.org/10.1007/s11157-018-9482-1>
- Morais, V. S., Barrada, R. V., Moura, M. N., Almeida, J. R., Moreira, T. F. M., Gonçalves, G. R., ... Freitas, M. B. J. G. (2020). Synthesis of manganese ferrite from spent Zn-MnO₂ batteries and its application as a catalyst in heterogeneous photo-Fenton processes. *Journal of Environmental Chemical Engineering*, 8(3), 103716. <https://doi.org/10.1016/j.jece.2020.103716>

- Neculita, C. M., & Rosa, E. (2019). A review of the implications and challenges of manganese removal from mine drainage. *Chemosphere*, 214, 491–510. <https://doi.org/10.1016/j.chemosphere.2018.09.106>
- Nogueira, C. A., & Margarido, F. (2015). Selective process of zinc extraction from spent Zn-MnO₂ batteries by ammonium chloride leaching. *Hydrometallurgy*, 157, 13–21. <https://doi.org/10.1016/j.hydromet.2015.07.004>
- Okal, J., Zawadzki, M., & Baranowska, K. (2016). Methane combustion over bimetallic Ru-Re/ γ -Al₂O₃ catalysts: Effect of Re and pretreatments. *Applied Catalysis B: Environmental*, 194, 22–31. <https://doi.org/10.1016/j.apcatb.2016.04.038>
- Olivares, J. A. (2006). Mass Spectrometry in Process Analysis. In *Encyclopedia of Analytical Chemistry* (pp. 1–16). <https://doi.org/10.1002/9780470027318.a2109>
- Ong, D. C., de Luna, M. D. G., Pingul-Ong, S. M. B., & Kan, C. C. (2018). Manganese and iron recovery from groundwater treatment sludge by reductive acid leaching and hydroxide precipitation. *Journal of Environmental Management*, 223(January), 723–730. <https://doi.org/10.1016/j.jenvman.2018.06.052>
- Ong, D. C., Tumampos, S. B., Kan, C. C., Pingul-Ong, S. M. B., Ensano, B. M. B., & De Luna, M. D. G. (2021a). Optimization of manganese recovery from groundwater treatment sludge for the production of highly-efficient Cu(II) and Pb(II) adsorbents. *Journal of Environmental Chemical Engineering*, 9(1), 104705. <https://doi.org/10.1016/j.jece.2020.104705>
- Ong, D. C., Tumampos, S. B., Kan, C. C., Pingul-Ong, S. M. B., Ensano, B. M. B., & De Luna, M. D. G. (2021b). Optimization of manganese recovery from groundwater treatment sludge

- for the production of highly-efficient Cu(II) and Pb(II) adsorbents. *Journal of Environmental Chemical Engineering*, 9(1). <https://doi.org/10.1016/j.jece.2020.104705>
- Park, Y. K., Kim, M. K., Jung, S. C., Shim, W. G., Jang, S. H., & Kim, S. C. (2021a). Effect of calcination temperature on properties of waste alkaline battery-based catalysts for deep oxidation of toluene and o-xylene. *Energy and Environment*, 32(3), 367–379. <https://doi.org/10.1177/0958305X20932551>
- Park, Y. K., Kim, M. K., Jung, S. C., Shim, W. G., Jang, S. H., & Kim, S. C. (2021b). Effect of calcination temperature on properties of waste alkaline battery-based catalysts for deep oxidation of toluene and o-xylene. *Energy and Environment*, 32(3), 367–379. <https://doi.org/10.1177/0958305X20932551>
- Park, Y. K., Song, H., Kim, M. K., Jung, S. C., Jung, H. Y., & Kim, S. C. (2021). Recycling of a spent alkaline battery as a catalyst for the total oxidation of hydrocarbons. *Journal of Hazardous Materials*, 403(September 2020), 123929. <https://doi.org/10.1016/j.jhazmat.2020.123929>
- Patil, D. S., Chavan, S. M., & Oubagaranadin, J. U. K. (2016). A review of technologies for manganese removal from wastewaters. *Journal of Environmental Chemical Engineering*, 4(1), 468–487. <https://doi.org/10.1016/j.jece.2015.11.028>
- Peng, N., Pan, Q., Liu, H., Yang, Z., & Wang, G. (2018). Recovery of iron and manganese from iron-bearing manganese residues by multi-step roasting and magnetic separation. *Minerals Engineering*, 126(May), 177–183. <https://doi.org/10.1016/j.mineng.2018.07.002>
- Piumetti, M., Fino, D., & Russo, N. (2015). Mesoporous manganese oxides prepared by solution combustion synthesis as catalysts for the total oxidation of VOCs. *Applied Catalysis B: Environmental*, 163, 277–287. <https://doi.org/10.1016/j.apcatb.2014.08.012>

- Post, J. E. (1999). Manganese oxide minerals: Crystal structures and economic and environmental significance. *Proceedings of the National Academy of Sciences of the United States of America*, 96(7), 3447–3454. <https://doi.org/10.1073/pnas.96.7.3447>
- Pulleri, J. K., Singh, S. K., Yearwar, D., Saravanan, G., Al-Fatesh, A. S., & Labhasetwar, N. K. (2021). Morphology Dependent Catalytic Activity of Mn₃O₄ for Complete Oxidation of Toluene and Carbon Monoxide. *Catalysis Letters*, 151(1), 172–183. <https://doi.org/10.1007/s10562-020-03278-w>
- Qi, W., Ran, J., Wang, R., Du, X., Shi, J., Niu, J., ... Ran, M. (2016). Kinetic consequences of methane combustion on Pd, Pt and Pd-Pt catalysts. *RSC Advances*, 6(111), 109834–109845. <https://doi.org/10.1039/c6ra21150j>
- Quintanilha, C. L., Afonso, J. C., Vianna, C. A., Gante, V., & Mantovano, J. L. (2014). Recovery of manganese and zinc via sequential precipitation from spent zinc-MnO₂ dry cells after fusion with potassium hydrogensulfate. *Journal of Power Sources*, 248, 596–603. <https://doi.org/10.1016/j.jpowsour.2013.09.111>
- R.D.W. Kemmitt and R.D. Peacock. (1973). *The Chemistry of Manganese, Technetium and Rhenium* (First). <https://doi.org/10.1016/C2013-0-05702-7>
- Rácz, R., & Ilea, P. (2013). Electrolytic recovery of Mn₃O₄ and Zn from sulphuric acid leach liquors of spent zinc-carbon-MnO₂ battery powder. *Hydrometallurgy*, 139, 116–123. <https://doi.org/10.1016/j.hydromet.2013.08.006>
- Rashid, R., Shafiq, I., Akhter, P., Iqbal, M. J., & Hussain, M. (2021). A state-of-the-art review on wastewater treatment techniques: the effectiveness of adsorption method. *Environmental Science and Pollution Research*, 28(8), 9050–9066. <https://doi.org/10.1007/s11356-021-12395-x>

- Ray, A., Bristow, T., Whitmore, C., & Mosely, J. (2018). On-line reaction monitoring by mass spectrometry, modern approaches for the analysis of chemical reactions. *Mass Spectrometry Reviews*, Vol. 37, pp. 565–579. <https://doi.org/10.1002/mas.21539>
- Reidies, A. H. (2000). Manganese Compounds. In *Ullmann's Encyclopedia of Industrial Chemistry* (Vol. 16, pp. 13–15). https://doi.org/10.1002/14356007.a16_123
- Ren, T., An, M., Hu, X., Ma, J., & Guo, Q. (2021). Development of inexpensive perovskite Mn-based oxygen carriers using the waste manganese sand for chemical looping gasification. *International Journal of Energy Research*, 45(2), 2416–2431. <https://doi.org/10.1002/er.5936>
- Rezaei, R., Moradi, G., & Sharifnia, S. (2019). Dry Reforming of Methane over Ni-Cu/Al₂O₃ Catalyst Coatings in a Microchannel Reactor: Modeling and Optimization Using Design of Experiments [Research-article]. *Energy & Fuels*, 33(7), 6689–6706. <https://doi.org/10.1021/acs.energyfuels.9b00692>
- Rubel, O., Nguyen, T., Tran, T., Gourley, S., Anand, S., Bommel, A. Van, ... Ivey, D. G. (n.d.). *Electrochemical Stability of ZnMn₂O₄: Understanding Zn-ion Rechargeable Battery*. 1–33.
- Sadeghabad, M. S., Bahaloo-Horeh, N., & Mousavi, S. M. (2019). Using bacterial culture supernatant for extraction of manganese and zinc from waste alkaline button-cell batteries. *Hydrometallurgy*, 188(December 2018), 81–91. <https://doi.org/10.1016/j.hydromet.2019.06.003>
- Sandoval-Bohorquez, V. S., Rozo, E. A. V., & Baldovino-Medrano, V. G. (2020). A method for the highly accurate quantification of gas streams by on-line chromatography. *Journal of Chromatography A*, 1626, 461355. <https://doi.org/10.1016/j.chroma.2020.461355>

- Satterfield, C. N. (1991). Acid and Zeolite Catalysts. *Heterogeneous Catalysis in Industrial Practice*, pp. 209–266.
- Sayilgan, E., Kukrer, T., Civelekoglu, G., Ferella, F., Akcil, A., Veglio, F., & Kitis, M. (2009). A review of technologies for the recovery of metals from spent alkaline and zinc-carbon batteries. *Hydrometallurgy*, 97(3–4), 158–166. <https://doi.org/10.1016/j.hydromet.2009.02.008>
- Scott Fogler, H. (1987). Elements of chemical reaction engineering. *Chemical Engineering Science*, 42(10), 2493. [https://doi.org/10.1016/0009-2509\(87\)80130-6](https://doi.org/10.1016/0009-2509(87)80130-6)
- Shen, B., Zhou, P., Chen, S., Yuan, H., Zhu, N., Sun, T., & Lou, Z. (2019). Manganese-based catalysts recovered from spent ternary lithium-ion batteries and its catalytic activity enhanced by a mechanical method. *Journal of Cleaner Production*, 213, 1346–1352. <https://doi.org/10.1016/j.jclepro.2018.12.248>
- Sher Shah, M. S. A., Oh, C., Park, H., Hwang, Y. J., Ma, M., & Park, J. H. (2020). Catalytic Oxidation of Methane to Oxygenated Products: Recent Advancements and Prospects for Electrocatalytic and Photocatalytic Conversion at Low Temperatures. *Advanced Science*, 7(23), 1–24. <https://doi.org/10.1002/advs.202001946>
- Shi, F., Wang, F., Dai, H., Dai, J., Deng, J., Liu, Y., ... Au, C. T. (2012). Rod-, flower-, and dumbbell-like MnO₂: Highly active catalysts for the combustion of toluene. *Applied Catalysis A: General*, 433–434, 206–213. <https://doi.org/10.1016/j.apcata.2012.05.016>
- Shu, J., Li, B., Chen, M., Sun, D., Wei, L., Wang, Y., & Wang, J. (2020). An innovative method for manganese (Mn²⁺) and ammonia nitrogen (NH₄⁺-N) stabilization/solidification in electrolytic manganese residue by basic burning raw material. *Chemosphere*, 253, 126896. <https://doi.org/10.1016/j.chemosphere.2020.126896>

- Shu, J., Liu, R., Liu, Z., Chen, H., & Tao, C. (2016a). Enhanced extraction of manganese from electrolytic manganese residue by electrochemical. *Journal of Electroanalytical Chemistry*, 780, 32–37. <https://doi.org/10.1016/j.jelechem.2016.08.033>
- Shu, J., Liu, R., Liu, Z., Chen, H., & Tao, C. (2016b). Simultaneous removal of ammonia and manganese from electrolytic metal manganese residue leachate using phosphate salt. *Journal of Cleaner Production*, 135, 468–475. <https://doi.org/10.1016/j.jclepro.2016.06.141>
- Shu, J., Wu, H., Chen, M., Peng, H., Li, B., Liu, R., ... Hu, Z. (2019). Fractional removal of manganese and ammonia nitrogen from electrolytic metal manganese residue leachate using carbonate and struvite precipitation. *Water Research*, 153, 229–238. <https://doi.org/10.1016/j.watres.2018.12.044>
- Sie, S. T., & Krishna, R. (1998). Process development and scale up: II. Catalyst design strategy. *Reviews in Chemical Engineering*, 14(3), 159–202. <https://doi.org/10.1515/REVCE.1998.14.3.159>
- Sihaib, Z., Puleo, F., Garcia-Vargas, J. M., Retailleau, L., Descorme, C., Liotta, L. F., ... Giroir-Fendler, A. (2017). Manganese oxide-based catalysts for toluene oxidation. *Applied Catalysis B: Environmental*, 209, 689–700. <https://doi.org/10.1016/j.apcatb.2017.03.042>
- Sobianowska-Turek, A., Szczepaniak, W., Maciejewski, P., & Gawlik-Kobylińska, M. (2016). Recovery of zinc and manganese, and other metals (Fe, Cu, Ni, Co, Cd, Cr, Na, K) from Zn-MnO₂ and Zn-C waste batteries: Hydroxyl and carbonate co-precipitation from solution after reducing acidic leaching with use of oxalic acid. *Journal of Power Sources*, 325(79), 220–228. <https://doi.org/10.1016/j.jpowsour.2016.06.042>

- Sobianowska-Turek, Agnieszka. (2018). Hydrometallurgical recovery of metals: Ce, La, Co, Fe, Mn, Ni and Zn from the stream of used Ni-MH cells. *Waste Management*, 77, 213–219. <https://doi.org/10.1016/j.wasman.2018.03.046>
- Sobianowska-Turek, Agnieszka, Szczepaniak, W., & Zabłocka-Malicka, M. (2014). Electrochemical evaluation of manganese reducers - Recovery of Mn from Zn-Mn and Zn-C battery waste. *Journal of Power Sources*, 270, 668–674. <https://doi.org/10.1016/j.jpowsour.2014.07.136>
- Soltanieh, M., Zohrabian, A., Gholipour, M. J., & Kalnay, E. (2016). A review of global gas flaring and venting and impact on the environment: Case study of Iran. *International Journal of Greenhouse Gas Control*, 49, 488–509. <https://doi.org/10.1016/j.ijggc.2016.02.010>
- Sotudeh-Gharebagh, R., & Chaouki, J. (2008). The Heterogeneous and Homogeneous Combustion of Methane Over Inert Particles. *The Canadian Journal of Chemical Engineering*, 81(6), 1182–1191. <https://doi.org/10.1002/cjce.5450810607>
- Staub, D., Meille, S., Le Corre, V., Chevalier, J., & Rouleau, L. (2015). Revisiting the Side Crushing Test Using the Three-Point Bending Test for the Strength Measurement of Catalyst Supports. *Oil & Gas Science and Technology – Revue d'IFP Energies Nouvelles*, 70(3), 475–486. <https://doi.org/10.2516/ogst/2013214>
- Stegarescu, A., Lung, I., Leoștean, C., Kacso, I., Opriș, O., Lazăr, M. D., ... Soran, M. L. (2020). Green Synthesis, Characterization and Test of MnO₂ Nanoparticles as Catalyst in Biofuel Production from Grape Residue and Seeds Oil. *Waste and Biomass Valorization*, 11(9), 5003–5013. <https://doi.org/10.1007/s12649-019-00805-8>
- Stranick, M. A. (1999). Mn₂O₃ by XPS. *Surface Science Spectra*, 6(1), 39–46. <https://doi.org/10.1116/1.1247889>

- Sun, L., Zhao, P., Liu, Y., Tan, B., Yu, C., Feng, N., ... Guan, G. (2021). Enhancing the catalytic activity of MnO₂ via structural phase transition for propane combustion: Promotional role of ionic liquid. *Journal of Environmental Chemical Engineering*, 9(6), 106453. <https://doi.org/10.1016/j.jece.2021.106453>
- Sun, Z., Cao, H., Xiao, Y., Sietsma, J., Jin, W., Agterhuis, H., & Yang, Y. (2017). Toward Sustainability for Recovery of Critical Metals from Electronic Waste: The Hydrochemistry Processes. *ACS Sustainable Chemistry and Engineering*, 5(1), 21–40. <https://doi.org/10.1021/acssuschemeng.6b00841>
- Survey, U. S. G. (2020). Mineral commodity summaries 2020. In *U.S Department OF The Interior, U.S Geological Survey*. Retrieved from <https://pubs.usgs.gov/periodicals/mcs2020/mcs2020.pdf>
- Takeda, A. (2003). Manganese action in brain function. *Brain Research Reviews*, 41(1), 79–87. [https://doi.org/10.1016/S0165-0173\(02\)00234-5](https://doi.org/10.1016/S0165-0173(02)00234-5)
- Thüne, P. C., & Niemantsverdriet, J. W. (Hans. (2009). Surface science models of industrial catalysts. *Surface Science*, 603(10–12), 1756–1762. <https://doi.org/10.1016/j.susc.2008.10.061>
- Tian, Y., Shu, J., Chen, M., Wang, J., Wang, Y., Luo, Z., ... Sun, Z. (2019). Manganese and ammonia nitrogen recovery from electrolytic manganese residue by electric field enhanced leaching. *Journal of Cleaner Production*, 236. <https://doi.org/10.1016/j.jclepro.2019.117708>
- Todorova, S., Stefanov, P., Naydenov, A., & Kolev, H. (2014). Catalytic oxidation of methane over Pd-MeO_x (Me = Mn, Co, Ni, Ce) catalysts - influence of metal oxides. *Revue Roumaine de Chimie*, 59(3–4), 251–257.

- Tomašić, V., & Jović, F. (2006). State-of-the-art in the monolithic catalysts/reactors. *Applied Catalysis A: General*, 311(1–2), 112–121. <https://doi.org/10.1016/j.apcata.2006.06.013>
- Toro, N., Jeldres, R. I., Órdenes, J. A., Robles, P., & Navarra, A. (2020). Manganese nodules in Chile, an alternative for the production of Co and Mn in the future—A review. *Minerals*, 10(8), 1–19. <https://doi.org/10.3390/min10080674>
- U.S. Geological Survey. (2021). *Manganese Commodity Summary 2021*. (703). Retrieved from <https://www.usgs.gov/centers/national-minerals-information-center/manganese-statistics-and-information>
- US EPA, O. (2021). *Recycling Basics*. 1–8. Retrieved from <https://www.epa.gov/recycle/recycling-basics>
- Vaudano, Pierre; Plattner, Eric; Comninellis, C. (1995). The Industrial Electrolytic Regeneration of $Mn_2(SO_4)_3$ for the Oxidation of Substituted Toluene to the Corresponding Benzaldehyde. *Chimia*, 49(1–2), 12. <https://doi.org/10.2533/chimia.1995.12>
- Velasco-Rozo, E. A., Ballesteros-Rueda, L. M., & Baldovino-Medrano, V. G. (2021). A Method for the Accurate Quantification of Gas Streams by Online Mass Spectrometry. *Journal of the American Society for Mass Spectrometry*, 32(8), 2135–2143. <https://doi.org/10.1021/jasms.1c00090>
- Walton, J., Alexander, M. R., Fairley, N., Roach, P., & Shard, A. G. (2016). Film thickness measurement and contamination layer correction for quantitative XPS. *Surface and Interface Analysis*, 48(3), 164–172. <https://doi.org/10.1002/sia.5934>
- Wang, C., Rosenfeldt, E., Li, Y., & Hofmann, R. (2020). External standard calibration method to measure the hydroxyl radical scavenging capacity of water samples. *Environmental Science and Technology*, 54(3), 1929–1937. <https://doi.org/10.1021/acs.est.9b06273>

- Wang, G., Zhang, J., Liu, L., Zhou, J. Z., Liu, Q., Qian, G., ... Richards, R. M. (2018). Novel multi-metal containing MnCr catalyst made from manganese slag and chromium wastewater for effective selective catalytic reduction of nitric oxide at low temperature. *Journal of Cleaner Production*, 183, 917–924. <https://doi.org/10.1016/j.jclepro.2018.02.207>
- Wang, G., Zhang, J., Zhou, J., & Qian, G. (2019). Production of an effective catalyst with increased oxygen vacancies from manganese slag for selective catalytic reduction of nitric oxide. *Journal of Environmental Management*, 239(February), 90–95. <https://doi.org/10.1016/j.jenvman.2019.03.056>
- Wang, N., Fang, Z., Peng, S., Cheng, D., Du, B., & Zhou, C. (2016). Recovery of soluble manganese from electrolyte manganese residue using a combination of ammonia and CO₂. *Hydrometallurgy*, 164, 288–294. <https://doi.org/10.1016/j.hydromet.2016.06.019>
- Wang, Xiuyun, Liu, Y., Zhang, Y., Zhang, T., Chang, H., Zhang, Y., & Jiang, L. (2018). Structural requirements of manganese oxides for methane oxidation: XAS spectroscopy and transition-state studies. *Applied Catalysis B: Environmental*, 229, 52–62. <https://doi.org/10.1016/j.apcatb.2018.02.007>
- Wang, Xu, Qiu, H., Liu, H., Shi, P., Fan, J., Min, Y., & Xu, Q. (2018). Recycling application of waste Li-MnO₂ batteries as efficient catalysts based on electrochemical lithiation to improve catalytic activity. *Green Chemistry*, 20(21), 4901–4910. <https://doi.org/10.1039/c8gc02183j>
- Wang, Y., Liu, Y., Cao, Q., Wang, C. A., & Che, D. (2011). Homogeneous combustion of fuel ultra-lean methane-air mixtures: Experimental study and simplified reaction mechanism. *Energy and Fuels*, 25(8), 3437–3445. <https://doi.org/10.1021/ef200484c>

- Watson, J. T., & Sparkman, O. D. (2007). *Introduction to Mass Spectrometry* (Fourth Ed.).
<https://doi.org/10.1002/9780470516898>
- Wei, Y., Ni, L., Li, M., & Zhao, J. (2017). A template-free method for preparation of MnO₂ catalysts with high surface areas. *Catalysis Today*, 297, 188–192.
<https://doi.org/10.1016/j.cattod.2016.12.044>
- Whelpton, R. (2019). Quality assurance | internal standards. In *Encyclopedia of Analytical Science* (3rd ed.). <https://doi.org/10.1016/B978-0-12-409547-2.14399-9>
- Winiarska, K., Klimkiewicz, R., Tylus, W., Sobianowska-Turek, A., Winiarski, J., Szczygieł, B., & Szczygieł, I. (2019). Study of the catalytic activity and surface properties of manganese-zinc ferrite prepared from used batteries. *Journal of Chemistry*, 2019.
<https://doi.org/10.1155/2019/5430904>
- Wu, F. F., Li, X. P., Zhong, H., & Wang, S. (2016). Utilization of Electrolytic Manganese Residues in Production of Porous Ceramics. *International Journal of Applied Ceramic Technology*, 13(3), 511–521. <https://doi.org/10.1111/ijac.12502>
- Xin, B., Chen, B., Duan, N., & Zhou, C. (2011). Extraction of manganese from electrolytic manganese residue by bioleaching. *Bioresource Technology*, 102(2), 1683–1687.
<https://doi.org/10.1016/j.biortech.2010.09.107>
- Xin, B., Jiang, W., Aslam, H., Zhang, K., Liu, C., Wang, R., & Wang, Y. (2012). Bioleaching of zinc and manganese from spent Zn-Mn batteries and mechanism exploration. *Bioresource Technology*, 106, 147–153. <https://doi.org/10.1016/j.biortech.2011.12.013>
- Xin, B., Jiang, W., Li, X., Zhang, K., Liu, C., Wang, R., & Wang, Y. (2012). Analysis of reasons for decline of bioleaching efficiency of spent Zn-Mn batteries at high pulp densities and

- exploration measure for improving performance. *Bioresource Technology*, *112*, 186–192.
<https://doi.org/10.1016/j.biortech.2012.02.133>
- Xu, F., Jiang, L., Dan, Z., Gao, X., Duan, N., Han, G., & Zhu, H. (2014). Water balance analysis and wastewater recycling investigation in electrolytic manganese industry of China - A case study. *Hydrometallurgy*, *149*, 12–22. <https://doi.org/10.1016/j.hydromet.2014.05.002>
- Xu, H., Yan, N., Qu, Z., Liu, W., Mei, J., Huang, W., & Zhao, S. (2017). Gaseous Heterogeneous Catalytic Reactions over Mn-Based Oxides for Environmental Applications: A Critical Review. *Environmental Science and Technology*, *51*(16), 8879–8892.
<https://doi.org/10.1021/acs.est.6b06079>
- Yang, Renchun, Ren, C., Teng, X., Chen, Z., Wu, S., & Zhang, W. (2017). Study of the Surface Oxygen Vacancies Evolvement on the Single and Bi-Components Manganese Oxide Precursors and their Catalytic Performance. *Catalysis Letters*, *147*(3), 727–737.
<https://doi.org/10.1007/s10562-017-1973-0>
- Yang, Ruizhi, Wang, Z., Dai, L., & Chen, L. (2005). Synthesis and characterization of single-crystalline nanorods of α -MnO₂ and γ -MnOOH. *Materials Chemistry and Physics*, *93*(1), 149–153. <https://doi.org/10.1016/j.matchemphys.2005.03.006>
- Ying, A. Y., Lu, Z., & Abdou, M. A. (1998). Mechanical behavior and design database of packed beds for blanket designs. *Fusion Engineering and Design*, *39–40*, 759–764.
[https://doi.org/10.1016/S0920-3796\(97\)00157-9](https://doi.org/10.1016/S0920-3796(97)00157-9)
- Yuan, A., Wang, X., Wang, Y., & Hu, J. (2009). Textural and capacitive characteristics of MnO₂ nanocrystals derived from a novel solid-reaction route. *Electrochimica Acta*, *54*(3), 1021–1026. <https://doi.org/10.1016/j.electacta.2008.08.057>

- Zakeri, M., Samimi, A., Shafiee Afarani, M., & Salehirad, A. (2018). Effects of porosity and pore size distribution on mechanical strength reliability of industrial-scale catalyst during preparation and catalytic test steps. *Particulate Science and Technology*, *36*(1), 96–103. <https://doi.org/10.1080/02726351.2016.1220437>
- Zeng, F., Pan, Y., Yang, Y., Li, Q., Li, G., Hou, Z., & Gu, G. (2016). Facile construction of Mn₃O₄-MnO₂ hetero-nanorods/graphene nanocomposite for highly sensitive electrochemical detection of hydrogen peroxide. *Electrochimica Acta*, *196*, 587–596. <https://doi.org/10.1016/j.electacta.2016.03.031>
- Zhang, K., Peng, X., Cao, Y., Yang, H., Wang, X., Zhang, Y., ... Jiang, L. (2019a). Effect of MnO₂ morphology on its catalytic performance in lean methane combustion. *Materials Research Bulletin*, *111*, 338–341. <https://doi.org/10.1016/j.materresbull.2018.11.023>
- Zhang, K., Peng, X., Cao, Y., Yang, H., Wang, X., Zhang, Y., ... Jiang, L. (2019b). Effect of MnO₂ morphology on its catalytic performance in lean methane combustion. *Materials Research Bulletin*, *111*(January 2018), 338–341. <https://doi.org/10.1016/j.materresbull.2018.11.023>
- Zhang, L., Wang, S., Lv, L., Ding, Y., Tian, D., & Wang, S. (2021). Insights into the Reactive and Deactivation Mechanisms of Manganese Oxides for Ozone Elimination: The Roles of Surface Oxygen Species. *Langmuir*, *37*(4), 1410–1419. <https://doi.org/10.1021/acs.langmuir.0c02841>
- Zhang, W., & Cheng, C. Y. (2007a). Manganese metallurgy review. Part I: Leaching of ores/secondary materials and recovery of electrolytic/chemical manganese dioxide. *Hydrometallurgy*, *89*(3–4), 137–159. <https://doi.org/10.1016/j.hydromet.2007.08.010>

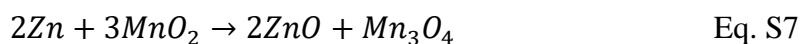
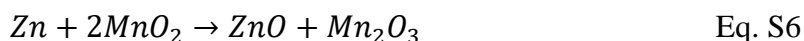
- Zhang, W., & Cheng, C. Y. (2007b). Manganese metallurgy review. Part II: Manganese separation and recovery from solution. *Hydrometallurgy*, 89(3–4), 160–177. <https://doi.org/10.1016/j.hydromet.2007.08.009>
- Zhang, W., & Cheng, C. Y. (2007c). Manganese metallurgy review. Part III: Manganese control in zinc and copper electrolytes. *Hydrometallurgy*, 89(3–4), 178–188. <https://doi.org/10.1016/j.hydromet.2007.08.011>
- Zhou, C., Wang, J., Liu, X., Chen, F., Di, Y., Gao, S., & Shi, Q. (2018). Magnetic and thermodynamic properties of α , β , γ and δ -MnO₂. *New Journal of Chemistry*, 42(11), 8400–8407. <https://doi.org/10.1039/c8nj00896e>
- Zhou, X., Luo, C., Wang, J., Wang, H., Chen, Z., Wang, S., & Chen, Z. (2021). Recycling application of modified waste electrolytic manganese anode slag as efficient catalyst for PMS activation. *Science of the Total Environment*, 762, 143120. <https://doi.org/10.1016/j.scitotenv.2020.143120>
- Zimmerman, J. B., Anastas, P. T., Erythropel, H. C., & Leitner, W. (2020). Designing for a green chemistry future. *Science*, 367(6476), 397–400. <https://doi.org/10.1126/science.aay3060>

Appendix C. Supplementary information chapter 2

1. Supplementary text

1.1 Availability of manganese species in the cathode of recycled waste batteries

The cathode powder of spent batteries has been characterized in several previous works (Ebin et al., 2016; Park, Song, et al., 2021; Agnieszka Sobianowska-Turek, Szczepaniak, & Zabłocka-Malicka, 2014), commonly composed by the phases $ZnMn_2O_4$, Mn_3O_4 , graphite, ZnO and Zn . Taking into account that batteries as in their original new state present as the cathode's component a mixture of MnO_2 and graphite (Almeida, Xará, Delgado, & Costa, 2006; Cabral, Pedrosa, Margarido, & Nogueira, 2013), it can be conclude that the other phases were formed after the usage of the batteries (eqs. S5 to S6) (Desai, Fernandes, & Dalal, 1985; Rącz & Ilea, 2013). As reported in the literature (Cabral et al., 2013; Desai et al., 1985), these reactions must carry out the migration of Zn ions from the anode to the cathode. Here, such migration was observed by analyzing the weight of cathode and anode as a function of voltage, as shown in Fig. S14A. It was possible to correlate the increase in the cathode weight and the decrease in anode weight with the drop of the battery voltage, which is directly related to the battery usage.



One of the findings of this work is the additional presence of MnO_2 , observed by the XRD pattern of the raw cathode powder recovered (Fig. S2). Such phase is associated with a fraction of the cathode that has not participated in the reactions shown above, turning in a partially spent battery. To analyze the usage level of the batteries collected in this work (up to 200 batteries), their voltage distribution was determined by boxplot analysis (Fig. S14B), finding that the median is around 1.36 V with a IQR (interquartile range) of 0.24 V. Since the maximum and minimum voltage of the alkaline batteries usable in electronic devices is expected to be around 1.7 and 1.1, respectively (Energizer Brands, 2018), it is clear that the median of the recycled batteries (1.36 V) showed only partial usage, which is consistent with the presence of MnO_2 .

The characteristic level of usage found for the recycled batteries population in this work was as expected for a public collection point. Depending on the electronic requirements of devices, it is common for batteries to be disposed of without being fully spent. However, the voltage distribution and composition reported in this work is relatively different from other spent batteries used in several investigations, in which the presence of MnO_2 is not reported. This fact implies that the battery samples used in these investigations might not be in the range of average usage for a waste battery, or at least indicates that the usable capacity varies with the geography. Since we show that the nature of the recovered cathode influences the nature of the synthesized value-added product, a future challenge for circular economy purposes is the easy normalization of the usage level of the discarded batteries.

1.2 Oxygen-associated properties analysis of MnO_x-based materials

The amount of adsorbed-surface and lattice oxygen, the reducibility, and the average oxidation state (AOS) of MnO_x have been correlated with the catalytic activity in oxidation reactions (Piumetti et al., 2015; Sher Shah et al., 2020; L. Sun et al., 2021; H. Xu et al., 2017; Yuan, Wang, Wang, & Hu, 2009). The concept behind these properties can be summarized as the oxygen that can be easily apported by the MnO_x, either from oxygen of the reaction feed that was adsorbed/dissociated in the surface or the lattice oxygen, to the reaction. Even there are different kinetic and surface phenomena that affect the catalytic process in transition metal oxides (G. Cheng et al., 2017; Xiuyun Wang et al., 2018), in this work, the analysis of those oxygen-associated properties can serve to determine the variations in oxidant capacity as a consequence of morphology and composition changes generated to the spent battery cathode by leaching treatments. In this sense, the materials developed were tested by O₂-TPD, H₂-TPR and XPS, and their results are presented in Fig. S10, S11 and S4, respectively. Two main O₂ desorption peaks were observed at 400-600 °C and 700-800 °C in O₂-TPD profiles (Fig. S10), which may be associated with oxygen migration from the surface lattice (O_{SL}) and bulk lattice (O_{BL}), respectively (Jampaiah et al., 2017). From desorption temperature, the materials can be arranged as follows: for O_{SL}, MnO₂-based nanorods < raw cathode ≈ NaOH-washed cathode < Mn₂O₃-based nanorods, and for O_{BL}, raw cathode < NaOH-washed cathode < Mn₂O₃-based nanorods ≈ MnO₂-based nanorods. As the desorption temperature is considered inverse to the oxygen mobility (L. Zhang et al., 2021), it can be inferred that the MnO₂-based nanorods and the raw cathode samples showed the highest mobility of O_{SL} and O_{BL}, respectively. Comparing the XRD (Fig. S2) and O₂-TPD results, it can be associated that the phases with the highest oxygen mobility are MnO₂ (92.4 % of

MnO₂-based nanorods) and ZnMn₂O₄ (67.4 % and 66.8 % of raw cathode and NaOH-washed nanorods, respectively). Three atypical behaviors were observed in the O₂-TPD profiles: first, the intermediate peak in the NaOH-washed cathode that can be associated with the presence of Mn₃O₄ (confirmed by XRD) formed during alkaline leaching; second, the band of O₂ desorption of MnO₂-based nanorods sample at 700-800 °C is plateau-shaped, which means greater resistance to bulk oxygen migration; finally, unlike the other materials, the fact that the O_{BL} desorption peak of Mn₂O₃-based nanorods sample is higher than O_{SL} desorption peak may be associated with a more reduced state on the surface (as Mn₂O₃) than in the bulk (as MnO₂).

On the other hand, two principal reduction bands were observed from the H₂-TPR profiles presented in Fig. S11. At each profile, it was expected to observe the bands corresponding to the reduction of Mn⁴⁺ to Mn³⁺ (lowest temperature band) and Mn³⁺ to Mn²⁺ (highest temperature band) (Y. Gao et al., 2020; Ji et al., 2019; Piumetti et al., 2015). For the raw cathode, NaOH-washed cathode and MnO₂-based nanorods, Mn⁴⁺ reduction was observed at 340 °C, but for Mn₂O₃-based nanorods was observed at 370 °C. In contrast, the second band was located at different temperatures, and the samples can be arranged according this Mn⁺³ temperature reduction: raw cathode > MnO₂-based nanorods > NaOH-washed cathode > Mn₂O₃-based nanorods. Likewise, an additional shoulder associated to chemisorbed oxygen was observed at 240 °C for MnO₂-based nanorods and at 260 °C for both raw cathode and NaOH-washed cathode, however, it was not observed for Mn₂O₃-based nanorods. The difference in the temperature associated to chemisorbed oxygen indicates differences in its adsorption energy and reactivity (Dey & Praveen Kumar, 2020). From XRD analysis (Fig. S2), it can be inferred that the reducibility result of the MnO₂-based nanorods sample is associated to MnO₂ phase, in fact, the H₂-TPR profile of this material is coherent with reported in literature for MnO₂. For the raw cathode, it is expected that its

reducibility is associated principally to ZnMn_2O_4 phase; because of a similar fraction of this phase in NaOH-washed cathode and raw cathode, their shift in the temperature of the reduction Mn^{3+} band can be associated with a content of around of 25 % of Mn_3O_4 phase. Finally, the differences in the reducibility profile of Mn_2O_3 -based nanorods respect to the other materials, can be attributed to the Mn_2O_3 phase content (81.4 % by XRD)

Complementary to O_2 -TPD and H_2 -TPR, the surface chemical composition of the materials was analyzed by XPS (Fig. S4). In general, the Mn 2p spectra (Fig. S4A) showed the characteristic two peaks for Mn 2p_{3/2} and Mn 2p_{1/2}, at averages Binding Energy (BE) of 641.67 eV and 654.07 eV, respectively. For these materials based on the cathode and its treatment, the average spin-orbit level energy spacing was 12.65 eV, which is ~1.1 eV higher than the values usually related to only Mn^{3+} based materials (Jahan, Tominaka, & Henzie, 2016; Menezes, Indra, Gutkin, & Driess, 2017; Stranick, 1999) indicating the presence of other Mn oxidation states, mainly Mn^{2+} and Mn^{4+} with different distributions. On the raw cathode and NaOH-washed cathode, the considerable signal of Zn 2p (see inserts on Fig. S4B) is consistent with the presence of ZnMn_2O_4 species (N. Guo, Wei, Deng, & Xu, 2015) and additional presence of ZnO species in these samples. For MnO_2 -based and Mn_2O_3 -based nanorods, the Zn 2p signal was negligible and some differences could be observed on the Mn 2p peaks. These results are consistent with other analysis that demonstrated around 98 % Zn remotion after the acid leaching (Table S2). The Mn 2p_{3/2} BE shifted to lower values of ~0.42 eV after the NaOH washing of the raw cathode (NaOH-washed cathode), 0.36 eV after acid treatment to raw cathode (MnO_2 -based nanorods) and 0.39 eV after the acid treatment to the NaOH-washed cathode (Mn_2O_3 -based nanorods). Those lower values indicated a change of MnO_x distribution towards higher Mn_2O_3 species (Han et al., 2006). Moreover, the observed narrowing of the Mn 2p_{3/2} peak could be associated with the increment of MnO_2 and also Mn_2O_3 species

(Biesinger et al., 2011) in the samples of MnO₂-based nanorods and Mn₂O₃-based nanorods, which agrees with the tendency observed by other techniques. The O 1s spectra (Fig. S4B) showed two peaks associated to surface lattice oxygen species (O_L) at ~530 eV and adsorbed oxygen species (O_{ads}) at ~531.8 eV (Renchun Yang et al., 2017). Additionally, a visible formation of a shoulder in MnO₂-based and Mn₂O₃-based nanorods was observed.

The quantification of the desorbed, reduced, and surface oxygen of the materials developed in this work and literature MnO_x references, determined by O₂-TPD, H₂-TPR, and XPS analysis, respectively, is presented in Table S3. It can be observed that MnO₂-based nanorods presented the highest consumption of H₂ because of the reduction of chemisorbed oxygen on the surface (O_{ads}) and of the Mn⁴⁺ species reduction (Mn⁴⁺ to Mn³⁺). Previously it was shown that this reduction occurred at the lowest temperatures (as shown in Fig. S11). The notable reducibility of MnO₂-based nanorods is aligned with the highest amount of oxygen that can be desorbed from surface lattice (O_{SL}) and bulk lattice (O_{BL}), which could be observed for all the MnO₂ phases referenced in the literature (Table S3). The value of average oxidation state (AOS, Table S3) of the materials was calculated by averaging the Mn^{α+} determined by the decomposition of Mn 2p spectra (Fig. S4A). The AOS determined for MnO₂-based nanorods correlates with the results of the oxygen-associated properties because high oxidation states are more susceptible to have more oxygen in its electrochemical micro-ambient. The relation of different types of oxygens determined in the different techniques tested and the synergistic process between them are yet unknown, but what is clear with Table S3 and Fig. S4, S10 and S11 results, is that the MnO₂-based nanorods presented the highest amount of oxygen in their structure, and a surface that can be activated with the lower thermodynamic requirement. Some results of MnO₂-based nanorods, as H₂ consumed, XPS O_{ads}/O_L ratio and the AOS, were compared with results from pure MnO₂ from literature data (Table

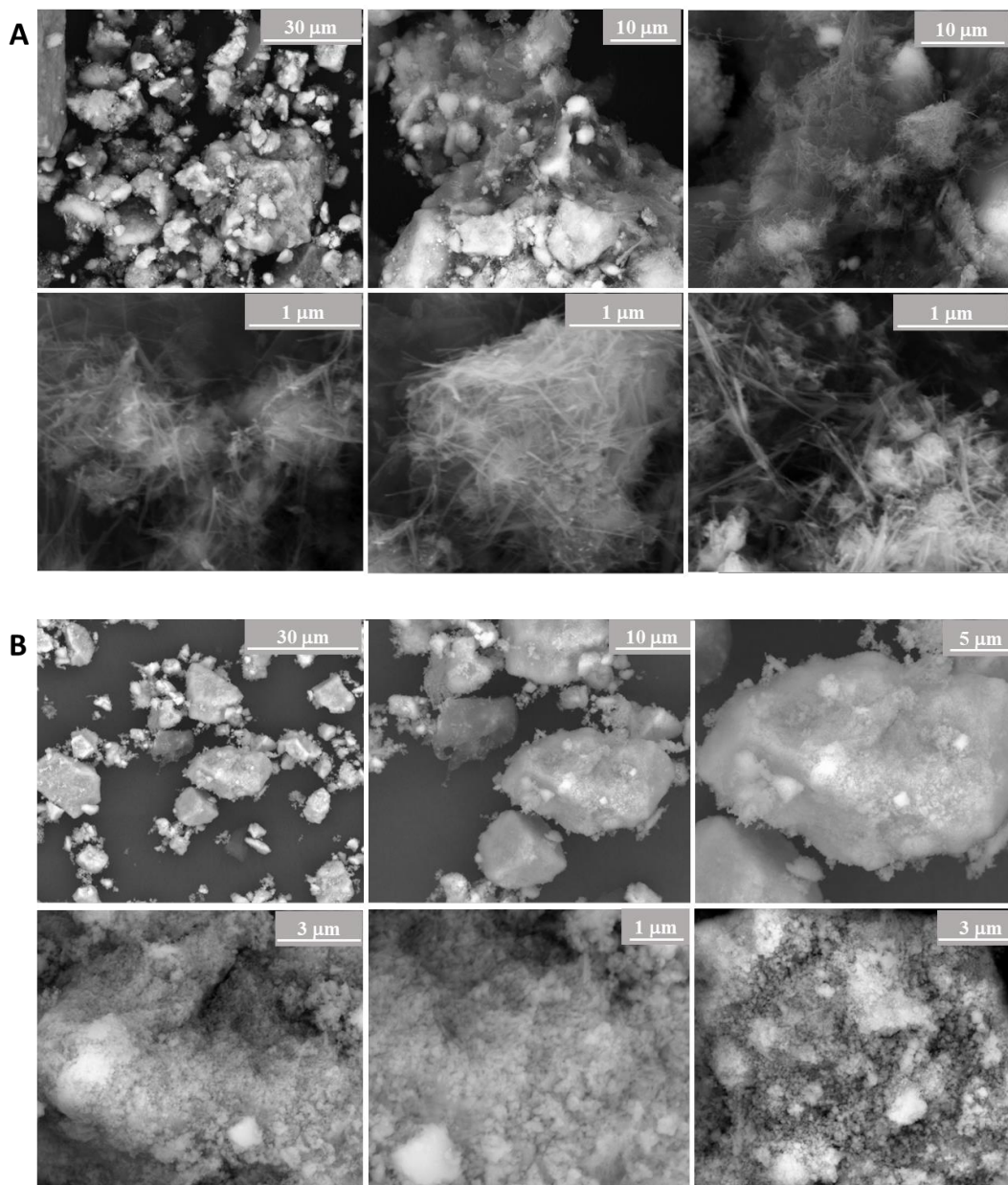
S3). Consistently, the value of H₂ consumed and XPS O_{ads}/O_L ratio fall in the average of reported by references, but here the AOS was lower for MnO₂-based nanorods than that reported in literature. This last result can be expected because the MnO₂-based nanorods was composed by 7.6 % of Mn₂O₃ (according XRD analysis) besides MnO₂.

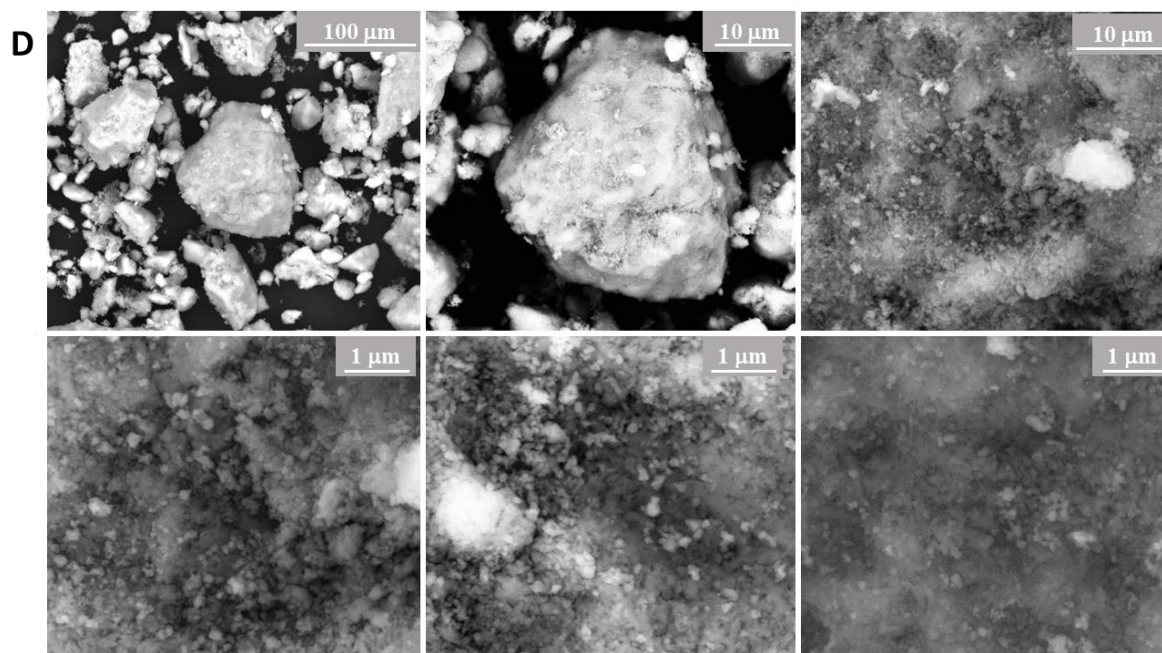
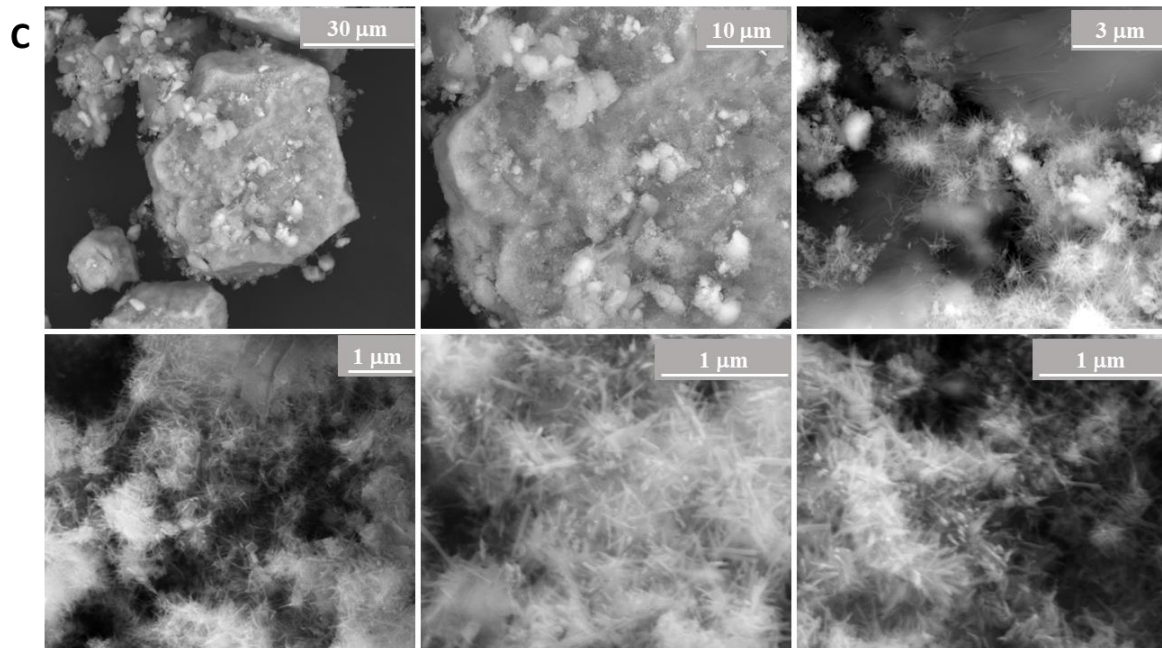
On the other hand, the raw cathode and the NaOH-washed cathode presented intermediate amounts of O₂ desorbed and ratio of (Mn⁴⁺→Mn³⁺)/(Mn³⁺→Mn²⁺) respect to that of MnO₂-based nanorods (which presented the higher amounts among the materials) and Mn₂O₃-based nanorods (which presented the lower amounts among the materials) reported in Table S3. As it was previously commented, these differences in oxygen-associated properties respect to the other materials are due to their composition rich in ZnMn₂O₄. As the oxygen amount, desorption and reduction temperatures are also intermediates, as it was presented in Fig. S10 and S11, respectively. In ZnMn₂O₄, the predominant Mn specie is Mn⁺³; with that in mind, the AOS determined for the raw cathode and the NaOH-washed cathode are congruent. The values from these samples were not compared with pure phases due to the lack of literature available for such results regarding ZnMn₂O₄. However, the results of oxygen-associated parameters were very close to Mn-oxides reported in literature as MnO_x, Mn₂O₃ and Mn₃O₄, included in Table S3. Comparatively, the Mn₂O₃-based nanorods had the lowest values of O₂ desorbed and (Mn⁴⁺→Mn³⁺)/(Mn³⁺→Mn²⁺) respect to the materials obtained from spent battery cathode. Due to the interesting coincidence between Mn₂O₃-based nanorods and Mn₂O₃ results from (L. Zhang et al., 2021), it is possible to inferred that this phase predominant in this type of nanorods (81.4 % from XRD quantification), has minor amount of oxygen-associated parameters that ZnMn₂O₄. In fact, the Mn₂O₃-based nanorods presented the lowest oxygen mobility, as shown in Fig. S10 and S11.

2. Supplementary figures

Figure S1.

SEM analysis of the MnO₂-based nanorods (A), raw cathode (B), Mn₂O₃-based nanorods (C), NaOH-washed cathode (D), and the benchmark (E).





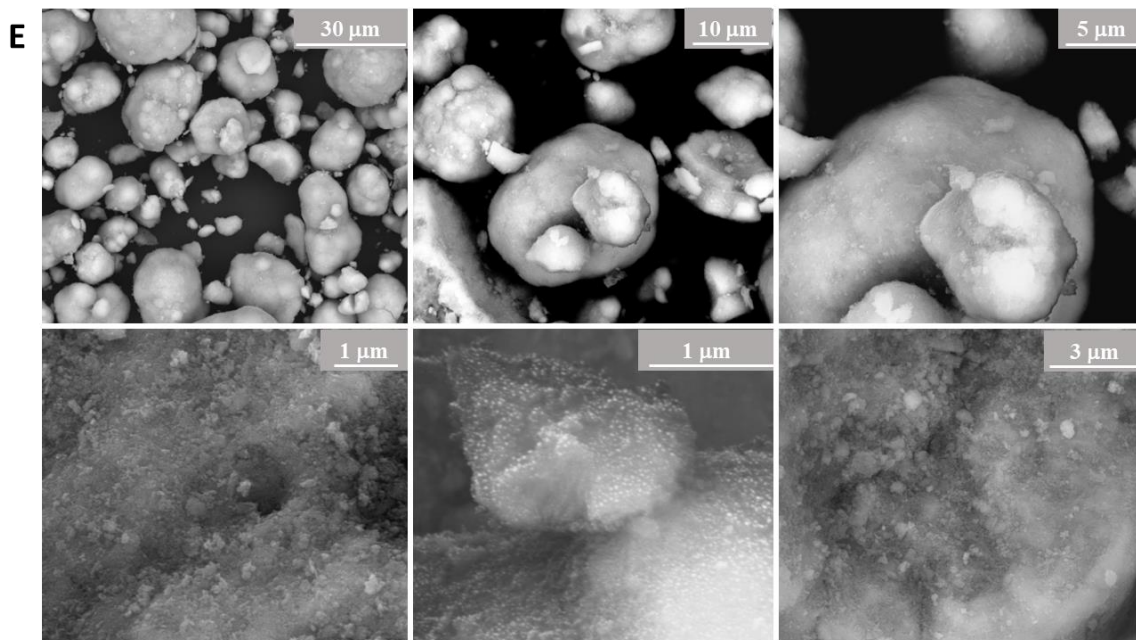


Figure S2.

X-ray diffraction patterns of raw cathode (A), NaOH-washed cathode (B), MnO₂-based nanorods (C), Mn₂O₃-based nanorods (D).

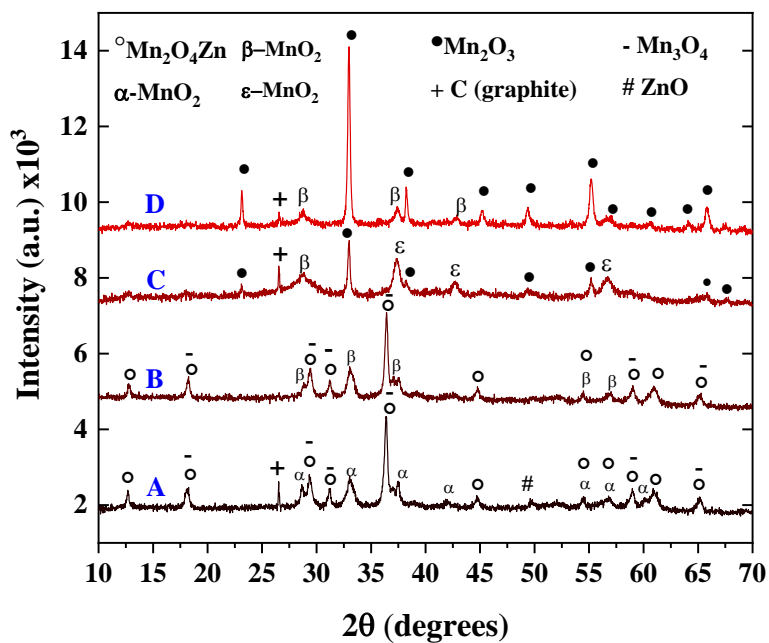


Fig. S3.

FTIR spectra of the raw cathode, NaOH-washed cathode, MnO₂-based nanorods (n-rods), and Mn₂O₃-based nanorods.

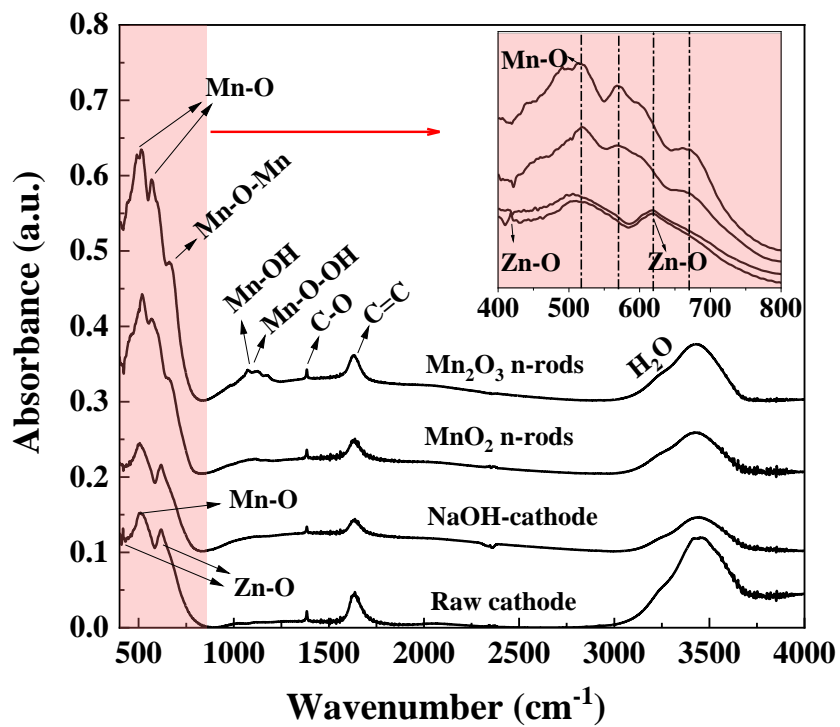


Figure S4.

XPS spectra of Mn 2p (A) and O 1s (B) for the raw cathode, NaOH-washed cathode, MnO₂-based nanorods, and Mn₂O₃-based nanorods.

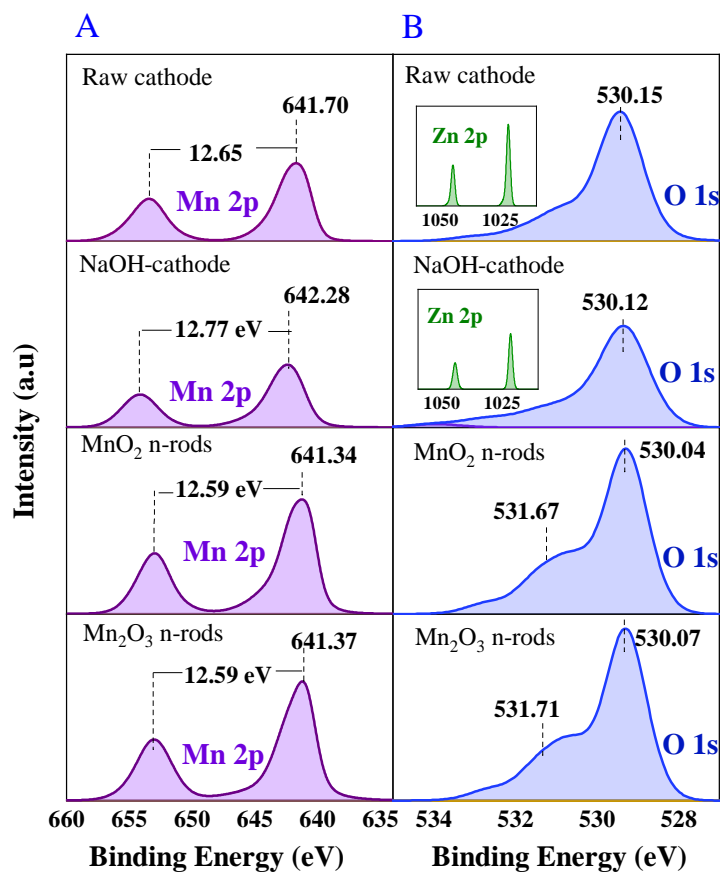


Figure S5.

N_2 adsorption-desorption isotherms and pore diameter distribution of the raw cathode (A), NaOH-washed cathode (B), MnO_2 -based nanorods (C), Mn_2O_3 -based nanorods (D).

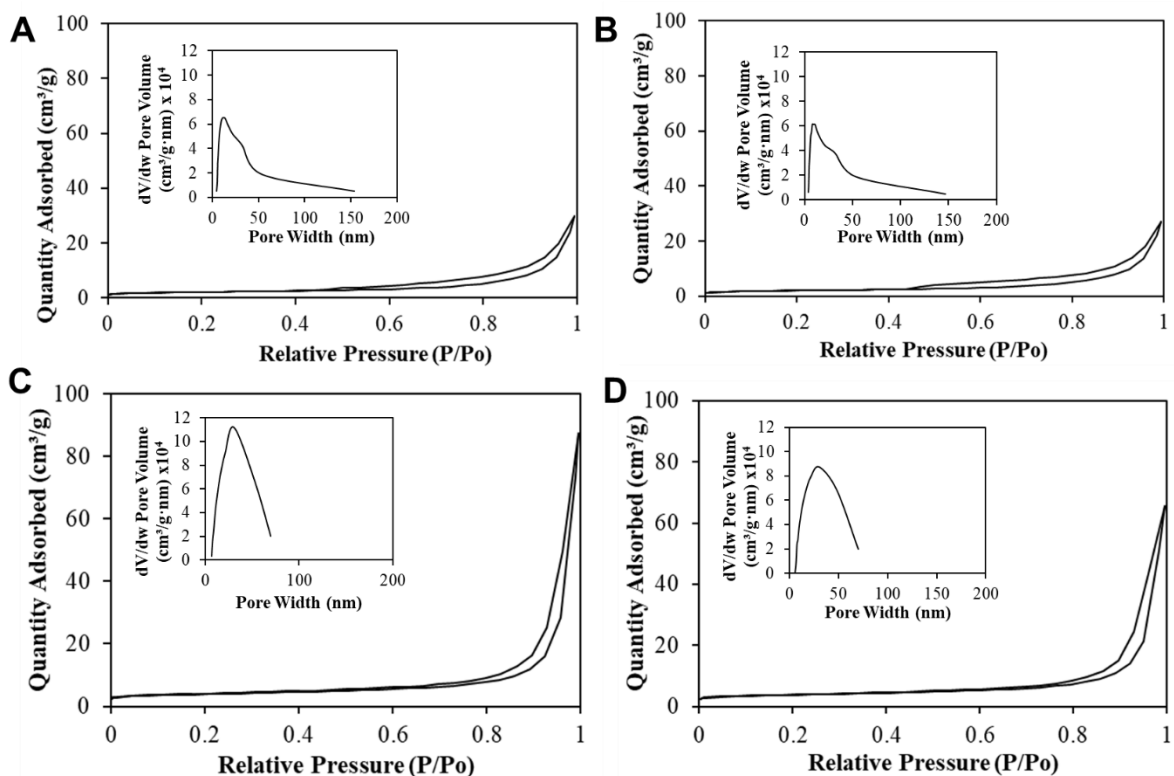


Figure S6.

UV-Vis spectroscopy analysis of the leach liquor extracted from NaOH washing of the cathode powder (A), the acid treatment of raw cathode (B), and the acid treatment of the NaOH-washed cathode (C). Right inserts correspond to images of the coloration of the leach liquor and their respective Zn and Mn concentration in mg/L.

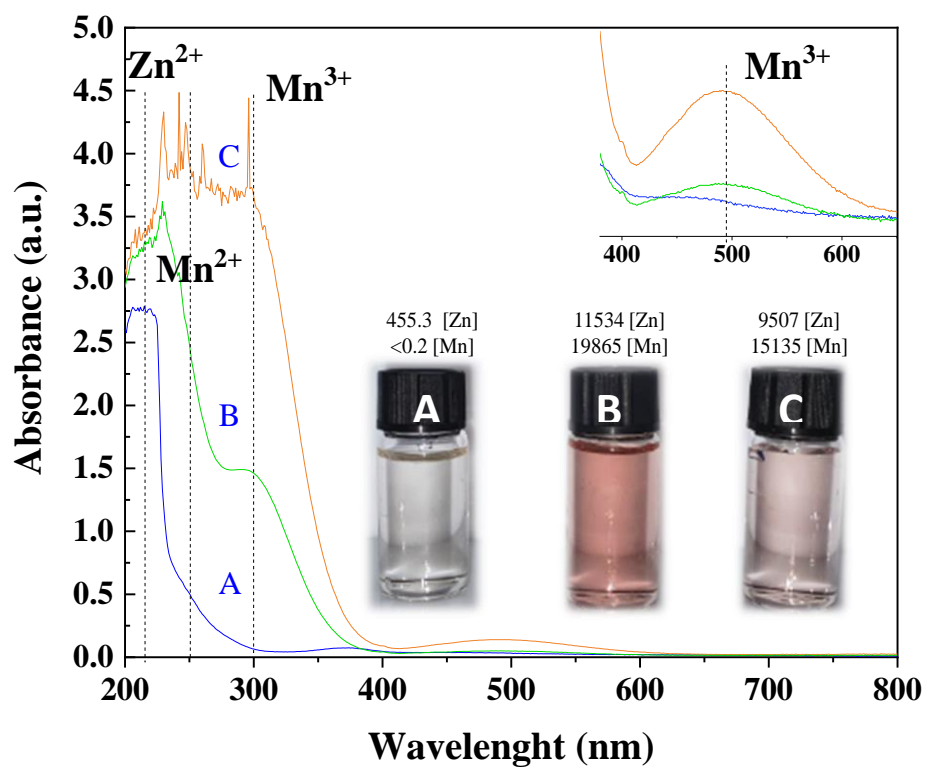


Figure S7.

Overlap of the pH and ζ -potential lectures from the acid treatment of raw cathode (A) and NaOH-washed cathode (B), with the Pourbaix diagram for Mn-H₂O system. The circles and the squares represent the points of analysis of ζ -potential and pH during each acid treatment of the materials.

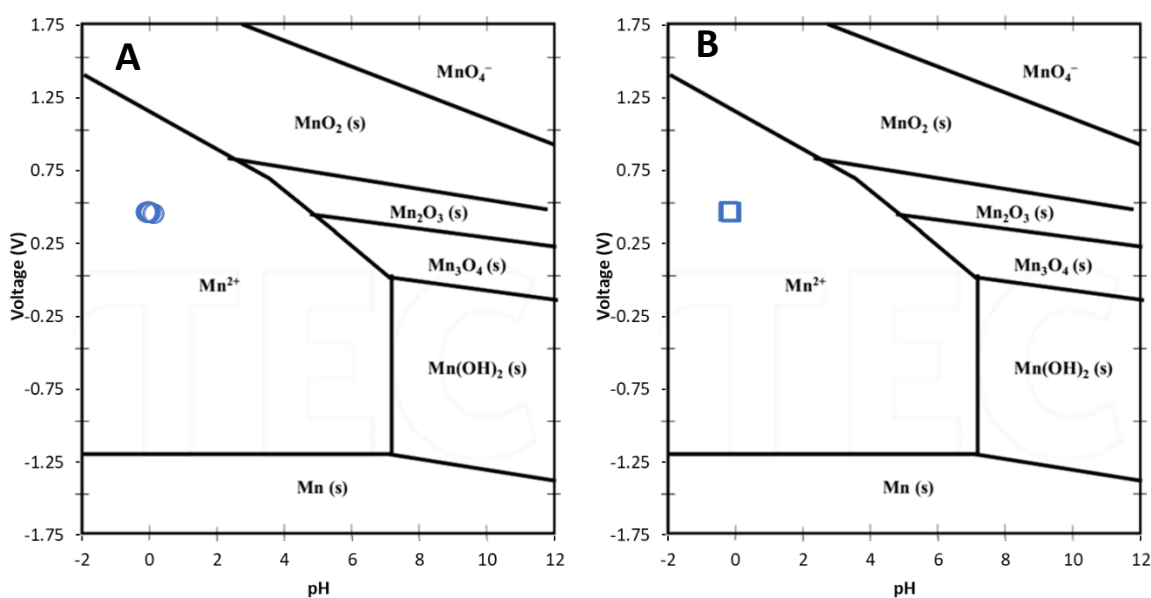


Figure S8.

Analysis of the conductivity (A), pH (B) and ζ -potential (C) lectures during the acid treatment of the raw cathode and NaOH-washed cathode.

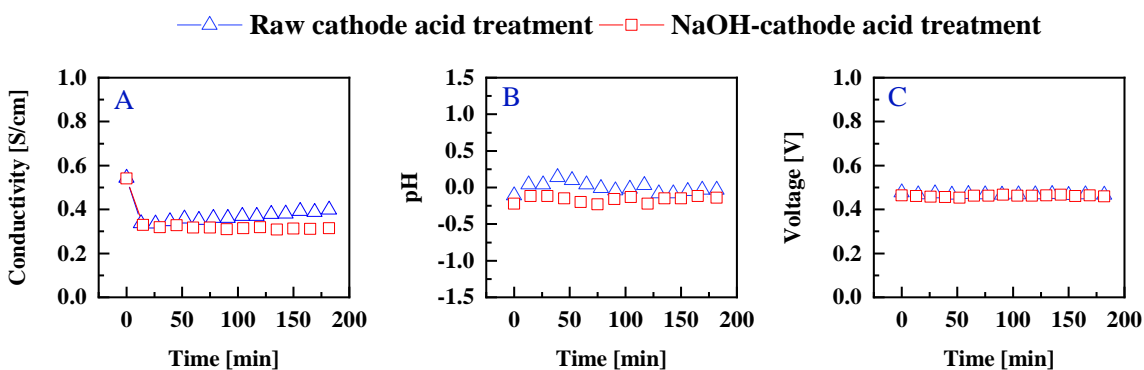


Figure S9.

Comparison between experimental specific reaction rate (R_{CH_4}), with its value theoretically determined as the sum of the individual contributions of the crystalline Mn phases composing the materials ($\sum R_{CH_4,i}$).

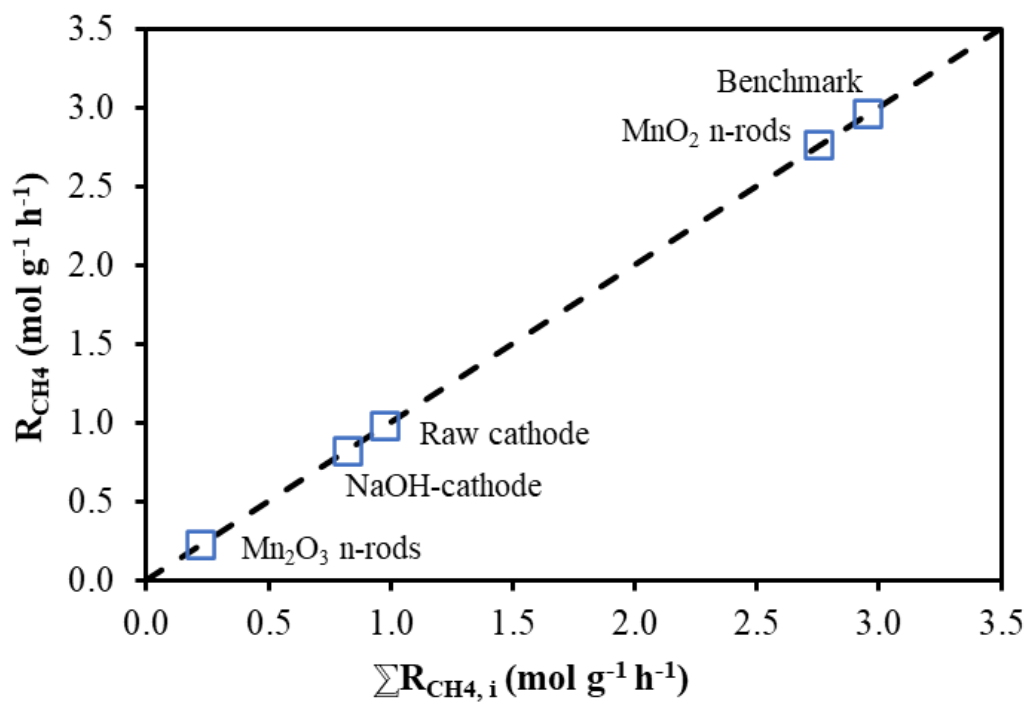


Figure S10.

*O*₂-TPD profiles of the raw cathode (A), NaOH-washed cathode (B), MnO₂-based nanorods (C), Mn₂O₃-based nanorods (D).

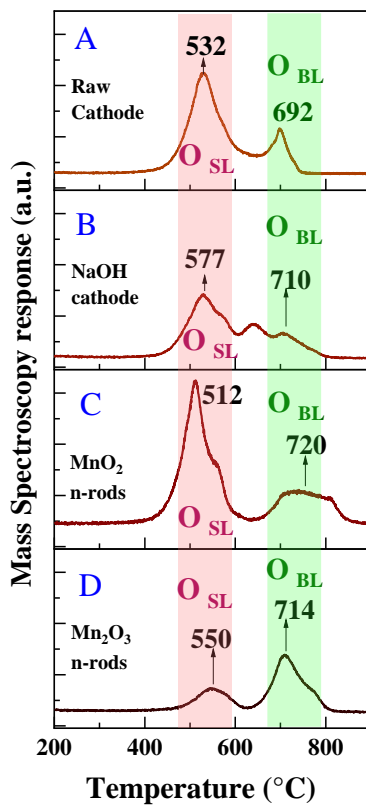


Figure S11.

H_2 -TPR profiles of the raw cathode (A), NaOH-washed cathode (B), MnO_2 -based nanorods (C), Mn_2O_3 -based nanorods (D).

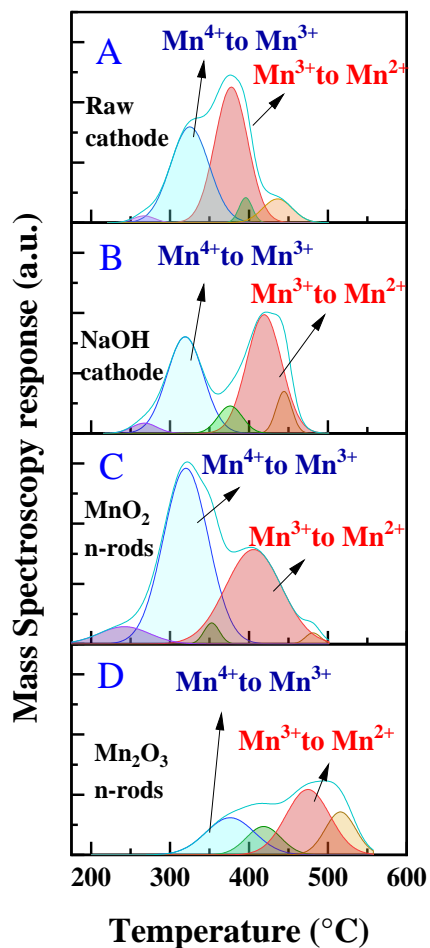


Figure S12.

Images of the manual dismantling of an AA spent alkaline battery, and the isolation of the cathode.



Figure S13.

General flowsheet of the nanorods synthesis from spent household alkaline Zn-Mn batteries.

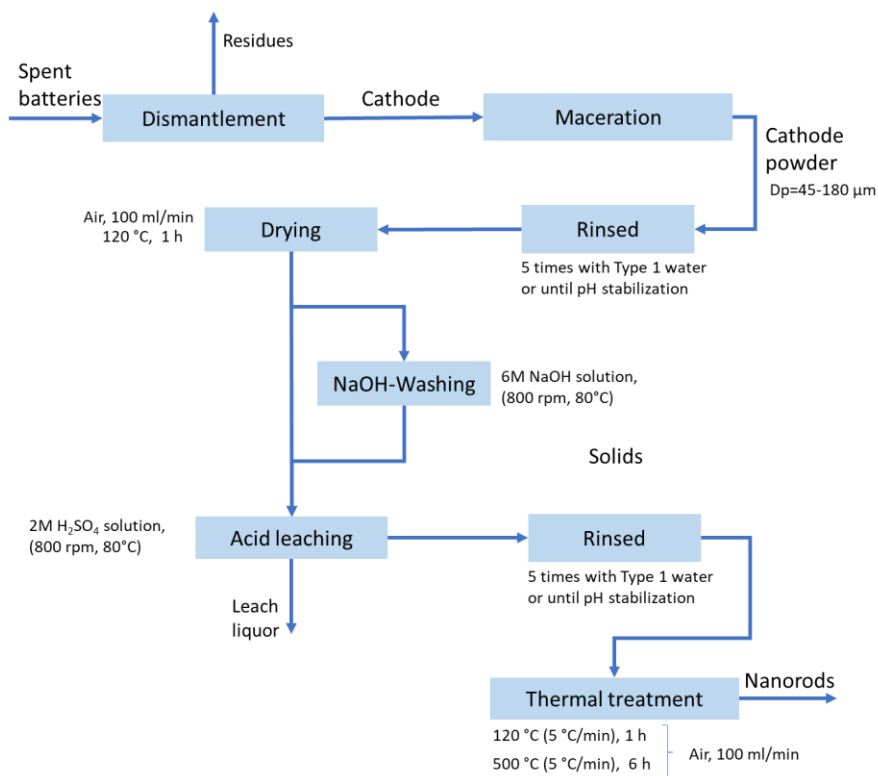


Figure S14.

Mass fraction of the cathode and anode recovered from the spent household batteries as a function of the residual voltage (A), and the distribution of residual voltage in the batteries dismantled (B).

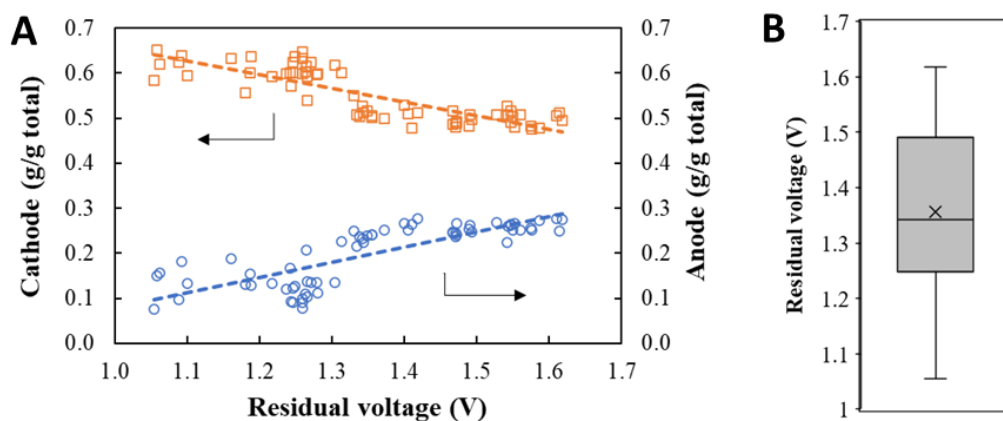
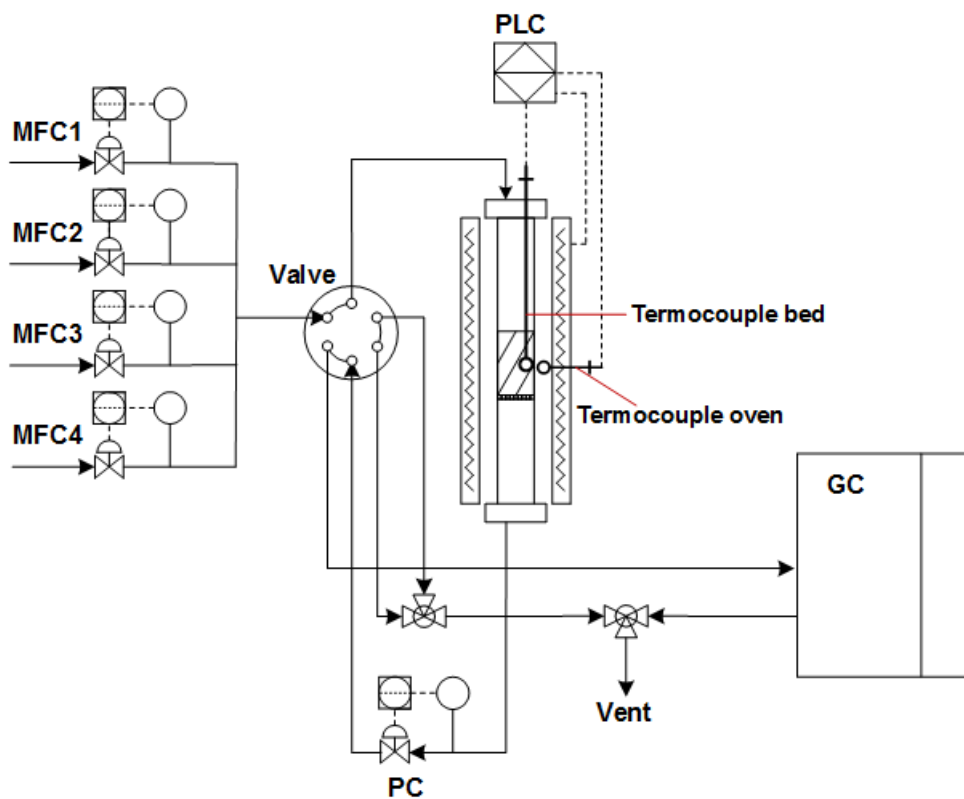


Figure S15.

Scheme of the reaction system, which couples the automated reactor on line with the gas chromatograph (GC).



3. Supplementary Tables

Table S1.

XRD phases percentage calculated by the Rietveld refinement results, with the analysis parameters.

Material	Solid from leaching						
	XRD phases (%)						
	ZnMn ₂ O ₄	α -MnO ₂	β -MnO ₂	ϵ -MnO ₂	Mn ₂ O ₃	Mn ₃ O ₄	ZnO
Raw cathode	69.9	16.8	-	-	10.5	2.4	0.4
Crystal system	tetragonal	tetragonal			cubic	orthothombic	hexagonal
Unit cell (Å)	a	5.7	9.8		9.4	3.0	3.4
	b	-	-		-	9.8	-
	c	9.2	2.8		-	9.6	5.2
χ^2 *	4.3						
NaOH-cathode	66.8	-	8.3	-	0.0	24.9	0.0
Crystal system	tetragonal		tetragonal			tetragonal	
Unit cell (Å)	a	5.7	4.4			5.8	
	b	-	-			-	
	c	9.2	2.9			9.4	
χ^2 *	2.4						
MnO₂ n-rods	0.0	-	13.7	78.7	7.6	0.0	0.0
Crystal system			tetragonal	hexagonal	cubic		
Unit cell (Å)	a		4.4	2.8	9.4		
	b		-	-	-		
	c		2.9	4.4	-		
χ^2 *	1.9						
Mn₂O₃ n-rods	0.0	-	18.6	-	81.4	0.0	0.0
Crystal system			tetragonal		cubic		
Unit cell (Å)	a		4.4		9.4		
	b		-		-		
	c		2.9		-		
χ^2 *	1.6						

*Rietveld FullProf refinement

Table S2.

Chemical analysis of solid (before and after) and liquor after the acid treatment of the cathode powder (either raw or NaOH-washed)

Material	Solid from leaching						Leach liquor				
	AAS metal content (wt. %)		SEM-EDS content (wt. %)				Graphite content (wt. %)	AAS metal content (µg/L)		UV-Vis (area) ^a	
	Mn	Zn	C	O	Mn	Zn		Mn	Zn	Zn ²⁺ +Mn ^{2,3+}	Mn ³⁺
Raw cathode	50.4	14.9	5.7	24.1	42.8	26.7	7.9	-	-	-	-
NaOH-cathode	51.9	11.5	3.0	25.1	68.5	1.0	4.5	0.0	0.5	86.5	0.0
MnO ₂ nanorods	58.3	0.2	4.9	25.5	68.1	0.9	5.9	19.9	11.5	537.5	24.0
Mn ₂ O ₃ nanorods	60.0	0.3	4.4	21.2	72.5	0.7	5.2	15.1	9.5	322.0	10.5

^aThe Zn²⁺+Mn^{2,3+} species were detected in spectra UV region, and Mn³⁺ species were detected at 494 nm in visible region.

Table S3.

Quantification of H₂ consumption during H₂-TPR test, O₂ desorbed by O₂-TPD and surface element molar ratio by XPS analysis.

Material	H ₂ consumption (mmol g ⁻¹) ^a				O ₂ desorbed (mmol g ⁻¹) ^b			Surface element molar ratio			Reference
	O _{ads} ^a	Mn ⁴⁺ → Mn ³⁺	Mn ³⁺ → Mn ²⁺	H ₂ total	O _{SL}	O _{BL}	O total	O _{ads} /O _L	Mn ⁴⁺ /Mn _#	AOS ^d	
Raw cathode	0.06	1.57	1.90	4.36	0.50	0.14	0.65	0.21	0.29	3.07	This work
NaOH-cathode	0.19	2.61	3.07	6.72	0.61	0.05	0.67	0.19	0.31	3.13	
MnO ₂ nanorod	0.62	5.64	3.78	11.53	0.80	0.23	1.02	0.28	0.37	3.19	
Mn ₂ O ₃ nanorod	0.00	2.13	3.37	6.13	0.09	0.22	0.31	0.29	0.23	2.99	
MnO _x	-	-	10.2	10.20	0.37	-	0.37	0.37	-	-	Li2021
MnO _x	-	-	-	6.70	-	-	-	0.26	-	-	Gao2020
MnO _x ^e	-	-	-	9.33	-	-	-	0.33	-	-	Wang2021
MnO ₂	-	-	-	14.01	-	-	-	0.28	-	-	Sun2021
MnO ₂ ^f	-	-	-	9.60	-	-	-	1.11	-	-	Li2019
MnO ₂ nanowire	-	-	-	7.34	-	-	-	0.25	-	3.74	Cheng2017
MnO ₂ nanorod	-	-	-	8.20	-	-	-	0.21	-	3.77	
MnO ₂	-	-	-	-	-	-	-	0.27	-	3.78*	Zhang2021
Mn ₂ O ₃	-	-	-	-	-	-	-	0.29	-	2.88	
Mn ₃ O ₄	-	-	-	-	-	-	-	0.26	-	2.48	
Mn ₃ O ₄	-	3.10	2.80	5.90	-	-	-	0.39	-	-	Ji2019

^aCalculated from H₂-TPR profiles. ^bCalculated from O₂-TPD profiles. ^cCalculated from XPS data. ^dAverage oxidation state. ^eAverage data from different MnO_x oxides. ^fAverage data from α, β, γ, and δ phases. Dashes in the table mean that the information was not reported.

Table S4.*Textural properties of materials synthesized.*

Material	Surface area (m²/g)	Pore width (nm)	Pore volume (m³/g)
Raw cathode	7.8	29.0	0.046
NaOH-washed cathode	7.5	27.9	0.042
MnO ₂ nanorods	13.9	38.6	0.112
Mn ₂ O ₃ nanorods	13.6	33.8	0.077

Table S5.*Mass balance of dismantling operation of spent household batteries.*

Component	Weight (g)	%
Cathode	13.37 ± 1.33	57.4
Outer shell + positive terminal	4.19 ± 0.45	18.0
Anode + ion Separator	4.45 ± 1.48	19.1
Negative terminal + collector + protective layer	1.27 ± 0.22	5.5
TOTAL	23.28 ± 0.44	100.0

4. References

- Abbasi, R., Wu, L., Wanke, S. E., & Hayes, R. E. (2012). Kinetics of methane combustion over Pt and Pt-Pd catalysts. *Chemical Engineering Research and Design*, 90(11), 1930–1942. <https://doi.org/10.1016/j.cherd.2012.03.003>
- Abid Charef, S., Affoune, A. M., Caballero, A., Cruz-Yusta, M., & Morales, J. (2017a). Simultaneous recovery of Zn and Mn from used batteries in acidic and alkaline mediums: A comparative study. *Waste Management*, 68, 518–526. <https://doi.org/10.1016/j.wasman.2017.06.048>
- Abid Charef, S., Affoune, A. M., Caballero, A., Cruz-Yusta, M., & Morales, J. (2017b). Simultaneous recovery of Zn and Mn from used batteries in acidic and alkaline mediums:

- A comparative study. *Waste Management*, 68, 518–526.
<https://doi.org/10.1016/j.wasman.2017.06.048>
- Akbari, E., Alavi, S. M., Rezaei, M., & Larimi, A. (2021). Catalytic Methane Combustion on the Hydrothermally Synthesized MnO₂Nanowire Catalysts. *Industrial and Engineering Chemistry Research*, 60(20), 7572–7587. <https://doi.org/10.1021/acs.iecr.1c00881>
- Akhtar, F., Andersson, L., Ogunwumi, S., Hedin, N., & Bergström, L. (2014). Structuring adsorbents and catalysts by processing of porous powders. *Journal of the European Ceramic Society*, 34(7), 1643–1666. <https://doi.org/10.1016/j.jeurceramsoc.2014.01.008>
- Almeida, M. F., Xará, S. M., Delgado, J., & Costa, C. A. (2006). Characterization of spent AA household alkaline batteries. *Waste Management*, 26(5), 466–476.
<https://doi.org/10.1016/j.wasman.2005.04.005>
- Analysis, G., Analysis, T., & Analysis, R. G. (n.d.). *Software for Hiden Mass Spectrometers*. Retrieved from <https://www.hidenanalytical.com/wp-content/uploads/2020/06/MASsoft-PC-Win-10-Software.pdf>
- Andak, B., Özduğan, E., Türdü, S., & Bulutcu, A. N. (2019). Recovery of zinc and manganese from spent zinc-carbon and alkaline battery mixtures via selective leaching and crystallization processes. *Journal of Environmental Chemical Engineering*, 7(5), 103372.
<https://doi.org/10.1016/j.jece.2019.103372>
- Andersson, R., Boutonnet, M., & Järås, S. (2012). On-line gas chromatographic analysis of higher alcohol synthesis products from syngas. *Journal of Chromatography A*, 1247, 134–145.
<https://doi.org/10.1016/j.chroma.2012.05.060>
- Anejionu, O. C. D., Whyatt, J. D., Blackburn, G. A., & Price, C. S. (2015). Contributions of gas flaring to a global air pollution hotspot: Spatial and temporal variations, impacts and

- alleviation. *Atmospheric Environment*, 118, 184–193.
<https://doi.org/10.1016/j.atmosenv.2015.08.006>
- Anthony, J. W., Bideaux, R. A., Bladh, K. W., & Nichols, M. C. (2006). Handbook of Mineralogy. In *Mineralogical Society of America* (Vol. 11). Retrieved from <http://www.handbookofmineralogy.org/>
- Arai, H., & Machida, M. (1991). Recent progress in high-temperature catalytic combustion. *Catalysis Today*, 10(1), 81–94. [https://doi.org/10.1016/0920-5861\(91\)80076-L](https://doi.org/10.1016/0920-5861(91)80076-L)
- Bach, S., Henry, M., Baffier, N., & Livage, J. (1990). Sol-gel synthesis of manganese oxides. *Journal of Solid State Chemistry*, 88(2), 325–333. [https://doi.org/10.1016/0022-4596\(90\)90228-P](https://doi.org/10.1016/0022-4596(90)90228-P)
- Baldovino-Medrano, V. G., Kartheuser, B., & Gaigneaux, E. M. (2019a). Production and testing of technical catalysts based on MnO₂ for the abatement of aromatic volatile compounds at the laboratory and pilot plant scales. *Catalysis Today*, 338(February), 81–92. <https://doi.org/10.1016/j.cattod.2019.03.029>
- Baldovino-Medrano, V. G., Kartheuser, B., & Gaigneaux, E. M. (2019b). Production and testing of technical catalysts based on MnO₂ for the abatement of aromatic volatile compounds at the laboratory and pilot plant scales. *Catalysis Today*, 338, 81–92. <https://doi.org/10.1016/j.cattod.2019.03.029>
- Barrett, E. P., Joyner, L. G., & Halenda, P. P. (1951). The Determination of Pore Volume and Area Distributions in Porous Substances. I. Computations from Nitrogen Isotherms. *Journal of the American Chemical Society*, 73(1), 373–380. <https://doi.org/10.1021/ja01145a126>
- Batey, J. H. (2014). The physics and technology of quadrupole mass spectrometers. *Vacuum*, 101(i), 410–415. <https://doi.org/10.1016/j.vacuum.2013.05.005>

- Baynham, A., Randall, D., & Hancy, C. (2017). Incinerators and Oxidizers. *EPA Air Pollution Control Cost Manual*, (November), 1–70. Retrieved from https://www.epa.gov/sites/production/files/2017-12/documents/oxidizersincinerators_chapter2_7theditionfinal.pdf
- Belardi, G., Lavecchia, R., Medici, F., & Piga, L. (2012). Thermal treatment for recovery of manganese and zinc from zinc-carbon and alkaline spent batteries. *Waste Management*, 32(10), 1945–1951. <https://doi.org/10.1016/j.wasman.2012.05.008>
- Belardi, G., Medici, F., & Piga, L. (2014). Influence of gaseous atmosphere during a thermal process for recovery of manganese and zinc from spent batteries. *Journal of Power Sources*, 248, 1290–1298. <https://doi.org/10.1016/j.jpowsour.2013.10.064>
- Bernardes, A. M., Espinosa, D. C. R., & Tenório, J. A. S. (2004). Recycling of batteries: A review of current processes and technologies. *Journal of Power Sources*, 130(1–2), 291–298. <https://doi.org/10.1016/j.jpowsour.2003.12.026>
- Biesinger, M. C., Payne, B. P., Grosvenor, A. P., Lau, L. W. M., Gerson, A. R., & Smart, R. S. C. (2011). Resolving surface chemical states in XPS analysis of first row transition metals, oxides and hydroxides: Cr, Mn, Fe, Co and Ni. *Applied Surface Science*, 257(7), 2717–2730. <https://doi.org/10.1016/j.apsusc.2010.10.051>
- Bischoff, C. F., Fitz, O. S., Burns, J., Bauer, M., Gentischer, H., Birke, K. P., ... Biro, D. (2020). Revealing the Local pH Value Changes of Acidic Aqueous Zinc Ion Batteries with a Manganese Dioxide Electrode during Cycling. *Journal of The Electrochemical Society*, 167(2), 020545. <https://doi.org/10.1149/1945-7111/ab6c57>

- Biswal, A., Mahakud, S., Bhuyan, S., Dash, B., Sarangi, C. K., Sanjay, K., ... Park, K. H. (2015). Recovery of Co metal and Electrolytic Manganese Dioxide (EMD) from Co-Mn sludge. *Hydrometallurgy*, 152, 159–168. <https://doi.org/10.1016/j.hydromet.2015.01.006>
- Blackburn, S., & Wilson, D. I. (2008). Shaping ceramics by plastic processing. *Journal of the European Ceramic Society*, 28(7), 1341–1351. <https://doi.org/10.1016/j.jeurceramsoc.2007.12.013>
- Blake, G. R. (2015). Particle density. *Methods of Soil Analysis, Part 1: Physical and Mineralogical Properties, Including Statistics of Measurement and Sampling*, 9(11121), 371–373. <https://doi.org/10.2134/agronmonogr9.1.c29>
- Blight, G. (2011). Mine Waste: A Brief Overview of Origins, Quantities, and Methods of Storage. *Waste*, 77–88. <https://doi.org/10.1016/B978-0-12-381475-3.10005-1>
- Buzatu, M., Săceanu, S., Ghica, V. G., Iacob, G., & Buzatu, T. (2013). Simultaneous recovery of Zn and MnO₂ from used batteries, as raw materials, by electrolysis. *Waste Management*, 33(8), 1764–1769. <https://doi.org/10.1016/j.wasman.2013.04.010>
- Buzatu, T., Popescu, G., Birloaga, I., & Săceanu, S. (2013). Study concerning the recovery of zinc and manganese from spent batteries by hydrometallurgical processes. *Waste Management*, 33(3), 699–705. <https://doi.org/10.1016/j.wasman.2012.10.005>
- Cabral, M., Pedrosa, F., Margarido, F., & Nogueira, C. A. (2013). End-of-life Zn-MnO₂ batteries: Electrode materials characterization. *Environmental Technology (United Kingdom)*, 34(10), 1283–1295. <https://doi.org/10.1080/09593330.2012.745621>
- Cai, X., Zhang, Y., Hu, H., Huang, Z., Yin, Y., Liang, X., ... Liang, J. (2020). Valorization of manganese residue to prepare a highly stable and active Fe₃O₄@SiO₂/starch-derived

- carbon composite for catalytic degradation of dye waste water. *Journal of Cleaner Production*, 258, 120741. <https://doi.org/10.1016/j.jclepro.2020.120741>
- Canda, L., Heput, T., & Ardelean, E. (2016). Methods for recovering precious metals from industrial waste. *IOP Conference Series: Materials Science and Engineering*, 106(1). <https://doi.org/10.1088/1757-899X/106/1/012020>
- Cano, R., Mackey, K., & McGlacken, G. P. (2018). Recent advances in manganese-catalysed C-H activation: Scope and mechanism. *Catalysis Science and Technology*, 8(5), 1251–1266. <https://doi.org/10.1039/c7cy02514a>
- Carrero, C. A., Schloegl, R., Wachs, I. E., & Schomaecker, R. (2014). Critical Literature Review of the Kinetics for the Oxidative Dehydrogenation of Propane over Well-Defined Supported Vanadium Oxide Catalysts. *ACS Catalysis*, 4(10), 3357–3380. <https://doi.org/10.1021/cs5003417>
- Castellanos-Beltran, I. J., Assima, G. P., & Lavoie, J. M. (2018). Effect of temperature in the conversion of methanol to olefins (MTO) using an extruded SAPO-34 catalyst. *Frontiers of Chemical Science and Engineering*, 12(2), 226–238. <https://doi.org/10.1007/s11705-018-1709-8>
- Chai, W. S., Cheun, J. Y., Kumar, P. S., Mubashir, M., Majeed, Z., Banat, F., ... Show, P. L. (2021). A review on conventional and novel materials towards heavy metal adsorption in wastewater treatment application. *Journal of Cleaner Production*, 296, 126589. <https://doi.org/10.1016/j.jclepro.2021.126589>
- Chen, B. R., Sun, W., Kitchaev, D. A., Mangum, J. S., Thampy, V., Garten, L. M., ... Schelhas, L. T. (2018). Understanding crystallization pathways leading to manganese oxide

- polymorph formation. *Nature Communications*, 9(1). <https://doi.org/10.1038/s41467-018-04917-y>
- Chen, H., Liu, R., Shu, J., & Li, W. (2015). Simultaneous stripping recovery of ammonia-nitrogen and precipitation of manganese from electrolytic manganese residue by air under calcium oxide assist. *Journal of Environmental Science and Health - Part A Toxic/Hazardous Substances and Environmental Engineering*, 50(12), 1282–1290. <https://doi.org/10.1080/10934529.2015.1055157>
- Chen, J., Arandiyana, H., Gao, X., & Li, J. (2015). Recent Advances in Catalysts for Methane Combustion. *Catalysis Surveys from Asia*, 19(3), 140–171. <https://doi.org/10.1007/s10563-015-9191-5>
- Cheng, G., Yu, L., He, B., Sun, M., Zhang, B., Ye, W., & Lan, B. (2017). Catalytic combustion of dimethyl ether over α -MnO₂ nanostructures with different morphologies. *Applied Surface Science*, 409, 223–231. <https://doi.org/10.1016/j.apsusc.2017.02.218>
- Cheng, Z., Mozammel, T., Patel, J., Lee, W. J., Huang, S., Lim, S., ... Li, C. (2018). A method for the quantitative analysis of gaseous mixtures by online mass spectrometry. *International Journal of Mass Spectrometry*, 434, 23–28. <https://doi.org/10.1016/j.ijms.2018.09.002>
- Christensen, K. A. (2007). Chapter 11 Design of industrial catalysts. In *Computer Aided Chemical Engineering* (Vol. 23). [https://doi.org/10.1016/S1570-7946\(07\)80014-9](https://doi.org/10.1016/S1570-7946(07)80014-9)
- Cook, K. D., Bennett, K. H., & Haddix, M. L. (1999). On-line mass spectrometry: A faster route to process monitoring and control. *Industrial and Engineering Chemistry Research*, 38(4), 1192–1204. <https://doi.org/10.1021/ie9707984>

- Das, A. P., Ghosh, S., Mohanty, S., & Sukla, L. B. (2014a). Consequences of manganese compounds: a review. *Toxicological and Environmental Chemistry*, 96(7), 981–997. <https://doi.org/10.1080/02772248.2015.1005428>
- Das, A. P., Ghosh, S., Mohanty, S., & Sukla, L. B. (2014b). Consequences of manganese compounds: a review. *Toxicological and Environmental Chemistry*, 96(7), 981–997. <https://doi.org/10.1080/02772248.2015.1005428>
- Das, A. P., Sukla, L. B., Pradhan, N., & Nayak, S. (2011). Manganese biomining: A review. *Bioresource Technology*, 102(16), 7381–7387. <https://doi.org/10.1016/j.biortech.2011.05.018>
- Dash, S. S., & Parida, K. M. (2007). Esterification of acetic acid with n-butanol over manganese nodule leached residue. *Journal of Molecular Catalysis A: Chemical*, 266(1–2), 88–92. <https://doi.org/10.1016/j.molcata.2006.10.031>
- Dautzenberg, F. M. (1989). *Ten Guidelines for Catalyst Testing*. 99–119. <https://doi.org/10.1021/bk-1989-0411.ch011>
- de Oliveira Demarco, J., Stefanello Cadore, J., da Silveira de Oliveira, F., Hiromitsu Tanabe, E., & Assumpção Bertuol, D. (2019). Recovery of metals from spent lithium-ion batteries using organic acids. *Hydrometallurgy*, 190(December 2018), 105169. <https://doi.org/10.1016/j.hydromet.2019.105169>
- Desai, B. D., Fernandes, J. B., & Dalal, V. N. K. (1985). Manganese dioxide - a review of a battery chemical Part II. Solid state and electrochemical properties of manganese dioxides. *Journal of Power Sources*, 16(1), 1–43. [https://doi.org/10.1016/0378-7753\(85\)80001-X](https://doi.org/10.1016/0378-7753(85)80001-X)

- Dey, S., & Praveen Kumar, V. V. (2020). The performance of highly active manganese oxide catalysts for ambient conditions carbon monoxide oxidation. *Current Research in Green and Sustainable Chemistry*, 3(May), 100012. <https://doi.org/10.1016/j.crgsc.2020.100012>
- Du, B., Zhou, C. bo, & Duan, N. (2014). Recycling of electrolytic manganese solid waste in autoclaved bricks preparation in China. *Journal of Material Cycles and Waste Management*, 16(2), 258–269. <https://doi.org/10.1007/s10163-013-0181-2>
- Du, B., Zhou, C., Li, X., Guo, T., & Wang, Z. (2015). A kinetic study of Mn(II) precipitation of leached aqueous solution from electrolytic manganese residues. *Toxicological and Environmental Chemistry*, 97(3–4), 349–357. <https://doi.org/10.1080/02772248.2015.1050188>
- Duan, N., Fan, W., Changbo, Z., Chunlei, Z., & Hongbing, Y. (2010). Analysis of pollution materials generated from electrolytic manganese industries in China. *Resources, Conservation and Recycling*, 54(8), 506–511. <https://doi.org/10.1016/j.resconrec.2009.10.007>
- Duan, N., Zhou, C., Chen, B., Jiang, W., & Xin, B. (2011). Bioleaching of Mn from manganese residues by the mixed culture of Acidithiobacillus and mechanism. *Journal of Chemical Technology and Biotechnology*, 86(6), 832–837. <https://doi.org/10.1002/jctb.2596>
- Dunlop, J. R., & Tully, F. P. (1993). A kinetic study of OH radical reactions with methane and perdeuterated methane. *Journal of Physical Chemistry*, 97(43), 11148–11150. <https://doi.org/10.1021/j100145a003>
- Dwivedi, D., Randhawa, N. S., Saroj, S., & Jana, R. K. (2017). An Overview of Manganese Recovery by Hydro and Pyro-Metallurgical Routes. *Journal of The Institution of Engineers (India): Series D*, 98(1), 147–154. <https://doi.org/10.1007/s40033-016-0119-7>

- Ebin, B., Petranikova, M., Steenari, B. M., & Ekberg, C. (2016). Production of zinc and manganese oxide particles by pyrolysis of alkaline and Zn-C battery waste. *Waste Management*, *51*, 157–167. <https://doi.org/10.1016/j.wasman.2015.10.029>
- Ebin, B., Petranikova, M., Steenari, B. M., & Ekberg, C. (2019). Recovery of industrial valuable metals from household battery waste. *Waste Management and Research*, *37*(2), 168–175. <https://doi.org/10.1177/0734242X18815966>
- Ellefson, R. E., Cain, D., & Lindsay, C. N. (1987). Calibration of mass spectrometers for quantitative gas mixture analysis. *Journal of Vacuum Science & Technology A: Vacuum, Surfaces, and Films*, *5*(1), 134–139. <https://doi.org/10.1116/1.574126>
- Elvidge, C. D., Bazilian, M. D., Zhizhin, M., Ghosh, T., Baugh, K., & Hsu, F. C. (2018). The potential role of natural gas flaring in meeting greenhouse gas mitigation targets. *Energy Strategy Reviews*, *20*, 156–162. <https://doi.org/10.1016/j.esr.2017.12.012>
- Energizer Brands, L. (2018). *Alkaline Manganese Dioxide Handbook and Application Manual*. 1–15.
- Falco, L., Quina, M. J., Gando-Ferreira, L. M., Thomas, H., & Curutchet, G. (2014). Solvent Extraction Studies for Separation of Zn(II) and Mn(II) from Spent Batteries Leach Solutions. *Separation Science and Technology (Philadelphia)*, *49*(3), 398–409. <https://doi.org/10.1080/01496395.2013.850510>
- Farzana, R., Rajarao, R., Hassan, K., Behera, P. R., & Sahajwalla, V. (2018). Thermal nanosizing: Novel route to synthesize manganese oxide and zinc oxide nanoparticles simultaneously from spent Zn–C battery. *Journal of Cleaner Production*, *196*, 478–488. <https://doi.org/10.1016/j.jclepro.2018.06.055>

- Farzana, R., Sayeed, M. A., Joseph, J., Ostrikov, K., O'Mullane, A. P., & Sahajwalla, V. (2020). Manganese Oxide Derived from a Spent Zn–C Battery as a Catalyst for the Oxygen Evolution Reaction. *ChemElectroChem*, 7(9), 2073–2080. <https://doi.org/10.1002/celec.202000422>
- Fawole, O. G., Cai, X. M., & Mackenzie, A. R. (2016). Gas flaring and resultant air pollution: A review focusing on black carbon. *Environmental Pollution*, 216, 182–197. <https://doi.org/10.1016/j.envpol.2016.05.075>
- Ferella, F., De Michelis, I., Beolchini, F., Innocenzi, V., & Vegliò, F. (2010). Extraction of zinc and manganese from alkaline and zinc-carbon spent batteries by citric-sulphuric acid solution. *International Journal of Chemical Engineering*, 2010. <https://doi.org/10.1155/2010/659434>
- Ferella, F., De Michelis, I., & Vegliò, F. (2008). Process for the recycling of alkaline and zinc-carbon spent batteries. *Journal of Power Sources*, 183(2), 805–811. <https://doi.org/10.1016/j.jpowsour.2008.05.043>
- Ferreira, B. S., Van Keulen, F., & Da Fonseca, M. M. R. (1998). Novel calibration method for mass spectrometers for on-line gas analysis. Set-up for the monitoring of a bacterial fermentation. *Bioprocess Engineering*, 19(4), 289–296. <https://doi.org/10.1007/s004490050522>
- Fu, J., He, Z., Wang, H., Liang, W., & Guo, C. (2010). Preparation of chemical manganese dioxide from manganese sulfate. *Mining Science and Technology*, 20(6), 877–881. [https://doi.org/10.1016/S1674-5264\(09\)60299-4](https://doi.org/10.1016/S1674-5264(09)60299-4)
- Gallegos, M. V., Falco, L. R., Peluso, M. A., Sambeth, J. E., & Thomas, H. J. (2013). Recovery of manganese oxides from spent alkaline and zinc-carbon batteries. An application as

- catalysts for VOCs elimination. *Waste Management*, 33(6), 1483–1490.
<https://doi.org/10.1016/j.wasman.2013.03.006>
- Gallegos, M. V., Peluso, M. A., Finocchio, E., Thomas, H. J., Busca, G., & Sambeth, J. E. (2017). Removal of VOCs by catalytic process. A study of MnZnO composites synthesized from waste alkaline and Zn/C batteries. *Chemical Engineering Journal*, 313, 1099–1111.
<https://doi.org/10.1016/j.cej.2016.11.001>
- Gancarczyk, A., Iwaniszyn, M., Piątek, M., Korpyś, M., Sinderka, K., Jodłowski, P. J., ... Kołodziej, A. (2018). Catalytic Combustion of Low-Concentration Methane on Structured Catalyst Supports. *Industrial & Engineering Chemistry Research*, 57(31), 10281–10291.
<https://doi.org/10.1021/acs.iecr.8b01987>
- Gangwar, D., & Rath, C. (2021). *Structural , optical and magnetic properties of α - and β -MnO 2 nanorods*. 557(April).
- Gao, J., Wang, Y., Ping, Y., Hu, D., Xu, G., Gu, F., & Su, F. (2012). A thermodynamic analysis of methanation reactions of carbon oxides for the production of synthetic natural gas. *RSC Advances*, 2(6), 2358. <https://doi.org/10.1039/c2ra00632d>
- Gao, Y., Wang, Z., Cui, C., Wang, B., Liu, W., Liu, W., & Wang, L. (2020). Amorphous manganese oxide as highly active catalyst for soot oxidation. *Environmental Science and Pollution Research*, 27(12), 13488–13500. <https://doi.org/10.1007/s11356-020-07909-y>
- Ghosh, S., & Das, A. P. (2017). Biobleaching of manganese from mining waste residues using *Acinetobacter* sp. *Geology, Ecology, and Landscapes*, 1(2), 77–83.
<https://doi.org/10.1080/24749508.2017.1332847>

- Ghosh, S., Mohanty, S., Akcil, A., Sukla, L. B., & Das, A. P. (2016). A greener approach for resource recycling: Manganese bioleaching. *Chemosphere*, *154*, 628–639. <https://doi.org/10.1016/j.chemosphere.2016.04.028>
- Gregorová, E., Pabst, W., Smith, D. S., & Zivcová, Z. (2009). *Thermal conductivity of porous alumina ceramics prepared using starch as a pore-forming agent*. *29*, 347–353. <https://doi.org/10.1016/j.jeurceramsoc.2008.06.018>
- Gunarathne, V., Rajapaksha, A. U., Vithanage, M., Alessi, D. S., Selvasembian, R., Naushad, M., ... Ok, Y. S. (2020). Hydrometallurgical processes for heavy metals recovery from industrial sludges. *Critical Reviews in Environmental Science and Technology*, *0(0)*, 1–41. <https://doi.org/10.1080/10643389.2020.1847949>
- Guo, M., Li, K., Liu, L., Zhang, H., Guo, W., Hu, X., ... Sun, T. (2019). Manganese-based multi-oxide derived from spent ternary lithium-ions batteries as high-efficient catalyst for VOCs oxidation. *Journal of Hazardous Materials*, *380*, 120905. <https://doi.org/10.1016/j.jhazmat.2019.120905>
- Guo, M., Li, K., Liu, L., Zhang, H., Hu, X., Min, X., ... Sun, T. (2019). Resource utilization of spent ternary lithium-ions batteries: Synthesis of highly active manganese-based perovskite catalyst for toluene oxidation. *Journal of the Taiwan Institute of Chemical Engineers*, *102*, 268–275. <https://doi.org/10.1016/j.jtice.2019.06.012>
- Guo, M., Li, K., Zhang, H., Min, X., Liang, J., Hu, X., ... Sun, T. (2020). Promotional removal of oxygenated VOC over manganese-based multi oxides from spent lithium-ions manganate batteries: Modification with Fe, Bi and Ce dopants. *Science of the Total Environment*, *740*, 139951. <https://doi.org/10.1016/j.scitotenv.2020.139951>

- Guo, M., Liu, L., Gu, J. nan, Zhang, H., Min, X., Liang, J., ... Sun, T. (2021). Catalytic performance improvement of volatile organic compounds oxidation over MnO_x and GdMnO₃ composite oxides from spent lithium-ion batteries: Effect of acid treatment. *Chinese Journal of Chemical Engineering*. <https://doi.org/10.1016/j.cjche.2020.08.015>
- Guo, N., Wei, X. Q., Deng, X. L., & Xu, X. J. (2015). Synthesis and property of spinel porous ZnMn₂O₄ microspheres. *Applied Surface Science*, 356, 1127–1134. <https://doi.org/10.1016/j.apsusc.2015.08.185>
- Haber, J. (1991). Manual on catalyst characterization (Recommendations 1991). *Pure and Applied Chemistry*, 63(9), 1227–1246. <https://doi.org/10.1351/pac199163091227>
- Hagelstein, K. (2009). Globally sustainable manganese metal production and use. *Journal of Environmental Management*, 90(12), 3736–3740. <https://doi.org/10.1016/j.jenvman.2008.05.025>
- Hammond, J. P. (2018). Quality Assurance: Spectroscopic Standards. In *Reference Module in Chemistry, Molecular Sciences and Chemical Engineering* (pp. 426–432). <https://doi.org/10.1016/B978-0-12-409547-2.00455-8>
- Han, Y. F., Chen, F., Zhong, Z., Ramesh, K., Chen, L., & Widjaja, E. (2006). Controlled synthesis, characterization, and catalytic properties of Mn₂O₃ and Mn₃O₄ nanoparticles supported on mesoporous silica SBA-15. *Journal of Physical Chemistry B*, 110(48), 24450–24456. <https://doi.org/10.1021/jp064941v>
- Hanf, L., Henschel, J., Diehl, M., Winter, M., & Nowak, S. (2020). Mn²⁺ or Mn³⁺? Investigating transition metal dissolution of manganese species in lithium ion battery electrolytes by capillary electrophoresis. *Electrophoresis*, 41(9), 697–704. <https://doi.org/10.1002/elps.201900443>

- He, C., Cheng, J., Zhang, X., Douthwaite, M., Pattisson, S., & Hao, Z. (2019). Recent Advances in the Catalytic Oxidation of Volatile Organic Compounds: A Review Based on Pollutant Sorts and Sources [Review-article]. *Chemical Reviews*, 119(7), 4471–4568. <https://doi.org/10.1021/acs.chemrev.8b00408>
- He, L., Fan, Y., Bellettre, J., Yue, J., & Luo, L. (2020). A review on catalytic methane combustion at low temperatures: Catalysts, mechanisms, reaction conditions and reactor designs. *Renewable and Sustainable Energy Reviews*, 119(November 2019). <https://doi.org/10.1016/j.rser.2019.109589>
- He, L., Fan, Y., Luo, L., Bellettre, J., & Yue, J. (2020). Preparation of Pt/γ-Al₂O₃ catalyst coating in microreactors for catalytic methane combustion. *Chemical Engineering Journal*, 380(August 2019). <https://doi.org/10.1016/j.cej.2019.122424>
- He, S., Jiang, D., Hong, M., & Liu, Z. (2021). Hazard-free treatment and resource utilisation of electrolytic manganese residue: A review. *Journal of Cleaner Production*, 306. <https://doi.org/10.1016/j.jclepro.2021.127224>
- He, S., Wilson, B. P., Lundström, M., & Liu, Z. (2021). Hazard-free treatment of electrolytic manganese residue and recovery of manganese using low temperature roasting-water washing process. *Journal of Hazardous Materials*, 402(July 2020). <https://doi.org/10.1016/j.jhazmat.2020.123561>
- Hedden, M., Francis, N., Haraldsen, J. T., Ahmed, T., & Constantin, C. (2015). Thermoelectric properties of nano-meso-micro β-MnO₂ powders as a function of electrical resistance. *Nanoscale Research Letters*, 10(1). <https://doi.org/10.1186/s11671-015-1000-6>

- Heinzle, E., Moes, J., Griot, M., Kramer, H., Dunn, I. J., & Bourne, J. R. (1984). On-line mass spectrometry in fermentation. *Analytica Chimica Acta*, 163(C), 219–229. [https://doi.org/10.1016/S0003-2670\(00\)81510-X](https://doi.org/10.1016/S0003-2670(00)81510-X)
- Heinzle, E., Oeggerli, A., & Dettwiler, B. (1990). On-line fermentation gas analysis: Error analysis and application of mass spectrometry. *Analytica Chimica Acta*, 238(C), 101–115. [https://doi.org/10.1016/S0003-2670\(00\)80528-0](https://doi.org/10.1016/S0003-2670(00)80528-0)
- Helmus, R., ter Laak, T. L., van Wezel, A. P., de Voogt, P., & Schymanski, E. L. (2021). patRoom: open source software platform for environmental mass spectrometry based non-target screening. *Journal of Cheminformatics*, 13(1), 1–25. <https://doi.org/10.1186/s13321-020-00477-w>
- Herndon, E. M., & Brantley, S. L. (2011). Movement of manganese contamination through the Critical Zone. *Applied Geochemistry*, 26(SUPPL.), S40–S43. <https://doi.org/10.1016/j.apgeochem.2011.03.024>
- Hoffmann, E. De, & Stroobant, V. (2007). Mass Spectrometry Principles and Applications Third Edition. In *Mass spectrometry reviews* (Vol. 29). Retrieved from <https://www.wiley.com/en-us/Mass+Spectrometry%3A+Principles+and+Applications%2C+3rd+Edition-p-9780470033111>
- Hohrenk, L. L., Itzel, F., Baetz, N., Tuerk, J., Vosough, M., & Schmidt, T. C. (2020). Comparison of Software Tools for Liquid Chromatography-High-Resolution Mass Spectrometry Data Processing in Nontarget Screening of Environmental Samples. *Analytical Chemistry*, 92(2), 1898–1907. <https://doi.org/10.1021/acs.analchem.9b04095>

- Holmes, N., Akien, G. R., Savage, R. J. D., Stanetty, C., Baxendale, I. R., Blacker, A. J., ... Bourne, R. A. (2016). Online quantitative mass spectrometry for the rapid adaptive optimisation of automated flow reactors. *Reaction Chemistry and Engineering*, *1*(1), 96–100. <https://doi.org/10.1039/c5re00083a>
- Hoseini, S., Rahemi, N., Allahyari, S., & Tasbihi, M. (2019). Application of plasma technology in the removal of volatile organic compounds (BTX) using manganese oxide nano-catalysts synthesized from spent batteries. *Journal of Cleaner Production*, *232*, 1134–1147. <https://doi.org/10.1016/j.jclepro.2019.05.227>
- Hoseini, S., Rahemi, N., Allahyari, S., Tasbihi, M., & Gharehabani, E. (2020). Effect of hydrometallurgical process parameters on the Mn₂O₃ nano catalysts derived from spent batteries used in the plasma catalytic oxidation of BTX. *Advanced Powder Technology*, *31*(10), 4187–4196. <https://doi.org/10.1016/j.apt.2020.08.026>
- Ippolito, N. M., Belardi, G., Medici, F., & Piga, L. (2016). Utilization of automotive shredder residues in a thermal process for recovery of manganese and zinc from zinc-carbon and alkaline spent batteries. *Waste Management*, *51*, 182–189. <https://doi.org/10.1016/j.wasman.2015.12.033>
- Işıldar, A., Rene, E. R., van Hullebusch, E. D., & Lens, P. N. L. (2018). Electronic waste as a secondary source of critical metals: Management and recovery technologies. *Resources, Conservation and Recycling*, *135*(December 2016), 296–312. <https://doi.org/10.1016/j.resconrec.2017.07.031>
- Ismail, O. S., & Umukoro, G. E. (2016). Modelling combustion reactions for gas flaring and its resulting emissions. *Journal of King Saud University - Engineering Sciences*, *28*(2), 130–140. <https://doi.org/10.1016/j.jksues.2014.02.003>

- Jahan, M., Tominaka, S., & Henzie, J. (2016). Phase pure α -Mn₂O₃ prisms and their bifunctional electrocatalytic activity in oxygen evolution and reduction reactions. *Dalton Transactions*, 45(46), 18494–18501. <https://doi.org/10.1039/c6dt03158g>
- Jampaiah, D., Velisoju, V. K., Venkataswamy, P., Coyle, V. E., Nafady, A., Reddy, B. M., & Bhargava, S. K. (2017). Nanowire Morphology of Mono- and Bidoped α -MnO₂ Catalysts for Remarkable Enhancement in Soot Oxidation. *ACS Applied Materials and Interfaces*, 9(38), 32652–32666. <https://doi.org/10.1021/acsami.7b07656>
- Jaya, H., Firdaus Omar, M., Md Akil, H., Arifin Ahmad, Z., & Noriman Zulkepli, N. (2016). Sawdust polyethylene composites. *BioResources*, 11(3), 6489–6504. Retrieved from https://bioresources.cnr.ncsu.edu/wp-content/uploads/2016/07/BioRes_11_3_6489_Jaya_OAAZ_Effect_Particle_Size_Mecha_Prop_Sawdust_HDPE_Comp_9342.pdf
- Jee, J. E., Pestovsky, O., & Bakac, A. (2010). Preparation and characterization of manganese(IV) in aqueous acetic acid. *Dalton Transactions*, 39(48), 11636–11642. <https://doi.org/10.1039/c0dt00476f>
- Ji, F., Men, Y., Wang, J., Sun, Y., Wang, Z., Zhao, B., ... Xu, G. (2019). Promoting diesel soot combustion efficiency by tailoring the shapes and crystal facets of nanoscale Mn₃O₄. *Applied Catalysis B: Environmental*, 242(October 2018), 227–237. <https://doi.org/10.1016/j.apcatb.2018.09.092>
- Kaiser, R. I., Jansen, P., Petersen, K., & Roessler, K. (1995). On line and in situ quantification of gas mixtures by matrix interval algebra assisted quadrupole mass spectrometry. *Review of Scientific Instruments*, 66(11), 5226–5231. <https://doi.org/10.1063/1.1146089>

- Kim, B. S., Lee, J. C., Jeong, S. B., Lee, H. I., & Kim, C. W. (2010). Kinetics of the volatilization removal of zinc from manganese dust. *Materials Transactions*, *51*(7), 1313–1318. <https://doi.org/10.2320/matertrans.M2010108>
- Kim, S. C., & Shim, W. G. (2010). Catalytic combustion of VOCs over a series of manganese oxide catalysts. *Applied Catalysis B: Environmental*, *98*(3–4), 180–185. <https://doi.org/10.1016/j.apcatb.2010.05.027>
- Kloprogge, J. T., Ponce, C. P., & Loomis, T. A. (2020). The Periodic Table: Nature's Building Blocks. In *The Periodic Table: Nature's Building Blocks*. <https://doi.org/10.1016/C2019-0-03114-7>
- Klusacek, K., & Schneider, P. (1981). Effect of size and shape of catalyst on pellet pore structure and effectiveness. *Chemical Engineering Science*, *36*, 523–527.
- Koivula, R., Pakarinen, J., Sivenius, M., Sirola, K., Harjula, R., & Paatero, E. (2009). Use of hydrometallurgical wastewater as a precursor for the synthesis of cryptomelane-type manganese dioxide ion exchange material. *Separation and Purification Technology*, *70*(1), 53–57. <https://doi.org/10.1016/j.seppur.2009.08.014>
- Kononov, R., Ostrovski, O., & Ganguly, S. (2008). Carbothermal reduction of manganese oxide in different gas atmospheres. *Metallurgical and Materials Transactions B: Process Metallurgy and Materials Processing Science*, *39*(5), 662–668. <https://doi.org/10.1007/s11663-008-9191-1>
- Kreutzer, M. T., Kapteijn, F., & Moulijn, J. A. (2006). Shouldn't catalysts shape up? Structured reactors in general and gas-liquid monolith reactors in particular. *Catalysis Today*, *111*(1–2), 111–118. <https://doi.org/10.1016/j.cattod.2005.10.014>

- Kularatne, R. K. A., Kasturiarachchi, J. C., Manatunge, J. M. A., & Wijeyekoon, S. L. J. (2009). Mechanisms of Manganese Removal from Wastewaters in Constructed Wetlands Comprising Water Hyacinth (*Eichhornia crassipes* (Mart.) Solms) Grown under Different Nutrient Conditions . *Water Environment Research*, *81*(2), 165–172. <https://doi.org/10.2175/106143008x370403>
- Kumar, S., García-Triñanes, P., Teixeira-Pinto, A., & Bao, M. (2013). Development of alkali activated cement from mechanically activated silico-manganese (SiMn) slag. *Cement and Concrete Composites*, *40*, 7–13. <https://doi.org/10.1016/j.cemconcomp.2013.03.026>
- Lahousse, C., Bernier, A., Grange, P., Delmon, B., Papaefthimiou, P., Ioannides, T., & Verykios, X. (1998). Evaluation of γ -MnO₂ as a VOC removal catalyst: Comparison with a noble metal catalyst. *Journal of Catalysis*, *178*(1), 214–225. <https://doi.org/10.1006/jcat.1998.2148>
- Lamaita, L., Peluso, M. A., Sambeth, J. E., & Thomas, H. J. (2005). Synthesis and characterization of manganese oxides employed in VOCs abatement. *Applied Catalysis B: Environmental*, *61*(1–2), 114–119. <https://doi.org/10.1016/j.apcatb.2005.03.014>
- Lan, J., Sun, Y., Guo, L., Li, Z., Du, D., & Zhang, T. C. (2019). A novel method to recover ammonia, manganese and sulfate from electrolytic manganese residues by bio-leaching. *Journal of Cleaner Production*, *223*, 499–507. <https://doi.org/10.1016/j.jclepro.2019.03.098>
- Lan, J., Sun, Y., Huang, P., Du, Y., Zhan, W., Zhang, T. C., & Du, D. (2020). Using Electrolytic Manganese Residue to prepare novel nanocomposite catalysts for efficient degradation of Azo Dyes in Fenton-like processes. *Chemosphere*, *252*, 126487. <https://doi.org/10.1016/j.chemosphere.2020.126487>

- Lannoo, S., Vilas-Boas, A., Sadeghi, S. M., Jesus, J., & Soares, H. M. V. M. (2019). An environmentally friendly closed loop process to recycle raw materials from spent alkaline batteries. *Journal of Cleaner Production*, 236, 117612. <https://doi.org/10.1016/j.jclepro.2019.117612>
- Larsen, D., & Mann, R. (2005). Origin of high manganese concentrations in coal mine drainage, eastern Tennessee. *Journal of Geochemical Exploration*, 86(3), 143–163. <https://doi.org/10.1016/j.gexplo.2005.06.001>
- Le Bourre, B., Neculita, C. M., Coudert, L., & Rosa, E. (2020). Manganese removal processes and geochemical behavior in residues from passive treatment of mine drainage. *Chemosphere*, 259, 127424. <https://doi.org/10.1016/j.chemosphere.2020.127424>
- Lee, S. A., Lee, J. J., You, G. R., Choi, Y. W., & Kim, C. (2015). Distinction between Mn(III) and Mn(II) by using a colorimetric chemosensor in aqueous solution. *RSC Advances*, 5(116), 95618–95630. <https://doi.org/10.1039/c5ra20396a>
- Leite, D. da S., Carvalho, P. L. G., de Lemos, L. R., Mageste, A. B., & Rodrigues, G. D. (2019). Hydrometallurgical recovery of Zn(II) and Mn(II) from alkaline batteries waste employing aqueous two-phase system. *Separation and Purification Technology*, 210(July 2018), 327–334. <https://doi.org/10.1016/j.seppur.2018.07.038>
- Li, H., Zhang, Z., Tang, S., Li, Y., & Zhang, Y. (2008). Ultrasonically assisted acid extraction of manganese from slag. *Ultrasonics Sonochemistry*, 15(4), 339–343. <https://doi.org/10.1016/j.ultsonch.2007.07.010>
- Li, K., Chen, C., Zhang, H., Hu, X., Sun, T., & Jia, J. (2019). Effects of phase structure of MnO₂ and morphology of δ -MnO₂ on toluene catalytic oxidation. *Applied Surface Science*, 496(July). <https://doi.org/10.1016/j.apsusc.2019.143662>

- Li, M., Hu, L., Zhong, H., He, Z., Sun, W., & Xiong, D. (2021). Efficient removal of diethyl dithiocarbamate with EDTA functionalized electrolytic manganese residue and mechanism exploration. *Journal of Hazardous Materials*, 410(November), 124582. <https://doi.org/10.1016/j.jhazmat.2020.124582>
- Li, M., Huang, F., Hu, L., Sun, W., Li, E., Xiong, D. L., ... He, Z. (2020). Efficient activation of peroxymonosulfate by a novel catalyst prepared directly from electrolytic manganese slag for degradation of recalcitrant organic pollutants. *Chemical Engineering Journal*, 401, 126085. <https://doi.org/10.1016/j.cej.2020.126085>
- Li, M., Zhong, H., He, Z., Hu, L., Sun, W., Loganathan, P., & Xiong, D. (2021). Degradation of various thiol collectors in simulated and real mineral processing wastewater of sulfide ore in heterogeneous modified manganese slag/PMS system. *Chemical Engineering Journal*, 413, 127478. <https://doi.org/10.1016/j.cej.2020.127478>
- Li, Yongchao, Huang, H., Xu, Z., Ma, H., & Guo, Y. (2020). Mechanism study on manganese(II) removal from acid mine wastewater using red mud and its application to a lab-scale column. *Journal of Cleaner Production*, 253, 119955. <https://doi.org/10.1016/j.jclepro.2020.119955>
- Li, Yongchao, Xu, Z., Ma, H., & Hursthouse, A. S. (2019). Removal of Manganese (II) from Acid Mine Wastewater : A Review of the Challenges and Opportunities with Special Emphasis on. *Water*, (1i).
- Li, Yongdan, Wu, D., & Lin, Y. S. (2004). Mechanical strength and reliability of solid catalysts. *China Particuology*, 2(2), 53–62. [https://doi.org/10.1016/s1672-2515\(07\)60024-4](https://doi.org/10.1016/s1672-2515(07)60024-4)

- Li, Yunqing, & Xi, G. (2005). The dissolution mechanism of cathodic active materials of spent Zn-Mn batteries in HCl. *Journal of Hazardous Materials*, 127(1–3), 244–248. <https://doi.org/10.1016/j.jhazmat.2005.07.024>
- Liang, S., Teng, F., Bulgan, G., Zong, R., & Zhu, Y. (2008). Effect of phase structure of MnO₂ nanorod catalyst on the activity for CO oxidation. *Journal of Physical Chemistry C*, 112(14), 5307–5315. <https://doi.org/10.1021/jp0774995>
- Lin, T., Yu, L., Sun, M., Cheng, G., Lan, B., & Fu, Z. (2016). Mesoporous α -MnO₂ microspheres with high specific surface area: Controlled synthesis and catalytic activities. *Chemical Engineering Journal*, 286, 114–121. <https://doi.org/10.1016/j.cej.2015.09.024>
- Liu, C., Han, Q., Chen, Y., Zhu, S., Su, T., Qu, Z., ... Huo, M. (2021). Resource Recycling of Mn-Rich Sludge: Effective Separation of Impure Fe/Al and Recovery of High-Purity Hausmannite. *ACS Omega*, 6(11), 7351–7359. <https://doi.org/10.1021/acsomega.0c05487>
- Liu, P. (2018). Recycling Waste Batteries: Recovery of Valuable Resources or Reutilization as Functional Materials. *ACS Sustainable Chemistry and Engineering*, 6(9), 11176–11185. <https://doi.org/10.1021/acssuschemeng.8b03495>
- Liu, X., Shi, L., Jiang, W., Zhang, J., & Huang, L. (2018). Taking full advantage of KMnO₄ in simplified Hummers method: A green and one pot process for the fabrication of alpha MnO₂ nanorods on graphene oxide. *Chemical Engineering Science*, 192, 414–421. <https://doi.org/10.1016/j.ces.2018.07.044>
- López, E., Gígola, C., Borio, D. O., & Bucalá, V. (2001). Catalytic combustion of methane over Pd/ γ -Al₂O₃ in a monolithic reactor: Kinetic study. *Studies in Surface Science and Catalysis*, 133(1961), 625–630. [https://doi.org/10.1016/s0167-2991\(01\)82023-1](https://doi.org/10.1016/s0167-2991(01)82023-1)

- Lu, J., Dreisinger, D., & Glück, T. (2014). Manganese electrodeposition — A literature review. *Hydrometallurgy*, *141*, 105–116. <https://doi.org/10.1016/j.hydromet.2013.11.002>
- Lyu, Y., Li, C., Du, X., Zhu, Y., Zhang, Y., & Li, S. (2020a). Catalytic oxidation of toluene over MnO₂ catalysts with different Mn (II) precursors and the study of reaction pathway. *Fuel*, *262*(August), 116610. <https://doi.org/10.1016/j.fuel.2019.116610>
- Lyu, Y., Li, C., Du, X., Zhu, Y., Zhang, Y., & Li, S. (2020b). Catalytic removal of toluene over manganese oxide-based catalysts: a review. *Environmental Science and Pollution Research*, *27*(3), 2482–2501. <https://doi.org/10.1007/s11356-019-07037-2>
- Malcolm, H. M., Wood, M., & Kingdom, U. (2004). IPCS Concise International Chemical Assessment Documents. Manganese and its compounds: Environmental aspects. *IPCS Concise International Chemical Assessment Documents*, (63), 1–37.
- Maryam Sadeghi, S., Vanpeteghem, G., Neto, I. F. F., & Soares, H. M. V. M. (2017). Selective leaching of Zn from spent alkaline batteries using environmentally friendly approaches. *Waste Management*, *60*, 696–705. <https://doi.org/10.1016/j.wasman.2016.12.002>
- Maynard, J. B. (2010). The chemistry of manganese ores through time: A signal of increasing diversity of earth-surface environments. *Economic Geology*, *105*(3), 535–552. <https://doi.org/10.2113/gsecongeo.105.3.535>
- Mears, D. E. (1971a). Diagnostic criteria for heat transport limitations in fixed bed reactors. *Journal of Catalysis*, *20*(2), 127–131. [https://doi.org/10.1016/0021-9517\(71\)90073-X](https://doi.org/10.1016/0021-9517(71)90073-X)
- Mears, D. E. (1971b). Tests for Transport Limitations in Experimental Catalytic Reactors. *Industrial and Engineering Chemistry Process Design and Development*, *10*(4), 541–547. <https://doi.org/10.1021/i260040a020>

- Melchor-Martínez, E. M., Macias-Garbett, R., Malacara-Becerra, A., Iqbal, H. M. N., Sosa-Hernández, J. E., & Parra-Saldívar, R. (2021). Environmental impact of emerging contaminants from battery waste: A mini review. *Case Studies in Chemical and Environmental Engineering*, 3(April). <https://doi.org/10.1016/j.cscee.2021.100104>
- Menezes, P. W., Indra, A., Gutkin, V., & Driess, M. (2017). Boosting electrochemical water oxidation through replacement of Oh Co sites in cobalt oxide spinel with manganese. *Chemical Communications*, 53(57), 8018–8021. <https://doi.org/10.1039/c7cc03749j>
- Michot, A., Smith, D. S., Degot, S., & Gault, C. (2008). Thermal conductivity and specific heat of kaolinite: Evolution with thermal treatment. *Journal of the European Ceramic Society*, 28(14), 2639–2644. <https://doi.org/10.1016/j.jeurceramsoc.2008.04.007>
- Minette, F., Lugo-Pimentel, M., Modroukas, D., Davis, A. W., Gill, R., Castaldi, M. J., & De Wilde, J. (2018). Intrinsic kinetics of steam methane reforming on a thin, nanostructured and adherent Ni coating. *Applied Catalysis B: Environmental*, 238, 184–197. <https://doi.org/10.1016/j.apcatb.2018.07.015>
- Mitchell, S., Michels, N. L., & Pérez-Ramírez, J. (2013). From powder to technical body: The undervalued science of catalyst scale up. *Chemical Society Reviews*, 42(14), 6094–6112. <https://doi.org/10.1039/c3cs60076a>
- Mocellin, J., Mercier, G., Morel, J. L., Blais, J. F., & Simonnot, M. O. (2015). Factors influencing the Zn and Mn extraction from pyrometallurgical sludge in the steel manufacturing industry. *Journal of Environmental Management*, 158, 48–54. <https://doi.org/10.1016/j.jenvman.2015.04.039>
- Mocellin, J., Mercier, G., Morel, J. L., Charbonnier, P., Blais, J. F., & Simonnot, M. O. (2017). Recovery of zinc and manganese from pyrometallurgy sludge by hydrometallurgical

- processing. *Journal of Cleaner Production*, 168, 311–321.
<https://doi.org/10.1016/j.jclepro.2017.09.003>
- Mohammadzadeh, J. S. S., & Zamaniyan, A. (2002). Catalyst Shape As a Design Parameter — Optimum Shape for. *Transport*, 80(May), Part A.
- Mohanty, S., Ghosh, S., Bal, B., & Das, A. P. (2018). A review of biotechnology processes applied for manganese recovery from wastes. *Reviews in Environmental Science and Biotechnology*, 17(4), 791–811. <https://doi.org/10.1007/s11157-018-9482-1>
- Morais, V. S., Barrada, R. V., Moura, M. N., Almeida, J. R., Moreira, T. F. M., Gonçalves, G. R., ... Freitas, M. B. J. G. (2020). Synthesis of manganese ferrite from spent Zn-MnO₂ batteries and its application as a catalyst in heterogeneous photo-Fenton processes. *Journal of Environmental Chemical Engineering*, 8(3), 103716.
<https://doi.org/10.1016/j.jece.2020.103716>
- Neculita, C. M., & Rosa, E. (2019). A review of the implications and challenges of manganese removal from mine drainage. *Chemosphere*, 214, 491–510.
<https://doi.org/10.1016/j.chemosphere.2018.09.106>
- Nogueira, C. A., & Margarido, F. (2015). Selective process of zinc extraction from spent Zn-MnO₂ batteries by ammonium chloride leaching. *Hydrometallurgy*, 157, 13–21.
<https://doi.org/10.1016/j.hydromet.2015.07.004>
- Okal, J., Zawadzki, M., & Baranowska, K. (2016). Methane combustion over bimetallic Ru-Re/ γ -Al₂O₃ catalysts: Effect of Re and pretreatments. *Applied Catalysis B: Environmental*, 194, 22–31. <https://doi.org/10.1016/j.apcatb.2016.04.038>
- Olivares, J. A. (2006). Mass Spectrometry in Process Analysis. In *Encyclopedia of Analytical Chemistry* (pp. 1–16). <https://doi.org/10.1002/9780470027318.a2109>

- Ong, D. C., de Luna, M. D. G., Pingul-Ong, S. M. B., & Kan, C. C. (2018). Manganese and iron recovery from groundwater treatment sludge by reductive acid leaching and hydroxide precipitation. *Journal of Environmental Management*, 223(January), 723–730. <https://doi.org/10.1016/j.jenvman.2018.06.052>
- Ong, D. C., Tumampos, S. B., Kan, C. C., Pingul-Ong, S. M. B., Ensano, B. M. B., & De Luna, M. D. G. (2021a). Optimization of manganese recovery from groundwater treatment sludge for the production of highly-efficient Cu(II) and Pb(II) adsorbents. *Journal of Environmental Chemical Engineering*, 9(1), 104705. <https://doi.org/10.1016/j.jece.2020.104705>
- Ong, D. C., Tumampos, S. B., Kan, C. C., Pingul-Ong, S. M. B., Ensano, B. M. B., & De Luna, M. D. G. (2021b). Optimization of manganese recovery from groundwater treatment sludge for the production of highly-efficient Cu(II) and Pb(II) adsorbents. *Journal of Environmental Chemical Engineering*, 9(1). <https://doi.org/10.1016/j.jece.2020.104705>
- Park, Y. K., Kim, M. K., Jung, S. C., Shim, W. G., Jang, S. H., & Kim, S. C. (2021a). Effect of calcination temperature on properties of waste alkaline battery-based catalysts for deep oxidation of toluene and o-xylene. *Energy and Environment*, 32(3), 367–379. <https://doi.org/10.1177/0958305X20932551>
- Park, Y. K., Kim, M. K., Jung, S. C., Shim, W. G., Jang, S. H., & Kim, S. C. (2021b). Effect of calcination temperature on properties of waste alkaline battery-based catalysts for deep oxidation of toluene and o-xylene. *Energy and Environment*, 32(3), 367–379. <https://doi.org/10.1177/0958305X20932551>
- Park, Y. K., Song, H., Kim, M. K., Jung, S. C., Jung, H. Y., & Kim, S. C. (2021). Recycling of a spent alkaline battery as a catalyst for the total oxidation of hydrocarbons. *Journal of*

- Hazardous Materials*, 403(September 2020), 123929.
<https://doi.org/10.1016/j.jhazmat.2020.123929>
- Patil, D. S., Chavan, S. M., & Oubagaranadin, J. U. K. (2016). A review of technologies for manganese removal from wastewaters. *Journal of Environmental Chemical Engineering*, 4(1), 468–487. <https://doi.org/10.1016/j.jece.2015.11.028>
- Peng, N., Pan, Q., Liu, H., Yang, Z., & Wang, G. (2018). Recovery of iron and manganese from iron-bearing manganese residues by multi-step roasting and magnetic separation. *Minerals Engineering*, 126(May), 177–183. <https://doi.org/10.1016/j.mineng.2018.07.002>
- Piumetti, M., Fino, D., & Russo, N. (2015). Mesoporous manganese oxides prepared by solution combustion synthesis as catalysts for the total oxidation of VOCs. *Applied Catalysis B: Environmental*, 163, 277–287. <https://doi.org/10.1016/j.apcatb.2014.08.012>
- Post, J. E. (1999). Manganese oxide minerals: Crystal structures and economic and environmental significance. *Proceedings of the National Academy of Sciences of the United States of America*, 96(7), 3447–3454. <https://doi.org/10.1073/pnas.96.7.3447>
- Pulleri, J. K., Singh, S. K., Yearwar, D., Saravanan, G., Al-Fatesh, A. S., & Labhasetwar, N. K. (2021). Morphology Dependent Catalytic Activity of Mn₃O₄ for Complete Oxidation of Toluene and Carbon Monoxide. *Catalysis Letters*, 151(1), 172–183. <https://doi.org/10.1007/s10562-020-03278-w>
- Qi, W., Ran, J., Wang, R., Du, X., Shi, J., Niu, J., ... Ran, M. (2016). Kinetic consequences of methane combustion on Pd, Pt and Pd-Pt catalysts. *RSC Advances*, 6(111), 109834–109845. <https://doi.org/10.1039/c6ra21150j>
- Quintanilha, C. L., Afonso, J. C., Vianna, C. A., Gante, V., & Mantovano, J. L. (2014). Recovery of manganese and zinc via sequential precipitation from spent zinc-MnO₂ dry cells after

- fusion with potassium hydrogenosulfate. *Journal of Power Sources*, 248, 596–603.
<https://doi.org/10.1016/j.jpowsour.2013.09.111>
- R.D.W. Kemmitt and R.D. Peacock. (1973). *The Chemistry of Manganese, Technetium and Rhenium* (First). <https://doi.org/10.1016/C2013-0-05702-7>
- Rącz, R., & Ilea, P. (2013). Electrolytic recovery of Mn₃O₄ and Zn from sulphuric acid leach liquors of spent zinc-carbon-MnO₂ battery powder. *Hydrometallurgy*, 139, 116–123.
<https://doi.org/10.1016/j.hydromet.2013.08.006>
- Rashid, R., Shafiq, I., Akhter, P., Iqbal, M. J., & Hussain, M. (2021). A state-of-the-art review on wastewater treatment techniques: the effectiveness of adsorption method. *Environmental Science and Pollution Research*, 28(8), 9050–9066. <https://doi.org/10.1007/s11356-021-12395-x>
- Ray, A., Bristow, T., Whitmore, C., & Mosely, J. (2018). On-line reaction monitoring by mass spectrometry, modern approaches for the analysis of chemical reactions. *Mass Spectrometry Reviews*, Vol. 37, pp. 565–579. <https://doi.org/10.1002/mas.21539>
- Reidies, A. H. (2000). Manganese Compounds. In *Ullmann's Encyclopedia of Industrial Chemistry* (Vol. 16, pp. 13–15). https://doi.org/10.1002/14356007.a16_123
- Ren, T., An, M., Hu, X., Ma, J., & Guo, Q. (2021). Development of inexpensive perovskite Mn-based oxygen carriers using the waste manganese sand for chemical looping gasification. *International Journal of Energy Research*, 45(2), 2416–2431.
<https://doi.org/10.1002/er.5936>
- Rezaei, R., Moradi, G., & Sharifnia, S. (2019). Dry Reforming of Methane over Ni-Cu/Al₂O₃ Catalyst Coatings in a Microchannel Reactor: Modeling and Optimization Using Design of

- Experiments [Research-article]. *Energy & Fuels*, 33(7), 6689–6706.
<https://doi.org/10.1021/acs.energyfuels.9b00692>
- Rubel, O., Nguyen, T., Tran, T., Gourley, S., Anand, S., Bommel, A. Van, ... Ivey, D. G. (n.d.).
Electrochemical Stability of ZnMn₂O₄: Understanding Zn-ion Rechargeable Battery. 1–33.
- Sadeghabad, M. S., Bahaloo-Horeh, N., & Mousavi, S. M. (2019). Using bacterial culture supernatant for extraction of manganese and zinc from waste alkaline button-cell batteries. *Hydrometallurgy*, 188(December 2018), 81–91.
<https://doi.org/10.1016/j.hydromet.2019.06.003>
- Sandoval-Bohorquez, V. S., Rozo, E. A. V., & Baldovino-Medrano, V. G. (2020). A method for the highly accurate quantification of gas streams by on-line chromatography. *Journal of Chromatography A*, 1626, 461355. <https://doi.org/10.1016/j.chroma.2020.461355>
- Satterfield, C. N. (1991). Acid and Zeolite Catalysts. *Heterogeneous Catalysis in Industrial Practice*, pp. 209–266.
- Sayilgan, E., Kukrer, T., Civelekoglu, G., Ferella, F., Akcil, A., Veglio, F., & Kitis, M. (2009). A review of technologies for the recovery of metals from spent alkaline and zinc-carbon batteries. *Hydrometallurgy*, 97(3–4), 158–166.
<https://doi.org/10.1016/j.hydromet.2009.02.008>
- Scott Fogler, H. (1987). Elements of chemical reaction engineering. *Chemical Engineering Science*, 42(10), 2493. [https://doi.org/10.1016/0009-2509\(87\)80130-6](https://doi.org/10.1016/0009-2509(87)80130-6)
- Shen, B., Zhou, P., Chen, S., Yuan, H., Zhu, N., Sun, T., & Lou, Z. (2019). Manganese-based catalysts recovered from spent ternary lithium-ion batteries and its catalytic activity

- enhanced by a mechanical method. *Journal of Cleaner Production*, 213, 1346–1352.
<https://doi.org/10.1016/j.jclepro.2018.12.248>
- Sher Shah, M. S. A., Oh, C., Park, H., Hwang, Y. J., Ma, M., & Park, J. H. (2020). Catalytic Oxidation of Methane to Oxygenated Products: Recent Advancements and Prospects for Electrocatalytic and Photocatalytic Conversion at Low Temperatures. *Advanced Science*, 7(23), 1–24. <https://doi.org/10.1002/advs.202001946>
- Shi, F., Wang, F., Dai, H., Dai, J., Deng, J., Liu, Y., ... Au, C. T. (2012). Rod-, flower-, and dumbbell-like MnO₂: Highly active catalysts for the combustion of toluene. *Applied Catalysis A: General*, 433–434, 206–213. <https://doi.org/10.1016/j.apcata.2012.05.016>
- Shu, J., Li, B., Chen, M., Sun, D., Wei, L., Wang, Y., & Wang, J. (2020). An innovative method for manganese (Mn²⁺) and ammonia nitrogen (NH₄⁺-N) stabilization/solidification in electrolytic manganese residue by basic burning raw material. *Chemosphere*, 253, 126896. <https://doi.org/10.1016/j.chemosphere.2020.126896>
- Shu, J., Liu, R., Liu, Z., Chen, H., & Tao, C. (2016a). Enhanced extraction of manganese from electrolytic manganese residue by electrochemical. *Journal of Electroanalytical Chemistry*, 780, 32–37. <https://doi.org/10.1016/j.jelechem.2016.08.033>
- Shu, J., Liu, R., Liu, Z., Chen, H., & Tao, C. (2016b). Simultaneous removal of ammonia and manganese from electrolytic metal manganese residue leachate using phosphate salt. *Journal of Cleaner Production*, 135, 468–475. <https://doi.org/10.1016/j.jclepro.2016.06.141>
- Shu, J., Wu, H., Chen, M., Peng, H., Li, B., Liu, R., ... Hu, Z. (2019). Fractional removal of manganese and ammonia nitrogen from electrolytic metal manganese residue leachate

- using carbonate and struvite precipitation. *Water Research*, 153, 229–238.
<https://doi.org/10.1016/j.watres.2018.12.044>
- Sie, S. T., & Krishna, R. (1998). Process development and scale up: II. Catalyst design strategy. *Reviews in Chemical Engineering*, 14(3), 159–202.
<https://doi.org/10.1515/REVCE.1998.14.3.159>
- Sihaib, Z., Puleo, F., Garcia-Vargas, J. M., Retailleau, L., Descorme, C., Liotta, L. F., ... Giroir-Fendler, A. (2017). Manganese oxide-based catalysts for toluene oxidation. *Applied Catalysis B: Environmental*, 209, 689–700. <https://doi.org/10.1016/j.apcatb.2017.03.042>
- Sobianowska-Turek, A., Szczepaniak, W., Maciejewski, P., & Gawlik-Kobylińska, M. (2016). Recovery of zinc and manganese, and other metals (Fe, Cu, Ni, Co, Cd, Cr, Na, K) from Zn-MnO₂ and Zn-C waste batteries: Hydroxyl and carbonate co-precipitation from solution after reducing acidic leaching with use of oxalic acid. *Journal of Power Sources*, 325(79), 220–228. <https://doi.org/10.1016/j.jpowsour.2016.06.042>
- Sobianowska-Turek, Agnieszka. (2018). Hydrometallurgical recovery of metals: Ce, La, Co, Fe, Mn, Ni and Zn from the stream of used Ni-MH cells. *Waste Management*, 77, 213–219.
<https://doi.org/10.1016/j.wasman.2018.03.046>
- Sobianowska-Turek, Agnieszka, Szczepaniak, W., & Zabłocka-Malicka, M. (2014). Electrochemical evaluation of manganese reducers - Recovery of Mn from Zn-Mn and Zn-C battery waste. *Journal of Power Sources*, 270, 668–674.
<https://doi.org/10.1016/j.jpowsour.2014.07.136>
- Soltanieh, M., Zohrabian, A., Gholipour, M. J., & Kalnay, E. (2016). A review of global gas flaring and venting and impact on the environment: Case study of Iran. *International Journal of Greenhouse Gas Control*, 49, 488–509. <https://doi.org/10.1016/j.ijggc.2016.02.010>

- Sotudeh-Gharebagh, R., & Chaouki, J. (2008). The Heterogeneous and Homogeneous Combustion of Methane Over Inert Particles. *The Canadian Journal of Chemical Engineering*, 81(6), 1182–1191. <https://doi.org/10.1002/cjce.5450810607>
- Staub, D., Meille, S., Le Corre, V., Chevalier, J., & Rouleau, L. (2015). Revisiting the Side Crushing Test Using the Three-Point Bending Test for the Strength Measurement of Catalyst Supports. *Oil & Gas Science and Technology – Revue d'IFP Energies Nouvelles*, 70(3), 475–486. <https://doi.org/10.2516/ogst/2013214>
- Stegarescu, A., Lung, I., Leoștean, C., Kacso, I., Opriș, O., Lazăr, M. D., ... Soran, M. L. (2020). Green Synthesis, Characterization and Test of MnO₂ Nanoparticles as Catalyst in Biofuel Production from Grape Residue and Seeds Oil. *Waste and Biomass Valorization*, 11(9), 5003–5013. <https://doi.org/10.1007/s12649-019-00805-8>
- Stranick, M. A. (1999). Mn₂O₃ by XPS. *Surface Science Spectra*, 6(1), 39–46. <https://doi.org/10.1116/1.1247889>
- Sun, L., Zhao, P., Liu, Y., Tan, B., Yu, C., Feng, N., ... Guan, G. (2021). Enhancing the catalytic activity of MnO₂ via structural phase transition for propane combustion: Promotional role of ionic liquid. *Journal of Environmental Chemical Engineering*, 9(6), 106453. <https://doi.org/10.1016/j.jece.2021.106453>
- Sun, Z., Cao, H., Xiao, Y., Sietsma, J., Jin, W., Agterhuis, H., & Yang, Y. (2017). Toward Sustainability for Recovery of Critical Metals from Electronic Waste: The Hydrochemistry Processes. *ACS Sustainable Chemistry and Engineering*, 5(1), 21–40. <https://doi.org/10.1021/acssuschemeng.6b00841>

- Survey, U. S. G. (2020). Mineral commodity summaries 2020. In *U.S Department OF The Interior, U.S Geological Survey*. Retrieved from <https://pubs.usgs.gov/periodicals/mcs2020/mcs2020.pdf>
- Takeda, A. (2003). Manganese action in brain function. *Brain Research Reviews*, 41(1), 79–87. [https://doi.org/10.1016/S0165-0173\(02\)00234-5](https://doi.org/10.1016/S0165-0173(02)00234-5)
- Thüne, P. C., & Niemantsverdriet, J. W. (Hans. (2009). Surface science models of industrial catalysts. *Surface Science*, 603(10–12), 1756–1762. <https://doi.org/10.1016/j.susc.2008.10.061>
- Tian, Y., Shu, J., Chen, M., Wang, J., Wang, Y., Luo, Z., ... Sun, Z. (2019). Manganese and ammonia nitrogen recovery from electrolytic manganese residue by electric field enhanced leaching. *Journal of Cleaner Production*, 236. <https://doi.org/10.1016/j.jclepro.2019.117708>
- Todorova, S., Stefanov, P., Naydenov, A., & Kolev, H. (2014). Catalytic oxidation of methane over Pd-MeOx (Me = Mn, Co, Ni, Ce) catalysts - influence of metal oxides. *Revue Roumaine de Chimie*, 59(3–4), 251–257.
- Tomašić, V., & Jović, F. (2006). State-of-the-art in the monolithic catalysts/reactors. *Applied Catalysis A: General*, 311(1–2), 112–121. <https://doi.org/10.1016/j.apcata.2006.06.013>
- Toro, N., Jeldres, R. I., Órdenes, J. A., Robles, P., & Navarra, A. (2020). Manganese nodules in Chile, an alternative for the production of Co and Mn in the future—A review. *Minerals*, 10(8), 1–19. <https://doi.org/10.3390/min10080674>
- U.S. Geological Survey. (2021). *Manganese Commodity Summary 2021*. (703). Retrieved from <https://www.usgs.gov/centers/national-minerals-information-center/manganese-statistics-and-information>

- US EPA, O. (2021). *Recycling Basics*. 1–8. Retrieved from <https://www.epa.gov/recycle/recycling-basics>
- Vaudano, Pierre; Plattner, Eric; Comninellis, C. (1995). The Industrial Electrolytic Regeneration of $\text{Mn}_2(\text{SO}_4)_3$ for the Oxidation of Substituted Toluene to the Corresponding Benzaldehyde. *Chimia*, 49(1–2), 12. <https://doi.org/10.2533/chimia.1995.12>
- Velasco-Rozo, E. A., Ballesteros-Rueda, L. M., & Baldovino-Medrano, V. G. (2021). A Method for the Accurate Quantification of Gas Streams by Online Mass Spectrometry. *Journal of the American Society for Mass Spectrometry*, 32(8), 2135–2143. <https://doi.org/10.1021/jasms.1c00090>
- Walton, J., Alexander, M. R., Fairley, N., Roach, P., & Shard, A. G. (2016). Film thickness measurement and contamination layer correction for quantitative XPS. *Surface and Interface Analysis*, 48(3), 164–172. <https://doi.org/10.1002/sia.5934>
- Wang, C., Rosenfeldt, E., Li, Y., & Hofmann, R. (2020). External standard calibration method to measure the hydroxyl radical scavenging capacity of water samples. *Environmental Science and Technology*, 54(3), 1929–1937. <https://doi.org/10.1021/acs.est.9b06273>
- Wang, G., Zhang, J., Liu, L., Zhou, J. Z., Liu, Q., Qian, G., ... Richards, R. M. (2018). Novel multi-metal containing MnCr catalyst made from manganese slag and chromium wastewater for effective selective catalytic reduction of nitric oxide at low temperature. *Journal of Cleaner Production*, 183, 917–924. <https://doi.org/10.1016/j.jclepro.2018.02.207>
- Wang, G., Zhang, J., Zhou, J., & Qian, G. (2019). Production of an effective catalyst with increased oxygen vacancies from manganese slag for selective catalytic reduction of nitric oxide.

- Journal of Environmental Management*, 239(February), 90–95.
<https://doi.org/10.1016/j.jenvman.2019.03.056>
- Wang, N., Fang, Z., Peng, S., Cheng, D., Du, B., & Zhou, C. (2016). Recovery of soluble manganese from electrolyte manganese residue using a combination of ammonia and CO₂. *Hydrometallurgy*, 164, 288–294. <https://doi.org/10.1016/j.hydromet.2016.06.019>
- Wang, Xiuyun, Liu, Y., Zhang, Y., Zhang, T., Chang, H., Zhang, Y., & Jiang, L. (2018). Structural requirements of manganese oxides for methane oxidation: XAS spectroscopy and transition-state studies. *Applied Catalysis B: Environmental*, 229, 52–62. <https://doi.org/10.1016/j.apcatb.2018.02.007>
- Wang, Xu, Qiu, H., Liu, H., Shi, P., Fan, J., Min, Y., & Xu, Q. (2018). Recycling application of waste Li-MnO₂ batteries as efficient catalysts based on electrochemical lithiation to improve catalytic activity. *Green Chemistry*, 20(21), 4901–4910. <https://doi.org/10.1039/c8gc02183j>
- Wang, Y., Liu, Y., Cao, Q., Wang, C. A., & Che, D. (2011). Homogeneous combustion of fuel ultra-lean methane-air mixtures: Experimental study and simplified reaction mechanism. *Energy and Fuels*, 25(8), 3437–3445. <https://doi.org/10.1021/ef200484c>
- Watson, J. T., & Sparkman, O. D. (2007). *Introduction to Mass Spectrometry* (Fourth Ed.). <https://doi.org/10.1002/9780470516898>
- Wei, Y., Ni, L., Li, M., & Zhao, J. (2017). A template-free method for preparation of MnO₂ catalysts with high surface areas. *Catalysis Today*, 297, 188–192. <https://doi.org/10.1016/j.cattod.2016.12.044>
- Whelpton, R. (2019). Quality assurance | internal standards. In *Encyclopedia of Analytical Science* (3rd ed.). <https://doi.org/10.1016/B978-0-12-409547-2.14399-9>

- Winiarska, K., Klimkiewicz, R., Tylus, W., Sobianowska-Turek, A., Winiarski, J., Szczygieł, B., & Szczygieł, I. (2019). Study of the catalytic activity and surface properties of manganese-zinc ferrite prepared from used batteries. *Journal of Chemistry*, 2019. <https://doi.org/10.1155/2019/5430904>
- Wu, F. F., Li, X. P., Zhong, H., & Wang, S. (2016). Utilization of Electrolytic Manganese Residues in Production of Porous Ceramics. *International Journal of Applied Ceramic Technology*, 13(3), 511–521. <https://doi.org/10.1111/ijac.12502>
- Xin, B., Chen, B., Duan, N., & Zhou, C. (2011). Extraction of manganese from electrolytic manganese residue by bioleaching. *Bioresource Technology*, 102(2), 1683–1687. <https://doi.org/10.1016/j.biortech.2010.09.107>
- Xin, B., Jiang, W., Aslam, H., Zhang, K., Liu, C., Wang, R., & Wang, Y. (2012). Bioleaching of zinc and manganese from spent Zn-Mn batteries and mechanism exploration. *Bioresource Technology*, 106, 147–153. <https://doi.org/10.1016/j.biortech.2011.12.013>
- Xin, B., Jiang, W., Li, X., Zhang, K., Liu, C., Wang, R., & Wang, Y. (2012). Analysis of reasons for decline of bioleaching efficiency of spent Zn-Mn batteries at high pulp densities and exploration measure for improving performance. *Bioresource Technology*, 112, 186–192. <https://doi.org/10.1016/j.biortech.2012.02.133>
- Xu, F., Jiang, L., Dan, Z., Gao, X., Duan, N., Han, G., & Zhu, H. (2014). Water balance analysis and wastewater recycling investigation in electrolytic manganese industry of China - A case study. *Hydrometallurgy*, 149, 12–22. <https://doi.org/10.1016/j.hydromet.2014.05.002>
- Xu, H., Yan, N., Qu, Z., Liu, W., Mei, J., Huang, W., & Zhao, S. (2017). Gaseous Heterogeneous Catalytic Reactions over Mn-Based Oxides for Environmental Applications: A Critical

- Review. *Environmental Science and Technology*, 51(16), 8879–8892.
<https://doi.org/10.1021/acs.est.6b06079>
- Yang, Renchun, Ren, C., Teng, X., Chen, Z., Wu, S., & Zhang, W. (2017). Study of the Surface Oxygen Vacancies Evolvement on the Single and Bi-Components Manganese Oxide Precursors and their Catalytic Performance. *Catalysis Letters*, 147(3), 727–737.
<https://doi.org/10.1007/s10562-017-1973-0>
- Yang, Ruizhi, Wang, Z., Dai, L., & Chen, L. (2005). Synthesis and characterization of single-crystalline nanorods of α -MnO₂ and γ -MnOOH. *Materials Chemistry and Physics*, 93(1), 149–153. <https://doi.org/10.1016/j.matchemphys.2005.03.006>
- Ying, A. Y., Lu, Z., & Abdou, M. A. (1998). Mechanical behavior and design database of packed beds for blanket designs. *Fusion Engineering and Design*, 39–40, 759–764.
[https://doi.org/10.1016/S0920-3796\(97\)00157-9](https://doi.org/10.1016/S0920-3796(97)00157-9)
- Yuan, A., Wang, X., Wang, Y., & Hu, J. (2009). Textural and capacitive characteristics of MnO₂ nanocrystals derived from a novel solid-reaction route. *Electrochimica Acta*, 54(3), 1021–1026. <https://doi.org/10.1016/j.electacta.2008.08.057>
- Zakeri, M., Samimi, A., Shafiee Afarani, M., & Salehirad, A. (2018). Effects of porosity and pore size distribution on mechanical strength reliability of industrial-scale catalyst during preparation and catalytic test steps. *Particulate Science and Technology*, 36(1), 96–103.
<https://doi.org/10.1080/02726351.2016.1220437>
- Zeng, F., Pan, Y., Yang, Y., Li, Q., Li, G., Hou, Z., & Gu, G. (2016). Facile construction of Mn₃O₄-MnO₂ hetero-nanorods/graphene nanocomposite for highly sensitive electrochemical detection of hydrogen peroxide. *Electrochimica Acta*, 196, 587–596.
<https://doi.org/10.1016/j.electacta.2016.03.031>

- Zhang, K., Peng, X., Cao, Y., Yang, H., Wang, X., Zhang, Y., ... Jiang, L. (2019a). Effect of MnO₂ morphology on its catalytic performance in lean methane combustion. *Materials Research Bulletin*, *111*, 338–341. <https://doi.org/10.1016/j.materresbull.2018.11.023>
- Zhang, K., Peng, X., Cao, Y., Yang, H., Wang, X., Zhang, Y., ... Jiang, L. (2019b). Effect of MnO₂ morphology on its catalytic performance in lean methane combustion. *Materials Research Bulletin*, *111*(January 2018), 338–341. <https://doi.org/10.1016/j.materresbull.2018.11.023>
- Zhang, L., Wang, S., Lv, L., Ding, Y., Tian, D., & Wang, S. (2021). Insights into the Reactive and Deactivation Mechanisms of Manganese Oxides for Ozone Elimination: The Roles of Surface Oxygen Species. *Langmuir*, *37*(4), 1410–1419. <https://doi.org/10.1021/acs.langmuir.0c02841>
- Zhang, W., & Cheng, C. Y. (2007a). Manganese metallurgy review. Part I: Leaching of ores/secondary materials and recovery of electrolytic/chemical manganese dioxide. *Hydrometallurgy*, *89*(3–4), 137–159. <https://doi.org/10.1016/j.hydromet.2007.08.010>
- Zhang, W., & Cheng, C. Y. (2007b). Manganese metallurgy review. Part II: Manganese separation and recovery from solution. *Hydrometallurgy*, *89*(3–4), 160–177. <https://doi.org/10.1016/j.hydromet.2007.08.009>
- Zhang, W., & Cheng, C. Y. (2007c). Manganese metallurgy review. Part III: Manganese control in zinc and copper electrolytes. *Hydrometallurgy*, *89*(3–4), 178–188. <https://doi.org/10.1016/j.hydromet.2007.08.011>
- Zhou, C., Wang, J., Liu, X., Chen, F., Di, Y., Gao, S., & Shi, Q. (2018). Magnetic and thermodynamic properties of α , β , γ and δ -MnO₂. *New Journal of Chemistry*, *42*(11), 8400–8407. <https://doi.org/10.1039/c8nj00896e>

- Zhou, X., Luo, C., Wang, J., Wang, H., Chen, Z., Wang, S., & Chen, Z. (2021). Recycling application of modified waste electrolytic manganese anode slag as efficient catalyst for PMS activation. *Science of the Total Environment*, 762, 143120. <https://doi.org/10.1016/j.scitotenv.2020.143120>
- Zimmerman, J. B., Anastas, P. T., Erythropel, H. C., & Leitner, W. (2020). Designing for a green chemistry future. *Science*, 367(6476), 397–400. <https://doi.org/10.1126/science.aay3060>